Master Curve Approach to Monitor Fracture Toughness of Reactor Pressure Vessels in Nuclear Power Plants

IAEA
International Atomic Energy Agency

Master Curve Approach
to Monitor Fracture Toughness
of Reactor Pressure Vessels
in Nuclear Power Plants

The following States are Members of the International Atomic Energy Agency:

AFGHANISTAN	GHANA	NIGERIA
ALBANIA	GREECE	NORWAY
ALGERIA	GUATEMALA	OMAN
ANGOLA	HAITI	PAKISTAN
ARGENTINA	HOLY SEE	PALAU
ARMENIA	HONDURAS	PANAMA
AUSTRALIA	HUNGARY	PARAGUAY
AUSTRIA	ICELAND	PERU
AZERBAIJAN	INDIA	PHILIPPINES
BAHRAIN	INDONESIA	POLAND
BANGLADESH	IRAN, ISLAMIC REPUBLIC OF	PORTUGAL
BELARUS	IRAQ	QATAR
BELGIUM	IRELAND	REPUBLIC OF MOLDOVA
BELIZE	ISRAEL	ROMANIA
BENIN	ITALY	RUSSIAN FEDERATION
BOLIVIA	JAMAICA	SAUDI ARABIA
BOSNIA AND HERZEGOVINA	JAPAN	SENEGAL
BOTSWANA	JORDAN	SERBIA
BRAZIL	KAZAKHSTAN	SEYCHELLES
BULGARIA	KENYA	SIERRA LEONE
BURKINA FASO	KOREA, REPUBLIC OF	SINGAPORE
BURUNDI	KUWAIT	SLOVAKIA
CAMEROON	KYRGYZSTAN	SLOVENIA
CANADA	LATVIA	SOUTH AFRICA
CENTRAL AFRICAN	LEBANON	SPAIN
REPUBLIC	LESOTHO	SRI LANKA
CHAD	LIBERIA	SUDAN
CHILE	LIBYAN ARAB JAMAHIRIYA	SWEDEN
CHINA	LIECHTENSTEIN	SWITZERLAND
COLOMBIA	LITHUANIA	SYRIAN ARAB REPUBLIC
CONGO	LUXEMBOURG	TAJIKISTAN
COSTA RICA	MADAGASCAR	THAILAND
CÔTE D'IVOIRE	MALAWI	THE FORMER YUGOSLAV
CROATIA	MALAYSIA	REPUBLIC OF MACEDONIA
CUBA	MALI	TUNISIA
CYPRUS	MALTA	TURKEY
CZECH REPUBLIC	MARSHALL ISLANDS	UGANDA
DEMOCRATIC REPUBLIC	MAURITANIA	UKRAINE
OF THE CONGO	MAURITIUS	UNITED ARAB EMIRATES
DENMARK	MEXICO	UNITED KINGDOM OF
DOMINICAN REPUBLIC	MONACO	GREAT BRITAIN AND
ECUADOR	MONGOLIA	NORTHERN IRELAND
EGYPT	MONTENEGRO	UNITED REPUBLIC
EL SALVADOR	MOROCCO	OF TANZANIA
ERITREA	MOZAMBIQUE	UNITED STATES OF AMERICA
ESTONIA	MYANMAR	URUGUAY
ETHIOPIA	NAMIBIA	UZBEKISTAN
FINLAND	NEPAL	VENEZUELA
FRANCE	NETHERLANDS	VIETNAM
GABON	NEW ZEALAND	YEMEN
GEORGIA	NICARAGUA	ZAMBIA
GERMANY	NIGER	ZIMBABWE

The Agency's Statute was approved on 23 October 1956 by the Conference on the Statute of the IAEA held at United Nations Headquarters, New York; it entered into force on 29 July 1957. The Headquarters of the Agency are situated in Vienna. Its principal objective is "to accelerate and enlarge the contribution of atomic energy to peace, health and prosperity throughout the world".

IAEA-TECDOC-1631

Master Curve Approach to Monitor Fracture Toughness of Reactor Pressure Vessels in Nuclear Power Plants

INTERNATIONAL ATOMIC ENERGY AGENCY
VIENNA, 2009

For further information on this publication, please contact:

Nuclear Power Engineering Section
International Atomic Energy Agency
Vienna International Centre
PO Box 100
1400 Vienna, Austria
email: Official.Mail@iaea.org

FOREWORD

A series of coordinated research projects (CRPs) have been sponsored by the IAEA, starting in the early 1970s, focused on neutron radiation effects on reactor pressure vessel (RPV) steels. The purpose of the CRPs was to develop correlative comparisons to test the uniformity of results through coordinated international research studies and data sharing.

The overall scope of the eighth CRP (CRP-8), Master Curve Approach to Monitor Fracture Toughness of Reactor Pressure Vessels in Nuclear Power Plants, has evolved from previous CRPs which have focused on fracture toughness related issues.

The ultimate use of embrittlement understanding is application to assure structural integrity of the RPV under current and future operation and accident conditions. The Master Curve approach for assessing the fracture toughness of a sampled irradiated material has been gaining acceptance throughout the world. This direct measurement of fracture toughness approach is technically superior to the correlative and indirect methods used in the past to assess irradiated RPV integrity.

Several elements have been identified as focal points for Master Curve use: (i) limits of applicability for the Master Curve at the upper range of the transition region for loading quasi-static to dynamic/impact loading rates; (ii) effects of non-homogeneous material or changes due to environment conditions on the Master Curve, and how heterogeneity can be integrated into a more inclusive Master Curve methodology; (iii) importance of fracture mode differences and changes affect the Master Curve shape.

The collected data in this report represent mostly results from non-irradiated testing, although some results from test reactor irradiations and plant surveillance programmes have been included as available. The results presented here should allow utility engineers and scientists to directly measure fracture toughness using small surveillance size specimens and apply the results using the Master Curve approach for RPV structural integrity assessment in nuclear power plants.

The IAEA wishes to thank the participants for their contributions, especially the CRP chairman, W. Server of ATI Consulting, USA. The IAEA officers responsible for this publication were K.S. Kang and L. Kupca of the Division of Nuclear Power.

EDITORIAL NOTE

CONTENTS

1. BACKGROUND

1.1. INTRODUCTION

The integrity of the reactor pressure vessel (RPV) is essential for the continued operation of a nuclear power plant (NPP). Most studies related to long term operation, beyond typical design life, have identified the RPV as the most critical component of the NPP. Essentially all commercial light water reactors use ferritic low alloy steels for the construction of the RPV, so structural integrity relies upon accurate knowledge of the change in fracture toughness of the RPV materials over the time of operation.

Surveillance programmes using small specimens (most typically 10 mm square Charpy V-notch) have been designed to assess changes in fracture properties over the operational life. However, the use of an indirect indexing method such as derived from Charpy V-notch test results, coupled with generic reference fracture toughness curves, is not the optimum approach that can be taken considering today's technology. Direct measurement of fracture toughness using small surveillance specimens is a better approach for assessing changes in fracture toughness. The analytical approach developed for ferritic steels, called the Master Curve method, can be used to directly apply fracture toughness properties as measured in the irradiated condition. These data can then be more clearly utilized for assuring structural integrity during continued operation.

The assurance of safe operation of RPV components has evolved since the early 1970s. The IAEA has sponsored a series of coordinated research projects (CRPs) that have led to a focus on RPV structural integrity application of measured irradiation fracture parameters using relatively small test specimens. The background and results from the progression of the CRPs are described next.

The first project (or CRP Phase 1), Irradiation Embrittlement of Reactor Pressure Vessel Steels, focused on standardization of methods for measuring embrittlement in terms of both mechanical properties and the neutron irradiation environment. Little attention was given at that time (early 1970s) to the direct measurement of irradiated fracture toughness by using small surveillance type specimens since elastic-plastic fracture mechanics was in its infancy. The main results from CRP Phase 1, including all reports from participating organizations, were published in 1975 in IAEA-TECDOC-176 [1].

CRP Phase 2, Analysis of the Behaviour of Advanced Reactor Pressure Vessel Steels under Neutron Irradiation, involved testing and evaluation by various countries of so-called advanced RPV steels that had reduced residual compositional elements (copper and phosphorus). Irradiations were conducted to fluence levels beyond expected end-of-life, and the results of CRP Phase 1 were used to guide the overall approach taken during CRP Phase 2. In addition to transition temperature testing using Charpy V-notch test specimens, some emphasis was placed on using tensile and early-design fracture toughness test specimens applying elastic-plastic fracture mechanics methods. Further progress in the application of fracture mechanics analysis methods for radiation damage assessment was achieved in this phase. Improvement and unification of neutron dosimetry methods provided better data with less inherent scatter. All results together with their analyses and raw data were summarized in IAEA Technical Reports Series (TRS) No. 265 [2].

CRP Phase 3 included the direct measurement of fracture toughness using irradiated surveillance specimens. Optimising Reactor Pressure Vessel Surveillance Programmes and

their Analyses was the title for CRP Phase 3, and significant accomplishments were achieved concerning fracture toughness testing and structural integrity methods, correlations between various toughness and strength measures for irradiated materials, emphasis on the need to understand embrittlement mechanisms, and potential mitigative measures for radiation embrittlement. One key achievement was the acquisition and testing of a series of RPV steels designed and selected for radiation embrittlement research. One of these materials was given the code JRQ, and it has been shown to be an excellent correlation monitor (or standard reference) material as documented in IAEA-TECDOC-1230 [3]. The CRP Phase 3 results, together with their analysis and raw data, have been summarized in an IAEA working document, Optimising Reactor Pressure Vessel Surveillance Programmes and their Analyses, distributed only to the CRP Phase 3 participants.

The main emphasis during CRP Phase 4, which began in 1995, was the experimental verification of the Master Curve approach for surveillance size specimens. This CRP was titled Assuring Structural Integrity of Reactor Pressure Vessels, and was directed at confirmation of the measurement and interpretation of fracture toughness using the Master Curve method with structural integrity assessment of irradiated RPVs as the ultimate goal. The main conclusion from CRP Phase 4 was that the Master Curve approach demonstrated that small size specimens, such as precracked Charpy, can be used to determine valid values of fracture toughness in the transition temperature region. Application included a large test matrix using the JRQ steel and other national steels including WWER materials. No differences in laboratory results were identified and dynamic fracture toughness data also followed the Master Curve.

Guidelines were developed and additional Master Curve testing was performed under CRP Phase 5, which was titled Surveillance Programme Results Application to Reactor Pressure Vessel Integrity Assessment. This CRP had two main objectives: (i) develop a large database of fracture toughness data using the Master Curve methodology for both precracked Charpy size bend (PCC) and one-inch thick (25.4 mm) compact tension (1T-CT) specimens to assess possible specimen bias effects; (ii) develop international guidelines for measuring and applying Master Curve fracture toughness results for RPV integrity assessment.

Some key results from CRP Phase 5 can be summarized below:

- Clear evidence was obtained to show that lower values of unirradiated T_0 are obtained using PCC specimens as compared to results from 1T-CT specimens. This bias in test results is very important when considering use of PCC specimens in evaluating RPV integrity. These results have been documented in IAEA-TECDOC-1435 [4].
- The Master Curve application guidelines have been published in Technical Reports Series No. 429 [5]. The general methodology for the IAEA Guidelines can follow either a deterministic or a probabilistic path for assessing RPV structural integrity. The deterministic path is one that has been adopted by the ASME Code in the USA using the reference temperature RT_{T0} as an alternative to RT_{NDT} for indexing the ASME Code K_{IC} curve. The German approach is essentially identical. The ongoing reassessment of the USA PTS screening criteria in the USA uses a probabilistic approach employing RT_{T0}. Other application approaches can be used as identified in TRS No. 429.
- ASTM Standard Test Method E1921-02 [6] was the basis for the fracture toughness testing and determination of T_0 for the surveillance-type test samples. Adjustments to the measured value of T_0 may be necessary to account for differences in the RPV material as compared to the surveillance material (i.e. they may not exactly match) and neutron fluence (i.e. a functional relationship with fluence for interpolation or

extrapolation is generally necessary). It should be noted that a later version of ASTM E1921-05 is now available and should be used in future testing work.

- Limited test results from different loading rates have shown a difference in the measured T_0 values [3] even within the allowable range in ASTM E1921-02. These results have been reported to the ASTM Committee E08 for consideration in tightening the ASTM E1921 loading rate requirements. ASTM E1921-03 revised loading rate requirements for quasi-static loading. ASTM E1921-05 maintains this reduced loading rate range.

- The shape of the Master Curve is assumed to be constant, and the data generated from JRQ and other national materials supported this assumption. Relevance to highly embrittled materials was not tested with the data generated in this CRP.

It is reasonable to expect that future determination of plant operating limits will be based on Master Curve methods. Under current codes and regulations, there are no specific requirements for Master Curve testing in RPV surveillance programmes. However, the need to more accurately assess RPV fracture toughness will drive some utilities to use modified surveillance specimens to measure Master Curve fracture toughness, in addition to the traditional Charpy V-notch (CVN) testing. For the vast majority of nuclear RPVs, significant margins against fracture can be demonstrated using current CVN-based methods. However, for plants that project significant embrittlement concerns during current or extended operating life, supplemental Master Curve testing may prove to be a critical, viable option.

The Master Curve approach for assessing the fracture toughness of a sampled irradiated material has been gaining acceptance throughout the world. This direct measurement approach is preferred over the correlative and indirect methods used in the past to assess irradiated RPV integrity. These indirect and correlative methods have used Charpy V-notch transition temperature shift (usually defined at the 41 J temperature, T_{41J}) as the measure of radiation embrittlement. These methods, when combined with reference fracture toughness curves, such as the ASME Code K_{IC} and K_{Ia} (or K_{IR}) curves allow the determination of a lower bound linear elastic fracture toughness that has consistently been shown to be conservative relative to measurement of actual fracture toughness. This conservatism stems primarily from the approach used to determine the initial reference transition temperature, RT_{NDT}, which is used as the first index to the ASME Code curves before irradiation effects become important. On average, the shift in Charpy transition temperature shift (ΔT_{41J}) due to neutron irradiation is close to the transition temperature shift in fracture toughness (ΔT_0 from the Master Curve method); otherwise, the overall approach using initial RT_{NDT} plus ΔT_{41J} would not be conservative. However, there is large scatter in the relationship between these two shifts, and caution is needed when assessing equivalence.

1.2. OBJECTIVE OF THE CRP

In the final evaluation for the application of the Master Curve in CRP Phase 5, three key areas were identified as needing further work:

(1) test specimen size, geometry, and constraint relative to the measurement and application of Master Curve T_0 values;
(2) effects of loading rate and qualification impact loading conditions on T_0;
(3) potential changes in the shape of the Master Curve for highly embrittled RPV materials.

Note that these issues were identified as being critical before the Master Curve methodology could be accepted for licensing applications. These three areas are the focus of this new CRP,

which is termed CRP Phase 8. Note that two other CRPs (CRP-6 and CRP-7) were focused on other aspects of RPV integrity, primarily for WWER steels.

A key consideration for RPV integrity is the understanding of constraint and any bias differences between the sample specimen(s) being tested (generally of one fixed specimen and loading geometry) and the hypothetical flaw assumed to exist in the RPV. The VOCALIST project sponsored by the European Commission has been addressing this particular topic and their results may be useful in this CRP. Further analytical and experimental work is needed to better quantify the differences and their significance.

The effect of loading rate can initially be broken down into two distinct aspects: (i) the effect of loading rate on the determined Master Curve T_0 values for loading rates within the loading rate range specified in ASTM E1921 for quasi-static loading; (ii) the effect of loading rate on Master Curve T_0 values for higher loading rates including impact conditions using instrumented PCC specimens. Qualification of impact fracture toughness testing is an important aspect of this topic area. The new CRP includes both aspects, but primarily focuses on the second element of loading rate effects, i.e. dynamic impact loading rate ranges.

The third topic involves possible changes in the Master Curve shape for highly embrittled materials and/or materials showing an intergranular fracture (IGF) mode. This task is crucial since the general shape of the Master Curve is considered to be invariant for most realistic irradiation conditions. If the Master Curve does change shape, the conditions and extent of deviation need to be defined.

A list of the participants involved in the various topic areas is provided in Table 1.1.

TABLE 1.1. PARTICIPANTS INVOLVED IN THE THREE TOPIC AREAS

| Country/Laboratory | Code | Topic area 1 | | Topic area 2 | | Topic area 3 |
		Exp. data	Analytical	RR	Exp. data	Exp. data
Belgium – SCK•CEN	BEL	✓	✓	✓	✓	✓
Czech Republic – NRI	NRI	✓		✓		✓
Finland – VTT	FIN	✓			✓	✓
Germany – FZD	FZD	✓	✓	✓	✓	✓
Hungary – AEKI	HUN	✓	✓	✓		✓
Japan – CRIEPI	CRI	✓	✓	✓	✓	
Japan – JAEA	JAE	✓	✓	✓	✓	✓
Rep. of Korea – KAERI	KOR	✓	✓	✓	✓	✓
Mexico – ININ	MEX	✓	✓		✓	
EU – JRC-IE	JRC	✓	✓	✓	✓	
Russian Federation – RRC-KI	RUS	✓			✓	✓
Spain – CIEMAT	ESP	✓	✓	✓	✓	
US Industry (ATI/W/EPRI)	USE	✓		✓	✓	✓
USA – ORNL	USO	✓	✓	✓	✓	✓

1.3. STRUCTURE AND APPLICATION

This report first reviews the identified topic areas in more detail and then provides the most relevant new test data or other collected data that provides better understanding and definition of Master Curve application limits. The key results from these topics are summarized at the end along with recommendations for future work relative to realistic component integrity assessment.

The results from the studies described in this report are applicable to utility engineers and scientists who are involved in the direct measurement of fracture toughness using small surveillance size specimens and application of the results using the Master Curve approach for RPV structural integrity assessment. This direct measurement approach has obvious advantages over the indirect methods used in the past for assessing radiation embrittlement effects. The Master Curve methodology is currently being applied in the ASME Boiler and Pressure Vessel Code (Sections III and XI), ASTM Standards, USNRC Regulations, German Regulations (KTA 3203), IAEA PTS Guidelines for WWER reactors, as well as the VERLIFE procedure, Unified Procedure for WWER Component Lifetime Assessment, and other industry guidance documents governing RPV integrity analysis.

1.4. REFERENCES

[1]   INTERNATIONAL ATOMIC ENERGY AGENCY, Co-ordinated Research Programme on Irradiation Embrittlement of Pressure Vessel Steels, IAEA-TECDOC-176, IAEA, Vienna (1975).
[2]   INTERNATIONAL ATOMIC ENERGY AGENCY, Analysis of the Behaviour of Advanced Reactor Pressure Vessel Steels under Neutron Irradiation, IAEA Technical Reports Series No. 265, IAEA, Vienna (1986).
[3]   INTERNATIONAL ATOMIC ENERGY AGENCY, Reference Manual on the IAEA JRQ Correlation Monitor Steel for Irradiation Damage Studies, IAEA-TECDOC-1230, IAEA, Vienna (2001).
[4]   INTERNATIONAL ATOMIC ENERGY AGENCY, Application of Surveillance Programme Results to Reactor Pressure Vessel Integrity Assessment, IAEA-TECDOC-1435, IAEA, Vienna (2005).
[5]   INTERNATIONAL ATOMIC ENERGY AGENCY, Guidelines for Application of the Master Curve Approach to Reactor Pressure Vessel Integrity in Nuclear Power Plants, IAEA Technical Reports Series No. 429, IAEA, Vienna (2005).
[6]   AMERICAN SOCIETY FOR TESTING AND MATERIALS, ASTM E 1921, Test Method for the Determination of Reference Temperature, T_0, for Ferritic Steels in the Transition Range, Annual Book of ASTM Standards, ASTM International, West Conshohocken (2002).

2. TOPIC AREAS

2.1. SPECIMEN SIZE, GEOMETRY, AND CONSTRAINT

The focus for this topic was on test specimen size and loading geometries to assess differences (often referred to as biases) between specimen types, specimen geometries, or specimen size. The fundamental reason for these biases results from the basic K_{Jc} fracture toughness parameter not uniquely characterizing the stress-strain field ahead of the crack tip under certain conditions. In these cases, the terminology of loss of constraint is used. The ultimate goal is to have an interrelationship between all typical specimen geometries and eventual application to a part-through flaw in an RPV. This topic area is critical for realistic structural integrity assessments, since most assessments use irradiated fracture toughness properties and application methods that are generally very conservative.

There were two portions relative to this topic area:

- experimental;
- analytical.

The analytical portion dealt with the use of finite element analyses and their qualification for assessing differences in constraint for two selected geometries. Round robin exercises were conducted to assess the use of different finite element codes at different institutes relative to assessing crack tip constraint conditions.

The experimental portion involved both mandatory and non-mandatory contributions. The mandatory portion involved tests or data on materials to be selected by each of the participants. Each participant was to select at least two of the following geometries for testing and/or assessment:

- single edge bend specimen [SE(B)] with specimen width to thickness equal to 1 [W/B = 1], which is referred to in this report as a precracked Charpy (PCC) specimen;
- SE(B) with W/B = 2;
- compact tension specimen [C(T)] with W/B = 2.

It was recommended that the same value of thickness (B) be used for the two specimen types selected. New material testing was not required, since previously obtained data could be supplied provided that appropriate data meeting different geometries or constraint conditions are available.

The non-mandatory portion involved additional testing on more or different specimen geometries. Study of the effects of shallow crack and deep crack specimens was also encouraged. Testing on a broader range of ferritic materials and conditions also was encouraged to cover more than just RPV steels. Other yield strengths and embrittlement processes were to be included (irradiation and thermally aged) where possible. Study of the relationship of specimen constraint to loading conditions in actual components with assumed or real flaws was also encouraged.

Specimen size, geometry, and constraint are further discussed in Section 3 of this report.

2.2. LOADING RATE EFFECTS AND QUALIFICATION OF IMPACT FRACTURE TOUGHNESS TESTING

Three specific loading rate ranges were identified for this study:

- quasi-static in the range of allowable loading rates within ASTM E1921-05;
- dynamic loading (intermediate rate between quasi-static and impact);
- impact using PCC specimen testing which requires test procedures for performing instrumented PCC testing and data analysis since none currently exist in standardized form.

This topic area has limited direct application since the loading rates in any actual RPV operating or accident conditions are not dynamic. However, knowledge of the loading rate dependence of T_0 can be used to adjust data generated at rates in the dynamic range to those needed for actual integrity assessment conditions. Additionally, many of the plant operating heat-up and cool-down curves were based on use of a reference fracture toughness curve (such as the ASME Code K_{IR} curve) which had a basis of a combination of crack arrest and dynamic fracture toughness. Even though a quasi-static K_{IC} reference fracture toughness curve is now more commonly used for normal operation and upset conditions, there are still areas where the K_{IR}-type curve is still needed.

Two such cases are:

- For extreme safety events such as pressurized thermal shock in which arrest may be important for assuring safety.
- For assessment of detected defects in the RPV embrittled zone. Thus, there appears a relationship between impact fracture toughness and crack arrest fracture toughness that could allow further use of impact fracture toughness test data.

The mandatory portion of this topic area required participation in a round robin exercise to validate the instrumented PCC testing and analysis procedures for impact loading using supplied specimens of JRQ material (10 tests per laboratory).

The non-mandatory portion suggested testing of additional ferritic steels. Other technical areas that potentially could be assessed from the data provided included:

- comparison of results from unloading compliance and monotonic loading in the quasi-static range;
- evaluation of the need for side grooves for PCC specimens;
- establishing a relationship between instrumented PCC test results and measured fracture toughness and T_0;
- evaluating methods for estimating K_{Ia} from instrumented PCC and instrumented Charpy V-notch (CVN) results;
- evaluating the effect of irradiation and/or yield strength changes on relationship of static and dynamic fracture toughness.

Loading rate effects and qualification of impact fracture toughness testing are further discussed in Section 4 of this report.

2.3. MASTER CURVE SHAPE

The overall scope of this topic area was to:

- Assess limits of applicability for Master Curve application at the upper range of the transition region in the standard Master Curve form.
- Determine the effects of heterogeneity (material and environment conditions).
- Evaluate the importance of fracture mode change on the Master Curve shape (i.e. upper shelf ductile and/or IGF modes).

Participation involved either data collection and/or new testing to assess potential Master Curve shape changes in highly embrittled materials (irradiated, thermally aged, or some other condition that induced IGF or other embrittlement). The data collected and generated was encouraged as much as possible relative to age and type of testing method. Temperature and the selected materials and conditions were selected to challenge the limits of a constant Master Curve shape.

Master Curve shape is further discussed in Section 5 of this report.

3. SPECIMEN SIZE, GEOMETRY, AND CONSTRAINT

3.1. BACKGROUND

The precracked Charpy V-notch (PCVN) and smaller specimens are identified as a critical issue for RPV integrity assessments due to the important link to RPV surveillance programmes. That specimen is the one most likely to be used because it is relevant to use of CVN surveillance specimens that may be reconstituted, precracked, and then tested as a PCVN specimen. In the United States of America, the NRC has applied an added factor of 4.5ºC to T_0 results based on PCVN specimen testing; however, the basis for that bias factor in T_0 for the PCVN specimen was based on a relatively small amount of information.

The observed differences in T_0 between results from PCVN specimens and compact specimens vary widely. Commonly, and for this report, the 1T compact specimen [1TC(T)] is defined as the reference specimen for comparisons of T_0 differences. Thus, references to a bias for the T_0 from a different type or size of fracture toughness specimen means the difference between the measured T_0 for that specimen relative to that measured with the 1TC(T) specimen. For a database of over 200 PCVN specimens and 35 1TC(T) specimens for HSSI Weld 72W, the T_0 based on PCVN tests was 21ºC lower than that based on the 1TC(T) specimens [1].

For the IAEA CRP-5 Surveillance Programme Results Application to Reactor Pressure Vessel Integrity Assessment, more than 300 PCVN and 1TC(T) specimens of A533B-1 steel (heat JRQ) were tested by different organizations and the T_0 based on the PCVN specimens was 12ºC lower than from the 1TC(T) specimens. Moreover, in the same CRP study, many other RPV steels were tested and showed differences from 12 to 45ºC (average of 22ºC), with the 3-point bend specimens giving the lower T_0 value in every case.

Questions regarding constraint limits for the MC method in general, and the PCVN specimen in particular, especially as a consequence of irradiation, must be resolved. The potential use of even smaller specimens highlights the significance of this issue, as evaluation of specimen size effects are needed to fully understand limits of applicability and associated uncertainties.

There are many potential reasons for the above observed differences in T_0. The primary focus is generally on different levels of constraint for the different specimen types. Differences in constraint for quasi-static loading rates are related to specimen geometry, size effects, and the relationship of crack length to specimen width. The thickness and ligament dimensions, for example, $W/B = 1$ and $W/B = 2$, are often identified. Other aspects are the potential effects of side-grooving and non-conservative limits on specimen size for K_{Jc} measuring capacity.

The American Society for Testing and Materials (ASTM) Standard Practice E1921 [2] specifies a relationship between specimen dimensions and measured fracture toughness to ensure that the measured K_{Jc} is not significantly affected by loss of constraint:

$$M_{lim} > b\sigma_{ys}E/K^2_{Jc}(1-\nu^2) \tag{3.1}$$

where b is the specimen remaining ligament, σ_{ys} is the material yield strength, E is Young's modulus, K_{Jc} is the measured cleavage fracture toughness, and ν is Poisson's ratio. The M_{lim} specified in E1921 is 30 and is the same for compact and three-point bend specimens.

Various analytical studies have concluded the need for M_{lim} values from 30 to 200, with the compact specimen geometry requiring a lower M_{lim} than that for the three-point bend

specimen. Moreover, numerous experimental studies generally tend to indicate the need for lower M_{lim} values than the numerical studies, but they also show disparate results.

A major focus of many analytical studies is the elastic crack tip T-stress. Gao and Dodds [3, 4] have proposed that the T-stress effects on constraint can account for the observed differences in T_0 for different specimen geometries. The T-stress is expressed as:

$$T = \beta K / \pi \pi a \qquad (3.2)$$

where β is a geometry dependent parameter. This parameter is generally evaluated computationally. As pointed out by Joyce and Tregoning [5], calculations of T-stress indicate that a C(T) specimen with a/W = 0.55–0.6 should give the same T-stress as for an SE(B) with a/W = 0.7–0.78. However, experiments by Joyce and Tregoning still show differences in T_0 with those a/W values. It seems to be an issue as to how well we know and understand the applicability of T-stress for various geometries. It is problematic that, for K_{Jc} measurements of RPV steels, the differences in constraint are considered to be relatively small compared with material variability and for typical sample sizes.

Other aspects involve testing techniques, for example, the measurement of specimen displacements needed to calculate the J-integral value at the onset of cleavage fracture. Experiments variously measure the crack-mouth opening displacement which is then converted to load-line displacement for J calculation, or the load-line displacement is measured directly.

However, there are different techniques used for load-line displacement in terms of where on the specimen they are made. Other factors to be considered are material factors such as strain hardening, and the J-integral formulations themselves. For example, various numerical studies show relatively wide differences in values of 0_p. It seems appropriate to question whether the existing J-formulations for C(T) and SE(B) specimens are correct.

Thus, this topic area was organized in two parts, an experimental part and an analytical part with a view towards each part complementing the other. The following sections describe the requirements for participation in the topic and discussions of both parts. For the experimental part, a list of participants, summary of the test matrix resulting from participant contributions, the test procedures and conditions, the materials to be tested, the results of the experiments, and discussion of the results are presented in Sections 3.1 through 3.3. For the analytical part, a list of participants, a description of the round robin analytical exercise, and discussion of results are presented in Sections 3.4 through 3.6. Finally, Section 3.7 of this section presents a summary of the results comparisons with results in the literature and, where appropriate, to results from previous IAEA CRPs.

3.2. TESTING PROCEDURES AND CONDITIONS

3.2.1. Description of requirements for participation

The formulation for this topic included both mandatory and non-mandatory parts. The focus of the mandatory portion is on specimen geometries to assess the potential bias between specimen types. It was specified that each participant provide MC test data on at least two of the following specimen types:

SE(B)   W/B = 1
SE(B)   W/B = 2

C(T)   W/B = 2

SE(T)   No W/B specified

It was recommended to use the same value of B (thickness) for the two selected geometries. It was also stated that new material testing was not required and that previously obtained data can be submitted with all CRP appropriate information.

The non-mandatory portion recommended additional materials, specimen geometries, and analyses be investigated. For example:

- Significant differences in constraint can be achieved with very shallow flaws, a/W = 0.1 compared with deep flaws, a/W = 0.5.
- Materials with different yield strengths and strain hardening.
- Comparison of data for an RPV steel in unirradiated and irradiated cases.
- Thermally aged materials.
- Evaluation of constraint in specimens with through-thickness cracks and comparison with flaw geometries in real components, such as a cylinder with a surface flaw.

For the new testing performed within this CRP, testing was conducted in accordance with ASTM E1921-05 [6] (except for the SE(T)) specimen that is not included in E1921 [2] and for which the CRP provided detailed information on the appropriate equations and methodology to be used. For the new testing, specific guidance was provided to participants to enhance the opportunity for evaluation of the effects of specimen geometry on T_0 differences. For example:

- Test temperatures should be chosen to produce valid data and not too far from T_0. For example, PCVN specimens should be tested at about T_0-20°C.
- Multiple temperature testing is allowed.
- The minimum number of test specimens recommended is 8 for any one condition, but participants were encouraged to test as many specimens as possible to enhance the opportunity for reduced statistical uncertainty.
- The same value of specimen thickness (B) was recommended for the different geometries.

Summary of experimental test matrix is shown in Table 3.1.

3.2.2. Information to be reported

A data reporting spreadsheet in Excel was developed and provided to each participant. The spreadsheet includes the source of data, the specimen type, specimen thickness, width, and crack depth, test temperatures, loading rate, standard deviation, and version of ASTM E1921 used. Data were reported from new tests performed during this CRP as well as from previously tested specimens.

3.3. CONTRIBUTIONS FOR EXPERIMENTAL PART

3.3.1. Experimental matrix

A summary of the test matrix resulting from participant contributions in the experimental part of Topic 1 are shown in Table 3.1, which shows the number of datasets for different materials by specimen type and geometry. As shown in the Table 3.1, a special focus was on the JRQ

steel because 8 participants tested to construct a larger database on one heat of steel for statistical evaluation.

3.3.2. Materials

For this topic, no specific material was required to be used by all participants. However, as shown in Table 3.1, the IAEA reference heat of A533, grade B, class 1 steel, designation JRQ, was selected by eight of the participants for testing. A detailed description of that material is available in Ref. [7]. Another relatively large dataset was made available for HSST Plate 13B, a plate of A533 grade B class 1 steel. Other materials include prototypic plates, forgings, and welds for PWRs, WWERs, and other ferritic materials for non-nuclear applications.

Large amounts of data on these various steels, ranging from 0.16T SE(B) to 1T SE(B) and 0.2C(T) to 1TC(T) specimens, with a/W values from 0.1 to 0.8, have been provided by the participants. The two large datasets, HSST Plate 13B and JRQ steel, provide opportunities for more extensive analysis to identify potential trends in effects of the various parameters of interest, e.g. specimen type, thickness, remaining ligament, and crack length-to-width ratio (a/W). Results from the other datasets provide the opportunity to compare results from smaller datasets with those from the larger datasets.

In addition to evaluation of the data, various constraint adjustments have been performed to evaluate their success in reducing the observed biases.

TABLE 3.1. SUMMARY OF EXPERIMENTAL TEST MATRIX

	SE(B) W/B=1	SE(B) W/B=2	C(T)	SE(T)/ Other	Steel
JRQ	10	7	11	1	8
Other Steels	3	4	7	1	6
All Steels	13	11	18	2	14
PCC-JRQ	10	5			
PCC-Others	3	3			
PCC-All	13	8	0	0	
.5T-JRQ	2	1			
.5T-Others	0	0			
.5T-All	2	1	0	0	
1T	1	1			
.2T-JRQ	1	0			
.8T-JRQ		1			
Multiple a/W-JRQ	3	1			
Multiple a/W-Others	2	2			
Multiple a/W-All	5	3			
.4T-JRQ			4		
.4T-Others			2		
.4T-All			6		
.5T-JRQ			3		
.5T-Others			1		
.5T-All			4		
1T-JRQ			4		
1T-Others			2		
1T-All			6		
2T-Others			1		
4T-Others			1		

Results of experimental part

Table 3.2 shows a summary of the test matrix for Plate 13B. Most of the tests were performed by USA organizations, with tests of PCVN (a/W = 0.5) and 0.4TSE(B) (a/W = 0.3, 0.65 and 0.75) performed by USI. As seen in the table, 29 1TC(T) specimens were tested to provide a good statistical basis for the reference T0. For the PCVN case, a total of 73 specimens with a/W = 0.5 were tested, including 20 specimens with side-grooves to investigate the effect of side-grooving. For other three-point bend specimens, variations in the width to thickness ratio (W/B), thickness, and a/W were investigated with at least the number of specimens recommended in ASTM E1921, but with much larger numbers in many cases. Finally, 0.4TC(T) specimens were also tested, including a set with very deep cracks (a/W = 0.8) to provide a remaining ligament (b = W-a) similar to that of a PCVN specimen with a crack of a/W = 0.5.

TABLE 3.2. TEST MATRIX FOR HSST PLATE 13B

Specimen type	Number of specimens				
	-120EC	-100EC	-85EC	-60EC	-36EC

0.4TSE(B) W/B = 1
  a/W = 0.5
  a/W = 0.3
  W/B = 2
  a/W = 0.3
  a/W = 0.5
  a/W = 0.65
  a/W = 0.75
	15 + 8* + 10SG
	20
	
	8*
		15 + 10SG
		
		8*
		7*
			15
			
			20		

1TSE(B)
  W/B = 1
  a/W = 0.5
  W/B = 2
  a/W = 0.5
				20
				
				17	

0.4TC(T)
  a/W = 0.5
  a/W = 0.8
	
	10
			18
			10		

1TC(T) a/W = 0.5			6	17	6

*Tests performed by US organizations

Figure 3.1 shows a plot of the 1TC(T) data and the master curve giving a T_0 of -69.1°C, where the tests at -60°C only gave a T_0 of -72.9°C. Figure 3.2 shows a plot of the PCVN data (a/W = 0.5) from USO and the master curve giving a T_0 of -106°C. Thus, the PCVN specimens for this material give a T_0 that is 37°C lower than that of the 1TC(T) specimens, a bias of -37°C. The USI tests of HSST Plate 13B with eight PCVN specimens (a/W = 0.5) resulted in a T_0 of -103°C, a result very close to that from the 65 tests by USO, providing an independent validation of this observed large bias result. A summary of all the test results for this material is provided in Table 3.3, which shows for each specimen type the number of specimens tested, the number of valid tests (by E1921), the T_0 result and two standard deviations on T_0. Figure 3.3 graphically depicts the effects of specimen type and geometry for

HSST Plate 13B, demonstrating a decreasing T_0 with decreasing specimen thickness and ligament, as well as crack depth for one PCVN case with an a/W = 0.3.
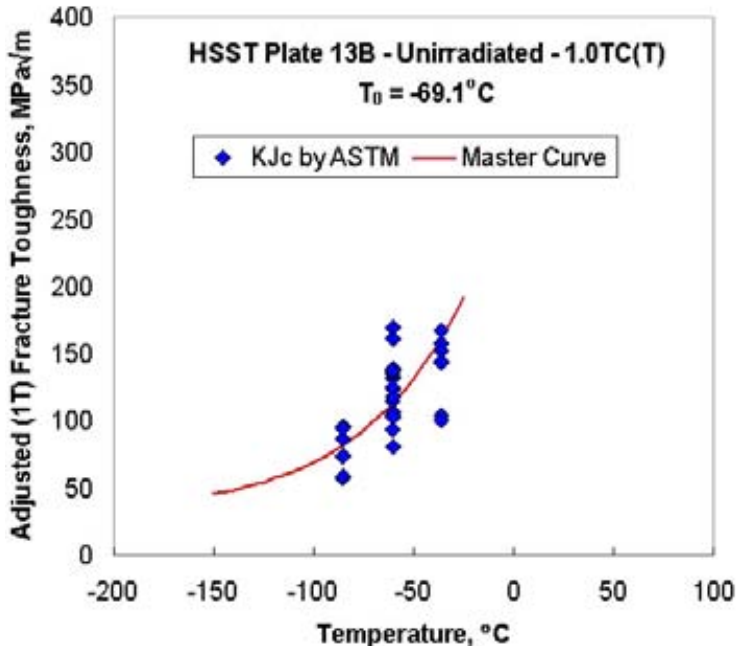
FIG. 3.1. Fracture toughness, K_{Jc}, results for 1TC(T) specimens of HSST Plate 13B showing master curve and T_0 of -69.1 ℃.
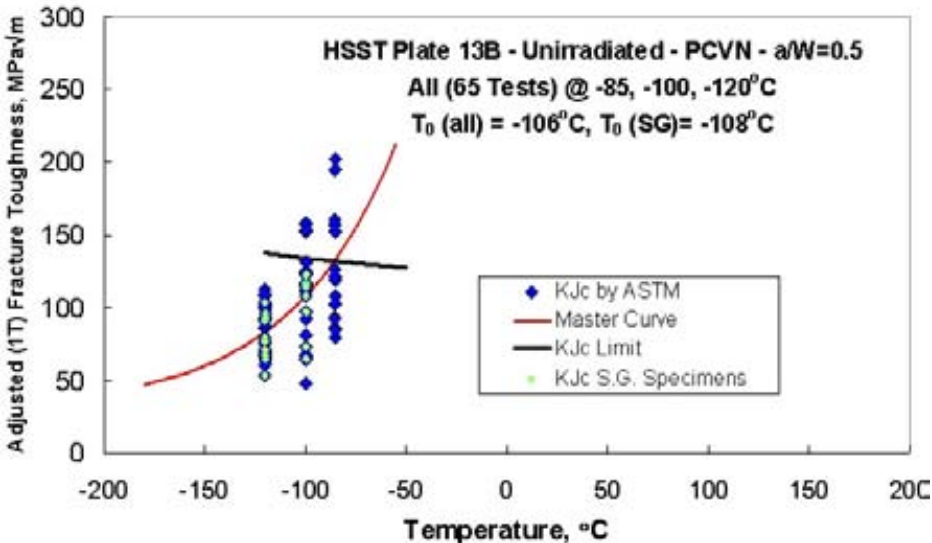
FIG. 3.2. Fracture toughness, K_{Jc} adjusted to 1T size, for PCVN specimens of HSST Plate 13B showing master curve and T_0 of -106 ℃. The side-grooved specimens are included in the overall analysis.

14
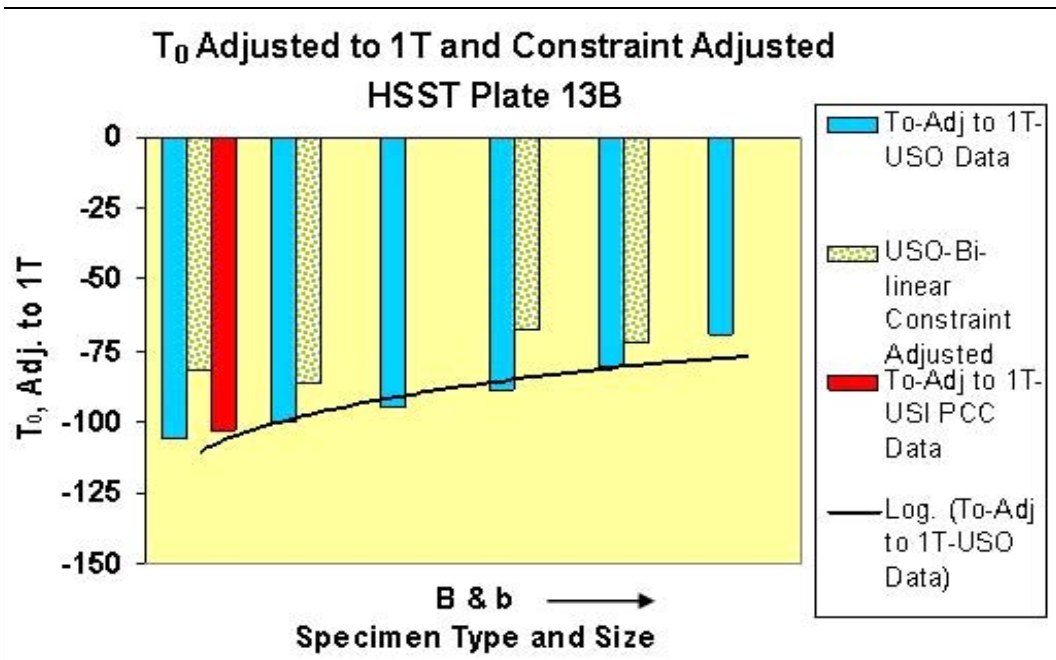
FIG. 3.3. Bar chart of T_0 for HSST Plate 13B showing a tendency for decreasing T_0 with decreasing specimen size (B and/or b) and crack depth.

TABLE 3.3. SUMMARY OF FRACTURE TOUGHNESS TEST RESULTS FOR HSST PLATE 13B

Specimen type	No. of test temps	No. of tested specimens N r		T_0, °C, 2σ	
1T C(T)	3	29	29	-69	6.7
1T SEB × 2B	1	17	17	-81	8.7
0.4TSEB × 2B (a/W = 0.3)	1	8	8	-87	
0.4TSEB × 2B (a/W = 0.65)	1	8	8	-100	
0.4TSEB × 2B (a/W = 0.75)	1	7	6	-90	
1T SEB × B	1	20	18	-89	8.2
0.4T C(T)	1	23	23	-95	7.5
0.4T SEB × 2B	1	20	17	-100	8.7
PCVN (a/W = 0.5)	3	65	41	-106	5.6
PCVN (a/W = 0.5)	1	8	8		
PCVN (a/W = 0.3)	1	19	16	-120	9.0

Figure 3.3 also shows bars representing an adjustment to T_0 using the Wasiluk, Petti, Dodds constraint adjustment scheme [8]. The following two equations are used to adjust the T_0 obtained from three-point bend specimens to that of a 1TC(T) specimen, the reference specimen geometry.

$$\text{SE(B), B} \times \text{2B: K-SE(B)/K-C(T)} = 1.10 + 0.00053 \, [175 - \text{M-SE(B)}] \qquad (3.3)$$

$$\text{SE(B), B} \times \text{B: K-SE(B)/K-C(T)} = 1.19 + 0.00180 \, [120 - \text{M-SE(B)}] \qquad (3.4)$$

where K-SE(B) is measured K_{Jc} for the bend specimen, K-C(T) is K_{Jc} for the 1TC(T) specimen, and M is the constraint parameter given in Equation 3.1. Table 3.4 shows the numerical results of those constraint corrections for Plate 13B. Note that the corrections apply only to a nominal deep cracked specimen (i.e. a/W ~ 0.5) and only to the bend specimens. The table shows the measured T_0, the adjusted T_0, and the number of valid specimens obtained for the as-measured case (N) as well as for the adjusted case (r). For the PCC specimens, the number of valid results increased from 47 in the as-measured case to 57 for the constraint adjusted case. Application of the Wasiluk, Petti, Dodds constraint correction changed the bias for the PCC specimen from -37°C to -13°C.

The Wasiluk, Petti, Dodds scheme provides an engineering approximation of a more fundamental stress-strain analysis which is dependent on the use of a finite element analysis of the specimen geometry. This procedure, discussed in Section 3.5.10 for the analytical portion of Topic area 1, was also used to perform a constraint adjustment of the PCC results for Plate 13B. The original model integrates over the plastic volume, whereas the Petti-Dodds model (referenced in Section 3.5.10) integrates over the volume for which σ_1 is greater than 2 times σ_y, where σ_1 is the maximum principal stress. Although a comparison of the two models has not been made here, it is believed the results should be similar. The result of that procedure is a constraint adjusted T_0 of -80.4°C, compared with the T_0 for the 1TC(T) specimen of -69°C, leaving a bias of about -11°C. Thus, this more complicated procedure, which requires a finite element analysis, results in a bias for the PCC specimens of Plate 13B similar to the Wasiluk, Petti, Dodds result of -13°C. Note that it is generally thought that this correction scheme tends to over correct the data for loss of constraint because the formulation does not account for the effect of plastic strain on the cleavage mechanism; however, it seems that an over-correction did not occur in this case.

With respect to adjustments for crack depth, Wallin developed a procedure for adjusting the T_0 for a deep cracked specimen to a shallow cracked specimen [9]. Table 3.5 shows the result obtained following adjustment of the deep cracked PCC specimen of Plate 13B to that of a specimen with a crack depth of a/W = 0.3. The adjustment in this case only decreased the T_0 for the deep cracked specimen by 2°C from the deep cracked value of -106°C to -108°C. This compares with the USO measured value of -120°C for a/W = 0.3.

Results for Plate JRQ from various participants tend to reflect similar trends as those just presented for Plate 13B. Some of the results are shown graphically in Figure 3.4. In most cases, the T_0 value increases with increasing thickness and/or remaining ligament similar to that shown for HSST Plate 13B. One notable example with an opposite result is shown in Figure 3.4 (e) where the PCC specimen results gave the highest T_0 value. A plot of the combined results in a manner similar to that shown for Plate 13B resulted in a similar trend, but exhibited significant scatter demonstrated by the different organizational results.

TABLE 3.4. RESULTS OF CONSTRAINT ADJUSTMENTS FOR TEST RESULTS FOR HSST PLATE 13B

Specimen type	No. of tested specimens, measured (Adj.)		T_0, ^{o}C		Adj. ΔT_0 ^{o}C
	N	r	Meas.	Adj.	
1TC(T) Ref. specimen	29	29	-69	-69	N.A.
1TSE(B) × 2B	17 (17)	17 (17)	-81	-72	9
1TSE(B) × B	20 (20)	18 (20)	-89	-68	21
0.4TC(T)	23	23	-95	N.A.	N.A.
0.4TSE(B) × 2B	20 (20)	17 (20)	-100	-87	13
PCC (a/W = 0.5)	65 (65)	41 (57)	-106	-82	24
PCC (a/W = 0.3)	19	16	-120	-	-

TABLE 3.5. RESULTS OF DEEP TO SHALLOW FLAW ADJUSTMENT FOR PCC SPECIMEN OF HSST PLATE 13B

Specimen type	No. of tested specimens, measured (Adj.)		T_0, ^{o}C		ΔT_0, °C
	N	r	Initial	Adj	
Measured PCC	65	41	-106	-108	-2
Constraint adjusted PCC	65	57	-82	-84	-2
PCC (a/W = 0.3)	19	16	-120	-	-

Figures 3.5 (a) and (b) show examples of results obtained from tests of PCC specimens with varying crack depths (a/W ratios). The plots show the expected decrease in T_0 with decreasing crack depth, reflective of the increase in apparent fracture toughness of specimens with shallow cracks. The difference in T_0 from a/W = 0.1 to 0.5 for the two different JRQ blocks is substantial, but cannot necessarily be attributed to variability between the two blocks as lab-to-lab variability is a confounding factor. Figure 3.5 (a) combines the data shown in Figures 3.5 (a) and (b) with a logarithmic curve fit chosen to represent the effect of increasing a/W. That fit indicates a T_0 value of -120°C at a/W = 0.1 and -63°C at a/W = 0.5. That fit appears to be dominated by the data from Figure 3.5 (a), but the curve fit to the data in Figure 3.5 (b) indicates a difference of about 50°C over the same range of a/W.

A similar effect with PCC specimen tests was observed for HSSI Plate 13B tested by USO and USI as shown in Figure 3.6. On the other hand, tests of 0.4TSE(B) specimens of the same material by both USO and USI with 0.4TSE(B) specimens with B × 2B geometry showed disparate results, as shown in Figure 3.7, as the specimens with a/W = 0.3 gave the highest

value of T_0. This result is likely reflective of various observations that conclude an a/W value of 0.3 does not truly represent a shallow flaw, but is close enough such that the scatter in results, depending on the specific material, is very high.

(a)

(b)

(c)

(d)
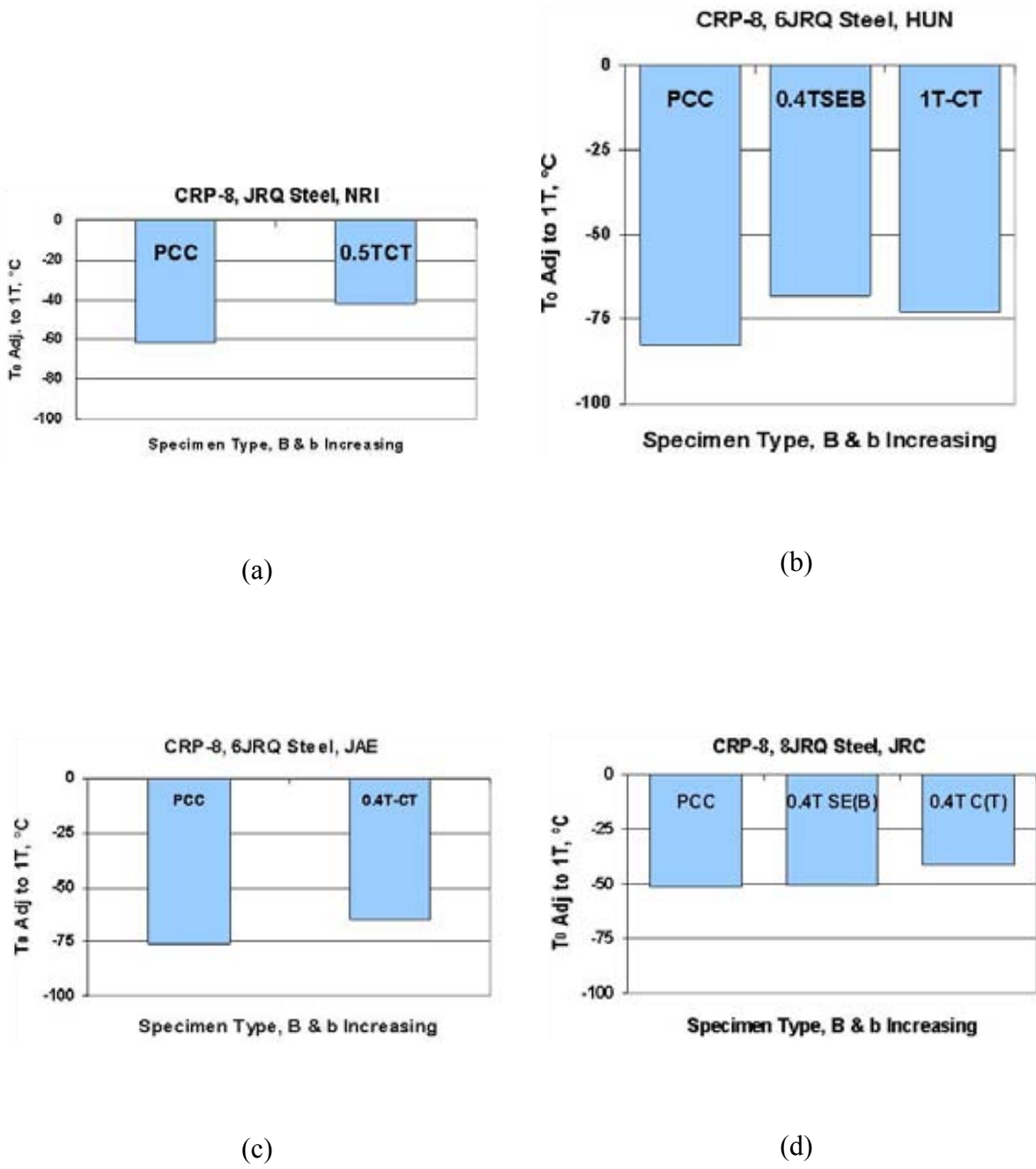
FIG. 3.4. Bar charts (a) through (d) showing T_0 results for Plate JRQ measured by different laboratories.
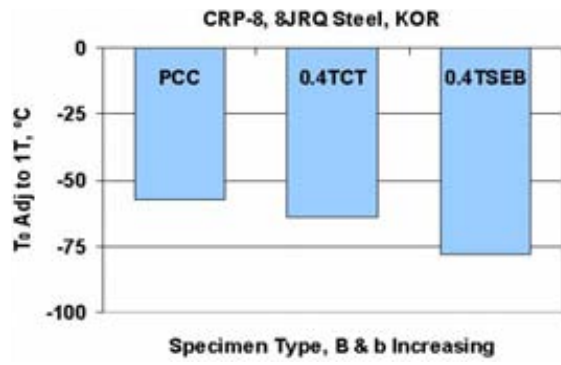
(e)
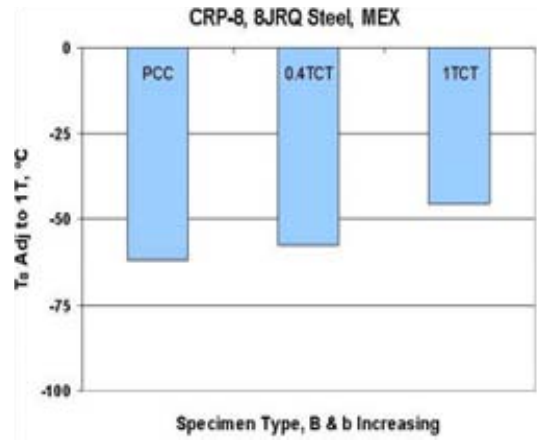
(f)
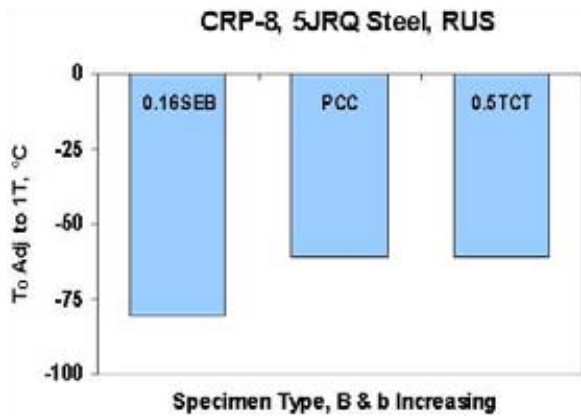
(g)
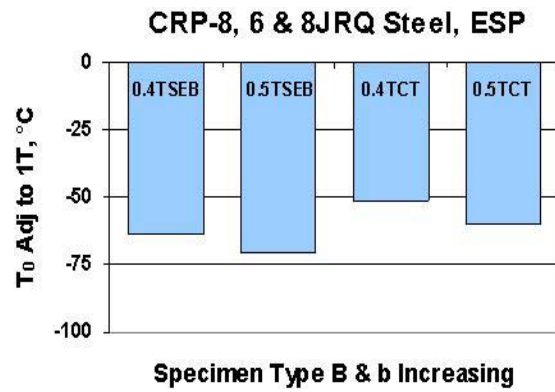
(h)

FIG. 3.4. (cont.) Bar charts (e) through (g) showing T_0 results for Plate JRQ measured by different laboratories.

CRP-8, 6JRQ Steel, HUN
PCC, T_0 vs a/W

(a)

CRP-8, 8 JRQ Steel, JRC & KOR
PCC, T_0 vs a/W

(b)

CRP-8, 6 & 8JRQ Steel, HUN, JRC, & KOR
PCC, T_0 vs a/W
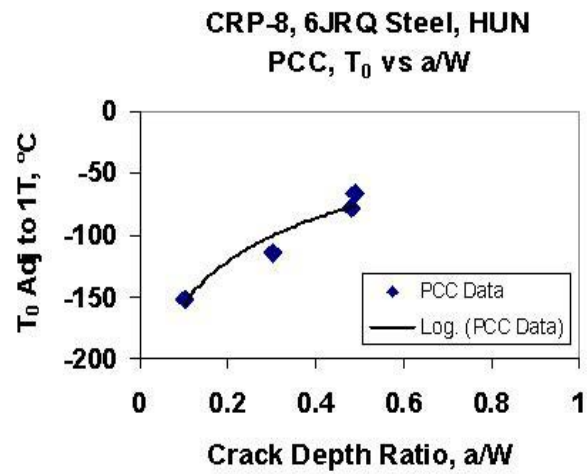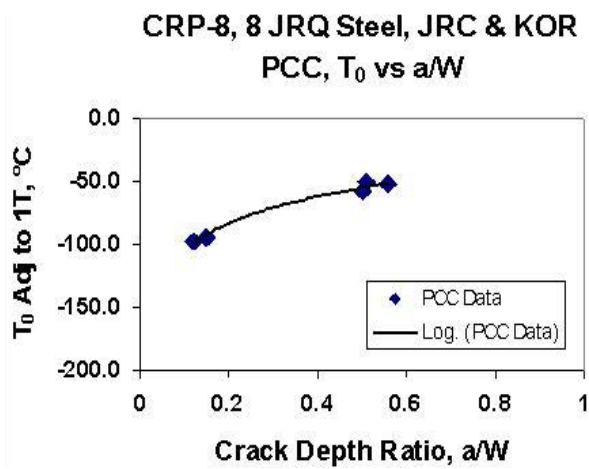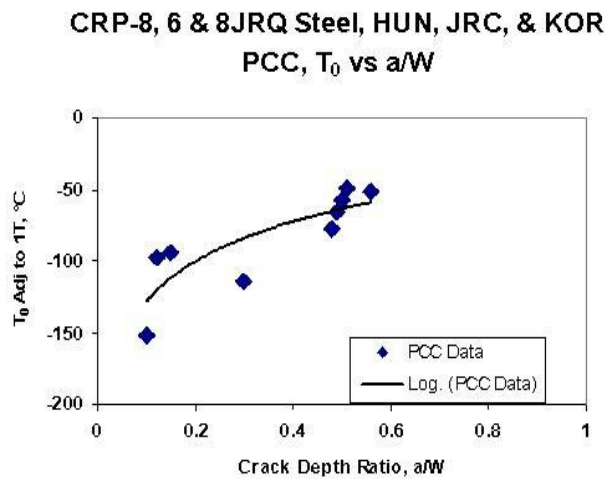
(c)

FIG. 3.5. Plots (a) through (c) of T_0 vs. crack depth (a/W) for JRQ steel from blocks 6JRQ and 8JRQ.

T₀ Adjusted to 1T for PCC Specimen, Vary a/W
HSST Plate 13B
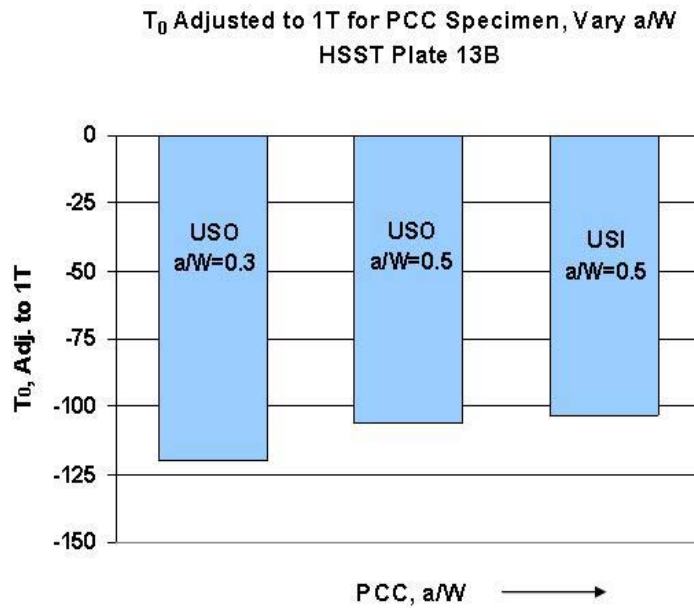
FIG. 3.6. Bar chart showing T_0 results for PCC tests of HSST Plate 13B with a/W ratios of 0.3 and 0.5, and for tests by USO and USI. As shown, the shallower crack result is almost 20°C lower than that for the deep crack result.

CRP-8, SEB (Bx2B) vs a/W
HSST Plate 13B
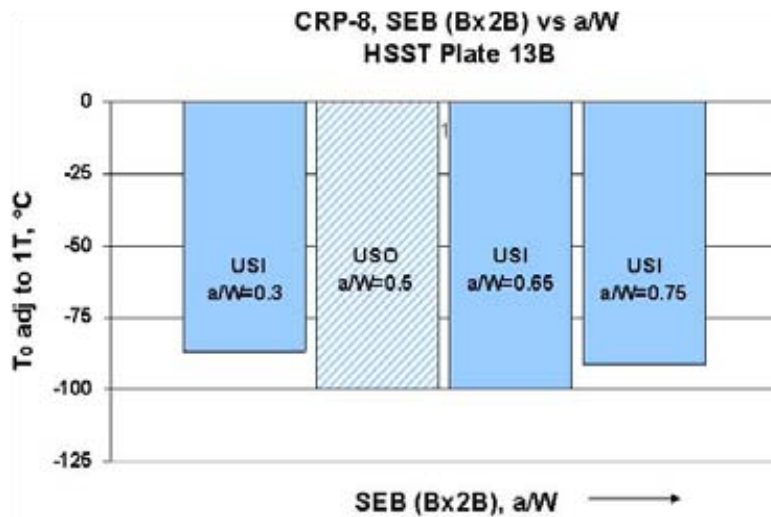
FIG. 3.7. Bar chart showing T_0 results for 0.4TSE(B) specimens of HSST Plate 13B with a/W ratios from 0.3 to 0.75, and for tests by USO and USI. The data for this geometry are disparate in that the T_0 value (-87°C) for the shallowest crack case is the highest of all the results.

Figure 3.8 shows a summary of the data for JRQ in terms of the PCC bias versus compact tension specimen size (xT), where x is in inches, e.g. 1T is one inch thick as in the usual format. As the figure shows, there is a substantial amount of scatter, with the average T_0 for

the PCC specimen being 11°C lower than that for compact specimens ranging from 0.4 to 1.0T. This value is similar to the average value of 12°C for JRQ from IAEA CRP-5.
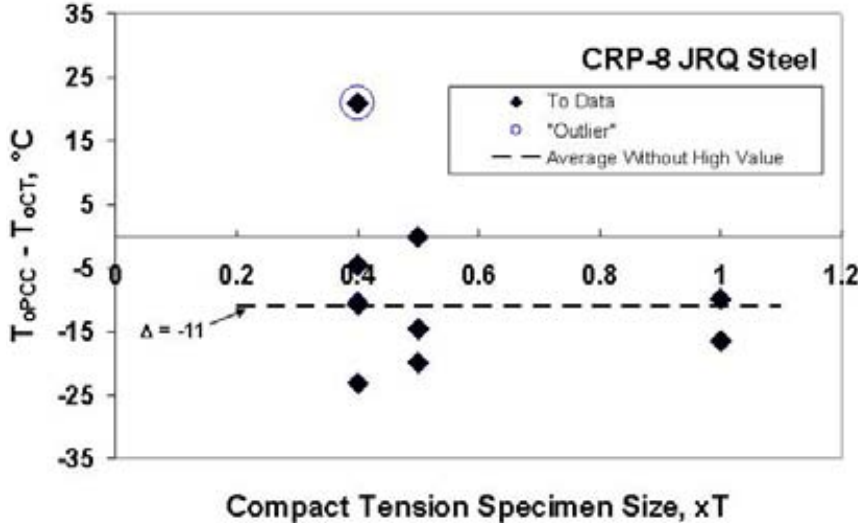
FIG. 3.8. Plot of differences between T_0 values for PCC specimens and compact specimens of size xT, where x is thickness in inches. The dashed line represents the average of all the values excluding that designated an outlier.

Table 3.6 provides results of tests by participants with so-called national steels. The data available for any one of the steels are insufficient to perform a detailed analysis, but the results can be evaluated in a normalized manner to show the effects of shallow flaws relative to deep flaws. Figure 3.9 shows the results graphically and the results are similar to those shown in Figures 3.5 (a)–(c) for the JRQ steel, with shallow flaws of a/W~0.1 exhibiting a T_0 on the order of 40 to 50°C lower than that for a deep flaw of a/W~0.5. The value of T_0 for the specimens with a/W = 0.5 are not shown, but can be derived from the data in the BIAS column. The rapid rise in T_0 vs. a/W in the figure is probably not really representative of the real constraint condition due to the sparse data in the a/W range between 0.1 and 0.5. Table 3.6 also provides an average value of 39°C bias for the specimens with such a shallow flaw. Although the standard deviation is relatively large, it is noted that there are only five values that contribute to the average which also includes lab-to-lab variations and five different steels. The table also provides some PCC data for an a/W value of 0.3 showing only a -2°C bias, meaning the constraint conditions are the same as for a deep flaw. Additionally, some results are shown for tests of 0.4TSEB specimens with shallow flaws. The bias values for the two cases with a/W = 0.1 are similar to those for the PCC specimen, but that for the case with a/W = 0.2 shows only a -1°C bias; this latter result is surprising because that flaw depth is generally considered a shallow flaw relative to constraint.

TABLE 3.6. EFFECT OF SHALLOW FLAWS ON T_0 FOR NATIONAL STEELS

Code	Material	Specimen	a/W	T_0, °C	Bias T_0(a/W = 0.5) -T_0(Meas.), °C
BEL	A508 Class 3	PCC	0.1	-117	-26
AREVA	22NiMoCr37	PCC	0.14	-137	-31
HUN	15H2MFA	PCC	0.1	-148	-50
KOR	SA508-3HT	PCC	0.13	-108	-50
JRC	PVRUF (A533B WM)	PCC	0.13	-133	-38
		Average			-39
		Standard deviation			10.9
HUN	15H2MFA	PCC	0.3	-99	-2
NRI	15Ch2NMFA	0.4TSEB	0.1	-167	-62
JRC	PVRUF (A533B BM)	0.4T SE(B)	0.1	-130	-35
JRC	PVRUF (A533B BM)	0.4T SE(B)	0.2	-96	-1
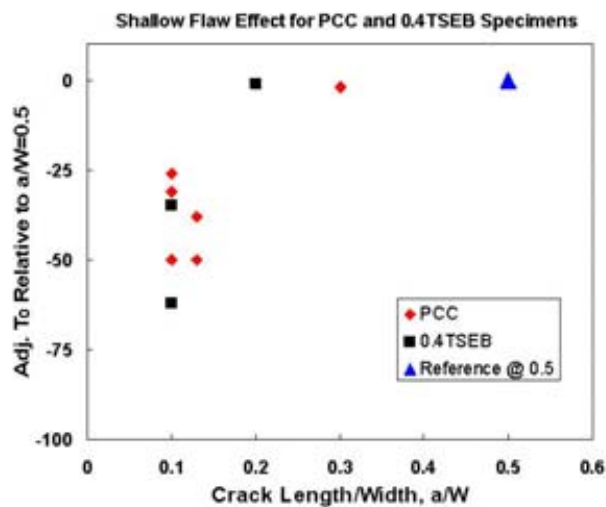
FIG. 3.9. Plot of T_0 v,s crack depth (a/W) for PCC and 0.4TSEB tests of various national steels.

Other results of testing national steels of different types and sizes are shown in Table 3.7.

TABLE 3.7. RESULTS OF TESTS FOR DIFFERENT SIZE SPECIMENS OF NATIONAL STEELS

Code	Material	Specimen comparison	T_0, °C	Bias, T_0(xT)-T_0(PCC), °C
FIN	SE 500 HR P.V. Steel	PCC 0.4TSEB	−179 −187	8
HUN	JFL	PCC 0.4TSEB	−106 −105	-1
KOR	SA508-3HT	PCC 0.4TCT	−58 −60	2
BEL	A508 Class 3	PCC 0.5TCT	−91 −87	-4
AREVA	22NiMoCr37	PCC 1TCT	−106 −95	-11
CRI	SFVQ1A	PCC 1TCT	−105 −102	-3
JRC	PVRUF (A533B BM)	PCC 1TCT	−95 −87	-8
CRI	SQV2A (Heat 1) (A533 Gr. B Cl. 1)	0.4TSEB 1TCT	−94 −87	-7
CRI	SQV2A (Heat 2) (A533 Gr. B Cl. 1)	0.4TSEB 1TCT	−114 −120	6

Not all the data provided by participants are shown because many of the results are singular in the sense that there were no data provided to allow for a comparison. There are only three cases for comparison of the bias for PCC to 1TC(T), with bias values from -3 to -11 which is similar to results for JRQ discussed earlier and shown in Figure 3.8. The table also shows some results comparing PCC to 0.4TSEB, and 0.4TSEB to 1TC(T), with a wide scatter of values indicated.

It is apparent from the results presented that the bias observed between the PCC specimen and larger specimens for Plate JRQ is not nearly as large as that obtained for Plate 13B (-11°C vs. -37°C) and for some of the results in the literature discussed in Section 3.1 (bias values as much as -45°C). This observation is consistent with observations in the literature that show significant variations in the bias that are dependent on the specific materials being tested. There are various methods for constraint adjustments, as discussed earlier and with one demonstrated, but there is not a consensus methodology available that accounts for the differences observed with different materials. Increasing the M_{lim} value in Equation 3.1 to ensure no loss of constraint for the PCC specimen is not a practicable solution because, as discussed in Section 3.1, the PCC specimen is derived from CVN specimens in RPV

surveillance capsules and larger specimens are normally not available. Resolution of these differences are needed for application of the master curve procedure to operating RPVs, but the research needed for such resolution is beyond the scope of this CRP.

3.4. FINITE ELEMENT ROUND ROBIN

3.4.1. Introduction

Finite element modelling is an important tool to support experimental studies aiming at understanding and clarifying bias/constraint/geometry issues. Such issues are particularly important for the application of the Master Curve as cleavage fracture is known to be particularly sensitive to constraint loss.

In the framework of the international acceptance of such tool for actual loss of constraint prediction, the validation of such tool is of prime importance. Therefore, within the CRP-8, Master Curve Approach to Monitor Fracture Toughness of Reactor Pressure Vessels in Nuclear Power Plants, the first part of a round robin exercise has been proposed and accepted during the IAEA meeting in Budapest on 11–13 May 2005.

As a result of the success of the first part of the round robin, the second part of the round robin was proposed and accepted during the IAEA meeting in Dresden on 6–8 November 2006. In this paragraph, the result of the round robin is presented and discussed.

3.4.2. Round robin specifications

Part 1 of the round robin specifications were carefully established in order to:

- Unambiguously define the problem in order to avoid large discrepancies in the results.
- Define a model that can, in a later stage, be used for actual modelling of loss of constraint. To reach this goal the model includes the following characteristics:

  o 3D elements which are needed to model out of plane loss of constraint;
  o an elastic-plastic incremental theory of plasticity;
  o a large strain displacement model;
  o a crack is inserted in the model.

- Use a simple and representative power law strain hardening law to extract useful results.
- Limit the amount of work needed to perform the exercise.

The model for the first part of the round robin is one quarter of a precracked Charpy specimen loaded in three point bending. The actual model and specifications are given in Appendix II. Figure 3.10 shows the elements and boundary conditions.
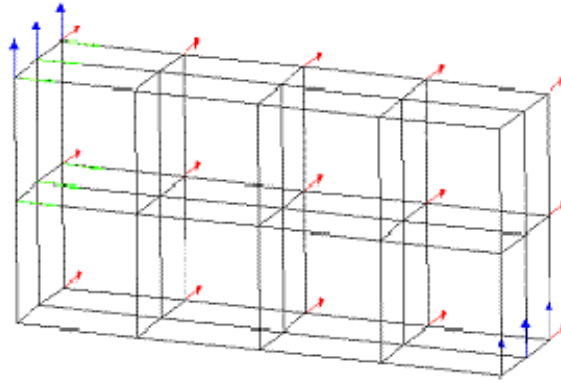
FIG. 3.10. Model of one quarter of a precracked Charpy specimen.

Part two of the round robin is based on part 1 and has been designed to:

- Decrease the mesh size to approach the actual solution of a fracture mechanic elastic-plastic problem.
- Use a simple mesh generation which might be more Central Process Unit (CPU) time consuming than an optimized mesh design.
- Use simple boundary conditions without trying to model the actual contact between specimen and roller.
- Be able to identify loss of constraint.

The model for the second part of the round robin is one quarter of a precracked Charpy specimen loaded in three point bending. The actual model and specifications are given in Appendix III. Figure 3.11 shows the boundary conditions for the deep and shallow crack; the mesh is such that crack tip elements have a size of 50 × 50 μm. The two geometries will be compared in terms of constraint differences measured using the Weibull stress and a simplified constraint correction methodology [10].

Deep crack   Shallow crack
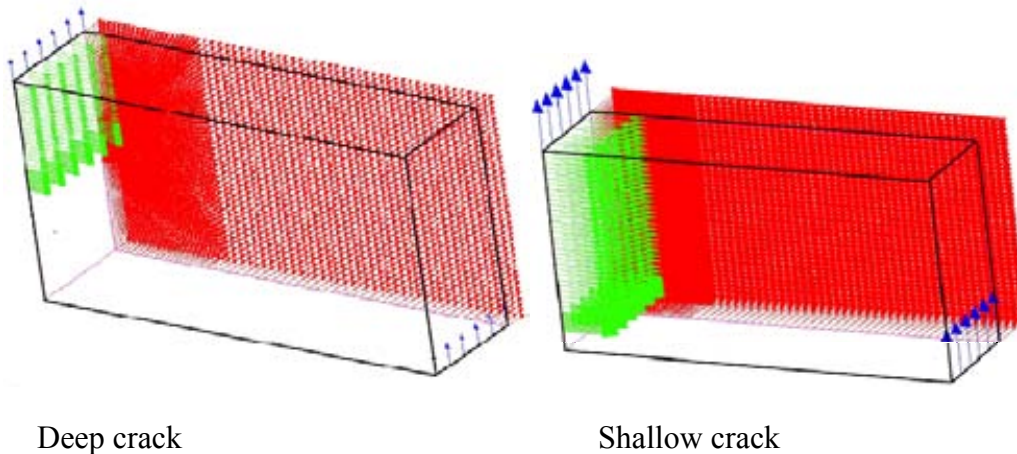
FIG. 3.11. Boundary conditions for the deep and shallow cracks.

3.4.3. Participants

Ten laboratories from nine different countries participated in the round robin. The participants are AEKI, CIEMAT, CRIEPI, FZR, ININ, JAEA, JRC, KAERI, ORNL and SCK•CEN. The results are presented in an anonymous way.

3.4.4. Round robin progress

For the first part of the round robin, all of the 10 participating laboratories submitted results. Results were received between May 2005 and August 2006 and before the November 2006 meeting. The foreseen date of completion set by each participant and the actual date of completion differed by less than 2 months. For experienced users, a typical two days work was needed to implement the specification, run the finite element code, extract the results and perform reporting.

Ten laboratories participated to the second part of the round robin. Results were received between February 2007 and February 2008 and before the final April 2008 meeting. For almost all participants, the foreseen date of completion set by each participant and the actual date of completion differed by less than 2 months. For experienced users, a typical two weeks work was needed to implement the specification, run the finite element code, extract the results and perform reporting.

3.4.5. Number of trials

In case the results submitted to the task coordinator differed substantially from the mean results, the laboratory was notified to verify their model for possible errors. In order not to bias the exercise, the mean results were never sent to any laboratory. Some laboratories only sent in one submission while other laboratories sent in up to 3 submissions. The average number of submission for part one and part two of the round robin are 1.5. This clearly indicates that errors are easily encountered in finite element models or results extraction. It also demonstrates the usefulness of a round robin exercise. For the second part of the round robin, the force displacement records were generally correct from the first trial but generating correct results for the Weibull stress has required additional effort. It is also interesting to note that differences are also found between laboratories using the same code. This can be attributed to the so called user effect. The user effect can be defined as any differences in calculations that use the same code version and the same specifications (e.g. initial and boundary conditions) for a given problem. This user effect and the need to reduce it have been extensively studied in Ref. [1] for nuclear system codes.

3.4.6. Finite element code

A finite element code is used to solve the non linear system of differential equations and is therefore considered to be an important element of the round robin. In total four different codes (listed in Table 3.4) were used. Laboratory 7 used two different finite element codes and produced two results for part one of the round robin.

TABLE 3.4. FINITE ELEMENT CODES USED

Code	Number of users part 1	Number of users part 2	Version
ABAQUS	6	5	6.3 to 6.7
ANSYS	2	2	8.1 and 9.0
MSC-MARC	2	2	2005 r2
SYSTUS	1	1	2005 to 2006

3.4.7. *Deviations from the requested specifications*

Only one laboratory (Laboratory 6) indicated that their calculations were not fully conforming to the requested specifications for part 1, and provided two results.

For the first results, the laboratory did not use the incremental theory of plasticity. Instead the laboratory used the deformation theory of plasticity using a Ramberg-Osgood law given by:

$$E\varepsilon = \sigma + \alpha \left(\frac{|\sigma|}{\sigma_x^o} \right)^{n-1} \sigma \tag{3.5}$$

with n, α and σ_x^o, determined in this case by mean values evaluated from fitting of the material model given in the specification. The values of the parameters were chosen equal to $n = 11.5$, $\alpha = 3.35$e-21 and $\sigma_x^o = 4.8$e6 Pa.

For the second result, the laboratory did use the incremental theory of plasticity but approximated the specified stress strain curve using the Ramberg-Osgood law given above. Moreover, instead of using the isotropic stress hardening option, a combined kinematic and isotropic hardening model was used.

Only one laboratory (Laboratory 3) indicated that their calculations were not fully conforming to the requested specifications for part 2, and indicated that the shallow crack SE(B) model used has 12 130 elements and 15 300 nodes, and the deep crack SE(B) model has 12 010 elements and 15 090 nodes. The deep crack mesh used by Laboratory 3 is given in Figure 3.12.
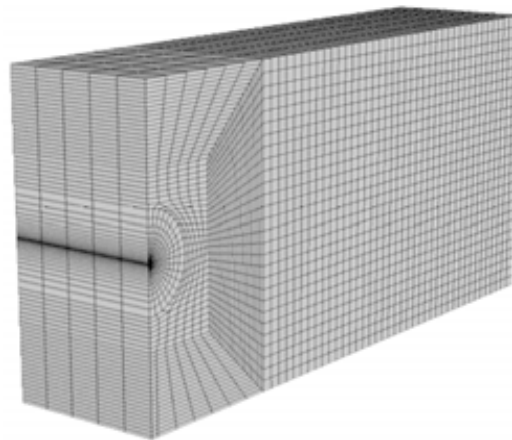
FIG. 3.12. Deep crack mesh used by Laboratory 3.

3.4.8. Results

Detailed tabulated results are given in Appendix 3 and Appendix 4. Force versus displacement curves are presented graphically in Figures 3.7 to 3.9. The displacement is either the load line displacement (LLD) or the crack mouth opening displacement (CMOD) which are defined in the specifications of the round robin. Some difference between the different laboratories can be observed but are relatively limited.
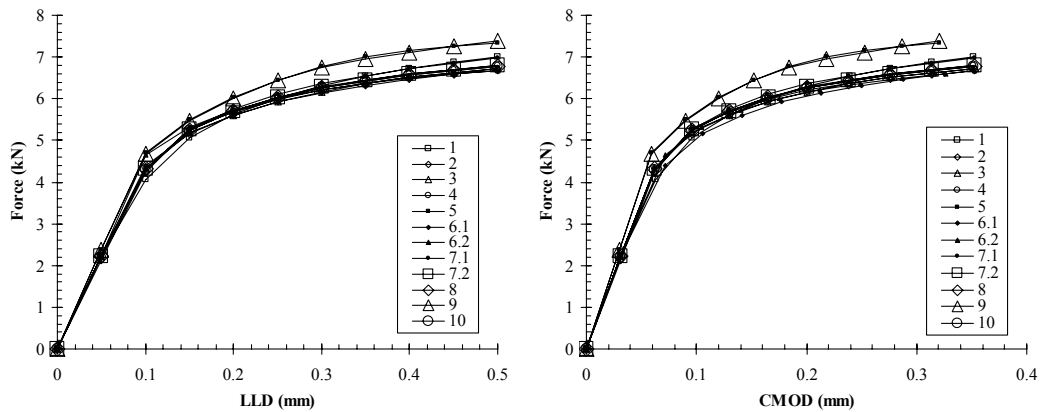
FIG. 3.13. Force versus displacement (round robin part 1).
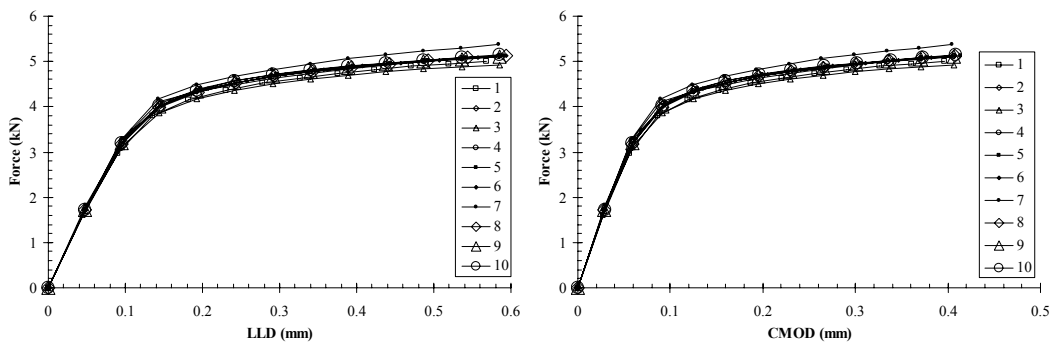
FIG. 3.14. Force versus displacement (round robin part 2, deep crack).
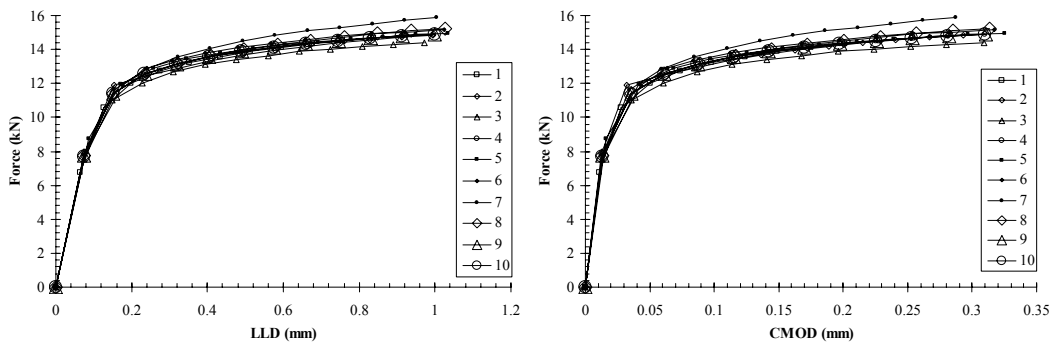
FIG. 3.15. Force versus displacement (round robin part 2, shallow crack).

To analyse the plastic volume and the Weibull stress, it is more appropriate to display the results as a function of the driving force K_J. The driving force is calculated from the force versus displacement record using the equations described in the ASTM E1921-05 [6]:

29

$$K_J = \sqrt{\frac{EJ}{(1-v^2)}} \qquad (3.6)$$

where J is the J-integral that can be decomposed in an elastic and a plastic component:

$$J = J_{el} + J_{pl} \qquad (3.7)$$

The elastic component of the J-integral is:

$$J_{el} = \frac{(1-v^2)K_{el}^{\ 2}}{E} \qquad (3.8)$$

where K_{el} is the elastic stress intensity factor:

$$K_{el} = \frac{FS}{BW^{3/2}} f(a_0/W) \qquad (3.9)$$

where F is the force, S the span, W the specimen width, B the specimen thickness and $f(a_0/W)$ a geometrical function given in Ref. [6].

The plastic component of the J-integral is:

$$J_{pl} = \frac{\eta A_p}{Bb_0} \qquad (3.10)$$

where b_0 is the ligament size, A_p the plastic part of the energy under the force versus displacement record and η is 1.9 when the load line displacement is used. When the CMOD is used the following equation applies:

$$\eta = \frac{S}{4W}\left(3.785 - 3.101(a_0/W) + 2.018(a_0/W)^2\right) \qquad (3.11)$$

For shallow cracks only the CMOD approach should be used (see Appendix 1). For deep cracks, K_J calculated from LLD and CMOD is compared in Figure 3.16. It is found that K_J is relatively equivalent using LLD and CMOD. In Figures 3.16–3.17 only J from CMOD is used.
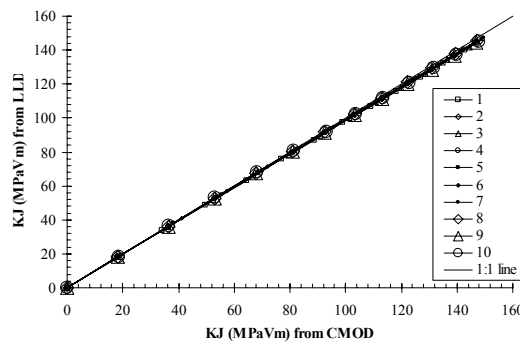
FIG. 3.16. K_J calculated from LLD and from CMOD (round robin part 2, deep crack).

The plastic volume (V_p) and the Weibull stress (σ_w) is plotted as a function of K_J in Figures 3.17 and 3.18. Some difference between the different laboratories can be observed. However, those differences are limited.
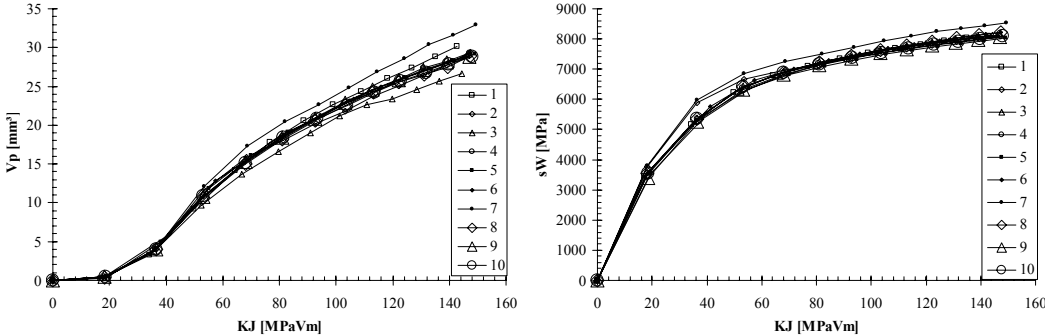
FIG. 3.17. Plastic volume and Weibull stress as a function of K_J
(round robin part 2, deep crack).
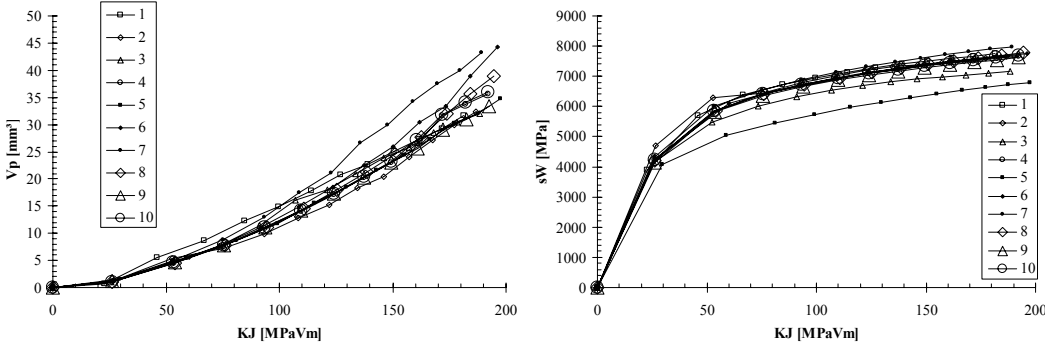
FIG. 3.18. Plastic volume and Weibull stress as a function of K_J
(round robin part 2, shallow crack).

3.4.9. Differences between the laboratories

For part one of the round robin, Laboratories 5 and 9 provided distinctively higher force value than the average (see Figure 3.13). Since both laboratories are the only ones using the ANSYS code, the bias must be a result of the finite element code. It is suspected that the finite element formulation of an 8-node hexahedral element is different from other finite element codes. It appears that ANSYS has two element types SOLID45 and SOLID185; both are 8 nodes, 8 integration points, isoparametric. However, SOLID45 is unable to model nearly incompressible materials. SOLID185 has an enhanced strain formulation with additional internal element DOFs that are used to prevent shear locking.

Excluding Laboratories 5 and 9, the differences are smaller than 3%. Laboratories 4, 8, 7.2 and 10 deliver results within 0.3% of each other. Therefore, the average of these 4 calculations is taken as the reference. The force difference is presented in Figure 3.19.

The remaining differences cannot be explained by the used finite element codes. Laboratories 2 and 7.1 are both using MSC-MARC and give results above and below the average. Laboratories 1, 3, 6.1, 6.2, 7.2 and 8 are using ABAQUS, and results are also above and below the reference.

The deviation of Laboratory 6.2 near the general yield can be due to the approximated strain-stress curve.

Remaining differences of up to 3% can be due to:

- overlooked and unreported non-full conformance to the model specifications or code specific options;
- convergence criterion and selected solver for the resolution of the non-linear equation;
- selection of the time step size.
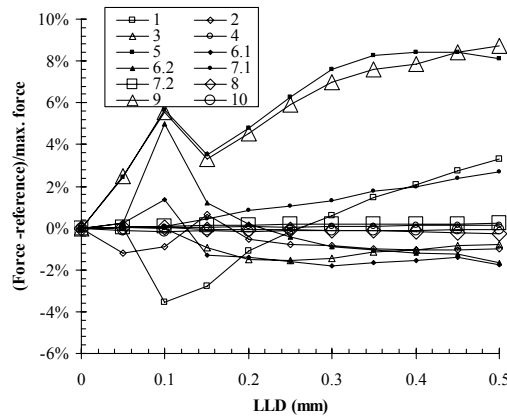
FIG. 3.19. Force minus the force average of laboratories 4, 8, 7.2 and 10 divided by the maximum force versus load line displacement (round robin part 1).

To investigate the differences between the different laboratories in part 2 of the round robin, the relative difference from a selected reference is calculated. The reference is subjectively selected to represent the median behaviour. In Figure 3.20, Laboratories 1, 3 and 7 deviate up to 4% from the rest of the results. This difference is not very large but cannot be attributed to a particular finite element code. For Laboratory 3, the difference can be identified as deriving from the difference in the mesh used for the calculation. The differences for Laboratories 1 and 7 are attributed to some user effect. The differences for the other laboratories are less than 2% and can be considered small.

After completion of the round robin, Laboratory 2 (MSC-MARC) discovered some software effect. Using a time step 10 times smaller than the one prescribed in the round robin, the results were in much better agreement with the other participants. This reveals that MSC-MARC needs smaller time step in order to properly integrate the behaviour law.

Deep crack   Shallow crack
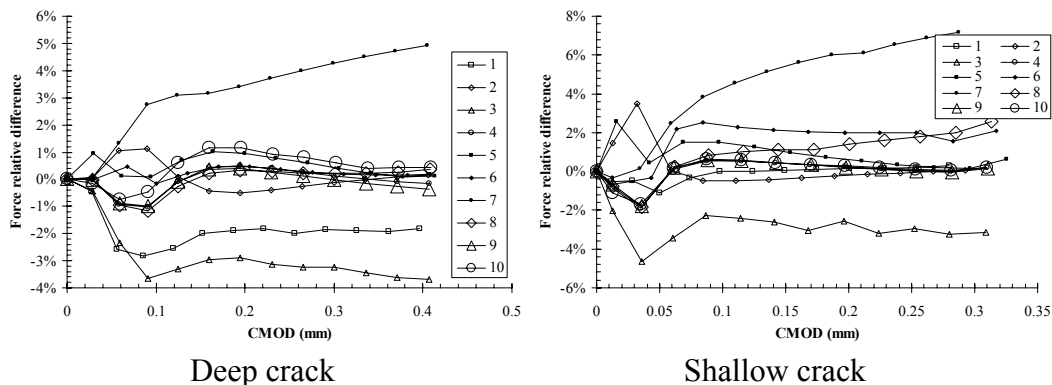
FIG. 3.20. Relative force difference for the round robin part 2. The reference is taken as the average of Laboratories 4 and 9.

The plastic volume and Weibull stress of the different laboratories are compared in Figures 3.21 and 3.22. Differences for those parameters are larger than the differences for the force versus displacement record. This might be due to the larger complexity to compute those values and to a larger sensitivity of those values to small variation in the resolution of the finite element problem. Results of Laboratories 3, 5 and 7 show the largest deviations. For Laboratory 3, the deviation can be attributed to the mesh difference in the vicinity of the crack tip. The variations of Laboratory 5 and 7 cannot be attributed to one particular finite element code but derived from a user effect.

After completion of the round robin and discussion of the results, two user effects were identified. Those user effects do not affect the force versus displacement record but can affect the Weibull stress and plastic volume calculation.

Finite element codes are ensuring equilibrium from stress computed at Gauss points. Therefore, user should use stress and strain information provided at Gauss point location by finite element code. However, it appears that some codes provide stress and strain at node location using an extrapolation/averaging method. It is not recommended to use this information to obtain the stresses inside the element.

Each participant is requested to compute integrals (i.e. plastic volume, Weibull stress). Those integrals are normally performed by calculating the sum of each quantity at Gauss point multiplied by the Gauss point weight and by the determinant of the Jacobian matrix of the shape functions. In practice, the Gauss point weight is 1/8 for 8 Gauss point elements. The determinant of the Jacobian matrix is generally not provided by finite element code at Gauss point location and is equal to the volume of the element but only in case of parallelepiped element. Some users have used this approximation and other users averaged the stress and strain at the centre of each element.
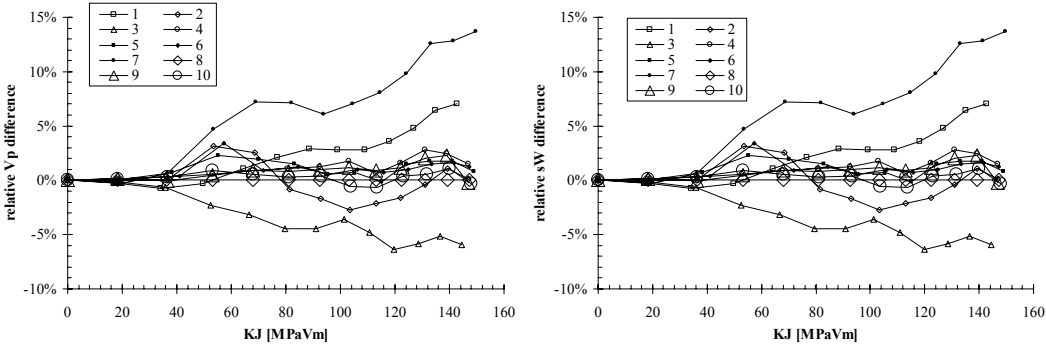
FIG. 3.21. Relative plastic volume and Weibull stress difference for the round robin part 2, deep crack. The reference is taken as Laboratory 8.
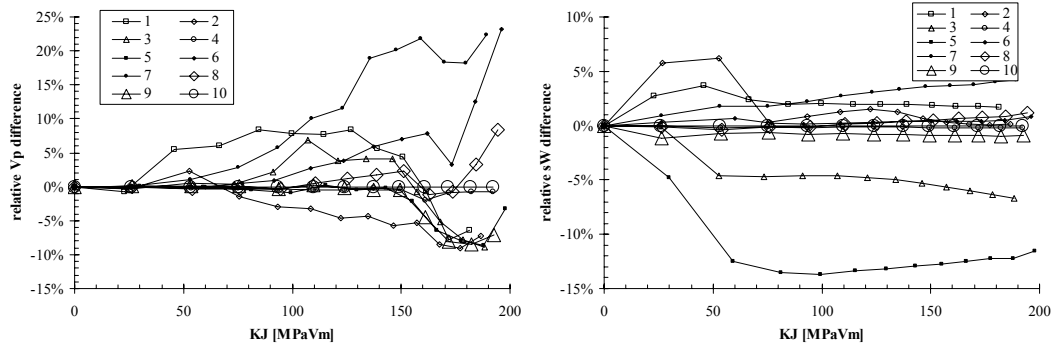
FIG. 3.22. Relative plastic volume and Weibull stress difference for the round robin part 2, shallow crack. The reference is taken as Laboratory 10.

3.4.10. Discussion

The effect of mesh size can be evaluated by comparing part 1 and part 2 of the round robin for the deep crack (see Figure 3.23). It is found, as expected, that the mesh in part 1 of the round robin is unable to capture the solution as it is much too coarse. The effect of mesh size can also be assessed by the fact that Laboratory 3 used a different mesh and still obtained similar results as the other laboratories. Which means that the mesh specified in the round robin part 2 should be close to convergence.
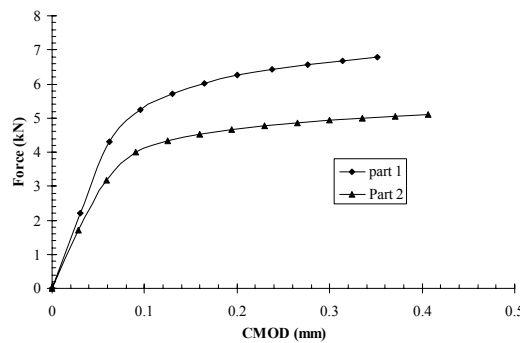
FIG. 3.23. Comparison of the force versus CMOD obtained for the deep crack using the mesh defined in part 1 and in part 2.

In the round robin 8 node brick elements were imposed. To evaluate the effect of the element type, Laboratory 4 performed a computation using the same mesh but using 20 node brick elements and 8 Gauss points. Although the number of element remains the same, the size of the problem increases due to the larger number of nodes and to the larger bandwidth of the stiffness matrix. Results are compared in Figures 3.24 and 3.25. Limited differences are found which confirm the convergence of the solution. In practical application, the user should develop an appropriate mesh and verify the convergence. The mesh specified in part 2 of the round robin exercise provide some guideline on appropriate mesh refinement.
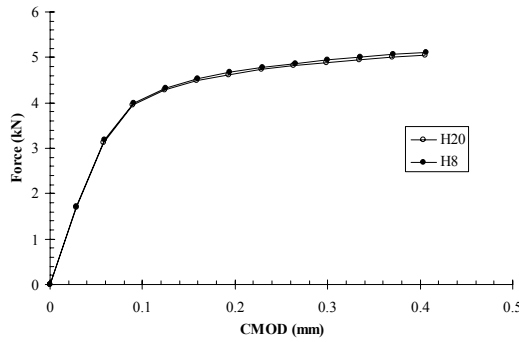
FIG. 3.24. Force versus CMOD for the deep crack using 8 and 20 nodes brick element.
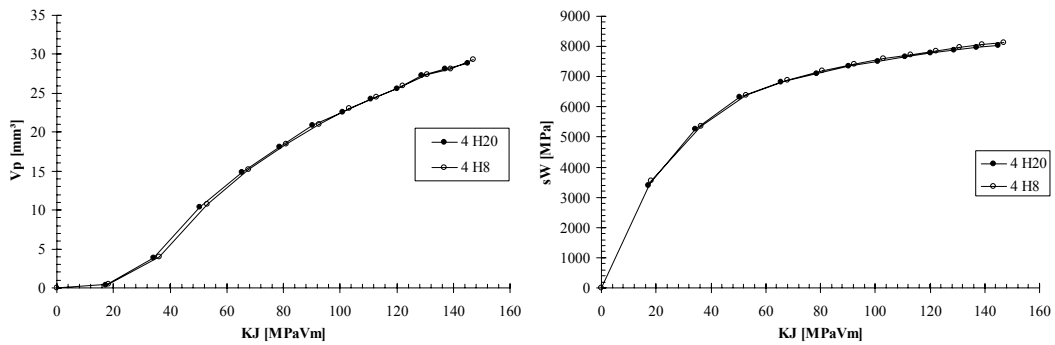
FIG. 3.25. Plastic volume and Weibull stress for the deep crack using 8 and 20 nodes brick elements.

The finite element round robin can be used to evaluate the difference of constraint between a shallow and a deep crack specimen. The procedure used is as follows: For a given plastic volume or Weibull stress, the K_J value is identified for both the deep and shallow crack. As the two geometries have the same plastic volume or Weibull stress, they have the same failure probability although the K_J driving force may differ between the two geometries.

The result of the procedure is given in Figure 3.26. For K_J above 40 MPa√m, the shallow crack specimen clearly displays loss of constraint for both the Weibull stress approach and the plastic volume approach. Using the plastic volume approach, the loss of constraint difference tends to decrease above 120 MPa√m. This is an artefact of the methodology that only evaluates the plastic zone size but not the level of stress in the volume. The self similarity of the stress field ahead of the crack tip probably disappears above 120 MPa√m and therefore, results in the inadequacy of the plastic volume methodology.

Testing PCCv at 25°C below the reference temperature results in a median fracture toughness of 87.6 MPa√m. This median fracture toughness corresponds to a PCCv median shallow crack fracture toughness of 136 MPa√m and 146 MPa√m for the volume and Weibull stress method respectively. Those fracture toughness values can be converted in temperature value using the master curve resulting in at reference temperature bias of 33°C and 39°C for the plastic volume and Weibull stress, respectively.
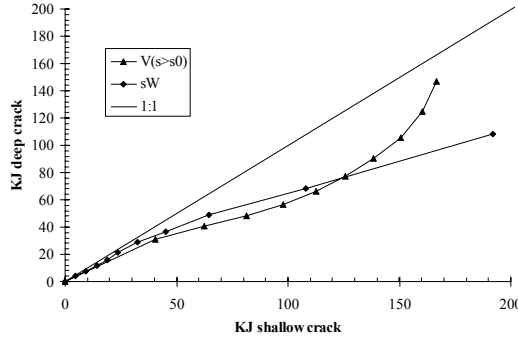
FIG. 3.26. Comparison of K_J from deep crack and shallow crack leading to the same failure probability.

The finite element round robin can also be used to address loss of constraint as a function of the loading level for each particular geometry. The f-function and g-function [4] are defined as:

$$f(M) = C \frac{V_p}{BK_J^4} \tag{3.12}$$

and

$$g(M) = D \frac{\sigma_w^m}{BK_J^4} \tag{3.13}$$

where C and D are constant and $M = b\,\sigma_{YS}/J$.

The f and g functions are constant under small scale yielding and tend to decrease for lower M values indicating loss of constraint. The C and D constants are set such that the f and g functions yield a value of one under high constraint. When f or g to the power of ¼ equal 0.5, it means that loss of constraint has occurred and that the measured fracture toughness is 2 times larger than under high constraint conditions.

The f and g functions to the power of ¼ are given in Figure 3.27. The plastic volume approach and the Weibull stress give similar loss of constraint functions as a function of loading. The figure indicates that loss of constraint starts at a M value of 200. In the current E1921 standard, the M limit is 30 for which relatively large loss of constraint is predicted using the current model. To reduce slightly the loss of constraint correction, we can make the hypothesis that the f or g function should only correct the portion above the minimum fracture toughness using:

$$K_{Jc,1T,SSY} = (K_{Jc} - K_{min})\left(\frac{B}{B_{1T}}\right)^{0.25} g^{0.25} + K_{min} \tag{3.14}$$

This equation could be used to correct each data point from a given test campaign.
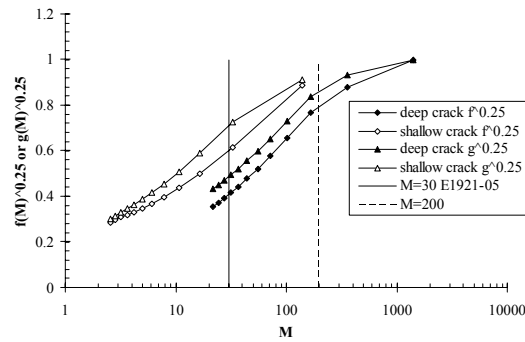
FIG. 3.27. Loss of constraint function for the deep crack and the shallow crack.

In this round robin the parameter of the plastic volume and Weibull model were specified. In actual problems, those parameters and their dependence with temperature would need to be identified using for example a procedure described in Ref. [3]. But, this is outside of the current round robin.

Many models exist such as the WST model [7], the Anderson and Dodds model [10], the Bordet model [11], the Prometey model [12]. All models are based on the weakest link and yield similar trends. However, the differences come from the level of complexity to identify the parameters needed for the models.

The boundary conditions were simplified to avoid modelling of complex contact condition between rollers and specimen. The modelling of the exact boundary condition is not believed to be important. However, in order to obtain meaningful results, it is important to use a proper strategy to simplify the contact condition. In practice, this issue was solved in this round robin by introducing few elastic elements at contact location and by using displacement information that are not affected by the amount of deformation of elements closed to the contact elements.

3.5. CONCLUSIONS AND RECOMMENDATIONS FOR FUTURE WORK

3.5.1. Conclusions

Fifteen laboratories contributed to the experimental portion of Topic area 1, Test Specimen Size, Geometry, and Constraint Relative to the Measurement and Application of Master Curve T_0 Values. Fracture toughness data were provided for three-point bend specimens of varying sizes from 0.16T to 1T and for compact specimens from 0.4T to 1T. Additionally, some participants tested specimens with crack depth (a/W) variations from 0.1 to 0.75. Two large datasets were available for analysis, HSST Plate 13B and JRQ steel, both RPV steels of the A533 grade B class 1 specification. Additionally, participants contributed data from tests of national steels.

It is apparent from the results presented in CRP-5 and in this CRP that the bias observed between the PCC specimen and larger specimens for Plate JRQ is not nearly as large as that obtained for Plate 13B (-11°C vs. -37°C) and for some of the results in the literature (bias values as much as -45°C). This observation is consistent with observations in the literature that show significant variations in the bias that are dependent on the specific materials being tested. This observation is also consistent for the data from the various national steels. For the varying crack depth data, the results exhibited T_0 differences from about 40 to 70°C between a/W = 0.1 and 0.5, with the shallow crack showing the lower T_0.

There are various methods for constraint adjustments, as discussed earlier and with two methods demonstrated for the Plate 13B data, but there is not a consensus methodology available that accounts for the differences observed with different materials. Increasing the M_{lim} value in Equation 3.1 (from ASTM E1921) to ensure no loss of constraint for the PCC specimen is not a practicable solution because the PCC specimen is derived from Charpy V-notch specimens in RPV surveillance capsules and larger specimens are normally not available. Resolution of these differences are needed for application of the Master Curve procedure to operating RPVs, but the research needed for such resolution is beyond the scope of this CRP.

Ten laboratories contributed to a finite element round robin in the framework of the consolidation of analytical tools needed to support loss of constraint issues in the application of the Master Curve. This exercise has been performed within the framework of the CRP-8. For part one of the round robin, it is found that the ANSYS code produces systematically higher forces. Remaining differences for the other finite element codes are very small and less than 3%.

For part two of the round robin, differences between the laboratories are limited. MSC-MARC would require smaller time step to yield equivalent results to the other finite element code that are using the time step prescribed in the specification. The remaining differences cannot be attributed to one particular finite element code. The differences are attributed to the so called user effect. Some of the user effects were identified during the discussion of the result of the round robin. To further track down those user effects, it is needed to compare the input file of the participant and to compare the subroutine used to post-treat the finite element results. However, this is currently outside of the scope of the round robin.

This round robin has been useful to qualify finite element codes and to identify possible errors in the input file. The round robin demonstrates that errors in the input file can be easily introduced. To avoid those errors, it is important to follow internal quality assurance and cross-check results again established references. This round robin should contribute to the reduction of the user effect. For laboratories that did not participate to the IAEA CRP-8, this round robin can serve as a very good opportunity to cross-check their methodology.

The second part of the round robin was used to evaluate the loss of constraint of each specimen and to compare the shallow and deep crack configuration. It is found that shallow crack specimens are more sensitive to loss of constraint than deep crack for a given specimen size. The difference in term of reference temperature is evaluated to be of about 40°C. For deep crack, loss of constraint is identified to appear at M values around 200.

3.5.2. Recommendations for future work

The scope of the round robin was limited to the precracked Charpy V-notch geometry. It is recommended to extend the work to compact tension geometry and to crack in structural application such crack subjected to pressurized thermal shock.

The issues related to the identification of micromechanical parameters and their dependence as a function of temperature has not been investigated in this study. Work is needed to allow engineering use of the methodology.

It is recommended that prior application of this methodology, that a quality assurance procedure is used in order to avoid error in the results. It is also important that users verify that mesh refinement and time step have reached convergence.

3.6. REFERENCES

[1] ASHLEY, R., EL-SHANAWANY, M., ELTAWILA, F., D'AURIA, F., Good Practices for User Effect Reduction, NEA/CSNI/R (98)22, Paris (1998).

[2] AMERICAN SOCIETY FOR TESTING AND MATERIALS, ASTM E 1921, Test Method for the Determination of Reference Temperature, T_0, for Ferritic Steels in the Transition Range, Annual Book of ASTM Standards, ASTM International, West Conshohocken (2002).

[3] RUGGIERI, C., GAO, X., DODDS, R.H., Jr., Transferability of the elastic-plastic fracture toughness using the Weibull stress approach: significance of parameter calibration, Engineering Fracture Mechanics **67** (2000) 101–117.

[4] PETTI, J.P., DODDS, R.H., Calibration of the Weibull stress scale parameter, σu, using the Master Curve, Engineering Fracture Mechanics **72** 1 (2005) 91–120.

[5] TREGONING, R.L., JOYCE, J.A., Investigation of Censoring Limits for Cleavage Fracture Determination. Fourth Symposium on Small Specimen Test Techniques, ASTM STP 1405, ASTM, West Conshohocken (2002).

[6] AMERICAN SOCIETY FOR TESTING AND MATERIALS, ASTM E1921-05 Standard Test Method for Determination of Reference Temperature, T_0, for Ferritic Steels in the Transition Range, Annual Book of ASTM Standards, ASTM International, West Conshohocken (2002).

[7] WALLIN, K., LAUKKANEN, A., New developments of the Wallin, Saario, Törrönen cleavage fracture model, Engineering Fracture Mechanics (2007).

[8] WASILUK, B., PETTI, J., DODDS, R.H., Jr., "Constraint Differences Between C(T) and SE(B) for the Euro-material", ASTM International, Salt Lake City (2004).

[9] WALLIN, K., PLANMAN, T., VALO, M., RINTAMAA, R., Applicability of miniature size bend specimens to determine the Master Curve reference temperature T_0, Engineering Fracture Mechanics **68** (2001) 1265–1296.

[10] ANDERSON, L., DODDS, R.H., Jr., Simple Constraint Corrections for Subsize Fracture Toughness Specimens, Small Specimen Test Techniques Applied to Nuclear Reactor Vessel Thermal Annealing and Plant Life Extension, ASTM STP 1204, Philadelphia (1993) 93–105.

[11] BORDET, S.R., KARSTENSEN, A.D., KNOWLES, D.M., WIESNER, C.S., A new statistical local criterion for cleavage fracture in steel. Part I: Model presentation, Engineering Fracture Mechanics **72** 3 (2005) 435–452.

[12] MARGOLIN, B., SHVETSOVA, V., GULENKO, A., KOSTYLEV, V., Prometey local approach to brittle fracture: Development and application, Engineering Fracture Mechanics, Moscow (2008).

4. LOADING RATE EFFECTS AND QUALIFICATION OF IMPACT FRACTURE TOUGHNESS TESTING

4.1. BACKGROUND

The Master Curve (MC) approach procedure standardised in ASTM E1921-05 is defined for quasi-static loading conditions. However, the use of the MC method for dynamic test is obvious. Namely impact toughness results on different RPV steels were already obtained in the frame of previous CRPs. Dynamic and impact tests conducted by Wallin [1], Joyce and Tregoning [2, 3]. Wallin [4] proposed an empirical relationship between loading rate dK/dt and increase of the reference temperature ΔT_0 (in K) based on the analysis of a large database mostly consisting of RPV steels.

$$\Delta T_0 = \frac{T_{01} \cdot \ln\left(\frac{dK_I}{dt}\right)}{\Gamma - \ln\left(\frac{dK_I}{dt}\right)} \quad (4.1)$$

where: T_{01} reference temperature measured under quasi-static conditions (in K)

Γ empirical function based on the Zener-Holloman Strain Rate parameter given by:

$$\Gamma = 9.9 \cdot \exp\left[\left(\frac{T_{01}}{190}\right)^{1.66} + \left(\frac{R_{el}}{722}\right)^{1.09}\right] \quad (4.2)$$

with: R_{eL} = quasi-static yield strength (in MPa).

To exclude the influence of the loading rate on the measured reference temperature a range is given in the ASTM E1921-05 standard. In the previous versions of ASTM E1921 (2003) the allowed loading rate was specified in terms of time take to reach 40% of the limit load (between 0.1 and 10 min). Investigations by Wallin, Hall and Yoon [5] and Joyce [6] have clearly shown that within this range the variation in T_0 is significantly larger than 10 K. In order to remain within this limit the allowed range was reduced in the current version of ASTM E1921 to dK/dt between 0.1 and 2 MPa√m/s.

At the same time the ASTM Technical Committee responsible for E1921 is working on developing an appendix for higher loading rates up to impact testing. The results of this CRP Topic area 2, Effects of loading rate and qualification impact loading conditions on T_0, will provide a significant contribution to this effort with test results covering the range between quasi-static loading rates (0.1 to 2 MPa√m/s) and impact loading rates (10^5 MPa√m/s using instrumented impact pendulum machines).

Impact toughness tests on precracked Charpy specimens have been performed by many institutions for several decades now. Indeed, the instrumentation of the striker made it possible to use the simple Charpy test for dynamic fracture mechanics testing and, thus to apply the results for the structural integrity assessment. In the range of lower shelf and the lower ductile-to-brittle transition (DBT) region, J-integral-based fracture toughness values, K_{Jc}, can be determined at the onset of cleavage crack initiation. The onset of cleavage fracture appears on the measured force versus time trace as a force drop.

The execution of the tests and the calculation of dynamic fracture toughness data of precracked Charpy specimens have not yet been defined by any official international standard. However, there are procedures and draft standards published by the Electric Power Research Institute (EPRI) in the report EPRI NP-119 [7, 8] and the Draft International Standard: ESIS, European Structure Integrity Society: Proposed Standard Methods for Instrumented Precracked Charpy Impact Testing of Steels – Combined K_{Id}, J_{Id} and CTOD Tests Methods, respectively.

The state of the art in the dynamic fracture toughness measurement using precracked Charpy size specimens was summarised by Lucon [9]. Based on these references, a set of guidelines has been developed for impact tests performed within Topic area 2 of this CRP.

4.2. INVESTIGATION OF LOADING RATE EFFECTS

4.2.1. Datasets analysed

CRP-8 participants were required to perform and evaluate the tests in accordance with the current version of ASTM E1921. The Master Curve datasets supplied by the participants for different blocks of JRQ and national steels are summarised in Appendix IIA. Figures 4.1 and 4.2 illustrate T_0 as a function of loading rates ranging from quasi-static to impact. The most comprehensive data are available for the JRQ steel (Figure 4.1), whereas for the national steels (Figure 4.2), the limited data available for each steel can only provide information about general trends.
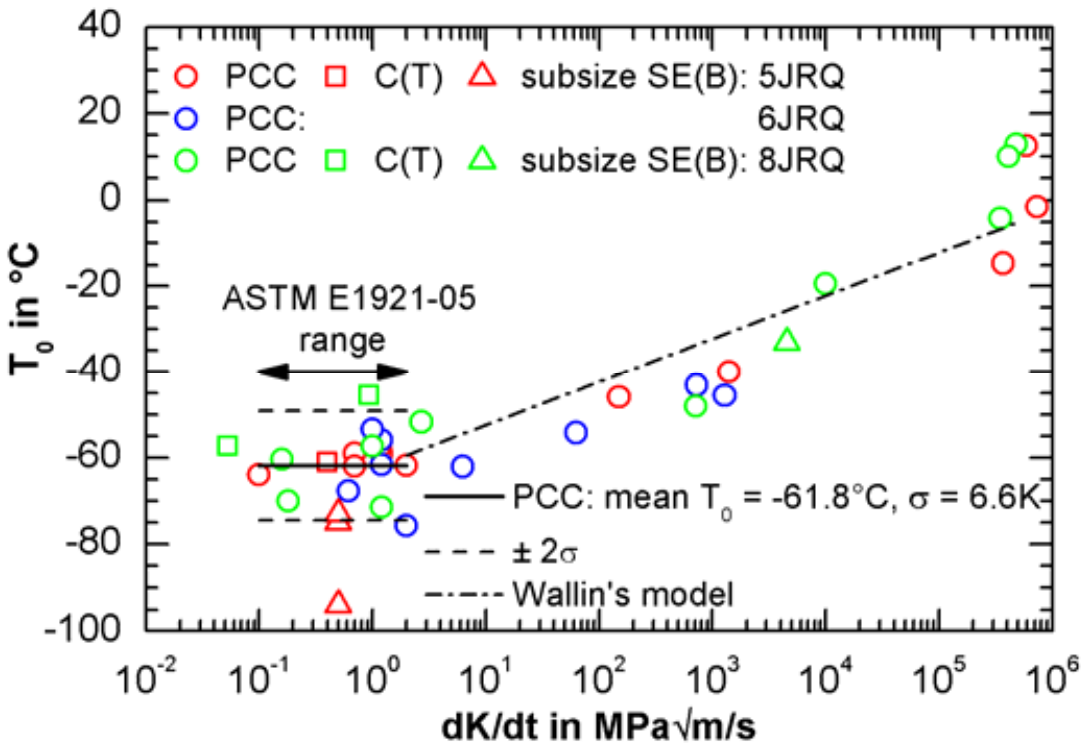
FIG. 4.1. Reference temperature T_0 vs. loading rate for different JRQ blocks (PCC specimens only) and comparison with the predictions of Equation 4.1 (Wallin's model).
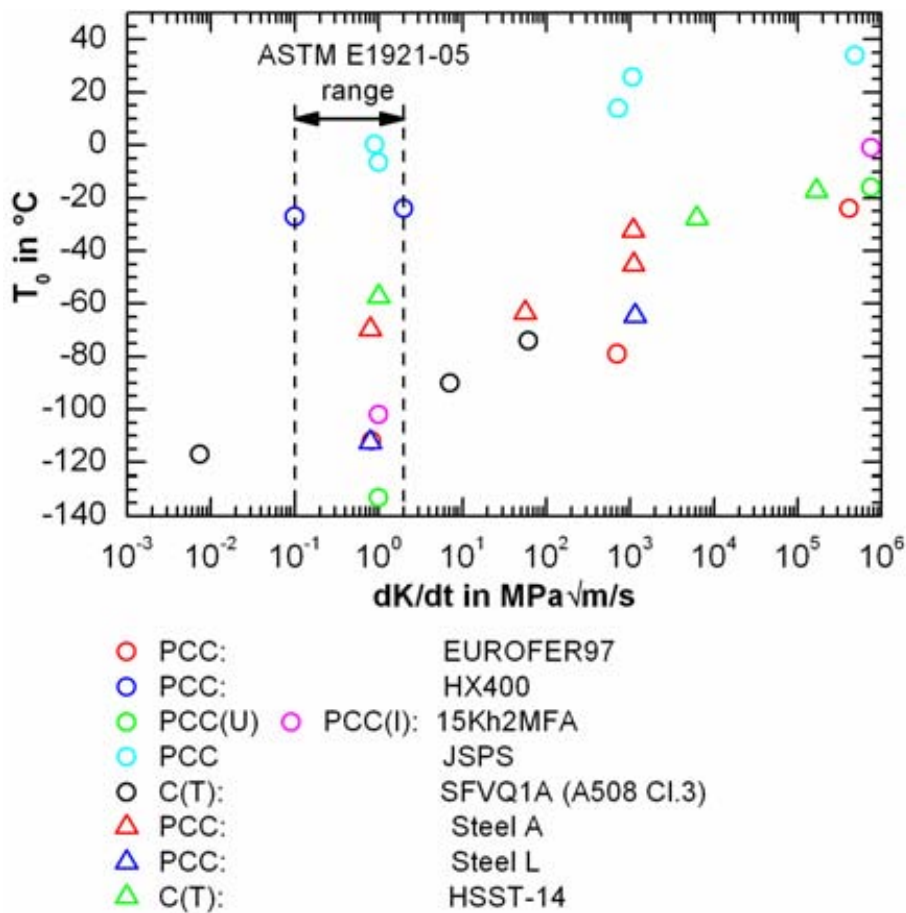
FIG. 4.2. Reference temperature T_0 vs. loading rate for the national steels.

4.2.2. Variation of T_0 within the quasi-static loading range (0.1–2 MPa√m/s)

As shown by Figures 4.1 and 4.2, there is no systematic variation of T_0 within the quasi-static loading range prescribed by ASTM E1921-08 (0.1 to 2 MPa√m/s). For JRQ, all T_0 values are within the ±2σ scatter band. The observed scatter is likely a result of variations between different JRQ plates, different specimen geometries (PCC and C(T)) and testing in different laboratories. The T_0 values determined with PCC specimens of the 5JRQ plate fall within a small scatter band, even through the tests were performed by different laboratories (Figure 4.1). This statement is substantially confirmed by the results obtained within the quasi-static range for the HX400 and JSPS steels (Figure 4.2).

4.2.3. Variation of T_0 outside the quasi-static loading range (below 0.1 MPa√m/s and above 2 MPa√m/s)

Above the 2 MPa√m/s limit, there is a clearly defined trend to increasing T_0 values with increasing loading rates [2, 4, 10]. As depicted in Figure 4.1, the shift of T_0 with increasing dK/dt for the JRQ steel can be satisfactorily predicted using Wallin's empirical relationship, Equation 4.1. This correlation predicts an increase of about 52 K between the upper limit of the quasi-static loading rate (2 MPa√m/s) and an impact loading rate of about 3.5×10^5 MPa√m/s, corresponding to impact loaded PCC specimens (see the round robin exercise described next). This variation is about 15 K lower than experimentally determined in the round robin exercise (see later data). The trend to higher T_0 values with increasing loading rate can also be observed for the national steels, but the results shown in Figure 4.2

indicate that the slope is material-dependent. Namely, JSPS, steel A and HSST-14 show a shallower slope compared with JRQ, EUROFER 97 and steel L.

4.3. IMPACT FRACTURE TOUGHNESS ROUND ROBIN EXERCISE ON PCC SIZE SPECIMENS

The round robin exercise (RRE) involves 12 participants. General guidelines for test conditions and analysis procedures are as follows:

- Loading rate: 1.2 m/s;
- Test temperature range: -30 to 10°C;
- Specimen geometry: SE(B), Charpy-type, Charpy V-notch + sharpened notch (for crack initiation) = total depth 2.5 mm; specimens 20% side-grooved;
- 10 specimens to be tested by each laboratory;
- Minimum response frequency of the acquisition system: 100 kHz;
- Minimum sampling rate: 2 μs;
- Precracking conditions: initiation of fatigue crack K_{max} = 25 MPa$\sqrt{m}$; finish sharpening K_{max} = 18.5 MPa$\sqrt{m}$;
- Side-grooving: according to E1921, §7.7;
- Pre-test dimensional measurements: B, B_N, W (precision: 0.01 mm);
- Status of machine/thermocouple calibration and temperature control/conditioning times/transfer time: in accordance with ASTM E23;
- Post-test crack size measurements: a_o, a_f (9-point average method, precision 0.01 mm).

From the dynamic test record, the absorbed impact energy is calculated from the area under the force-displacement curve up to the onset of cleavage fracture. Force is directly measured and displacement is calculated, by double numerical integration of force/time data according to Equations 4.1 and 4.2.

$$V(t) = V_0 - \frac{1}{m} \int_{t_0}^{t} F(t)dt \tag{4.3}$$

$$s(t) = \int_{t_0}^{t} V(t)dt \tag{4.4}$$

m   mass of the pendulum hammer
F   impact force measured at the pendulum striker
V   actual velocity of the pendulum hammer
V_0 initial impact velocity of the pendulum hammer
s   deflection of the specimen

The J integral at the onset of cleavage fracture (Equation 4.5), is determined per ASTM E1921-05 in analogy to the standards ISO/DIS 12135 Metallic Materials – Unified Method of Test for the Determination of Quasi-static Fracture Toughness and ASTM E1820 Standard Test Method for Measurement of Fracture Toughness.

$$J_c = J_{el} + J_{pl} = \frac{K_c^2(1-v^2)}{E} + \frac{2W_{c(pl)}}{B_N b_0} \qquad (4.5)$$

B_N specimen net thickness between side grooves
b_0 specimen ligament
E   Young's modulus calculated as a function of test temperature T using:
J_{el} elastic component of the J-integral
J_p plastic component of the J-integral
K_c stress intensity at the onset of cleavage failure
$W_{c(pl)}$ plastic part of the area under the force-deflection curve
v   Poisson's ratio

$$K_c = \left[\frac{F_c \cdot S}{\sqrt{B \cdot B_N . W^3}} \right] \cdot f(a/W) \qquad (4.6)$$

where:

F_c force at cleavage failure determined at the onset of the force drop in the force deflection curve
S   span value of the anvils (for a DIN 300 J pendulum: 42 mm)
B   specimen thickness
W   specimen width
f(a/W)   specimen stress intensity function for SE(B) specimens

$$f(a_0/W) = \frac{3 \cdot \sqrt{\frac{a_0}{W}} \cdot \left[1.99 - \left(\frac{a_0}{W}\right) \cdot \left(1 - \frac{a_0}{W}\right) \cdot \left(2.15 - 3.93 \cdot \left(\frac{a_0}{W}\right) + 2.7 \cdot \left(\frac{a_0}{W}\right)^2 \right) \right]}{2 \cdot \left(1 + \frac{2a_0}{W}\right) \cdot \left(1 - \frac{a_0}{W}\right)^{1,5}} \qquad (4.7)$$

The total absorbed impact energy W_{tot} is calculated from the area under the force-displacement curve up to the onset of cleavage fracture. This energy value contains some contributions not related to fracturing the specimen. The true specimen initiation energy, $W_{c(pl)}$, is determined according to Equation 4.8.

$$W_{c(pl)} = W_{tot} - \frac{C_0 \cdot F_c^2}{2} \qquad (4.8)$$

with C_0 = reciprocal of the initial elastic slope

The initial elastic slope is determined according to the ESIS draft on proposed standard methods for instrumented precracked Charpy impact testing of steels.

Acceptable force values F_c are obtained when the inertial oscillations have been sufficiently dampened, namely after 3 complete oscillations (3τ, with τ = period of force oscillation) [7−9]. J_c values are transformed into values of plain strain stress intensity factor K_{Jc} according to ASTM E1921-05 using Equation 4.9.

44

$$K_{Jc} = \sqrt{\frac{E \cdot J_c}{1 - \nu^2}}$$ (4.9)

The calculated K_{Jc} are used to evaluate the reference temperature T_0 following ASTM E1921-05.

Dynamic yield strength properties for the calculation of the validity limit K_{lim} should be evaluated according to:

$$\sigma_{yd} = \frac{4 \cdot F_{gy}}{C \cdot B_N (W - a_0)^2} \cdot \frac{S}{4} = \frac{C' \cdot F_{gy}}{B_N \cdot (W - a_0)^2} \cdot \frac{S}{4}$$ (4.10)

where:

a_0 initial crack length
C   constraint factor (C' = C/4); for precracked Charpy size SE(B): ISO-tup C' = 3.13; ASTM-tup C' = 2.98
F_{gy} force at general yield

Additional options available for estimating yield strength in case of elevated loading rates are described in Appendix IIC along with other comparisons of quasi-static and impact loading Master Curve results.

4.3.1. Master Curve results provided by the participants

Twelve organizations signed up for the round robin exercise; each of them received from JRC Petten 10 precracked and side-grooved Charpy specimens of JRQ material (plate 8JRQ44). Later, one of the participants pulled out due to the unavailability of the testing machine. Consequently, the round robin exercise counted eleven participants. Each participant sent in the results using the data reporting spreadsheets supplied by the topic area leaders.

Table 4.1 summarizes the original results of the Master Curve analyses provided by the round robin participants (number of specimens tested N, number of valid data r, sum of weighting factors $\sum n_i$, reference temperature T_0, standard deviation σ_{T0}, average loading rate dK/dt). For reference purposes, the Table 4.1 also reports the results obtained by FZD at quasi-static loading rate (1.2 MPa√m/s) on PCVN specimens of the same plate (8JRQ44).

Each participant tested 10 specimens; Laboratory 4 supplied only 8 valid results, due to a fault in the acquisition system. All participants provided valid reference temperatures ($\sum n_i \geq 1$); invalid tests ranged from a minimum of 0 to a maximum of 3.

TABLE 4.1. RESULTS SUPPLIED BY THE ROUND ROBIN EXERCISE PARTICIPANTS

Lab No.	N	r	$\sum n_i$	T_0 (°C)	σ_{T0} (°C)	dK/dt (MPa√m/s)
1	10	9	1.40	-2.3	6.0	3.51E+05
2	10	9	1.40	1.6	6.0	3.21E+05
3	10	7	1.12	-9.9	6.8	3.70E+05
4	8	8	1.18	10.0	6.6	4.14E+05
5	10	10	1.57	2.1	5.7	3.29E+05
6	10	9	1.32	4.6	6.0	3.44E+05
7	10	8	1.33	-20.4	6.4	2.69E+05
8	10	9	1.40	-1.1	6.0	3.36E+05
9	10	7	1.07	-2.5	6.8	4.25E+05
10	10	9	1.40	-3.8	6.0	5.02E+05
Average values			1.32	-2.2	6.2	3.66E+05
FZD	8	8	1.29	-71.4	6.4	1.2

T_0 values reported by participants range from -20.4 to 10.0°C, corresponding to a maximum difference of 30.4°C. The difference between dynamic (average value) and quasi-static reference temperature is 69.2°C. Individual Master Curves for RRE datasets are compared in Figure 4.3.
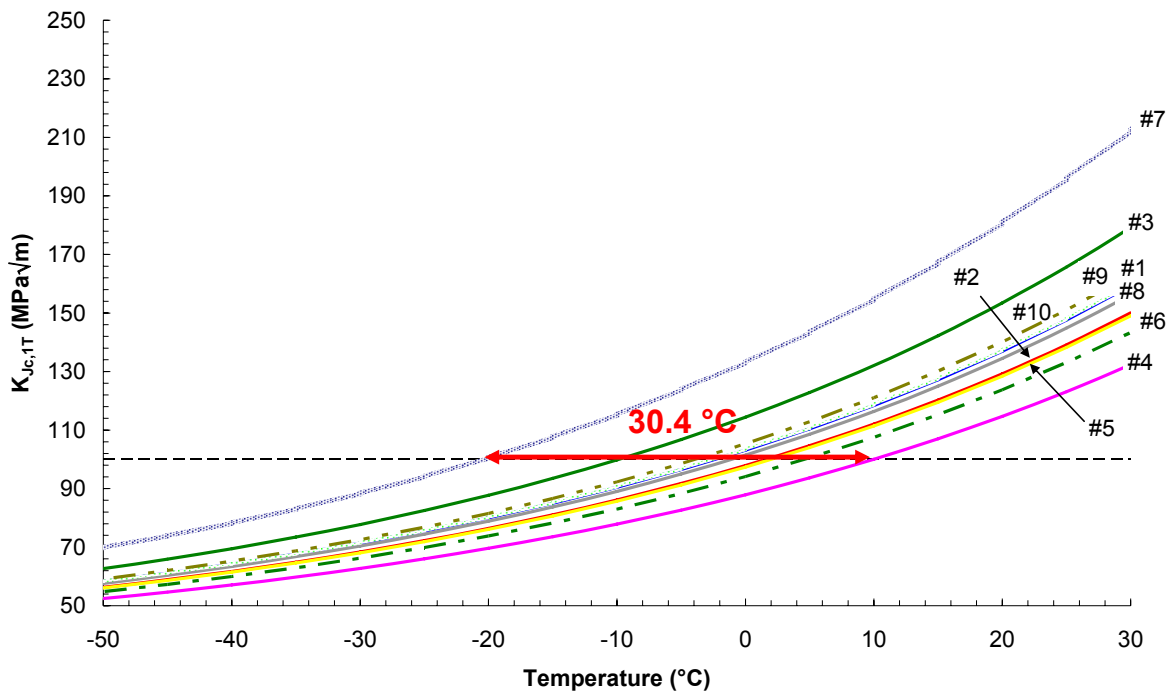
FIG. 4.3. Master Curves supplied by the round robin participants.

Individual K_{Jc} test results (normalized to 25 mm reference thickness), including quasi-static data, are plotted in Figure 4.4 as a function of the difference between test temperature and reference temperature reported by the corresponding lab ($T_{0, lab}$). This normalized representation shows that impact fracture toughness values measured in the round robin exercise effectively follow the Master Curve and its tolerance bounds.

An overall Master Curve analysis was performed on the individual K_{Jc} values supplied by the participants (98 data points; 85 valid). The results are shown in Table 4.2 and Figure 4.5. The increase with respect to the quasi-static value (-71.4°C) is now 67.2°C.

TABLE 4.2. RESULTS OF THE OVERALL MASTER CURVE ANALYSIS PERFORMED ON THE ROUND ROBIN DATASET

N	r	$\sum n_i$	T_0 (°C)	σ_{T0} (°C)
98	85	13.21	-4.2	2.0
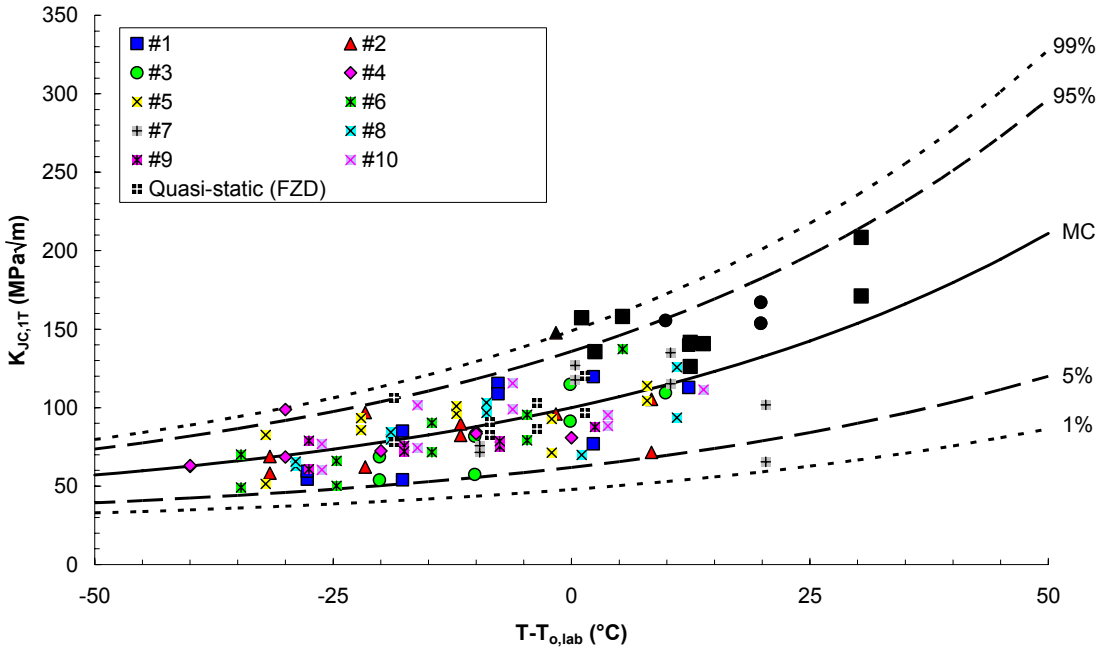
FIG. 4.4. Normalized fracture toughness values measured in the round robin exercise compared to the Master Curve and its tolerance bounds. Black symbols represent invalid (censored) data. Quasi-static data measured by FZD are also included.
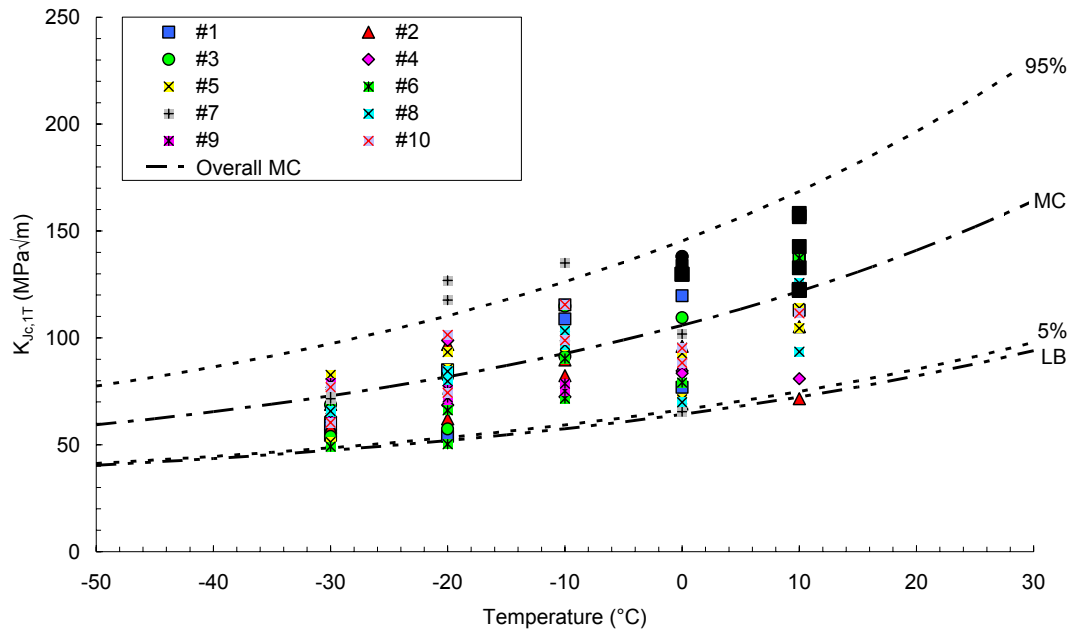
FIG. 4.5. Overall Master Curve analysis of the round robin dataset (with 5%–95% tolerance bounds and margin-adjusted 5% tolerance bound). Black symbols represent invalid (censored) data.

Individual T_0 values supplied by the participants, with $\pm 2\sigma$ error bars, are compared in Figure 4.6 with the result of the overall analysis ($T_{0, \, all} \pm 2\sigma$).
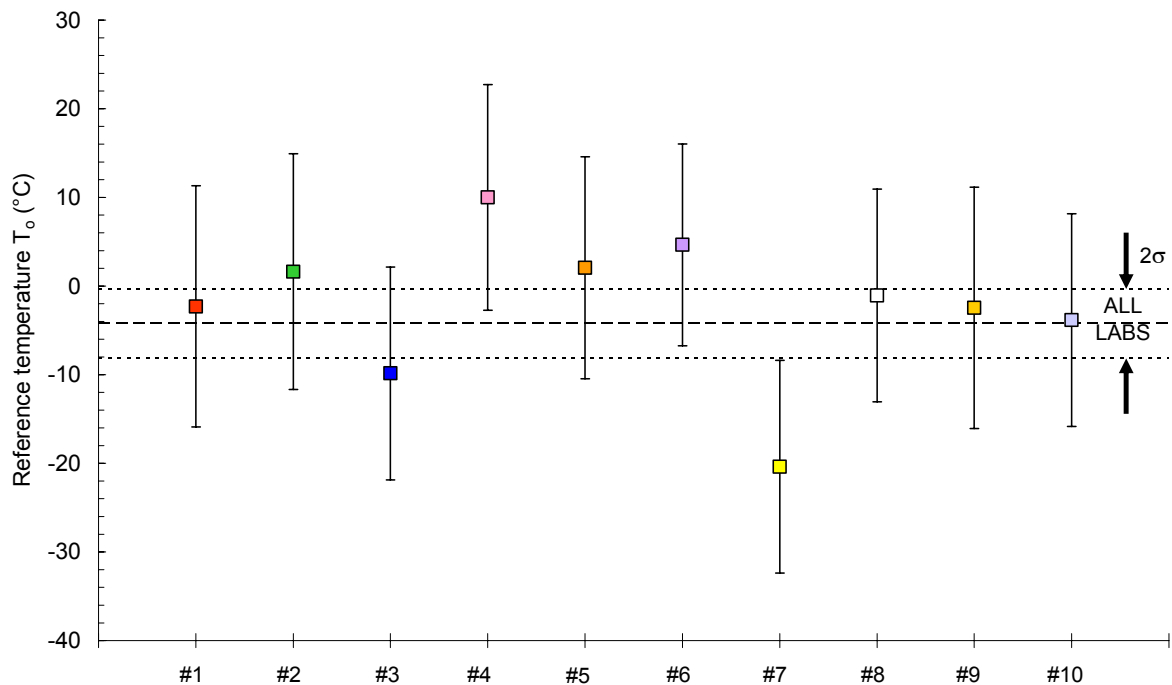
FIG. 4.6. Comparison between individual and overall Master Curve reference temperatures with $\pm 2\sigma$ error bars.

It is noted that for one dataset (Laboratory 7), the error bars do not overlap with the 95% confidence interval around $T_{0, \, all}$. Furthermore, examination of Figures 4.3 and 4.5 shows that

Laboratory 7 has supplied data which fall way above the general trend and could therefore be considered potential outliers (K_{Jc} values too high, T_0 too low).

If this dataset is excluded, the maximum difference between individual reference temperature drops to 19.8°C; the results of the updated overall Master Curve analysis are shown in Table 4.3 and Figure 4.7. Figure 4.8 also shows that, after removing the potential outlier, the error bands of all remaining datasets do overlap with the overall analysis. Furthermore, it can be noted that the lowest and the highest reference temperatures (from Laboratories 3 and 4, respectively) are not statistically different at the 95% ($\pm 2\sigma$) confidence level.

More detailed investigations, which confirm the nature of the outlier dataset, are presented in Appendix IIE.

TABLE 4.3. RESULTS OF THE UPDATED OVERALL MASTER CURVE ANALYSIS AFTER EXCLUDING DATA FROM LABORATORY 7

N	r	$\sum n_i$	T_0 (°C)	σ_{T0} (°C)	dK/dt (MPa√m/s)
88	77	11.98	-0.8	2.1	3.77E+05
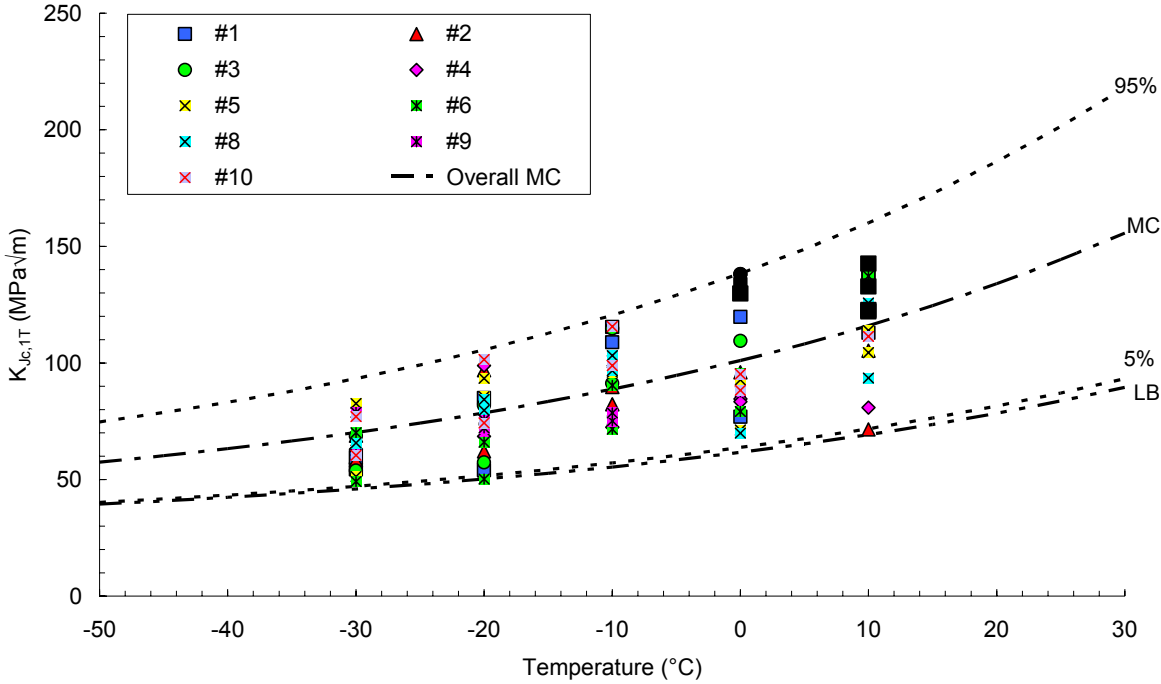
FIG. 4.7. Overall updated Master Curve analysis of the round robin dataset after excluding data from Laboratory 7. Black data points represent invalid (censored) data.
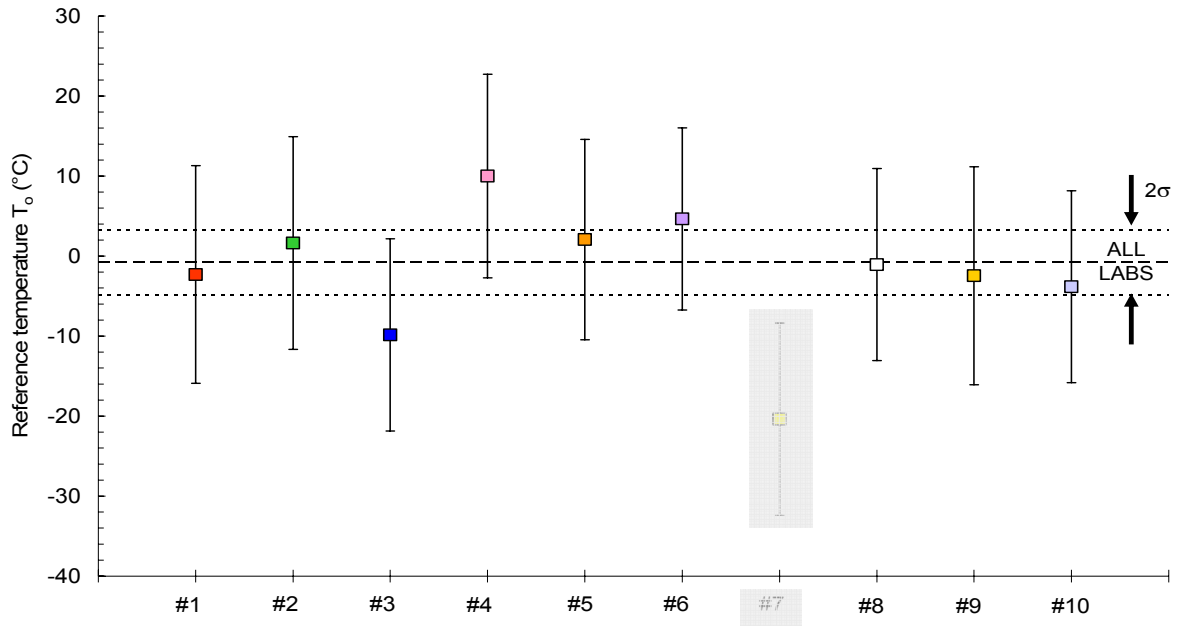
FIG. 4.8. Comparison between individual and overall Master Curve reference temperatures after removing data from Laboratory 7.

4.3.2. Common re-evaluation of the RRE datasets

In order to investigate the influence of possible subjective interpretations of the analysis method, all individual test results were re-analysed by Forschungszentrum Dresden-Rossendorf (FZR) in strict accordance with the guidelines given in §4.3.1. Re-analysis consisted in re-evaluating all individual K_{Jc} results (on the basis of original time, displacement and force data supplied by participants) and re-calculating individual T_0 values according to ASTM E1921-05.

The re-analysis was conducted using two different approaches for the evaluation of the elastic and plastic components of the energy absorbed up to cleavage (and therefore, of the J-integral):

(a) using the fitted slope of the initial elastic portion of the force/displacement record;
(b) using the theoretical compliance C_o, calculated as the sum of the specimen compliance C_S (obtained by FZD using FEM for a precracked Charpy specimen with a/W = 0.5) and the machine compliance C_M, which was requested to each participant as one of the input data.

Re-evaluated T_0 using the two approaches are compared to original values in Table 4.4. In the case of approach (b), T_0 could be re-evaluated only for those participants who provided their machine compliance in the Test Report form (6 out of 10).

Variations up to 19.4°C (Laboratory 10) for approach (a) and up to 13.3°C (Laboratory 3) for approach (b) were obtained; in most cases, variations are of the same order of magnitude as the standard deviations σ_{T0} or lower. In general, recalculated T_0 were found to be slightly higher than the original submissions (average differences = 4.2 and 4.7°C for the two approaches respectively). Such variations should not be attributed to the Master Curve calculations (which were carried out using the same EXCEL97 subroutine for all

participants), but to differences in the calculation of individual K_{Jc} values based on the original time/displacement/force data supplied by the participants.

Again, the reference temperature obtained by FZD at quasi-static strain rates is indicated in Table 4.4. The dynamic increase of T_0 is now 73.4°C using the measured compliance and 76.6°C using the theoretical compliance.

TABLE 4.4. COMPARISON BETWEEN ORIGINAL ($T_{0, or}$) AND RE-CALCULATED ($T_{0, re}$) USING APPROACHES (a) AND (b) VALUES

Lab No.	$T_{0, or}$ (°C)	$T_{0, re(a)}$ (°C)	$T_{0, re(a)} - T_{0, or}$ (°C)	$T_{0, re(b)}$ (°C)	$T_{0, re(b)} - T_{0, or}$ (°C)
1	-2.3	3.5	5.8	6.5	8.8
2	1.6	3.7	2.1	-0.5	-2.1
3	-9.9	-5.2	4.7	3.4	13.3
4	10.0	1.6	-8.4	3.0	-8.4
5	2.1	1.7	-0.4	-	-
6	4.6	11.8	7.2	8.5	3.9
7	-20.4	-22.3	-1.9	-	-
8	-1.1	-1.3	-0.2	-	-
9	-2.5	11.3	13.8	10.2	12.7
10	-3.8	15.6	19.4	-	-
Average	-2.2	2.0	4.2	5.2	7.4
Quasi-static loading rate (FZD tests) T_0 = -71.4°C					

After re-analysis according to approach (a), the maximum difference between individual T_0 values increases from 30.4 to 37.9°C (Figure 4.9). A normalized representation of the re-analysed dataset, using the differences between test temperatures and recalculated T_0, is given in Figure 4.10 (including quasi-static data). These and the following analyses cannot be repeated for approach (b) since the theoretical compliance is not available for all participants.
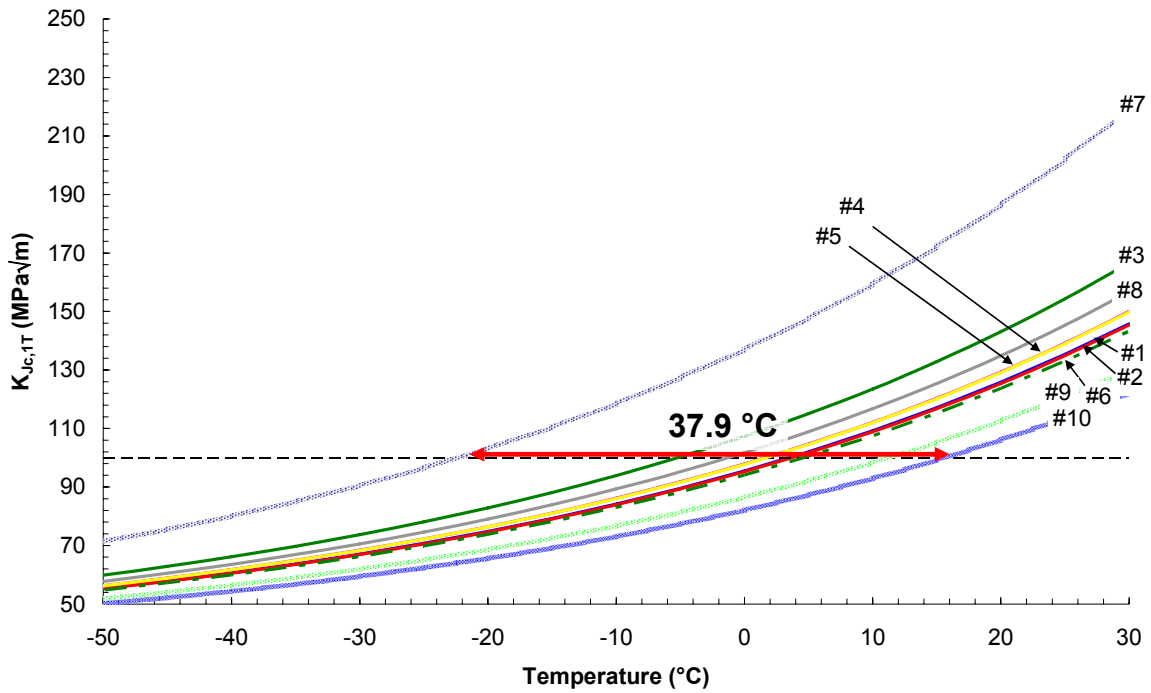
FIG. 4.9. Individual Master Curves for round robin participants after re-analysis by FZD.
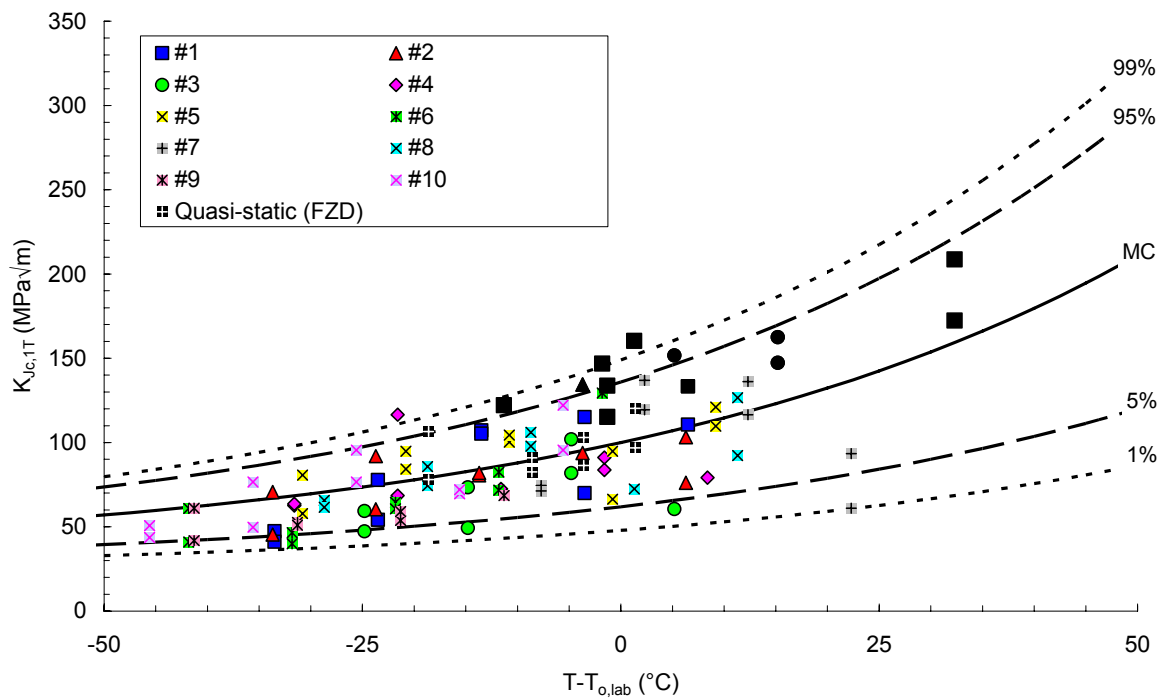
FIG. 4.10. Normalized fracture toughness values measured in the round robin exercise after re-analysis by FZD. Black symbols represent invalid (censored) data.

Results of the overall Master Curve analysis of the re-analysed dataset are provided in Table 4.5 and Figure 4.11. The overall reference temperature slightly increases (-2.3°C).

52

TABLE 4.5. RESULTS OF THE OVERALL MASTER CURVE ANALYSIS PERFORMED
ON THE ROUND ROBIN DATASET AFTER RE-ANALYSIS BY FZD

N	r	$\sum n_i$	T_0 (°C)	σ_{T0} (°C)
98	87	13.55	-2.3	1.9
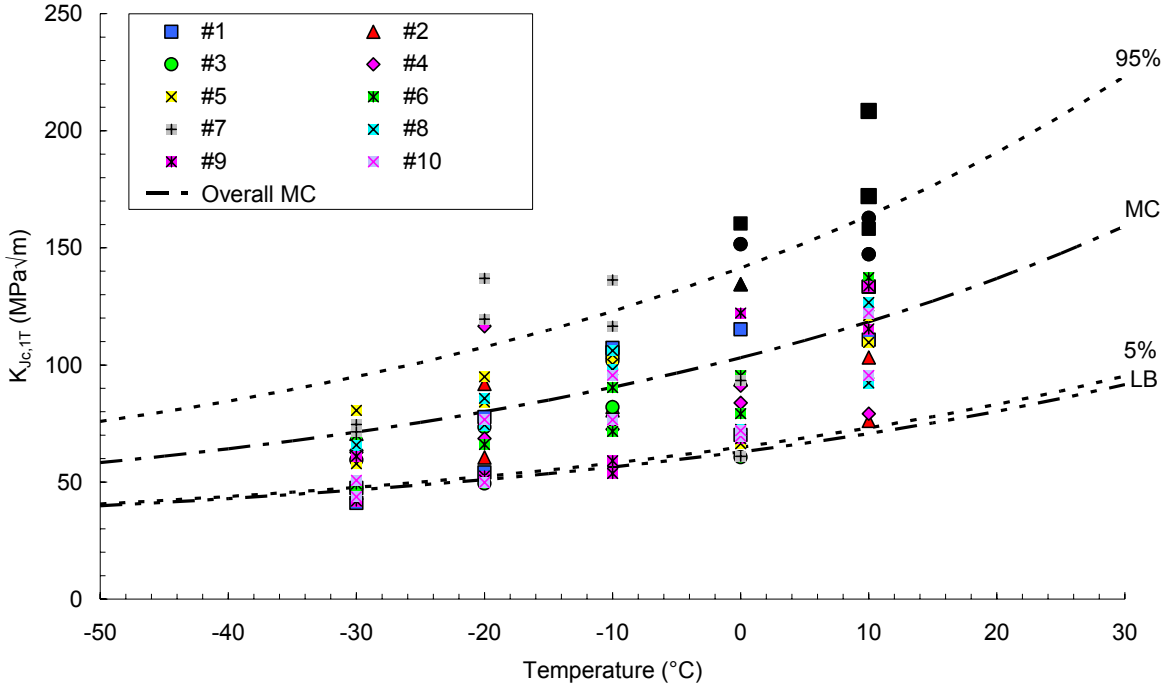
*FIG. 4.11. Overall Master Curve analysis of the round robin dataset,
after re-analysis by FZD.*

Re-calculated T_0 values, with ±2σ error bars, are compared in Figure 4.12 to the outcome of
the overall Master Curve analysis.

Even after re-analysis, the potential outlier nature of Laboratory 7 is confirmed.
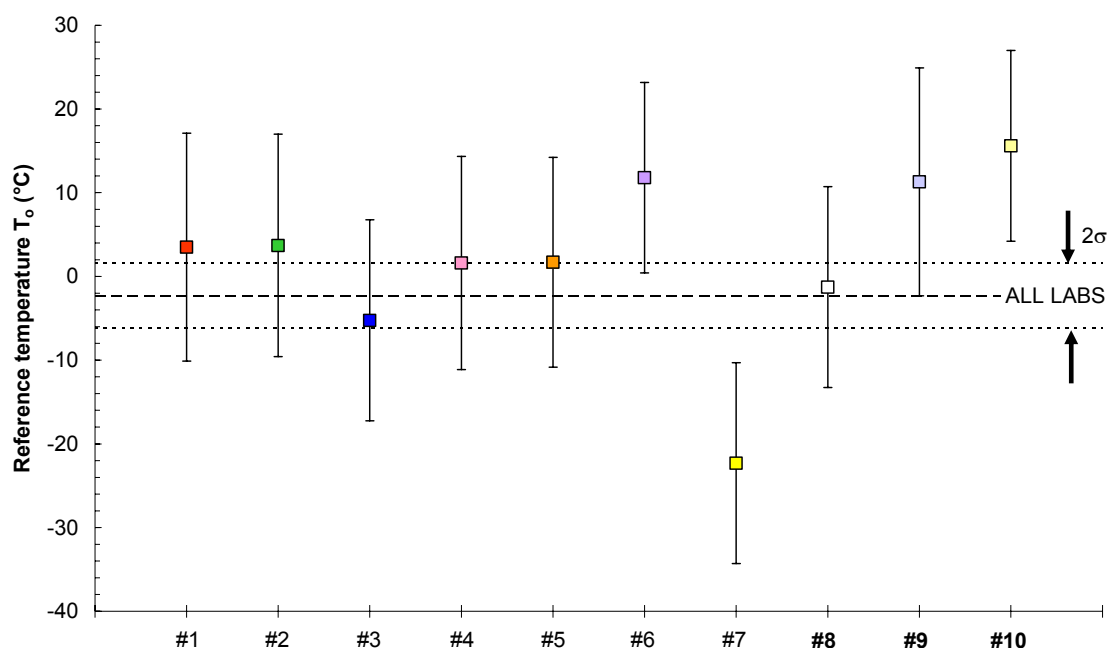
FIG. 4.12. Comparison between individual and overall Master Curve reference temperatures ($T_0 \pm 2\sigma$) after re-analysis by FZD.

4.3.3. *Influence of impact striker radius on the reference temperature*

Approximately one third of the RRE participating laboratories (Laboratories 3, 8 and 10) used an instrumented striker conforming to the ASTM E23 standard, that is with a tup radius of 8 mm. The remaining seven laboratories used a 2 mm striker, i.e. conforming to the ISO 148 standard.

The values of Master Curve reference temperature obtained by the individual laboratories allow assessing a possible influence of striker radius on the results of impact toughness testing. Note that Laboratory 7 is not included in this assessment.

Using the original T_0 and K_{Jc} values reported by participants, the assessment is given in Figure 4.13 (T_0 vs. striker radius) and Figure 4.14 (comparison between Master Curves obtained by separately analysing 2 mm and 8 mm striker data). The corresponding analyses on RRE data re-analysed by FZD (§4.3.2) are shown in Figures 4.15 and 4.16.
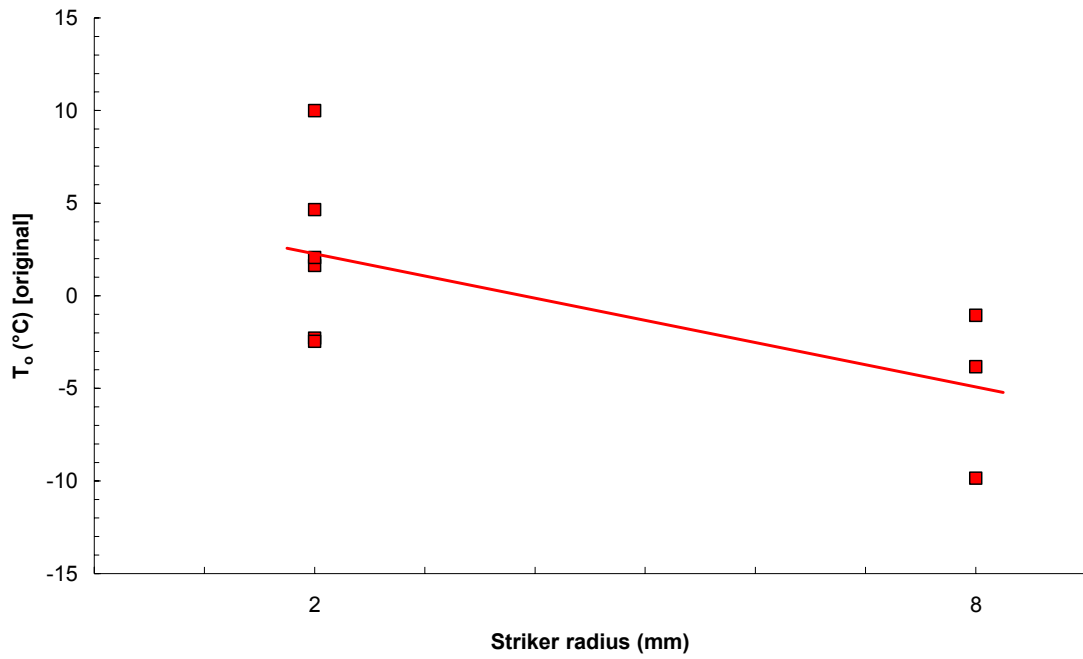
FIG. 4.13. Influence of striker radius on T_0 (original RRE submissions).
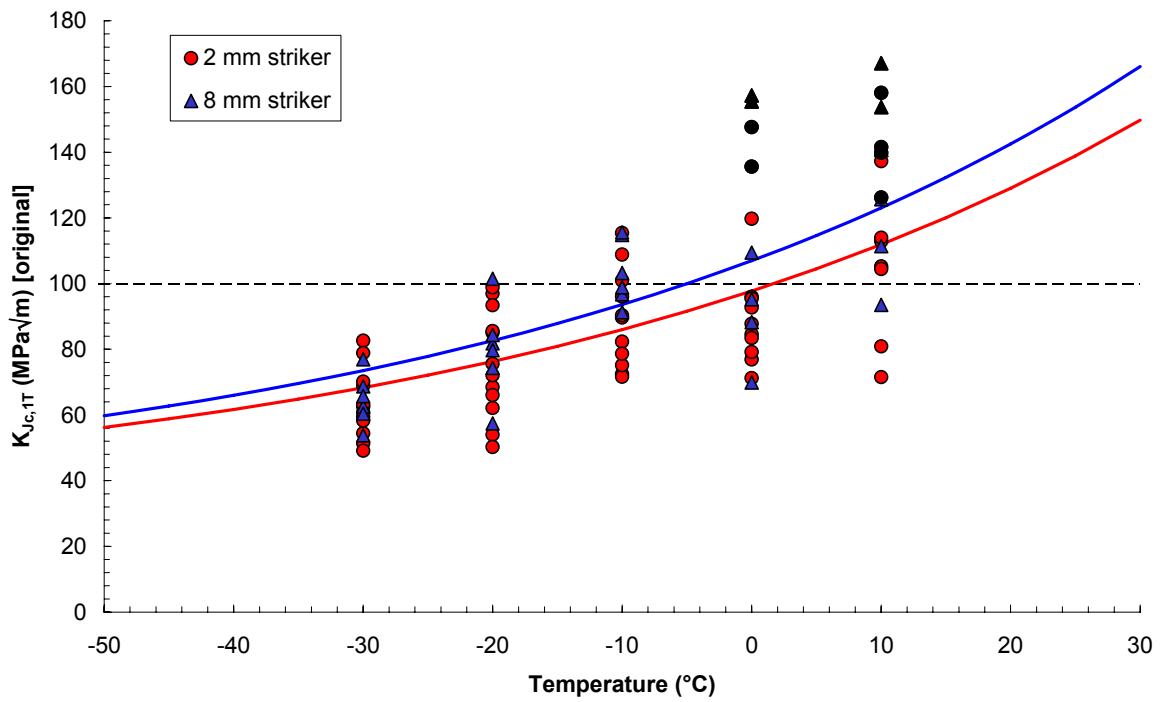
FIG. 4.14. Master Curves obtained from 2 mm and 8 mm striker test results (original RRE submissions). Black symbols are invalid (censored) data.
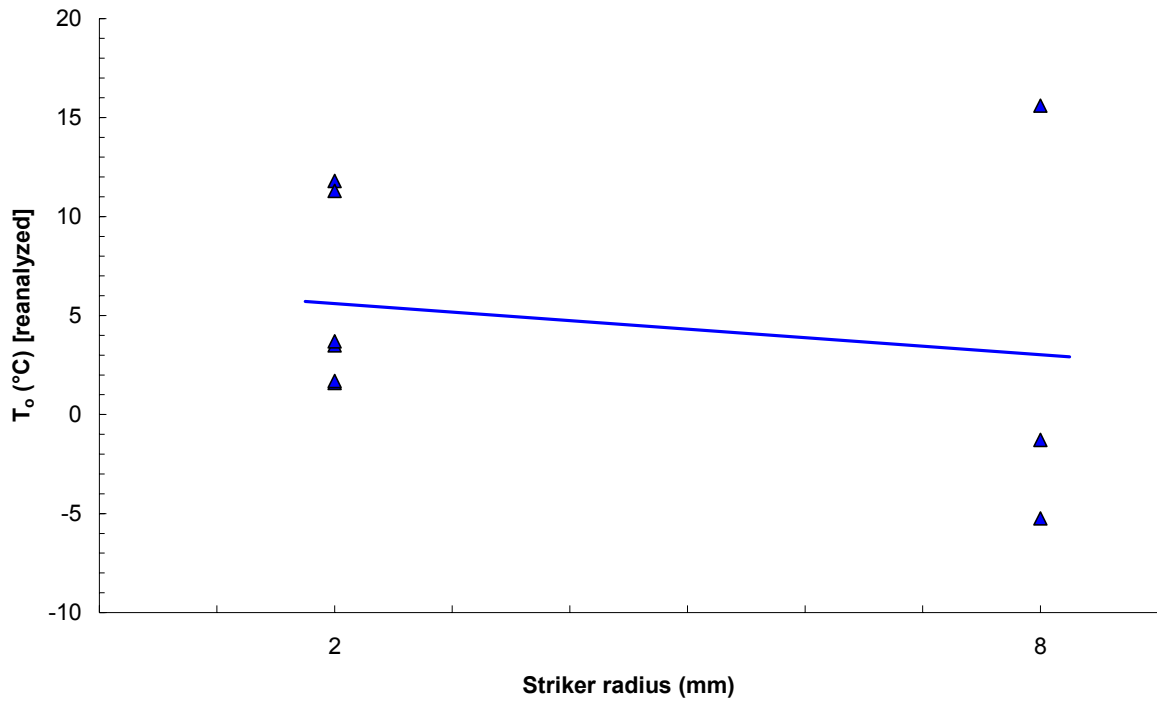
FIG. 4.15. Influence of striker radius on T_0 (RRE data re-analysed by FZD).
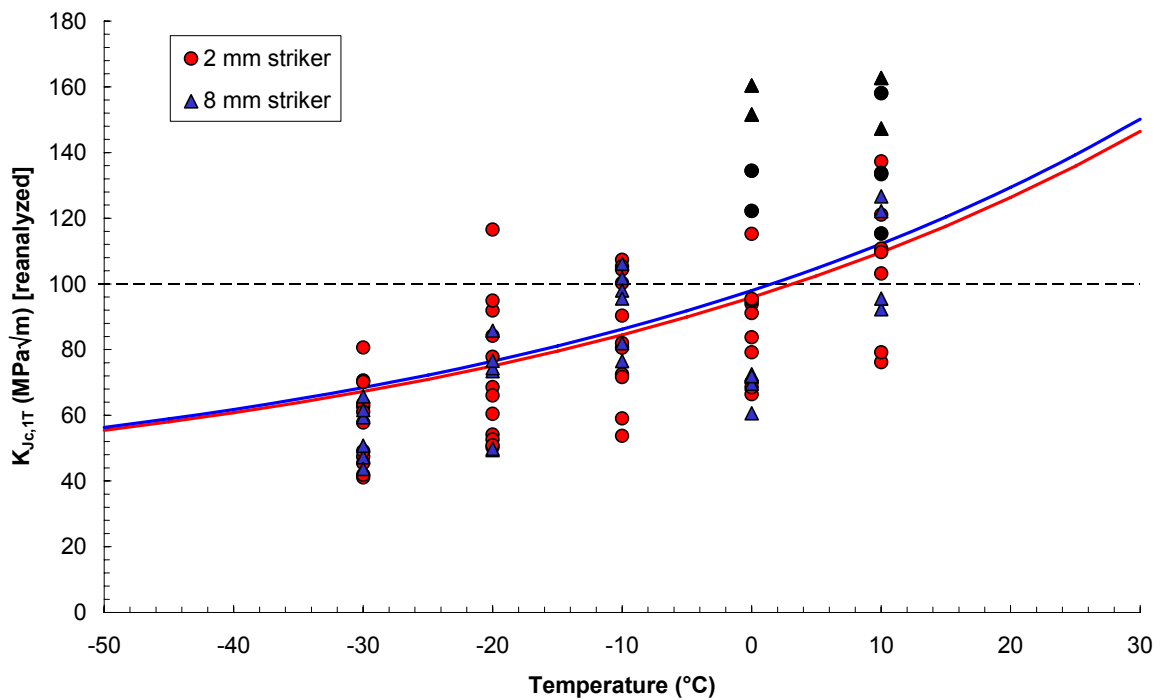
FIG. 4.16. Master Curves obtained from 2 mm and 8 mm striker test results (RRE data re-analysed by FZD). Black symbols are invalid (censored) data.

Original RRE data show a decrease of T_0 with striker radius, but if re-analysed data are considered the effect becomes negligible (see also the Master Curves in Figure 4.16).

However, when considering overall reference temperatures with $\pm 2\sigma$ ($\pm 95\%$) confidence limits (Table 4.6), T_0 values from both strikers are statistically undistinguishable.

TABLE 4.6. RESULTS OF OVERALL MASTER CURVE ANALYSES ON 2 MM AND 8 MM STRIKER DATA, USING ORIGINAL AND RE-ANALYSED RRE DATA

RRE data	Striker radius (mm)	No. of labs	T_0 (°C)	σ_{T0} (°C)
Original	2	6	1.7	2.5
	8	3	-5.0	3.6
Re-analysed	2	6	3.2	2.5
	8	3	1.5	3.6

4.3.4. Conclusions from the round robin exercise

- Except for one laboratory (which appears to have force calibration problems), the results supplied by the participants are very consistent and show reasonable scatter.
- The Master Curve approach has proven to be fully applicable to impact fracture toughness measurements obtained in the ductile-to-brittle transition region.
- Despite the lack of an official test standard, the guidelines supplied to the participants for the execution and evaluation of the tests have proven to be reliable and can be easily implemented by the testing laboratories.
- The quality of impact fracture toughness measurements strongly depends on the quality of force values. Hence, a reliable calibration of the instrumented striker is of primary importance.
- Although the JRQ material is known to be a fairly inhomogeneous material (particularly through the plate thickness), the results obtained from the round robin exercise are quite satisfactory and can be probably considered above expectations.
- The currently proposed requirement on the time to fracture ($t_f > 5\tau$, with τ = period of oscillation) appears too restrictive and can cause significant non-conservatism in the Master Curve analysis. A less stringent requirement ($t_f > 3\tau$) should be recommended.
- No clear influence of instrumented striker radius (2 mm vs. 8 mm) on impact toughness results has been detected.

4.3.5. Force interlaboratory comparison using ERM specimens

As previously stated, the RRE results had shown the existence of an outlier laboratory (No. 7); the most likely cause appeared to be an incorrect calibration of the instrumented striker, which provided excessively high force values (Figures 4.9 to 4.12).

It was therefore decided to perform an interlaboratory comparison (ILC) among the RRE participants based on general yield (F_{gy}) and maximum (F_m) force measurements, using ERM (European Reference Materials) Charpy-V specimens from the high energy level (KV ~ 150 J) supplied by the Institute for Reference Materials and Measurements (IRMM) in Geel, Belgium. The specimens were purchased and distributed to all participating laboratories by EC-JRC; each laboratory received two ERM specimens to be tested in as-received condition using the same pendulum machine and instrumented striker used for the RRE and full impact velocity (i.e. 5–5.5 m/s).

Instrumented force measurements were returned by 9 of the 10 institutes which took part in the RRE. Laboratory 6 was unable to provide data since the machine used for the RRE was a small-capacity 80 J pendulum which cannot be used to test ERM high energy specimens. Laboratory 7 tested 4 specimens instead of 2.

For each one of the 20 instrumented tests performed, the following information was provided:

- force at general yield, F_{gy};
- maximum force, F_m;
- absorbed energies KV (encoder or dial reading) and W_t (integrated).

The availability of the two latter values (KV and W_t) allowed investigating the so-called dynamic force correction approach, which consists in adjusting force and deflection values until absorbed energies from the pendulum encoder (KV) and under the instrumented test record (W_t) are equal [9].

The most accurate way to apply this procedure is by iteratively correcting force values until KV = W_t, since deflections are calculated from time and force measurements, as well as using the pendulum mass and the initial impact velocity. However, in a first approximation forces can be adjusted by simply using the ratio KV/W_t as a correction factor. Within this ILC, reported values of F_{gy} and F_m have been corrected using the accurate procedure mentioned above, with the exception of Laboratory 8, which did not provide raw force/time data; in this case, the approximate procedure was employed. The aim was to verify whether the interlaboratory consistency improved or became worse.

Table 4.7 reports the original ILC results in terms of force and absorbed energy values. Figures 4.17 and 4.18 show the original (uncorrected) data provided by the participants for F_{gy} and F_m respectively. Significant scatter is observed; the standard deviations are 10.5% for F_{gy} and 14.6% for F_m with respect to the mean values. Moreover, Laboratory 7 is confirmed as an outlier with force values which once again appear too high.

TABLE 4.7. ORIGINAL RESULTS OF THE ILC

Lab No.	Striker rad.(mm)	Spec. id	F_{gy} (kN)	F_m (kN)	KV (J)	W_t (J)
1	2	16	17.95	22.80	151.70	152.10
		17	17.69	22.93	145.20	145.60
		Mean	17.82	22.86	148.45	148.85
2	2	6	16.29	22.72	160.01	156.54
		7	16.45	22.80	157.21	153.13
		Mean	16.37	22.76	158.61	154.84
3	8	18	19.56	25.47	136.30	139.88
		21	19.35	25.55	137.80	139.70
		Mean	19.46	25.51	137.05	139.79
4	2	19	18.97	26.07	150.30	163.69
		20	18.94	26.00	157.10	172.76
		Mean	18.96	26.04	153.70	168.23
5	2	8	18.61	23.98	149.20	148.10
		27	19.89	23.92	145.10	143.90
		Mean	19.25	23.95	147.15	146.00
7	2	1	22.52	32.21	168.19	203.12
		3	22.65	31.95	162.12	194.68
		4	22.25	31.90	159.70	192.74
		5	22.32	31.59	153.50	186.81
		Mean	22.44	31.91	160.88	194.34
8	8	23	20.02	23.14	139.65	134.04
		25	19.25	23.21	145.07	141.82
		Mean	19.64	23.18	142.36	137.93
9	2	22	16.65	20.54	149.70	130.09
		24	16.63	20.38	150.56	129.82
		Mean	16.64	20.46	150.13	129.95
10	8	10	18.95	25.94	134.36	140.33
		26	19.08	26.01	142.63	146.29
		Mean	16.64	20.46	150.13	129.95
Average values			19.20	25.46	149.77	155.76
Standard deviation (abs)			2.01	3.71	9.19	22.48
Standard deviation (%)			10.5%	14.6%	6.1%	14.4%
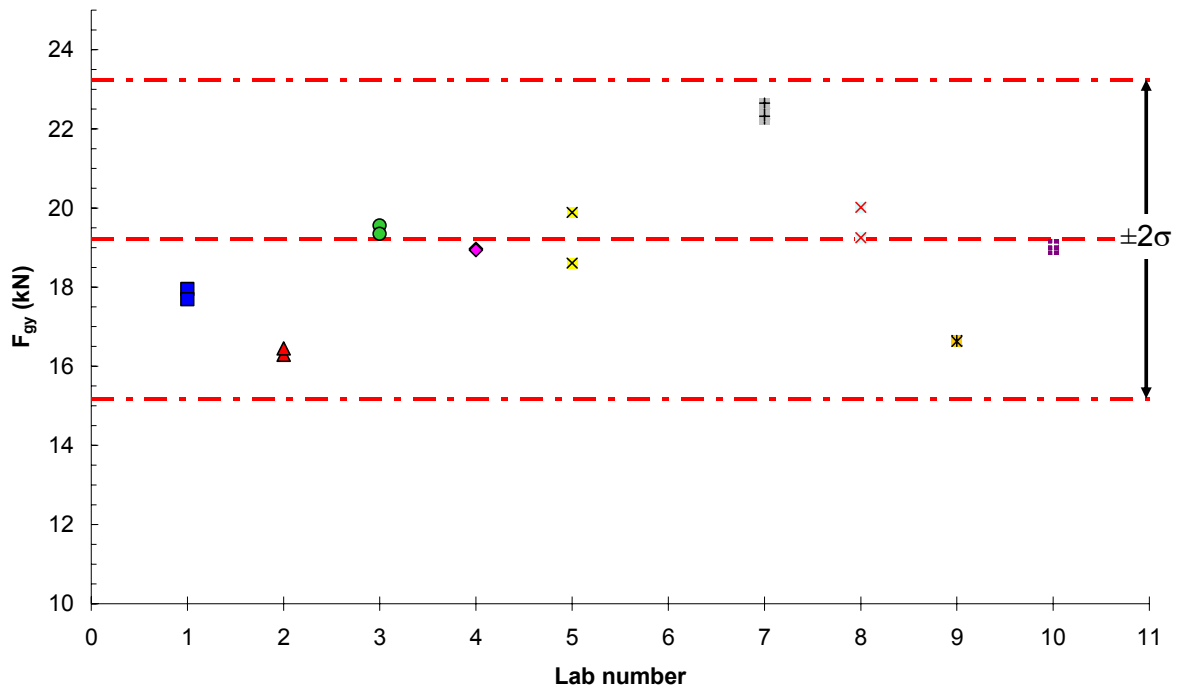
FIG. 4.17. Original values of force at general yield returned by ILC participants.
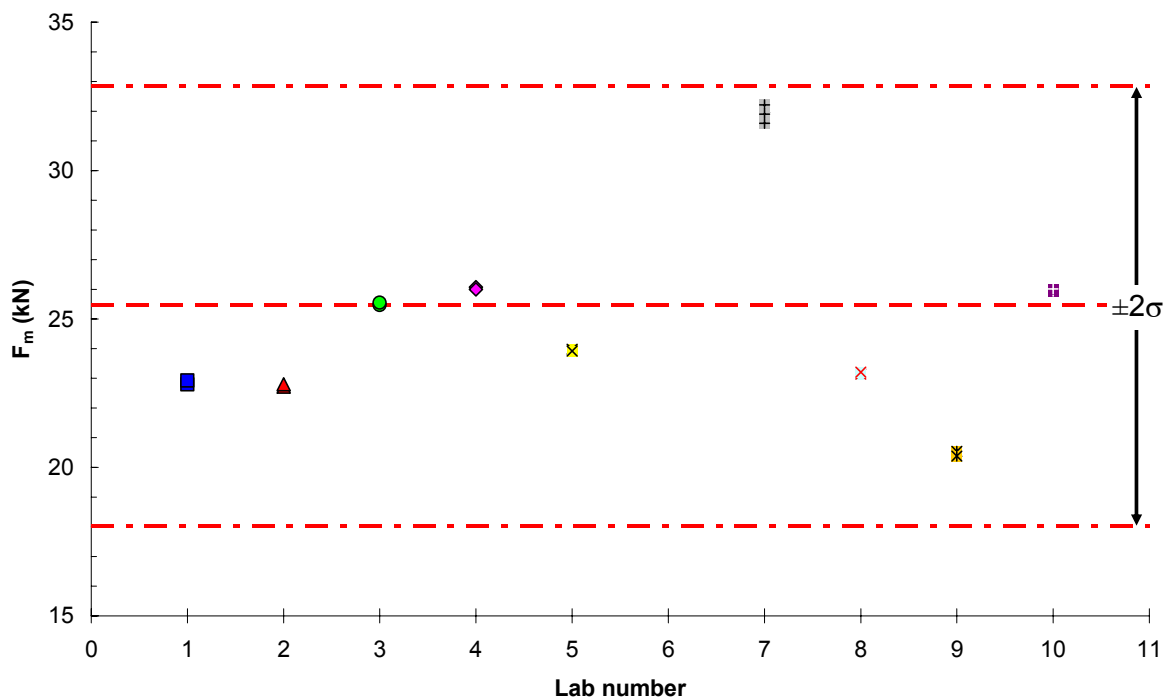
FIG. 4.18. Original values of maximum force returned by ILC participants.

As previously stated, the dynamic force correction approach was applied to the original ILC results.

The corrected ILC results are provided in Table 4.8, in terms of correction factor and instrumented force values.

TABLE 4.8. CORRECTED ILC RESULTS

Lab No.	Spec. id	Corr. factor	F_{gy} (kN)	F_m (kN)
1	16	0.990	17.77	22.57
	17	0.993	17.58	22.77
	Mean		17.68	22.67
2	6	1.028	16.75	23.37
	7	1.034	17.01	23.57
	Mean		16.88	23.47
3	18	0.951	18.60	24.22
	21	0.965	18.68	24.67
	Mean		18.64	24.44
4	19	0.902	17.11	23.52
	20	0.892	16.89	23.19
	Mean		17.00	23.35
5	8	1.010	18.79	24.21
	27	1.011	20.11	24.19
	Mean		19.45	24.20
7	1	0.760	17.12	24.49
	3	0.772	17.49	24.67
	4	0.767	17.06	24.46
	5	0.759	16.94	23.98
	Mean		17.15	24.40
8	23	1.042	20.86	24.11
	25	1.023	19.69	23.74
	Mean		20.27	23.93
9	22	1.135	18.89	23.31
	24	1.142	18.98	23.27
	Mean		18.94	23.29
10	10	0.951	18.02	24.67
	26	0.971	18.52	25.25
	Mean		18.27	24.96
Average values			18.14	23.91
Standard deviation (abs)			1.18	0.70
Standard deviation (%)			6.5%	2.9%

The effect is beneficial for the force at general yield (Figure 4.19), where the standard deviation decreases from 10.5% to 6.5%, and very beneficial for the maximum force (Figure 4.20), where the standard deviation drops from 14.6% to just 2.9%. In both cases, the anomaly represented by Laboratory 7 practically disappears.
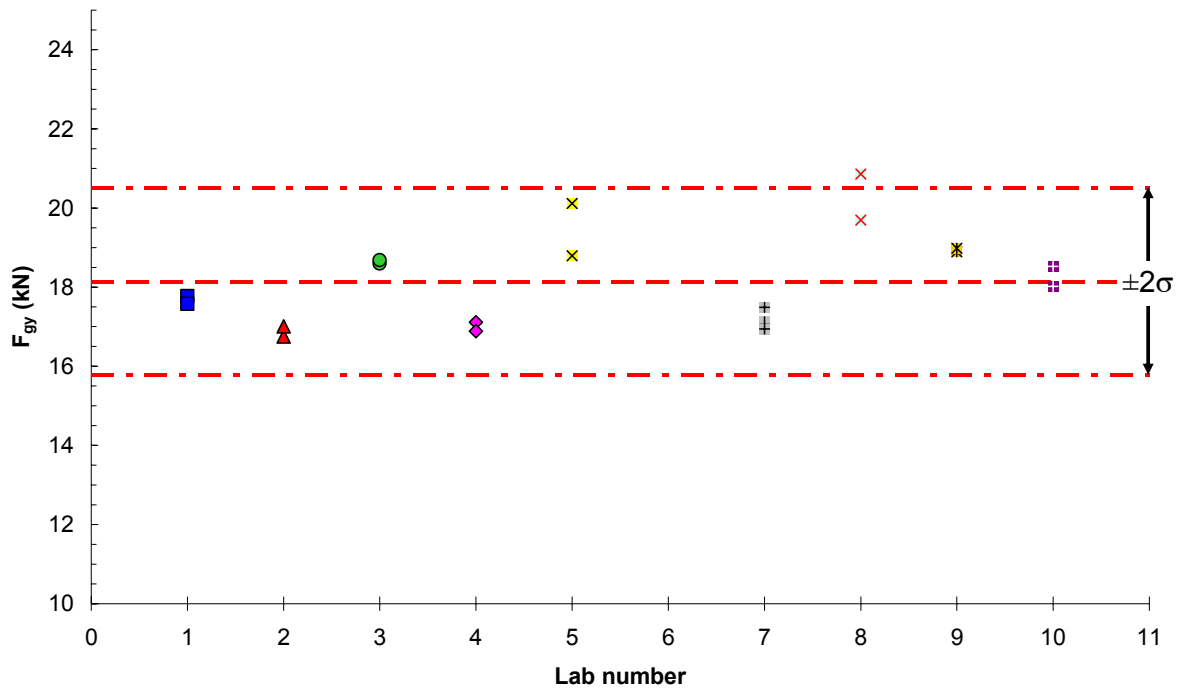
FIG. 4.19. Values of F_{gy} after dynamic force correction.
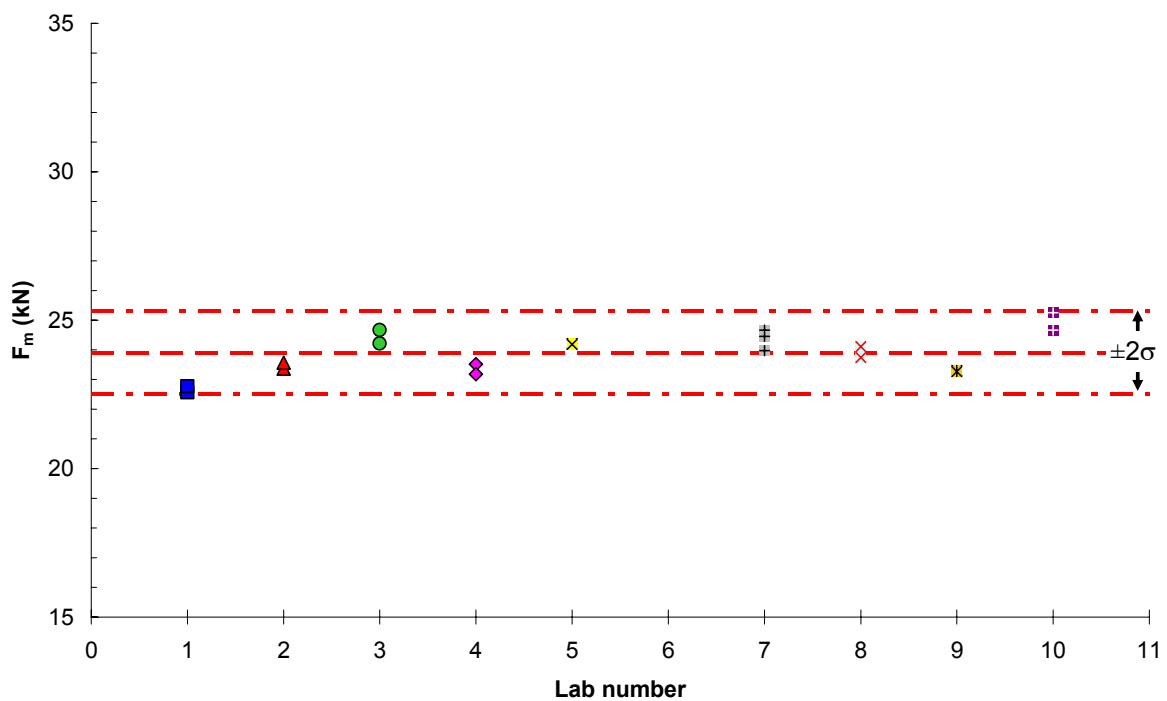
FIG. 4.20. Values of F_m after dynamic force correction.

It could somehow be expected that the dynamic force correction would have a more significant effect on F_{gy} than on F_m, since the former parameter has an intrinsic higher dispersion due to the subjectivity of its determination with respect to the maximum force.

4.3.6. *Conclusions from the interlaboratory comparison*

- The original results provided by the ILC participants show considerable scatter: Standard deviation is 10.5% for F_{gy} and 14.6% for F_m.
- Laboratory 7 confirms its nature of potential outlier.
- The influence of striker radius (2 mm vs. 8 mm) cannot be unambiguously resolved, due to the presence of only three laboratories using 8 mm strikers.
- After applying the dynamic force correction to the original data, the following is observed:

  o the standard deviation is considerably reduced (to 6.5% for F_{gy} and 2.9% for F_m);
  o the within-laboratory consistency (*k* statistics) remains substantially acceptable;
  o the between-laboratory consistency (*h* statistics) is somewhat improved, particularly in the case of Laboratory 7.

4.4. CONCLUSIONS AND RECOMMENDATIONS FOR FUTURE WORK

4.4.1. *Conclusions*

The Master Curve reference temperature T_0 is reasonably constant within the quasi-static range of loading rates as defined by ASTM E1921-05(08), i.e. between 0.1 and 2 MPa√m/s. For higher loading rates, T_0 increases steadily with dK/dt and the rate of increase (loading rate sensitivity) decreases with with increasing quasi-static T_0 and appears poorly correlated to the yield strength of the material. Below 0.1 MPa√m/s, Wallin's empirical model provides reasonable and useful predictions of the variation of T_0 as a function of loading rate.

The RRE conducted within CRP-8 has demonstrated the full applicability of the Master Curve approach to impact fracture toughness measurements obtained in the dutcile-to-brittle transition regime. The guidelines provided by the future ISO/ASTM standards for test execution and data analysis have proven to be reliable and easy to implement; the test method appears mature enough to be implemented into official standards. Reliable calibration of the instrumented impact striker is a key issue, and the dynamic adjustment based on the equalization of dial and integrated energies has proven very helpful in reducing scatter and improving the between-laboratory consistency. The shape of the instrumented striker (2 mm or 8 mm radius) seems to have negligible influence on the measured T_0.

4.4.2. *Recommendations for future work*

The influence of loading rate on T_0 could be further investigated by significantly enlarging the available experimental basis with results contained in large databases such as the one currently mantained by EPRI.

The usefulness of performing fracture toughness measurements at loading rates higher than quasi-static for RPV assessments could be emphasized by establishing correlations between crack arrest toughness (K_{Ia}) and dynamic/impact fracture toughness (K_{Id}), namely:

- by comparing the ASME KIR lower bound curve to lower bound Master Curves (corresponding to low fracture probabilities) obtained from dynamic/impact toughness measurements;
- by determining an equivalent dynamic RT_{T0} (similar to the quasi-static one in ASME Code Cases N-629 and N-631) for indexing the ASME lower bound KIR curve;

- definition of a threshold dynamic loading rate representative for the equivalent dynamic RT_{T0};
- by corroborating or revising the existing correlations (Wallin, Fabry, AREVA etc.) between instrumented Charpy arrest forces (Fa, T4kN etc.) and crack arrest parameters (K_{Ia}/NDT).

From an experimental point of view, this would imply:

- collecting and re-assessing the existing crack arrest and dynamic/impact fracture toughness data on a few well-characterized RPV steels (e.g. plate HSST-02);
- generating a limited amount of new crack arrest data on other relevant RPV steels, for which a large database of dynamic fracture toughness data is available (e.g. JRQ);
- generating new dynamic/impact fracture toughness data (K_{Id}, $T_{0, dyn}$) for some or all the selected materials.

4.5. REFERENCES

[1] WALLIN, K., "Summary of the IAEA/CRP3 Fracture Mechanical Results", Proceedings IAEA Specialists Meeting, IAEA working material, Espoo (1999).

[2] JOYCE, J.A., On the Utilization of High Rate Pre-Cracked Charpy Test Results and the Master Curve to Obtain Accurate Lower Bound Toughness Predictions in the Ductile-To-Brittle Transition, ASTM STP 1329, Small Specimen Test Techniques, ASTM, Philadelphia (1998) 253–273.

[3] TREGONING, R.L., JOYCE, J.A., "Investigation of censoring limits for cleavage fracture determination", Fourth Symposium on Small Specimen Test Techniques, ASTM, West Conshohocken (2002).

[4] WALLIN, K., Effect of Strain Rate on the Fracture Toughness Reference Temperature T_0 for Ferritic Steels, Recent Advances in Fracture, the Minerals, Metals & Materials Society (1997).

[5] HALL, J.B., YOON, K.K., "Quasi-static loading rate effect on the master curve reference temperature of ferritic steels and implications", Proceedings of the ASME Pressure Vessels and Piping Conference, Cleveland (2003).

[6] JOYCE, J.A., TREGONING, R.L., ROE, C., On setting testing rate limitations for the master curve reference temperature, T_0, ASTM E 1921, Journal of Testing and Evaluation **34** 2 (2006).

[7] MCCORNELL, P., SERVER, W.L., "EPRI instrumented impact test procedures", Proceedings C.S.N.I. Specialists Meeting on Instrumented Precracked Charpy Testing, EPRI NP-2102-LD, Palo Alto (1980) 1-1–1-22.

[8] IRELAND, D.R., "A review of the proposed standard method of test for impact testing precracked Charpy specimen of metallic materials", Proceedings C.S.N.I. Specialists Meeting on Instrumented Precracked Charpy Testing, EPRI NP-2102-LD, Palo Alto (1980) 1-23–1-63.

[9] LUCON, E., Dynamic Toughness Testing of Pre-Cracked Charpy V-Notch Specimens, BLG-808, SCK-CEN, Mol (1999).

[10] VIEHRIG, H.-W., BÖHMERT, J., DZUGAN, J., Use of Instrumented Charpy Impact Tests for the Determination of Fracture Toughness Values, From Charpy to Present Impact Testing, ESIS-Publication 30, Elsevier Science Ltd. and ESIS (2002) 245.

5. MASTER CURVE SHAPE

5.1. BACKGROUND

The Master Curve methodology is based on a cleavage fracture model that assumes randomly distributed fracture initiators in a macroscopically homogeneous matrix. The generic form assumed for the fracture toughness vs. temperature function makes the MC model universal for practically all ferritic steels, provided the basic assumptions of the model are satisfied. Substantial empirical evidence has been collected that demonstrates this generality. Recent efforts have also documented a physical basis for the MC methodology [1]. As global utilisation of the Master Curve methodology continues to expand its application is being extended to materials that approach the documented limits of applicability. Further research is needed to clarify the limits of applicability on materials where the basic assumptions of the Master Curve methodology are not fully satisfied. This knowledge will help to identify whether the model should be applied in its basic or some modified form or if it should be applied at all under certain conditions.

5.2. DEFINITION AND VERIFICATION OF TEMPERATURE DEPENDENCE

5.2.1. Original Master Curve shape definition

The transition curve definition for ferritic steels, as specified in ASTM E1921 [2], was originally derived in 1991 from data measured on various quenched and tempered structural steels [3]. The data was taken from different sources and included measurements on irradiated and unirradiated pressure vessel steels with the transition temperature (T_0) ranging from 109 to 36$^\mathrm{o}$C. After the statistical size correction of these data, which had been measured with different size specimens, the curve shape (K_0 vs. temperature) was determined from the maximum likelihood fit to the data (see Figure 5.1). The determined good fit was then proposed for a universal functional form of the temperature dependence of fracture toughness in the transition region and, afterwards, it was included in ASTM E1921.

The estimated K_0 vs. temperature (corresponding to 63.2% fracture probability) defines the median K_{Jc} vs. temperature (T) as follows:

$$K_{Jc} = 30 + 70 \cdot \exp[0.019 \cdot (T - T_0)] \; MPa\sqrt{m} \tag{5.1}$$

The formula (Equation 5.1) has shown to describe the elastic-plastic K_{Jc} temperature dependence for most structural steels independent of their yield strength and composition. In the current standard (ASTM E1921-05), the procedure is specified to cover ferritic steels with yield strength ranging from 270 to 870 MPa. Since its definition, the curve shape has been verified in various research programmes like that on the Euro Reference Material [4] covering not only pressure vessel and other conventional structural steels but also more alloyed ones. Results from the round robin test programme using the Euro Reference Material (22NiMoCr37) are given in Figure 5.2.
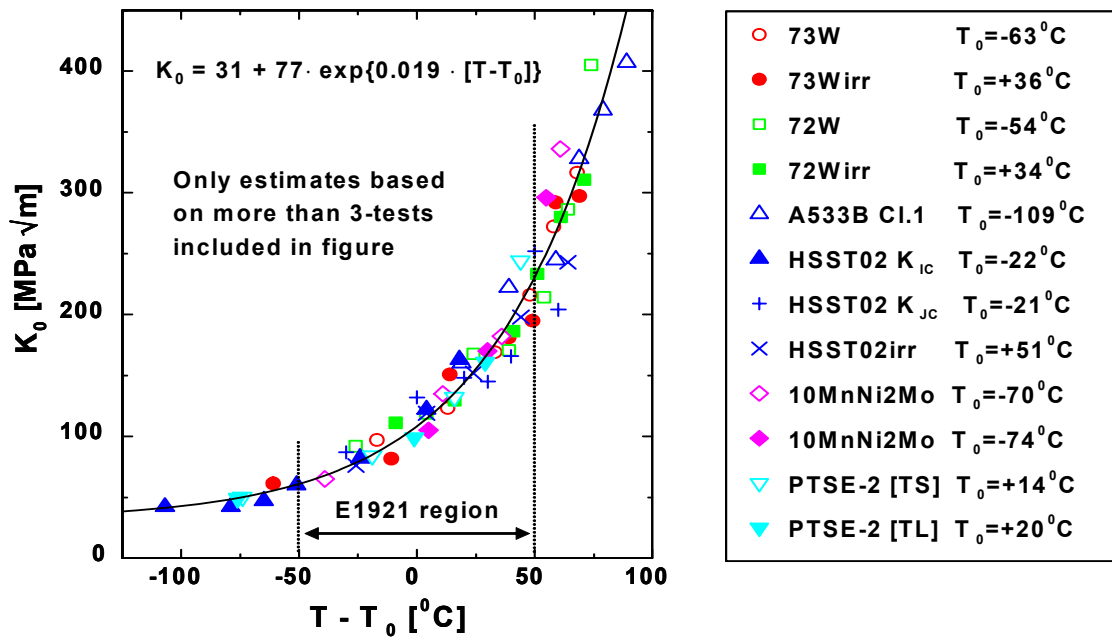
FIG. 5.1. Original datasets used to determine the standard Master Curve temperature dependence and the estimated K_0 vs. temperature curve [3].
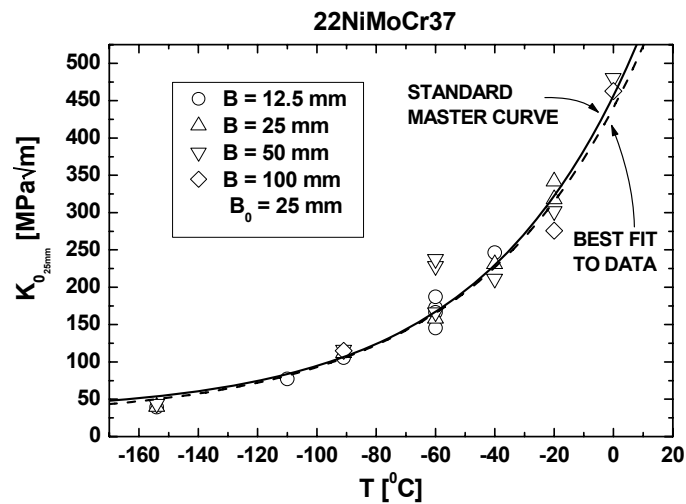
FIG. 5.2. Master Curve shape comparison to the Euro Reference Material A data measured with different size specimens (thickness 12.5–100 mm) [4].

5.2.2. Effect of irradiation

For RPV applications, the curve shape issue may become critical if the curve shape exhibited by the irradiated material deviates from that of the unirradiated material. The importance of this possibility has been clearly recognized but so far only few investigations on this subject have been published [5]. Reasons for this lack of information are obviously the availability and difficulty of examining highly irradiated materials. On the other hand, present results from irradiation and plant surveillance programmes strongly suggest that the curve shape issue is unlikely to become a critical issue even for highly irradiated materials. Test results showing significant curve shape change due to irradiation have occasionally been reported, but the true reason behind this behaviour has seldom been adequately documented and clarified.

The transition curve shape on irradiated materials has already been studied as part of the general curve shape definition study associated with the MC techniques development [6, 7]. The first attempts to model the temperature dependence of some irradiated and unirradiated RPV steels were based on application of the local approach models (RKR, HRR, and Beremin) on the crack tip stress distribution, and the temperature dependence of the material yield strength derived from these models. The agreement with the predicted and measured behaviour was, however, poor, and only after introduction of the statistical cleavage fracture model (WST) could the observed transition behaviour be modelled satisfactorily [6, 7]. These studies also suggested that the constant transition curve shape could be generally applicable for structural steels including irradiated conditions. This finding was essential and meant that the procedure could be presented as a universal estimation procedure for fracture toughness including irradiated conditions.

In the basic study [6] the derived transition curve shape was verified by comparing the MC prediction with the experimental data of two irradiated pressure vessel steels (72W and 73W). The significance of this study is important because: (i) the transition temperature shifts of the materials were large, 91°C and 100°C, and (ii) both datasets were large enough to allow analysis of the curve shape statistically. The comparison was made in two parts so that data for T-ΔT below and above -40°C were analysed separately. The results showed that the transition curve shape is practically unaffected by irradiation, as shown in Figure 5.3. The conclusion from the study, covering also several other unirradiated materials, was that the transition curve shape is not sensitive to material's yield strength, composition, or the prior neutron irradiation.

As part of the curve shape studies with highly irradiated materials, one also should consider the changes irradiation induced microstructural changes in the material affecting not only the re-distribution of alloying and impurity elements, but also the fracture mode. The fracture mode change from cleavage to GBF-type or quasi-cleavage (discussed in Section 5.3) means that the cleavage fracture model [7], in its basic form, tends to become gradually more inaccurate as the proportion of GBF increases. Finally, at high enough proportions of GBF the cleavage fracture model does not properly describe the fracture behaviour. Refined physical and fracture models that take into account material microstructural characteristics considering irradiation exposure are under development to be applied for engineering purposes.
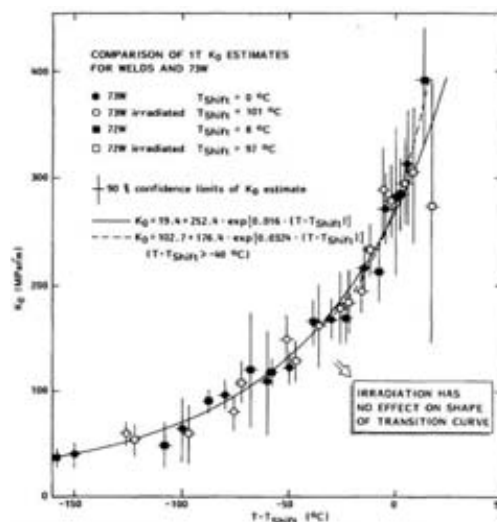
FIG. 5.3. Effect of irradiation on the temperature dependence of parameter K_0 for welds 72W and 73W [6].

5.3. LIMITS OF MASTER CURVE APPLICABILITY

Master Curve inconsistency issues, i.e. where the measured and predicted behaviour do not agree, that have been reported so far have typically dealt with situations where one or more of the basic assumptions (usually either the fracture mode or homogeneity) was not satisfied and application of the MC required extrapolation outside the scope of the basic model. In these situations it is not appropriate to identify a conflict with respect to the measured behaviour resulting from the model itself. Modified MC applications are already available for inhomogeneous materials (the SINTAP-procedure and the multi-modal or bi-modal MC model).

Application of the standard Master Curve methodology has recently been studied both in the IAEA CRP-5 [8] and the ATHENA programmes, as well as in the preceding CRPs and several other projects. One objective of the present CRP is to study applicability of the Master Curve methodology by extending it beyond the standard scope of application. Based on the results from previous CRPs in this series this evaluation was structured to clarify the limits of the Master Curve approach and develop guidance to analyse data falling outside established applicability limits or general cases where the basic assumptions of the model are not fulfilled. Examples of application issues to be addressed include:

- inhomogeneity;
- intergranular fracture;
- low upper shelf toughness;
- highly irradiated materials.

For (irradiated) RPV materials the K_{Jc} vs. T curve shape issue should be regarded as one that may be associated with any of the above abnormal material conditions. Though these conditions are exceptional, they should be considered in RPV applications where large T_0 shifts may exist together with variations in material properties owing to large wall thicknesses and fluence variations. Any of these factors can contribute to abnormalities in fracture toughness data measured with small specimens increasing the total uncertainty of results.

The above applicability issues are discussed in detail in the CRP-5 final report [9] and in the MC guidelines prepared during CRP-5 [8]. These same issues were discussed, from a consensus point of view, in the ATHENA programme completed in 2004.

5.3.1. Intergranular fracture

For properly heat-treated, as-received ferritic structural steels the standard MC approach can normally be applied, without consideration of validity constraints, provided the testing requirements specified in ASTM E1921 are fulfilled. A deviation from the standard K_{Jc} vs. temperature dependence (which defines the MC shape) is anticipated if intergranular fracture (IGF), due to thermal ageing or irradiation, begins to dominate or significantly affect the fracture behaviour. The existence of fracture modes other than pure cleavage usually, but not necessarily, means that one of the basic premises for applicability of the Master Curve methodology is not fulfilled.

Previous studies have revealed characteristics of GBF and how it affects the fracture behaviour of ferritic steels, for example:

- IGF may be a stress- or strain-controlled event, depending on temperature. This suggests that the deviation from typical cleavage fracture behaviour depends on temperature.
- Materials with 100% intergranular fracture have been shown to follow the MC if the T_0 value is low, i.e. less than about 0°C, when the fracture is likely stress-controlled rather than strain-controlled.
- At higher temperatures GBF becomes strain-controlled and is thus not expected to be significantly affected by temperature (Master Curve application is not recommended).
- GBF proportions less than about 50% have been observed not to affect the MC analysis.

To date no cases with a significant shape effect have been reported (excluding GBF and other clear fracture mode cases). On the other hand, there have been cases showing at least moderate correspondence on extremely brittle material conditions (high yield strength and high T_0) such as reported by Prometey [10]. Correspondingly, the irradiated model alloys with moderate to very high T_0, as well as high proportions of GBF in the most brittle materials, which were tested and analysed in the FRAME project behave well in line with the MC predictions (Figures 5.4 and 5.5) so that even the most brittle alloys could be analysed with the standard procedure.
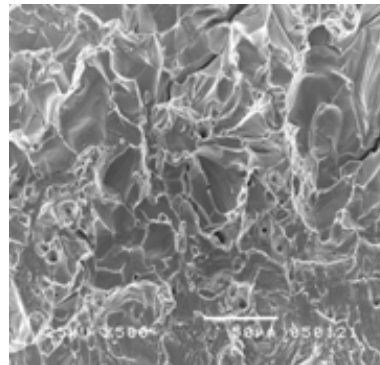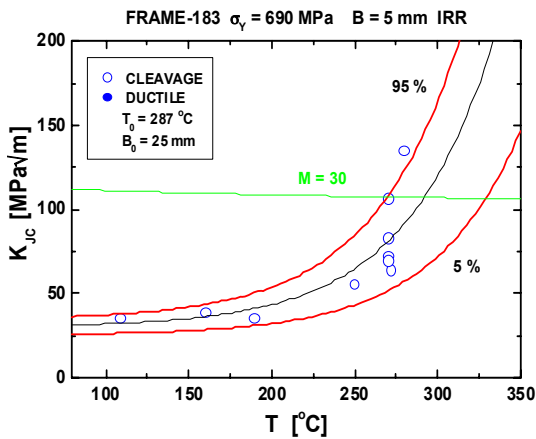
Specimen G02:

IGF: 75%

$T_{test} = 272°C$,

$K_{Jc} = T_{test} = 272°C$

$K_{Jc} = T_{test} = 272°C$

$K_{Jc} = 80 MPa\sqrt{m}$

FIG. 5.4. Master Curve fit to model alloy No. 183 data (irradiated material condition, $T_0 = 287°C$) and fracture surface of a specimen tested at $272°C$.
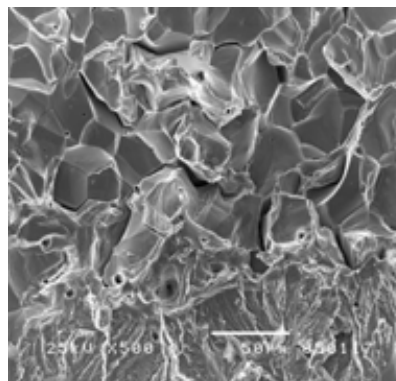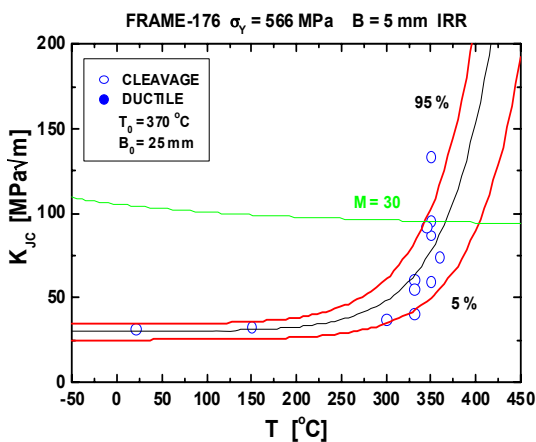
Specimen C01:

IGF: 90%

$T_{test} = 331°C$

$K_{Jc} = 47 MPa\sqrt{m}$

FIG. 5.5. Master Curve fit to model alloy No. 176 data (irradiated material condition, $T_0 = 370°C$) and fracture surface of a specimen tested at $331°C$.

Previous results on brittle materials suggest that deviations in the transition curve shape, for reasons other than IGF, may occur in the upper transition region at relatively high K_{Jc} levels. Experimentally such a situation is thus most likely encountered with large specimens if the material has high yield strength and the T_0 near or above 100°C. Also, the upper shelf toughness should not be too low, which further limits the number of steels suitable for investigating experimentally the curve shape issue. The most suitable materials for this purpose would thus be:

- Quenched and tempered steels with high yield strength and with various compositions and heat treatments (Cr steels, steels alloyed with Ni, micro-alloyed steels) resulting in different microstructures (precipitates etc.).
- Tempered martensitic steels.
- Only a few experimental investigations are available on the characteristics of grain boundary fracture toughness, covering the whole transition region from the lower to upper shelf. This means that additional testing may be required in cases where the IGF mode is likely or suspected.

5.3.2. Inhomogeneous materials

The Master Curve approach is based on the weakest link theory [7], in which the material is assumed to contain randomly distributed defects or cleavage fracture initiators. It is assumed that the material is macroscopically homogeneous, having uniform and isotropic strength and toughness properties. In addition to macroscopic homogeneity, the material is assumed to have an essentially single phase microstructure. Significant deviations from either or both of these assumptions may result in anomalous fracture behaviour that does not comply with the predicted behaviour of 'homogeneous' materials. Inhomogeneity typically appears as an excessive scatter exceeding that shown by the Master Curve model. On the other hand, both the temperature dependence of K_{Jc} and the T_0 estimation are typically not very sensitive to macroscopic inhomogeneity, or may even be totally unaffected. The same kind of behaviour is expected of materials with a (virtually) two phase structure, caused, for example, by large non-metallic inclusions or other impurities, which may result in an excessive scatter in K_{Jc} data if the specimen size is small in relation to the size of these particles.

Macroscopic inhomogeneity may exist, for example, in cross-sections of multipass welds between the beads of the weld or between the weld metal and the heat affected zone material. Similarly, large components such as forgings and thick, hot-rolled plates may experience macroscopic inhomogeneity in the thickness direction. If macroscopic inhomogeneity is known to exist at different locations and/or orientations in a component or structure, the Master Curve analysis should, if possible, be performed separately for each relevant area and orientation with approximately uniform properties. Depending on the application and the consistency of the experimental versus predicted behaviour, an adjusted Master Curve analysis can be performed to ensure the quality of the estimation.

The basic Master Curve is intended for use on macroscopically homogeneous ferritic steels. Whenever necessary, the consistency of any measured data with the Master Curve standard prediction, namely, whether the material should be analysed as an inhomogeneous case, can be checked by applying the structural integrity assessment procedure (SINTAP) [11]. If abnormal behaviour is encountered, the data should be analysed with a modified Master Curve model that takes into account the material inhomogeneity [12, 13]. The methodology for random inhomogeneity forms an integral part of the SINTAP structural integrity assessment procedure. The method includes a censoring procedure for data exceeding the

50% fracture probability to ensure a conservative lower bound determination for inhomogeneous materials. The SINTAP method (for analysing random inhomogeneous materials) is also applicable for datasets including several different materials.

The SINTAP method does not represent the same accuracy as a standard MC analysis of a homogeneous dataset [14, 15]. For a homogeneous material, the SINTAP method provides on the average a 10% lower fracture toughness estimate than the standard MC. For inhomogeneous datasets, the difference will be larger.

A simple extension of the MC has been developed to analyse material inhomogeneities governed by two separate (bi-modal) MC distributions [12]. The method has been shown to be extremely efficient in describing e.g. weld heat-affected zone (HAZ) data.

The use of the bi-modal distribution should be limited to datasets of a sufficient size to provide information about the inhomogeneity in question. The bi-modal fit to the data can be very good, but a small dataset may not describe the distribution very accurately. The accuracy of the estimated parameters will be a function of dataset size, occurrence probability (probability of hitting the different zones) and degree of censoring.

5.3.3. *Low upper shelf toughness*

To make an accurate assessment of vessel integrity, it may be necessary to identify the temperature above which upper shelf behaviour is expected (and, thus, at which the Master Curve cannot be expected to work) or, ideally, to develop a model of the fracture toughness behaviour on the upper shelf that can be used together with the Master Curve to describe the fracture toughness of RPV steels across the entire range of temperatures encountered in RPV service. This becomes especially important for materials exhibiting a low upper shelf fracture toughness since a low upper shelf toughness limits applicability of the Master Curve approach.

Limited information has been written regarding a relationship between transition and upper shelf toughness behaviour, either from the standpoint of the temperature dependence of the mean toughness or the temperature dependence of the scatter about the mean. Recently an empirical and physical basis for a common dependency between the transition temperature, T_0, and the onset of upper shelf, T_{US}, has been developed [16]. The developed methodology provides an approach to predict the upper shelf toughness behaviour of ferritic steels based solely on the measured T_0. This relationship has been empirically demonstrated with available data [14] and was further investigated as an element of this topic area.

The proposed correlation for estimating the level of T_{US} from the value of T_0, or vice versa, is based on the empirical result determining the intersection point of the mean fracture toughness transition curve (defined as T_0) and the mean upper shelf curve (denoted as T_{US}) as follows:

$$T_{US} = 0.794 \cdot T_0 + 50.1 \text{ (standard deviation 8.4}^\text{o}\text{C)} \tag{5.2}$$

Appendix IIIC provides details on the development of this relationship.

5.3.4. *Highly irradiated materials*

Many of the reported abnormal fracture behaviour cases have been associated with thermally embrittled or highly irradiated materials. In assessing data on such material conditions, one should separate factors associated with true material properties (microstructure, fracture

mode, materials macroscopic homogeneity) from those which result from other factors like testing conditions and procedures (standards used, allowed ductile crack growth, assurance of data quality etc.), specimen preparation (pre-fatigue before or after irradiation, reconstitution), homogeneity of irradiation conditions (fluence, temperature) and extraction of specimens (location and orientation). The true reason for the abnormal fracture behaviour has unfortunately seldom been checked out (which may be difficult if the test data has been collected from several test series measured a long time ago).

It has been presented, without consideration of possible reasons for the observed behaviour, that highly irradiated steels (with high T_0 temperature) might show the fracture toughness vs. temperature curve shape which markedly deviates from the assumed Master Curve shape [10], but with moderately irradiated steels the deviation would be negligible. On the other hand, there are several examples of materials with T_0 well above $100^{\circ}C$ which show consistent fracture toughness vs. temperature dependence with the Master Curve form. One of these is the KS01 weld which is very sensitive to irradiation embrittlement and represents an extreme case in this respect. In general, based on fractographic studies, IGF is suspected to be one potential reason for low fracture toughness values also in the upper transition region.

It is obvious that the curve shape change on irradiated materials is definitely a material-specific issue and often, deduced from the scatter of data, associated with existence of fracture modes other than cleavage. If the dominating fracture mode is IGF, as observed in heavily irradiated or embrittled steels, the Master Curve approach may not be applicable. In such cases, further analysis is recommended to ensure a conservative estimate for fracture toughness.

5.4. REVIEW OF THE ANALYSED DATA

5.4.1. Provided data

The materials reviewed in Topic area 3 consisted of mostly different RPV base and weld metals from various surveillance and test programmes. As for this topic area, the most interesting data (i.e. that which provide information on the correspondence and deviations between the measured data and the MC estimations), are those which include measurements from the whole transition region and from the upper transition area (also beyond the upper K_{Jc} and T limits specified in ASTM E1921). The aim was also to collect data on materials which have a high T_0, either due to irradiation or thermal ageing, to characterize their transition behaviour. Only relatively large datasets and only fracture mechanics tests were included. Some of these data are given in Refs [9, 10].

Besides surveillance materials, some thermally aged materials from completed research programmes, as well as materials irradiated in high flux reactors, were characterized in the database. In a few cases only the specimen fracture surfaces had been examined.

5.4.2. Results of analyses of selected datasets

Because the data provided for the CRP-8 are mostly surveillance test results measured with small specimens around the 100 MPa√m K_{Jc} level, only limited if any information about the upper transition behaviour is available. The relevant data show mostly consistent K_{Jc} vs. temperature dependence with respect to the assumed MC shape. In general, the data analysed so far in the CRP-8 reveal no new information invalidating the correspondence of MC predictions vs. measured data. In no respect do the reviewed data question the validity of the standard curve shape including highly irradiated and thermally aged material conditions.

When small size specimens are used, the upper validity limit for K_{Jc} becomes so low that it is impossible to produce valid test data at the high levels of K_{Jc}. In typical surveillance test programmes the measured values are around 100 MPa√m or even well below this level, near the lower shelf area. Such datasets may be sufficient to give valid estimates for T_0, but they are poor or not appropriate for verifying the upper transition behaviour, near the upper shelf area. Therefore, only datasets where the T_0 temperature was high (well above 0°C) and where data existed above the 100 MPa√m level were selected for further analyses.

One of the highest T_0 values reported was 164°C (irradiated JRQ by FZD). The fracture toughness data measured by FZD on the JRQ after irradiation to the T_0 of 124–164°C are shown in Figure 5.6 [15]. The data show consistent temperature dependence with the MC form up to 140 MPa√m (Figure 5.6). The same result applies to the data measured by JAEA on a reference pressure vessel steel with a high P content (Figure 5.7). JAEA had studied the transition curve shape with different aged and irradiated (modified) A533B-1 grades (various contents of P) and found no violation in respect of the standard median curve.

ORNL reported slightly lower shape factors for very brittle RPV materials ($T_0 > 100$°C) compared to unirradiated materials, but these data do not suggest modification of the MC shape assumption due to irradiation. In total, 851 irradiated base and weld metals were included in this study.
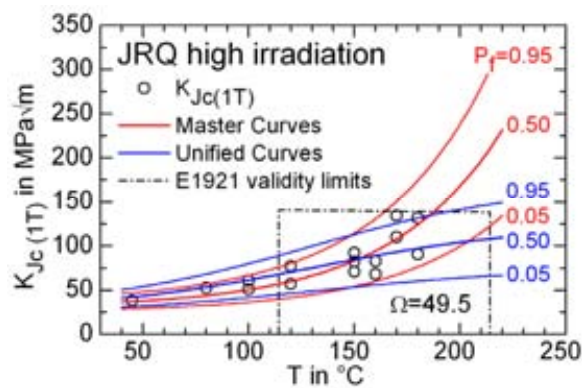
FIG. 5.6. Fracture toughness data measured for irradiated JRQ with high T_0 (data by FZD) [15].
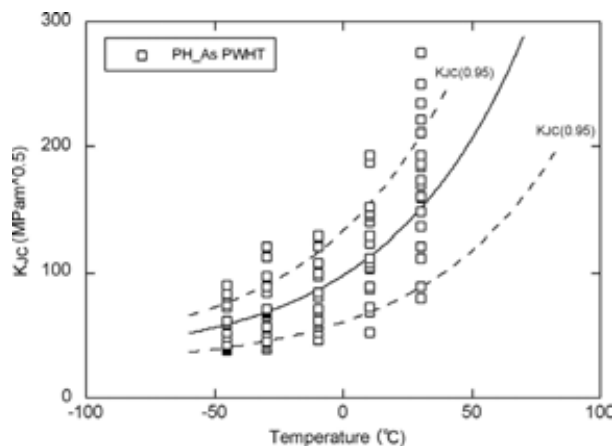
FIG. 5.7. Fracture toughness data measured for a model PV steel with high P content.

VTT reported re-analysed results from the thermally aged Prometey PTSE-1 material (15X2MFA) which showed macroscopic inhomogeneity, presumably due to the different extraction depths of specimens (Figure 5.8a). The SINTAP analysis of these data increased the value of T_0 from 88 to 96°C (Figure 5.8b).

The KS-01 (a Germain model steel), which is very sensitive to irradiation embrittlement due to the high copper and nickel contents, has been analysed previously by ORNL and VTT. The data of the irradiated material is presented in Figures 5.9a–b, showing very low K_{Jc} values measured at and above 200°C (Figure 5.9a). The SINTAP analysis (Figure 5.9b) corrected the value of T_0 from 133 to 148°C. The reason for the low values is unclear, but they are suspected in part to be due to ductile tearing or GBF (although none is reported). The same result was reported by ORNL for the irradiated and unirradiated KS-01 steel ($\Delta T_0 = 160^\circ$C), although some low values (discussed below) existed. Similar type results have been obtained for irradiated WWER-440 RPV materials by NRI and VTT.

The data measured on irradiated KS01 with T_0 as high as 133–271°C by MPA and ORNL provide information near the upper shelf region on this very brittle material. In the standard validity area there is generally no deviation from the MC form. Beyond this limit ORNL had measured low values, but, as the ductile values from the terminated tests performed at 180 and 200°C indicate, there appears to be a very large scatter in the measured values in this temperature area. Also, it should be noted that the lowest data had been measured with 0.5T CT specimens while the main part of the data had been measured with 1T CT specimens. More data are therefore needed to determine the onset and level of the upper shelf as well as the true temperature dependence above 180°C. In general, the presented KS01 data are mostly consistent with the MC predictions.

The data measured by SCK•CEN and VTT on the irradiated (3.1 $\times$ 10^{19} n/cm^2, E >1 MeV, T_{irr} = 150°C) Euro Reference Material, a 22NiMoCr37 type grade (Material A), showed a moderate scatter and T_0 = 69°C (Figure 5.10a). The value of T_0 was increased to 74°C using the SINTAP analysis (Figure 5.10b), suggesting an almost negligible effect of inhomogeneity despite the apparent large data scatter.

(a)   (b)
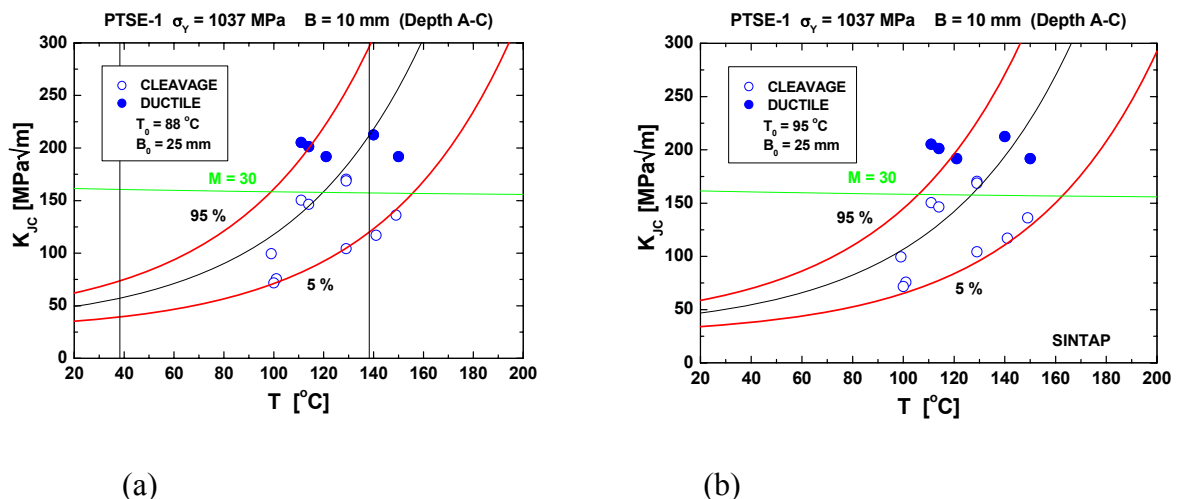
FIG. 5.8. The PTSE-1 data measured at different depths of the RPV wall block (15X2MFA) which were re-analysed for CRP-8: normal MC analysis (a) and SINTAP analysis (b).

74
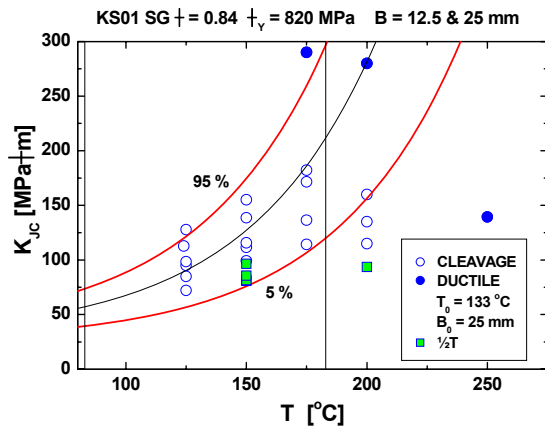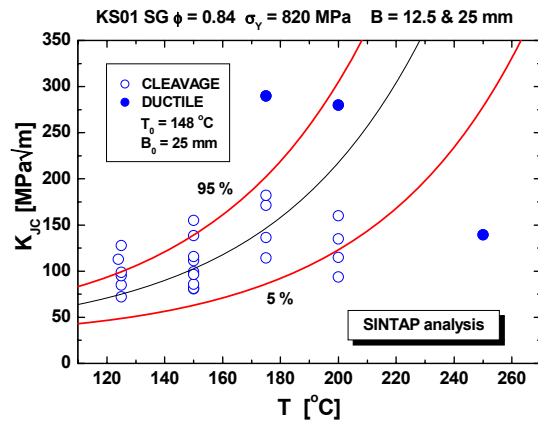
(a)   (b)

FIG. 5.9. Fracture toughness data measured on irradiated KS-01 weld with different size specimens. The values of T_0 are 133^oC, based on normal MC analysis (a), and 148^oC based on SINTAP analysis (b).
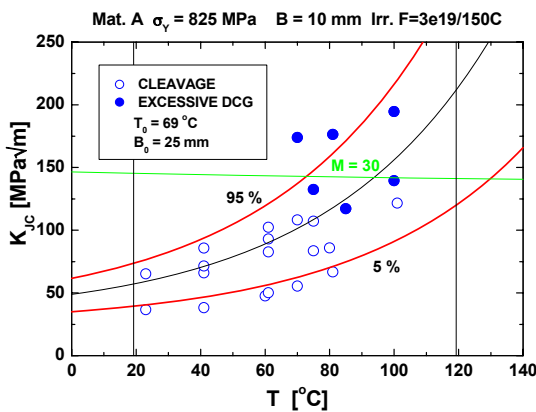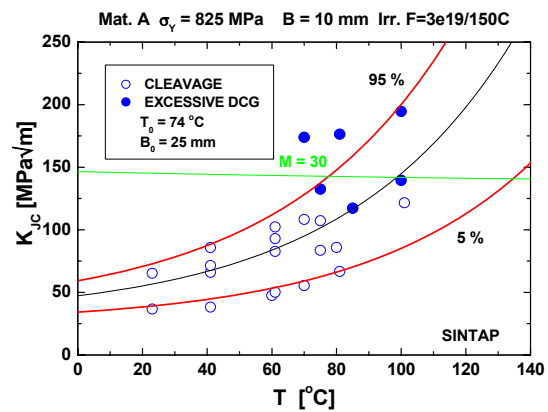
(a)   (b)

FIG. 5.10. Fracture toughness data measured on irradiated Material A (22NiMoCr37) with 10×10 mm 3-PB specimens. The values of T_0 are 69^oC based on normal MC analysis (a) and 74^oC based on SINTAP analysis (b) (excessive ductile crack growth data included as censored values).

5.5.   ESTIMATION OF THE MASTER CURVE C-PARAMETER

The standard MC procedure includes the assumption of a constant temperature dependence which is defined by the C-parameter (0.019 $1/^oC$), see Equation 5.1. Estimation of the C-parameter may also be used to improve the fit to the dataset if this is large enough and contains data from a range of temperature. Examples of such datasets are those determined on welds 72W and 73W (the combined analysis is given in Figure 5.3) for which it is known that the measurements are not affected by excessive ductile tearing. When analysed separately the following C-factors are obtained for these materials (Table 5.1).

TABLE 5.1. C-FACTORS ESTIMATED FOR WELDS 72W AND 73W

Material	C – factor (1/^{o}C)	Number of data points
72W non-irradiated	0.018	11
72W irradiated	0.016	9
73W non-irradiated	0.019	9
73W irradiated	0.017	8

The results show that the materials exhibit practically an identical temperature dependence, with the best estimate C = 0.019 1/^{o}C, and no effect of irradiation on the temperature dependence. Consequently, when plotted against T-T_0, these data can well be presented as one dataset (compare Figure 5.11), showing no deviations due to the temperature dependence. The standard value for the C-parameter (ASTM E1921) was originally derived from this result [6].

Afterwards, the curve shape issue has further been studied by estimating datasets measured on different base metals and welds in unirradiated and irradiated conditions. This work was started in 2006 by estimating two WWER-1000 datasets, originally issued by Prometey [10]. The results of the extended MC analyses performed for these datasets are given in Figures 5.11a–b. The obtained C-values are 0.014 1/^{o}C (unirradiated material) and 0.012 1/^{o}C (irradiated materials), i.e. in both cases the value is lower than the assumption 0.019 1/^{o}C. It should be noted that in this case the unirradiated material also showed lower temperature dependence than assumed and that the difference between the irradiated and unirradiated materials was smaller than could be expected from the previous results published on this material. The re-analysed datasets are large enough and cover a wide temperature range, such as to ensure reliable estimates for the C-parameter. As a result the materials can well be described with one average C-parameter (0.013 1/^{o}C).
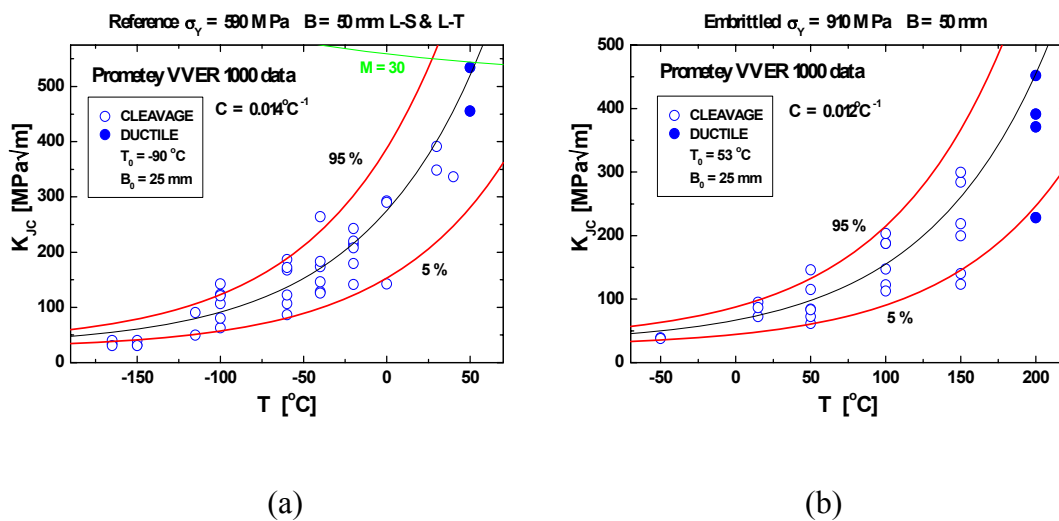
FIG. 5.11. C-parameter estimations made for the Prometey dataset in reference condition (a) and in embrittled condition (b).

To further verify the assumed K_{Jc} vs. T curve shape, 10 datasets previously determined from various surveillance programmes and round robin type joint projects were re-analysed for the CRP-8 by estimating the true K_{Jc} vs. temperature dependence and possible deviations from the assumed curve shape. Most of the analysed datasets had been measured on unirradiated, irradiated and/or annealed WWER-440 base and weld metals. For comparison, some western

type RPV materials, characterised in joint projects, were included in the comparison. The analysed materials and the result of the analysis, i.e. the T_0 temperatures and the estimated C-parameters, are summarised in Table 5.2 and in Figure 5.12.

The estimated C-parameters vary between 0.015 and 0.026 1/°C. Except for the maximum value, estimated for a WWER-440 BM dataset (only 7 valid data points), the values are mostly close to the standard value 0.019 1/°C. The average value of all estimates is 0.021 1/°C and the standard deviation 0.0036 1/°C, which suggests that there is no systematic deviation from the assumed value. Although the results in general show a weak or negligible dependence of the C-parameter on T_0, the relatively low values measured for the irradiated JRQ and the WWER-440 weld material, with $T_0 = 99$°C and 66°C, respectively, may be indications of the effect of irradiation (Figures 5.12 and 5.13). The irradiated Material A result ($C = 0.023$ 1/°C), where the number and distribution of data should already ensure a reliable estimate, is the most pronounced deviation from this trend (Figures 5.12 and 5.14). For the unirradiated Material A (Figure 5.15) the C estimate is close to that of the irradiated material, which means that the standard estimation provides on both material conditions more conservative lower bound estimates (Figures 5.14 and 5.15). The C-value estimate of the thermally aged A508 Cl.3 ($T_0 = 64$°C) is close to the standard value (Figure 5.16).

TABLE 5.2. SUMMARY OF RE-ANALYSED DATASETS AND THE VALUES OF T_0 AND C-PARAMETER

Material	Condition [c]	T_0 (°C)	T_0 C-estim. (°C)	C (1/°C)	Number of data points	Number of valid data
WWER-440 WM	R	-43	-42	0.025	16	10
WWER-440 WM	I	66	68	0.015	12	10
WWER-440 WM	IA	-25	-26	0.022	15	12
WWER-440 BM	R	-47	-48	0.017	15	8
WWER-440 BM	I	27	29	0.026	15	7
A508 Cl.3 BM	Ag	64	63	0.021	27	22
WWER-440 WM	IAI	27	27	0.019	12	8
A533B Cl.1 [a]	I	99	98	0.018	18	9
A508 Cl.2 [b]	R	-104	-106	0.025	49	26
A508 Cl.2 [b]	I	69	68	0.023	24	18

[a] JRQ: IAEA CRP-3 round robin programme.
[b] Euro Reference Material A, irradiation at 150°C.
[c] R: unirradiated, I: irradiated, A: recovered, Ag: thermally aged.

TABLE 5.3. SUMMARY OF MATERIAL DATA PROVIDED

Institute	Material [a]	Fluence (E>1 MeV)	T_0 (°C)	Condition [b]	Remarks
NRI	WWER-440 BM & WM		+15…+109	I	
	IAEA RRE WM		+42…+60	I	
AREVA NP	Material A			R	
	NiCrMo WM	2.2×10^{19} n/cm^2		I	40–50 mm WOL specimens
FZD	JFL, JRQ	20×10^{19} n/cm^2		I	
	WWER-440 BM			I	GBF ≈ 20%
	JFL		-45…-37		
	JRQ		+124 and +164	I	
AEKI	WWER-440 Weld 502		+30…+84	I	
	WWER-1000		+31	I	High Ni cont.
	JRQ		+62	I	
JAEA	A533B-1 (mod.):			A+I	0.057% P content
	1.	1.9×10^{19} n/cm^2	+117 (SINTAP)		Tests at 90°C
	2.	5.3×10^{19} n/cm^2	+218 (SINTAP)		Tests at 200°C
KAERI	Mod. 9Cr-1Mo-V		-68		Ferritic - mart. steel
CIEMAT	JRQ			A	Incl. GBF
	16MND5 (A508Cl.3)		$\Delta T_0 \approx 90$°C	A	
ORNL	HSSI WM 72W, 73W			R, I	
	KS-01 WM		$\Delta T_0 = 160$°C	R, I	
	Midland WM	3.4×10^{19} n/cm^2		R, I	
SCK•CEN	EUROFER 97 F82H, T91, HT9	High fluence		I	RPV steels, high fluence
EPRI & ATI	Western steels Linde 80 WM			R & I	
VTT	WWER-440 WM			R, I, IA etc.	
	22NiMoCr37 (Mat. A)	3.1×10^{19} n/cm^2	+69 (irradiated)	R, I	
	PTSE-1 (15X2MFA)		+80…+163	A	Diff. size specimens, various depth

[a] BM: base metal, WM: weld metal
[b] R: reference, I: irradiated, A: annealed
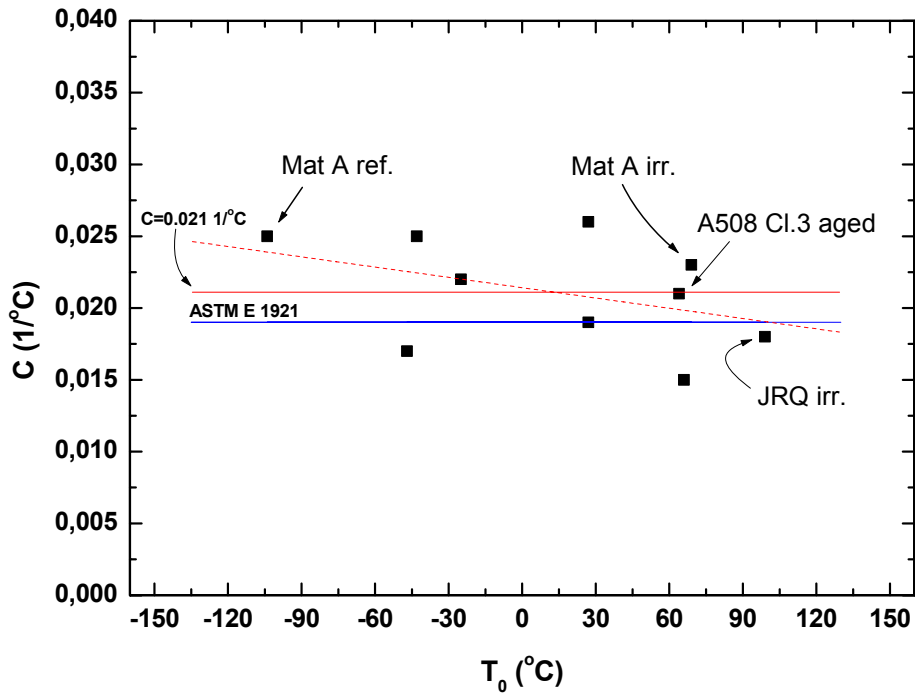
FIG. 5.12. Estimated C-parameters and least squares fits of 10 datasets measured on WWER-440 and three other RPV materials in different conditions (Euro Reference Material A, thermally aged A508 Cl.3 and irradiated JRQ).
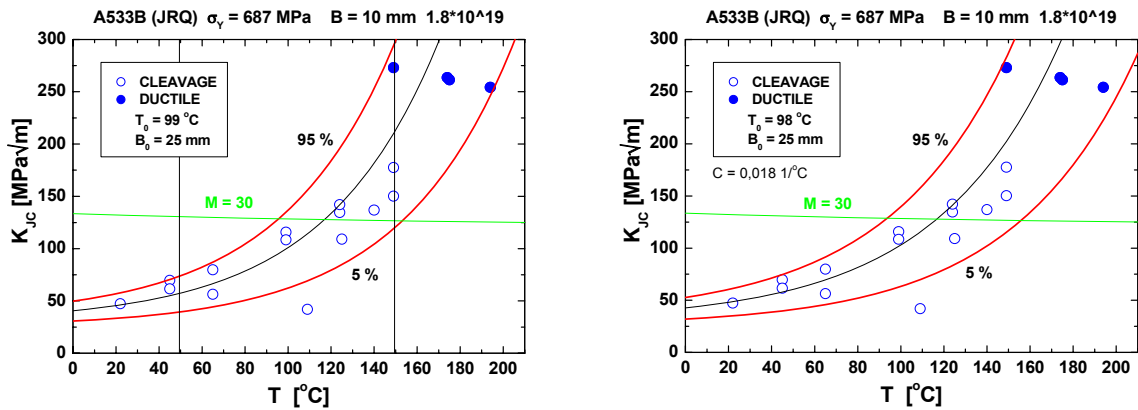
FIG. 5.13. Master Curve analysis of the irradiated A533B Cl.1 (JRQ). The values of T_0 are 99^oC and 98^oC (C-estimation) and $C = 0.018$ $1/^oC$.
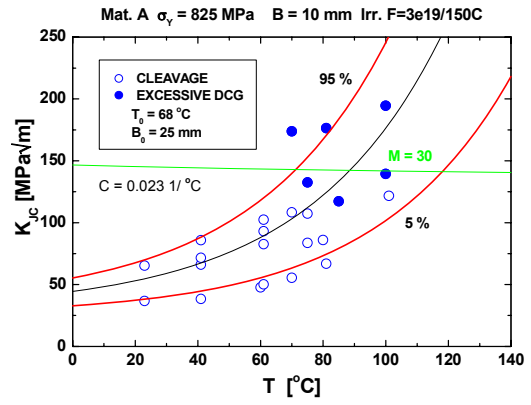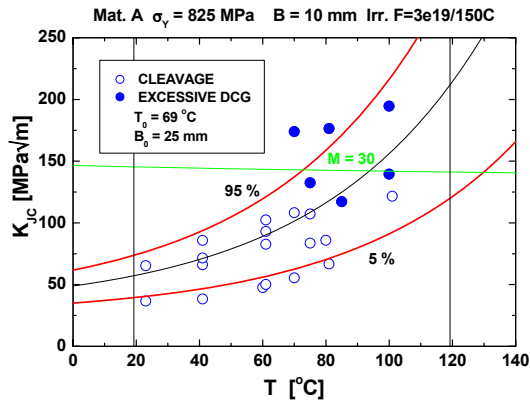
FIG. 5.14. Master Curve analysis of the irradiated Material A (22NiMoCr37). The values of T_0 are 69^oC and 68^oC (C-estimation) and $C = 0.023$ $1/^oC$.
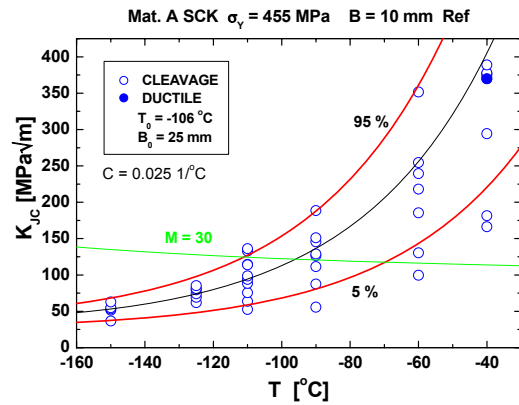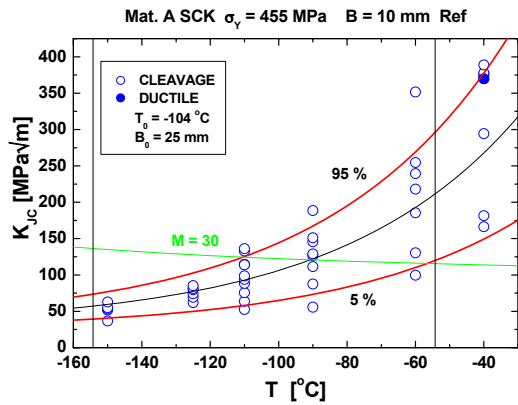
FIG. 5.15. Master Curve analysis of the unirradiated Material A (22NiMoCr37). The values of T_0 are -104^oC and -106^oC (C-estimation) and $C = 0.025$ $1/^oC$.
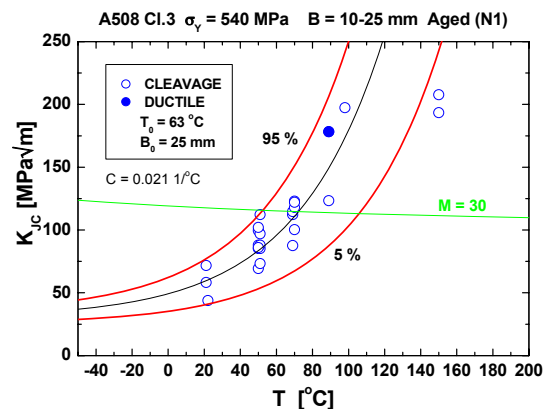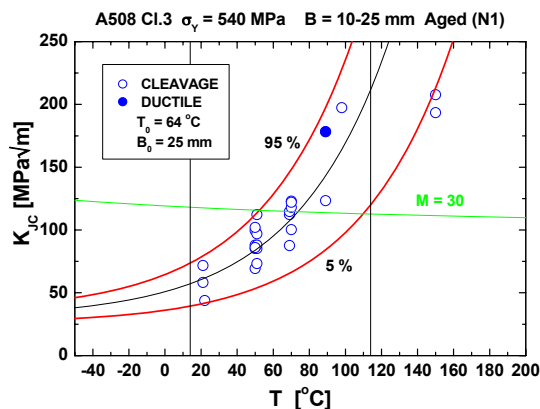
FIG. 5.16. Master Curve analysis of the thermally aged A508 Cl.3. The values of T_0 are 64^oC and 63^oC (C-estimation) and $C = 0.021$ $1/^oC$.

A more comprehensive study on the C-factor material dependence, to be published elsewhere, has similarly revealed a similar type, moderate, variation of the C-factor and no or very weak dependence of this factor on the material fracture toughness. In addition, the variation seems to occur equally to both directions of the present assumption, with the mean value close to 0.019 1/°C, which suggests that there is no need to change the present curve shape assumption. Neither do the first results support the justification presented for the Unified Curve model, i.e. that a marked curve shape change would occur due to irradiation at high T_0. A gradual change in the mean behaviour, with high uncertainty, is possible but the present results give no basics to present a universal model for predicting this behaviour.

5.6. THE UNIFIED CURVE MODEL FOR ESTIMATING THE CURVE SHAPE

A special procedure, so-called Unified Curve, has been proposed for highly irradiated steels by the Russian CRISM Prometey [18, 19]. The special feature in this model is that it includes a parameter for estimating the effect of irradiation or the degree of embrittlement on the transition curve shape. The method has similarities with the basic MC method, such as the definition of the size correction, scatter and the lower shelf. The main difference is the functional form of the transition curve which in the Unified Curve is established by a tanh-type function including a variable (Ω) for estimating the temperature dependence of fracture toughness in the transition region.

The temperature dependence of fracture toughness at fracture probability $P_f = 0.5$ for specimens with thickness B = 25 mm from RPV steel for any degree of material embrittlement may, according to the Unified Curve procedure, be described by:

$$K_{Jc(med)} = K_{Jc}^{shelf} + \Omega \cdot \left(1 + \tanh\left(\frac{T-130}{105}\right)\right) \quad MPa\sqrt{m} \tag{5.3}$$

where $K_{Jc}^{shelf} = 26$ MPa√m, Ω is the parameter that depends on the degree of embrittlement and T is temperature (°C).

It follows from Equation 5.3 that:

$$\Omega = K_{Jc(med)|T=130°C} - K_{Jc}^{shelf} \tag{5.4}$$

According to the definition (Equation 5.3) the parameter Ω decreases as the degree of embrittlement increases.

For comparison, the unirradiated and irradiated Material A data were also analysed with the UC method by estimating the mean K_{Jc} vs. T with a best-estimate power-curve fit to the datasets. The yielded Ω parameters, Figures 5.17 and 5.18, were 342 MPa√m (unirradiated material) and 125 MPa√m (irradiated material). Compared to the MC median estimate, the UC estimate for the irradiated material gives distinctly lower fracture toughness estimates in the upper transition region. In this case, however, the difference is mainly caused by the censoring procedure applied in the MC estimation. In the UC estimation (Figure 5.18) the data points below the M = 30 curve are all included in the analysis, with equal weight, while the data above this curve are excluded. For the unirradiated material the UC and the MC estimates coincide (Figure 5.17).
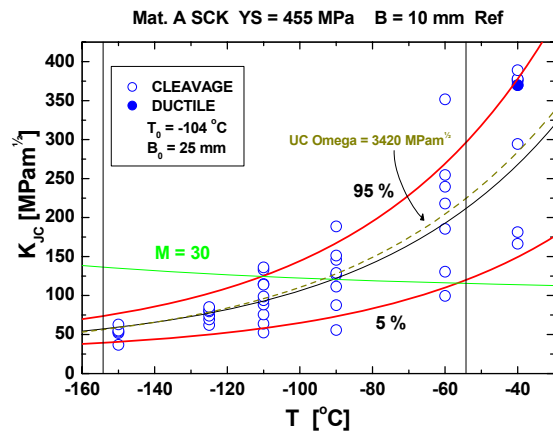
FIG. 5.17. Comparison of MC and UC median K_{Jc} curves estimated for the unirradiated Material A. Data censoring has been applied only in the MC analysis.
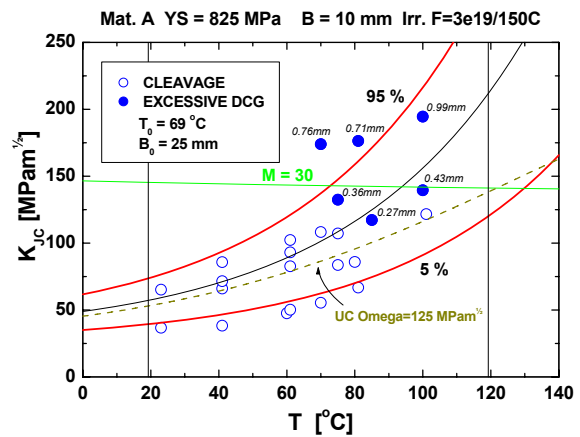
FIG. 5.18. Comparison of MC and UC median K_{Jc} curves estimated for the irradiated Material A. The data points with excessive ductile crack growth have been censored in the MC analysis and only data below the M = 30 curve are included in the UC analysis (without censoring). The mean crack growth values measured from the censored 6 specimens are given in the figure.

5.7. DISCUSSION

It has been presented, without consideration of possible reasons for the observed behaviour, that highly irradiated steels with high T_0 might show the fracture toughness vs. temperature dependence which markedly deviates from the assumed Master Curve shape [10], but with moderately irradiated steels the deviation would be negligible. On the other hand, there are several examples of materials with T_0 well above 100°C which show consistent fracture toughness vs. temperature dependence with the Master Curve form. One of these is the KS01 weld which is very sensitive to irradiation embrittlement and represents an extreme case in this sense. Based on fractographic studies on RPV steels GBF is one potential reason for low fracture toughness values also in the upper transition region.

Significant macroscopic inhomogeneity or large proportions of GBF often means deviation from the statistical cleavage fracture model and the ASTM E1921 requirements based on the weakest link theory, according to which the material is assumed to contain randomly distributed defects or cleavage fracture initiators. Such materials typically exhibit anomalously scattered fracture toughness in the transition region appearing as deviations in respect of the standard tolerance bound.

Determination of material's fracture toughness vs. temperature dependence exactly is complicated due to several factors which may affect the measured fracture toughness. Excluding the pure experimental factors, like material macroscopic inhomogeneity and the effect of ductile tearing etc., there still remains the inherent statistical scatter of fracture toughness and the limitations of the procedure itself, especially the narrow temperature range available for obtaining valid test results with sub-size specimens. Since small specimens (Charpy size or smaller) are mostly used for testing irradiated materials with high T_0, which

82

are suspected to predominantly exhibit abnormal shape factors, it may be impossible to determine from such surveillance data statistically reliable estimates for the true temperature dependence if the test temperature range is narrow. Extrapolation is possible to a certain extent, but at least some data from large specimens are necessary to demonstrate that the behaviour is truly material-specific. In this respect the Prometey and the Material A data as well as those measured for thermally aged materials with large specimens (e.g. the NESC and PTSE programmes) provide a valuable verification on curve shape besides the original data measured previously on welds 72W and 73W.

The ductile tearing preceding cleavage initiation on the other hand tends to increase the probability of cleavage initiation and thus decrease the fracture toughness, whereas the possible loss of constraint tends to increases the fracture toughness. In addition, with highly irradiated materials the upper shelf may be very low which should be taken into account when extrapolating to higher temperatures.

Another question is how material-specific the temperature dependence really is. It is well known that the proportion of GBF tends to increase with irradiation exposure or the degree of embrittlement. On the other hand, material's susceptibility to GBF may greatly vary depending on the material composition and purity. Significant curve shape change has been reported to occur mainly on WWER-1000 type RPV materials, but also other cases like the KS-01 data have been reported. The present results do not support the assumption that the possible curve shape change would be a general phenomenon associated with neutron irradiation exposure (or thermal ageing) so that it could be described by one simple, universal model like the Unified Curve model. Nor do the results confirm the gradual change in the curve shape as a function of T_0, although a weak correlation may exist. On the contrary, the scatter in the estimated C-values suggests that there has to be other factors besides, or instead of, the T_0 explaining the possible decreasing C value with temperature. Due to the small number of relevant test data this scatter is also at least partly due to the inherent scatter of fracture toughness and the resulting uncertainty in the C-parameter estimation. The magnitude of the scatter in the C values shall thus primarily be judged in relation to the statistical uncertainty of the T_0 determination and the scatter of fracture toughness. The present results do not confirm the general dependence of the C-parameter on T_0.

It is emphasised that so far a great majority of results, including those given here, seem to confirm that there is no need to change the assumption of the constant C-parameter or the value of it from that given in ASTM E1921. The value 0.019 1/^{o}C is based on test data measured on large specimens including also irradiated conditions and considering possible uncertainties like the effect of ductile tearing. The derived C value has proven to describe correctly the behaviour of most of structural steels and normally there is no need to estimate the C-parameter case-specifically. The estimation is not even recommended, if it is not known beforehand that the material may show abnormal K_{Jc} vs. temperature dependence and in any case for data which is not fully representative or otherwise suitable for such estimation.

On the other hand, it is recommended that very brittle materials (with T_0 above $\approx$100°C) are always analysed case-specifically taking into account the possibility of exceptional temperature dependence and the occurrence of large proportions of GBF. In such cases the Master Curve C-parameter adjustment or the Unified Curve estimation can be used to improve the consistency of the prediction with the measured data as well as to increase the conservative of the lower bound estimates and possible extrapolations from the measured data.

5.8. CONCLUSIONS

The presented data do not clearly indicate the existence of a general trend of the decreasing FT in the upper transition region in terms of material's fracture toughness (T_0). Additional test results on very brittle material conditions, seldom allowed in real structures, are needed to demonstrate their behaviour. The conclusions from the present study are as follows:

- The constant C-parameter assumption given in ASTM E1921 provides a good approximation for most irradiated materials exhibiting moderate fracture toughness.
- Irradiation may slightly lower the fracture toughness in the upper transition region in relation to that predicted by the standard curve shape, but the effect after moderate T_0 shift values (up to about $100^{\circ}C$) seems to be negligible.
- It is recommended that very brittle materials (with T_0 above $\approx 100^{\circ}C$) should be analysed case-specifically, using e.g. the SINTAP procedure, for conservatively addressing the true fracture toughness. Extrapolation to higher temperatures should be made taking into account the possibly lowered upper shelf fracture toughness.
- Datasets including values below the 2% lower bound curve are recommended to be analysed with the SINTAP or the multi-modal model for inhomogeneous materials to ensure conservative estimates for T_0 and the lower bound K_{Jc}.
- More FT data following the ASTM E1921 standard but covering the whole transition region on highly irradiated materials are needed to demonstrate their true transition behaviour and its possible dependence on the fluence with different materials.

5.9. REFERENCES

[1] ELECTRIC POWER RESEARCH INSTITUTE, Materials Reliability Program: Establishing a Physically Based, Predictive Model for Fracture Toughness Transition Behavior of Ferritic Steels (MRP-53), EPRI, Palo Alto (2001).
[2] AMERICAN SOCIETY FOR TESTING AND MATERIALS, ASTM E 1921-05, Standard Test Method for Determination of Reference Temperature, T_0, for Ferritic Steels in the Transition Range, Annual Book of ASTM standards, ASTM International, West Conshohocken (2007) 1203–1222.
[3] WALLIN, K., "Fracture toughness transition curve shape for ferritic structural steels", Joint FEFG/ICF International Conference on Fracture of Engineering Materials and Structures, Singapore (1991).
[4] WALLIN, K., Master Curve Analysis of Ductile to Brittle Transition Region Fracture Toughness Round Robin Data. The "EURO" Fracture Toughness Curve, VTT Publications 367, Technical Research Centre of Finland, Espoo (1998).
[5] WALLIN, K., The effect of ductile tearing on cleavage fracture probability in fracture toughness testing, Engineering Fracture Mechanics **32** (1989) 523–531.
[6] WALLIN, K., Irradiation damage effects on the fracture toughness transition curve shape for reactor pressure vessel steels, International Journal of Pressure Vessel Piping **55** (1993) 61–79.
[7] WALLIN, K., Validity of Small Specimen Fracture Toughness Estimates Neglecting Constraint Corrections, Constraint Effects in Fracture: Theory and Applications, ASTM STP 1244, Annual Book of ASTM standards, ASTM International, Philadelphia (1995) 519–537.
[8] INTERNATIONAL ATOMIC ENERGY AGENCY, Guidelines For Application of the Master Curve Approach to Reactor Pressure Vessel Integrity in Nuclear Power Plants, IAEA Technical Reports Series No. 429, IAEA, Vienna (2005).

[9]   INTERNATIONAL ATOMIC ENERGY AGENCY, Application of Surveillance Programme Results to Reactor Pressure Vessel Integrity Assessment, IAEA-TECDOC-1435, IAEA, Vienna (2005).

[10] MARGOLIN, B., SHVETSOVA V., GULENKO A., ILYIN A., NIKOLAEV V., SMIRNOV V., Fracture toughness predictions for a reactor pressure vessel steel in the initial and highly embrittled states with the Master Curve approach and a probabilistic model, International Journal of Pressure Vessel Piping **79** (2002) 219–231.

[11] BRITISH STEEL, SINTAP - Structural Integrity Assessment Procedures for European Industry, Project BE95-1426, Final Procedure, British Steel, Rotherham (1999).

[12] WALLIN, K., NEVASMAA, P., LAUKKANEN, A., PLANMAN, T., Master curve analysis of inhomogeneous ferritic steels, Engineering Fracture Mechanics **71** 16–17, (2004) 2329–2346.

[13] PLANMAN, T., SERVER, W., WALLIN, K., ROSINSKI, S., "Application of the Master Curve approach for abnormal material conditions", Proceedings of ASME PVP 2007/CREEP 8 Conference, San Antonio (2007).

[14] ELECTRIC POWER RESEARCH INSTITUTE & U.S. DEPARTMENT OF ENERGY, Materials Reliability Program: Implementation Strategy for Master Curve Reference Temperature, T_0 (MRP-101), EPRI, Palo Alto, U.S. Department of Energy, Washington (2004).

[15] ZURBUCHEN, C., VIEHRIG, H.W., "Master Curve applicability to highly neutron irradiated reactor pressure vessel steels — Results of a BMWi grant project", Proceedings of 33.MPA-Seminar, Stuttgart (2007) 1861–5414.

[16] ERICKSONKIRK, M., The relationship between the transition and upper-shelf fracture toughness of ferritic steels, Fatigue Fracture Engineering Material Structure **29** (2006) 672–684.

[17] BRUMOVSKY, M., "Master Curve application to embrittled RPVs of VVER type reactors", ASME Pressure Vessel and Piping Symposium, Atlanta (2001).

[18] MARGOLIN, B., GULENKO, A., NIKOLAEV, V., RYADKOV, L., A new engineering method for prediction of the fracture toughness temperature dependence for RPV steels, International Journal of Pressure Vessel Piping **80**, (2003) 817–829.

[19] MARGOLIN, B., GULENKO, A., NIKOLAEV, V., RYADKOV, L., Prediction of the dependence of $K_{JC}(T)$ on neutron fluence for RPV steels on the basis of the Unified Curve concept, International Journal of Pressure Vessel Piping **82** (2005) 679–686.

[20] NANSTAD, R.K., et al., Irradiation Effects on Fracture Toughness of Two High-Copper Submerged-Arc Welds, HSSI Series 5. NUREG/CR5913. Vol. 1., U.S. Nuclear Regulatory Commission, Washington (1992).

6. CONCLUSIONS AND RECOMMENDATIONS

From 1971 until the present time, the IAEA has contributed significantly to the dissemination of knowledge regarding issues related to the structural integrity of reactor pressure vessels. Through the establishment of CRPs that have brought together experts from a variety of organizations in many of the world's nuclear power producing countries, advances in the engineering materials field have been evaluated and published in the forms of special CRP IAEA-TECDOC reports, Technical Reports Series, and technical journal papers. With the advancements in materials science and engineering over the past 37 years, the IAEA CRPs have taken advantage of those advancements by incorporating them in the evaluations of the specific issues and objectives of each particular CRP. Major advances in elastic-plastic fracture mechanics that allow for determination of fracture toughness of RPV steels with a relatively few number of relatively small specimens using the Master Curve methodology was the key advancement further investigated in CRP-8. The technical aspects of elastic-plastic fracture mechanics combined with the assembly of large databases have allowed the Master Curve approach to be further validated leading to potential improved safety in operating RPVs.

The main conclusions and some recommendations are provided next for each CRP-8 topic area. More detailed conclusions as well as recommendations for future work are summarized at the end of each topic area section.

6.1. TEST SPECIMEN BIAS, CONSTRAINT, AND GEOMETRY

A key consideration for RPV integrity is the understanding of constraint and bias between the sample specimen(s) being tested (generally of one or two geometries) and the flaw assumed to exist in the RPV. Results from CRP-5 showed that lower values of unirradiated T_0 are obtained using PCC specimens as compared to results from 1T-CT specimens. More than 300 PCC and 1T-CT specimens of A533B-1 steel (heat JRQ) were tested in CRP-5 by many different organizations; the T_0 based on the PCC specimens was 12ºC lower than from the 1T-CT specimens. Moreover, many other RPV steels were tested and showed differences from 12 to 45ºC, with the three-point bend specimens giving the lower T_0 value in every case. This bias in test results between different geometries and sizes is very important when considering use of PCC specimens in evaluating RPV integrity. Issues regarding constraint limits for the Master Curve method in general and the PCC specimen in particular, especially as a consequence of irradiation, must be understood. The potential use of even smaller specimens highlights the significance of this topic, as evaluation of specimen size effects are needed to fully understand limits of applicability and associated uncertainties.

Fifteen laboratories contributed to the experimental portion of Topic area 1, Test Specimen Size, Geometry, and Constraint Relative to the Measurement and Application of Master Curve T_0 Values, and fracture toughness data were provided for three-point bend specimens of varying sizes from 0.16T to 1T and for compact specimens from 0.4T to 1T. Additionally, some tests were conducted with crack depth (a/W) variations from 0.1 to 0.75. Two large datasets were available for analysis, HSST Plate 13B and JRQ steel, both RPV steels of the A533 Grade B Class 1 specification. Additionally, tests for many national steels were included. The results from these datasets were analysed in detail.

There are various methods for constraint adjustments, but there is not a consensus methodology available that accounts for the differences observed with different materials. Increasing the constraint limit (M = 30 in ASTM E1921) to ensure no loss of constraint for

the PCC specimen is not a practicable solution because the PCC specimen is derived from Charpy V-notch specimens in RPV surveillance capsules, and larger specimens are normally not available. Resolution of these differences are needed for application of the Master Curve procedure to operating RPVs, but the research needed for such resolution is beyond the scope of this CRP.

A series of finite element round robin exercises were conducted involving ten laboratories to better quantify the differences in fracture toughness specimens relative to the RPV and their significance. It was determined that shallow crack specimens are more sensitive to loss of constraint than those with deep cracks for a given specimen size. The difference in terms of reference temperature was evaluated to be about 40°C. For deep crack specimens, loss of constraint was identified to appear at M constraint values of around 200, which is consistent with others reported in the literature. However, experimental results suggest that this limit is too restrictive, and key experimental results have been evaluated showing that specimen geometry and size.

Also, part one of the round robin found that the ANSYS code produces systematically higher forces while other remaining differences for the other finite element codes are very small and less than 3%. For part two of the round robin, differences between the laboratories are limited. MSC-MARC would require smaller time step to yield equivalent results to the other finite element code that are using the time step prescribed in the specification. The remaining differences cannot be attributed to one particular finite element code. The differences are attributed to the so called user effect. This round robin has been useful to qualify finite element codes and to identify possible errors in the input file. The round robin demonstrates that errors in the input file can be easily introduced. To avoid those errors, it is important to follow internal quality assurance and cross check results again established references. The user effect should be eliminated if these specific measures are taken.

It is recommended that further work be conducted to resolve the fundamental reasons for loss of constraint to varying amounts for different steels and the relationship between T_0 as measured from PCC specimens and other specimen geometries and sizes (including the traditional norm of using 1T-CT specimens). This work also needs to include typical cracks either assumed or measured in real structural applications, such as pressurized thermal shock. The issues related to the identification of micromechanical parameters and their dependence as a function of temperature has not been investigated in this study. Work is needed to allow engineering use of the methodology. Also relative to finite element usage, it is recommended that a quality assurance procedure be established and used in order to avoid error in the results; it is also crucial that mesh refinement and time steps have reached convergence.

6.2. LOADING RATE EFFECTS AND QUALIFICATION OF IMPACT FRACTURE TOUGHNESS TESTING

The effect of loading rate within the loading rate range specified in ASTM E1921-05 for quasi-static loading, and the effect of loading rate for higher loading rates including impact conditions using instrumented PCC specimens were examined. A major focus was on dynamic instrumented impact loading which includes a round robin exercise using the JRQ steel. Except for one laboratory (which appeared to have force calibration problems), the results supplied by the participants are very consistent and show reasonable scatter. Based on the results from this round robin exercise, the Master Curve approach has proven to be fully applicable to impact fracture toughness measurements obtained in the ductile-to-brittle transition region, but it is clear that the quality of impact fracture toughness measurements

strongly depends on the quality of instrumented force values. Hence, a reliable calibration of the instrumented striker is of primary importance.

The Master Curve reference temperature T_0 is reasonably constant within the quasi-static range of loading rates as defined by ASTM E1921-05(08), i.e. between 0.1 and 2 MPa√m/s. For higher loading rates, T_0 increases steadily with dK/dt and the rate of increase (loading rate sensitivity) decreases with with increasing quasi-static T_0 and appears poorly correlated to the yield strength of the material. Below 0.1 MPa√m/s, Wallin's empirical model provides reasonable and useful predictions of the variation of T_0 as a function of loading rate.

Full applicability of the Master Curve approach to impact fracture toughness measurements obtained in the dutcile-to-brittle transition regime has been shown. The guidelines provided by the future ISO/ASTM standards for test execution and data analysis have proven to be reliable and easy to implement; the test method appears mature enough to be implemented into official standards. The shape of the instrumented striker (2 mm or 8 mm radius) seems to have negligible influence on the measured T_0.

Future work should continue to be investigated on the influence of loading rate on T_0 using the results contained in large databases, such as the one developed several years ago by EPRI. The usefulness of performing fracture toughness measurements at loading rates higher than quasi-static for RPV assessments could be emphasized by establishing correlations between crack arrest toughness (K_{Ia}) and dynamic/impact fracture toughness (K_{Id}). The measurement of impact T_0 values could be used for comparison with the ASME K_{IR} lower bound curve to lower bound Master Curves (corresponding to low fracture probabilities) obtained from dynamic/impact toughness measurements. This comparison can be achieved by: (i) determining an equivalent dynamic RT_{T0} (similar to ASME Code Cases N-629 and N-631) for indexing the ASME lower bound K_{IR} curve; (ii) defining a threshold dynamic loading rate representative for the equivalent dynamic RT_{T0}; and/or (iii) corroborating or revising correlations between instrumented Charpy arrest forces (F_a, T_{4kN} etc.) and crack arrest parameters (K_{Ia}/NDT). From an experimental point of view, this activity could involve several possible actions:

- collecting and re-assessing the existing crack arrest and dynamic/impact fracture toughness data on a few well-characterized RPV steels (e.g. HSST-02);
- generating a limited amount of new crack arrest data on other relevant RPV steels, for which a large database of dynamic fracture toughness data is available (e.g. JRQ);
- enerating new dynamic/impact fracture toughness data (K_{Id}, $T_{0, dyn}$) for other selected materials.

A future CRP could be organized to focus on the use of dynamic/impact T_0 measurements as the basis for assessing crack arrest fracture toughness. This CRP could focus on most, if not all, of the recommendations made above.

6.3. MASTER CURVE SHAPE

Possible changes in the Master Curve shape for highly irradiated materials, and/or materials that show an intergranular fracture mode, is a concern relative to structural integrity application since the general shape of the Master Curve is considered to be invariant for most realistic irradiation conditions. For properly heat-treated, as-received ferritic structural steels, the standard Master Curve approach can normally be applied, without consideration of validity constraints, provided the testing requirements specified in ASTM E1921 are fulfilled.

A deviation from the standard K_{Jc} vs. temperature dependence (which defines the Master Curve shape) may be anticipated if intergranular fracture (IGF), due to thermal ageing or irradiation, begins to dominate or significantly affects the fracture behaviour. The existence of fracture modes other than pure cleavage usually, but not necessarily, means that one of the basic premises for applicability of the Master Curve methodology is not fulfilled.

If the Master Curve does change shape, the conditions and extent of deviation need to be defined. One major conclusion from this task is that irradiation may slightly lower the fracture toughness in the upper transition region in relation to that predicted by the standard curve shape, but the effect after moderate T_0 shift values (up to about 100°C) seems to be negligible. It is recommended that very brittle materials (with T_0 above ~100°C) should be analysed on a case-specific basis, using a procedure to evaluate data for heterogeneity. Datasets including values below the 2% lower bound curve are recommended to be analysed with the SINTAP or the multi-modal model for inhomogeneous materials to assure conservative estimates for T_0 and the lower bound K_{Jc}. More large-specimen fracture toughness data following the ASTM E1921 standard, but covering the whole transition region on highly irradiated materials, are needed to demonstrate their true transition behaviour and its possible dependence on fluence with different RPV steels.

APPENDIX I
TOPIC AREA 1

IA. RECOMMENDED PROCEDURE FOR SHALLOW CRACK TESTING

IA.1. INTRODUCTION

CRP-8 Topic area 1 concentrates on three interrelated subjects: bias, constraint and geometry effect on the reference temperature, T_0, for ferritic steels in the transition range. The bias subject focus on the difference between C(T) and SE(B) configuration due to constraint differences between the two geometries. The effect of constraint can be emphasis when using shallow crack specimen or through specimen geometry (e.g. tension versus bend loading).

The use of shallow crack SE(B) is particularly attractive to generate information in low constraint condition. However, the ASTM E1921-05 does not currently cover the use of this configuration.

In order to allow proper interpretation of the data generated within the CRP-8, the use of the ASTM E1921-05 procedure is recommended except for the points described bellow.

IA.2. SPECIFIC PROCEDURE

IA.2.1. Fatigue precracking

For SE(B) (*a*/W~0.1), a specific fatigue precracking procedure is recommended. Indeed, the initial sharp notch for initiating the fatigue crack could affect the stress field ahead of a shallow crack. To avoid the effect of the initial notch, the notch should be machined after precracking. For example, the initial specimen dimension of the specimen are B = 10, W = 13.5, L = 55 with a sharp notch of 3 mm depth. After precracking over a distance of about 1.5 mm, the specimen width, W, is reduced to 10 mm through machining. The initial notch of 3 mm depth is therefore removed (see Figure IA.1).
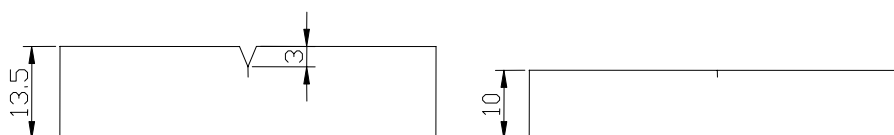
FIG. IA.1. Example of precracked PCC specimen prior and after machining.

IA.2.2. η-factor

The η-factor based on the load line given in the ASTM E1921-05 is inadequate for shallow SE(B). In this case, the η-factor depends on the crack length to width ratio and on the strain hardening exponent of the material. An alternative approach has been developed for shallow crack relying on a specific η-factor based on the CMOD. This formulation has been extended and given by the following equation:

$$\eta_{CMOD} = \frac{S}{4W}\left(3.785 - 3.101(a_0/W) + 2.018(a_0/W)^2\right) \qquad \text{(IA.1)}$$

IA.2.3. Measurement of CMOD

As an integral notch for clip gauge would affect the stress state ahead of a shallow crack, attachable knifes are used to measure the crack mouth opening displacement (CMOD).
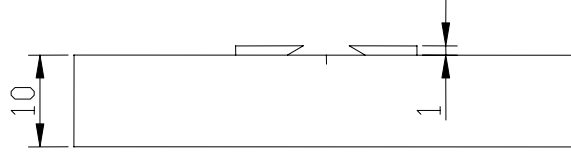
FIG. IA.2. Example of precracked PCC with knifes for CMOD measurement.

In Figure IA.2, the knives are 1 mm thick; therefore, the displacement is measured one millimetre above the specimen surface. This offset distance can be accounted for using the plastic rotation factor r_p.

$$CMOD = CMOD_Z \frac{a_0 + r_p(W - a_0)}{a_0 + r_p(W - a_0) + Z} \tag{IA.2}$$

where $CMOD_Z$ is the measured clip gauge displacement, a_0 the initial crack length, Z the distance between the knife edge and the specimen surface and r_p the plastic rotation factor equal to 0.44 for a_0/W between 0.45 and 0.55. For shallow cracks, the plastic rotation factor depends on the crack length to width ratio and on the material strain hardening exponent.

Using finite element calculations, the plastic rotation factor can be obtained using the following equation:

$$\frac{CTOD_p}{CMOD_p} = \frac{r_p(W - a_0)}{a_0 + r_p(W - a_0)} \tag{IA.3}$$

where CTOD is the crack tip opening displacement.

The r_p value for the material of interest ($n = 10$) and $a_0/W = 0.15$ is given as 0.261. However a value of 0.5 is also used in the same procedure. On the other hand an r_p value of 0.27 for $a_0/W = 0.15$ is using the ratio between the CMOD and the load line displacement (LLD).

$$\frac{LLD_p}{CMOD_p} = \frac{S/4}{a_0 + r_p(W - a_0)} \tag{IA.4}$$

The plastic rotation factor can also be obtained from the following equation:

$$\frac{\eta_{LLD}}{\eta_{CMOD}} \frac{S}{4W} = r_p + (1 - r_p)a_0/W \tag{IA.5}$$

where CTOD is the crack tip opening displacement. This definition is believed to be more appropriate for our application. The assumption of a rigid body rotating around a rotation point does not hold close to the crack tip.

The plastic rotation factor for the material of interest ($n = 10$) and $a_0/W = 0.15$ is calculated from Equation IA.5 to be 0.37.

From experimental and computational evidence, the following equation is suggested:

$$r_p = 0.3 + 0.5a_0/W \qquad a_0/W < 0.3 \tag{IA.6}$$

yielding a value of 0.375 for $a_0/W = 0.15$.

It should be noted that in the specific case ($a_0 = 1.5$, $W = 10$, $Z = 1$, $r_p = .37$) an error of 10% on r_p only affect the measured CMOD by 2% and the measured fracture toughness by 1%. Therefore, Equations IA.2 and IA.6 are recommended when the CMOD is measured above the specimen surface.

IB.   SPECIFICATIONS FOR THE FINITE ELEMENT ROUND ROBIN PART 1

In order to study constraint in fracture toughness specimens, 3-dimensional elastic-plastic calculations are needed. Therefore, the exercise is based on a simple model including both features.

IB.1. SELECTED GEOMETRY

The geometry, axis and origin are defined in Figure IB.1. It is a single edge bend SE(B) specimen loaded in three point bend with a span of S = 40 mm. The dimensions correspond to a precracked Charpy (PCC) specimen W = 10 mm, B = 10 mm. The crack length is a = 5 mm.
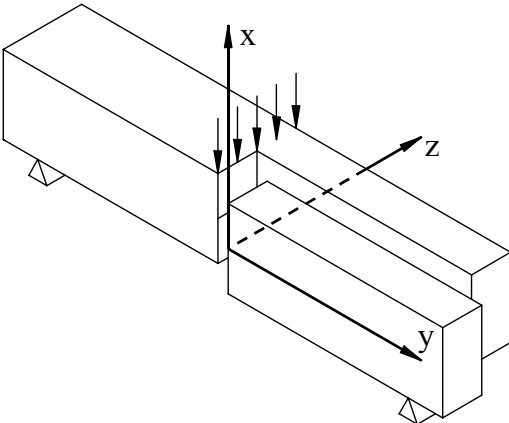
FIG. IB.1. PCC in 3PB loading. Only one fourth of the geometry is simulated.

IB.2. FINITE ELEMENT MESH

8-node isoparametric hexahedral elements with 8 Gauss points are recommended. The mesh contains 16 element and 45 nodes as follows (Figure IB.2):
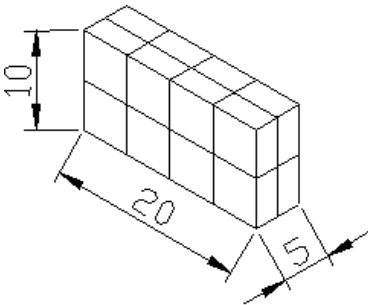
FIG. IB.2. Mesh recommended for the exercise.

IB.3. FINITE ELEMENT BOUNDARY CONDITION

Symmetry conditions are imposed to the planes defined by the equations y = 0 and z = 5. However, for nodes located on the plane y = 0, the nodes with an x-coordinate strictly lower than 0 are not constraint in y to allow the crack to open. The nodes on the support have fixed displacement in the $\vec{X}$ direction. Force is simulated by applying a displacement in the $-\vec{X}$ direction on nodes in the load line. Constraints are illustrated in Figure IB.3.
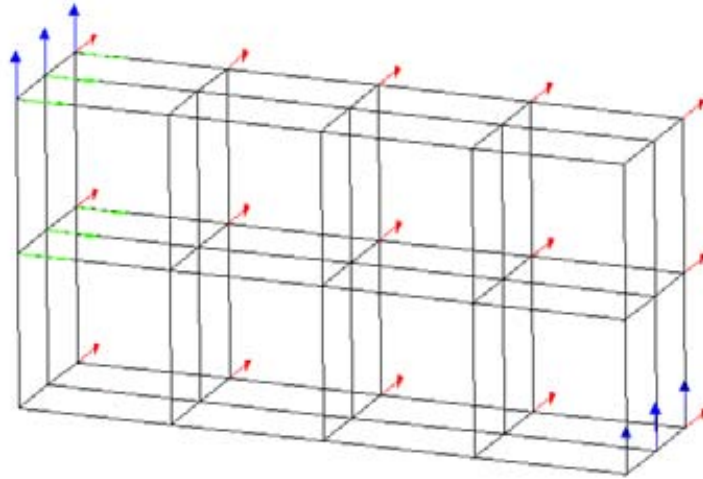
FIG. IB.3. Finite element boundary condition.

IB.4. MATERIAL PROPERTY

The incremental theory of plasticity is recommended in combination with an isotropic strain-hardening model based on the Von Mises criterion with uniaxial true stress versus true strain described by a power law:

$$\frac{\sigma}{\sigma_{YS}} = \begin{cases} \dfrac{\varepsilon}{\varepsilon_{YS}} & if \ \sigma < \sigma_{YS} \\ \left(\dfrac{\varepsilon}{\varepsilon_{YS}}\right)^{n} & if \ \sigma \geq \sigma_{YS} \end{cases} \tag{IB.1}$$

with

$$E \, \varepsilon_{YS} = \sigma_{YS} \tag{IB.2}$$

The hardening exponent is n = 0.1, the Young's modulus is E = 207 GPa, the Poisson ratio is v = 0.3 and the yield stress is σ_{YS} = E/500. Large strains and displacements should be taken into account using a Lagrangian formulation.

IB.5. EXPECTED RESULTS

Simulation should be performed up to a Load Line Displacement of 0.5 mm in increments of 0.05 mm. 'Force' is the reaction force on the support: multiply by 4 to take the 2 symmetry planes into account. LLD is the applied displacement. CMOD is twice the displacement in the y direction of the node located at coordinate (x = -5, y = 0, z = 5).

Any deviation from the recommendations in this guide should be reported, as well as the name of the finite element code used.

Force (kN)	LLD (mm)	CMOD (mm)
0	0	0
	0.05	
	0.1	
	0.15	
	0.2	
	0.25	
	0.3	
	0.35	
	0.4	
	0.45	
	0.5	

IB.6. EXAMPLE OF INPUT FILE

Node	X	y	Z	Node	X	y	Z
1	-5	0	0	23	0	10	2.5
2	-5	5	0	24	0	15	2.5
3	-5	10	0	25	0	20	2.5
4	-5	15	0	26	5	0	2.5
5	-5	20	0	27	5	5	2.5
6	0	0	0	28	5	10	2.5
7	0	5	0	29	5	15	2.5
8	0	10	0	30	5	20	2.5
9	0	15	0	31	-5	0	5
10	0	20	0	32	-5	5	5
11	5	0	0	33	-5	10	5
12	5	5	0	34	-5	15	5
13	5	10	0	35	-5	20	5
14	5	15	0	36	0	0	5
15	5	20	0	37	0	5	5
16	-5	0	2.5	38	0	10	5
17	-5	5	2.5	39	0	15	5
18	-5	10	2.5	40	0	20	5
19	-5	15	2.5	41	5	0	5
20	-5	20	2.5	42	5	5	5
21	0	0	2.5	43	5	10	5
22	0	5	2.5	44	5	15	5
				45	5	20	5

Element	Node1	Node2	Node3	Node4	Node5	Node6	Node7	Node8
1	1	2	17	16	6	7	22	21
2	2	3	18	17	7	8	23	22
3	3	4	19	18	8	9	24	23
4	4	5	20	19	9	10	25	24
5	6	7	22	21	11	12	27	26
6	7	8	23	22	12	13	28	27
7	8	9	24	23	13	14	29	28
8	9	10	25	24	14	15	30	29
9	16	17	32	31	21	22	37	36
10	17	18	33	32	22	23	38	37
11	18	19	34	33	23	24	39	38
12	19	20	35	34	24	25	40	39
13	21	22	37	36	26	27	42	41
14	22	23	38	37	27	28	43	42
15	23	24	39	38	28	29	44	43
16	24	25	40	39	29	30	45	44

- node 31 to 45 to be constraint in z direction (symmetry plane, see Figure IB.4);
- node 6, 21, 36, 11, 26, 41 be constraint in y direction (symmetry plane);
- node 5, 20, 35 to be constraint in the x direction (support);
- displacement to be applied in the –x direction on nodes 11, 26, 41.
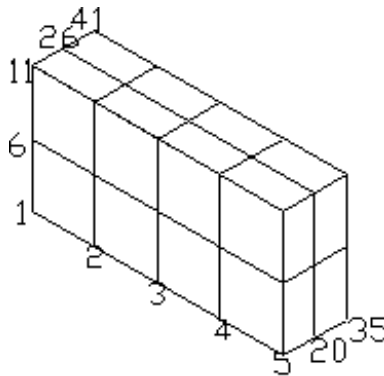
FIG. IB.4. Node number.

IC.   SPECIFICATIONS FOR THE FINITE ELEMENT ROUND ROBIN PART 2

The objective of this round robin is to quantify loss of constraint using finite element tools and to qualify this analytical tool trough round robin exercise.

IC.1. SELECTED GEOMETRY

The geometry, axis and origin are defined in Figure IC.1. It is a single edge bend SE(B) specimen loaded in three point bend with a span of S = 40 mm. The dimensions correspond to a precracked Charpy (PCC) specimen W = 10 mm, B = 10 mm. Two models are selected the deep crack a = 5 mm and the shallow crack a = 1 mm.
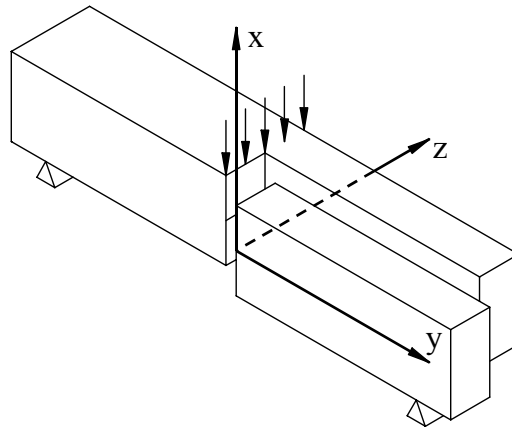
*FIG. IC.1. PCC in 3PB loading. Only one fourth of the geometry is simulated.
(Deep crack configuration.)*

IC.1.1. Finite element mesh

8-node isoparametric hexahedral elements with 8 Gauss points are recommended.

The mesh for the shallow crack and deep crack is divided in 4 and 5 macro cell respectively according to Figure IC.2. Each cell is subdivided regularly according to the following table and illustrated in Figure IC.3. Element size at crack tip position is 50 µm by 50 µm by 1 mm.

Macro cell	Shallow crack (number of elements)	Deep crack (number of elements)
1	40×40×5	40×40×5
2	20×40×5	20×40×5
3	20×30×5	20×23×5
4	40×30×5	40×23×5
5		20×23×5
Total elements	21 000	21 200
Total nodes	25 986	26 184

Shallow crack   Deep crack
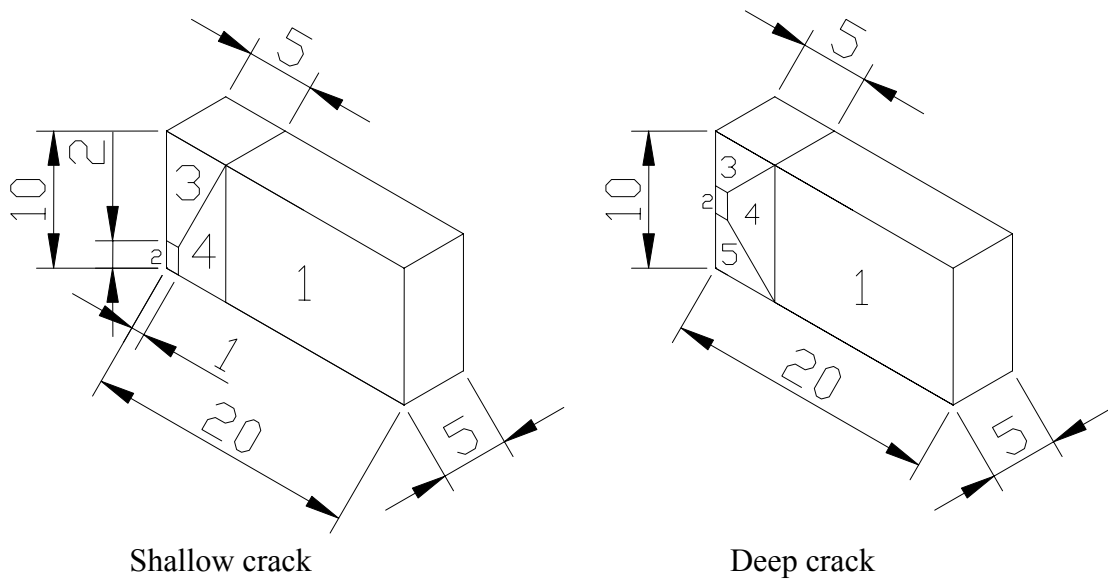
FIG. IC.2. Macro cells recommended for the exercise.
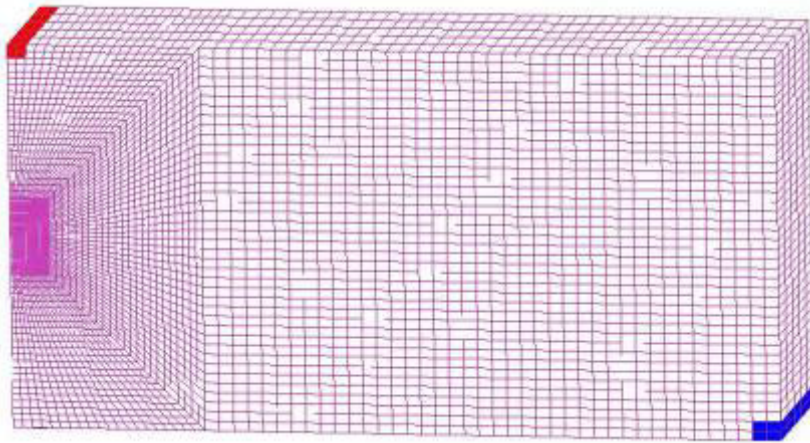
Deep crack
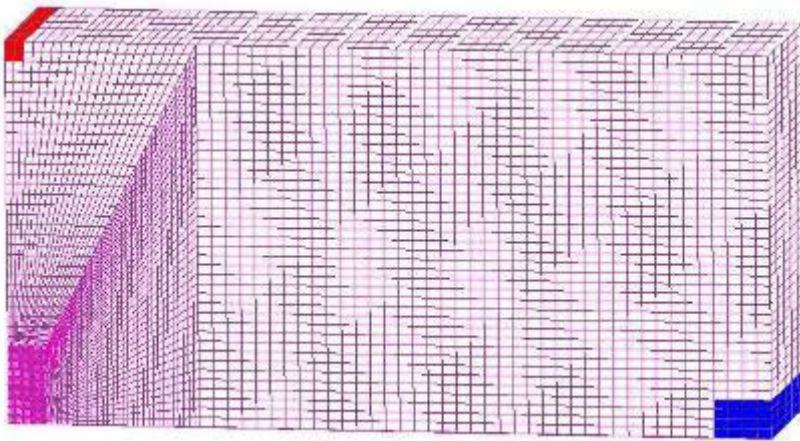
Shallow crack

FIG. IC.3. *Meshing of the macro cell. Element in red and blue are elastic elements as explain in the material properties paragraph.*

IC.2. FINITE ELEMENT BOUNDARY CONDITION

Symmetry conditions are imposed to the planes defined by the equations $y = 0$ and $z = 5$. However, for nodes located on the plane $y = 0$, the nodes with an x-coordinate strictly lower than 0 are not constraint in y to allow the crack to open. The nodes on the support have fixed displacement in the $\vec{X}$ direction. Force is simulated by applying a displacement in the $-\vec{X}$ direction on nodes in the load line. Constraints are illustrated in Figure IC.4.

Deep crack

Shallow crack
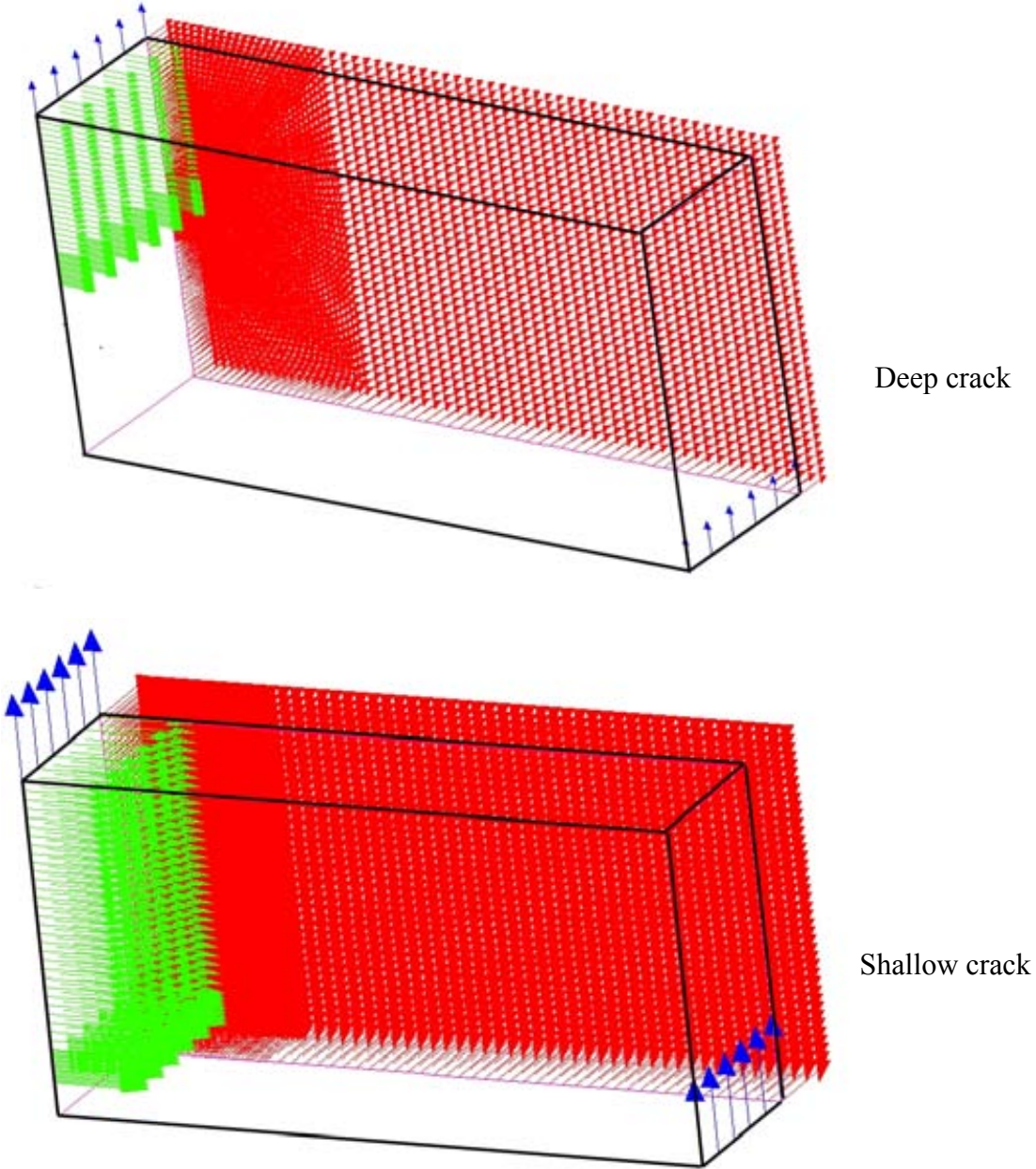
FIG. IC.4. Boundary condition.

IC.3. MATERIAL PROPERTY

The incremental theory of plasticity is recommended in combination with an isotropic strain-hardening model based on the Von Mises criterion with uniaxial true stress versus true strain described by a power law:

$$\frac{\sigma}{\sigma_{YS}} = \begin{cases} \dfrac{\varepsilon}{\varepsilon_{YS}} & if \ \ \sigma < \sigma_{YS} \\ \left(\dfrac{\varepsilon}{\varepsilon_{YS}}\right)^{n} & if \ \ \sigma \geq \sigma_{YS} \end{cases} \tag{IC.1}$$

with:

$$E \, \varepsilon_{YS} = \sigma_{YS} \tag{IC.2}$$

The hardening exponent is $n = 0.1$, the Young's modulus is $E = 207$ GPa, the Poisson ratio is $\nu = 0.3$ and the yield stress is $\sigma_{YS} = E/500$.

Large strains and displacements should be taken into account using a Lagrangian formulation.

To avoid excessive plastic deformation of the specimen, fully elastic elements, with material properties $E = 207$ GPa and $\nu = 0.3$, are placed at the support and at the place of imposed displacement (see Figure IC.3). For the deep-crack specimen the size of the beams is $2 \times 2 \times 5$ elements. For the shallow-crack specimen the beam size is $2 \times 2 \times 5$ and $4 \times 4 \times 5$ (support).

IC.4. EXPECTED RESULTS

Simulation should be performed up to an imposed displacement of:

- 0.6 mm in increments of 0.05 mm for the deep crack geometry;
- 1.2 mm in increments of 0.1 mm for the shallow crack geometry.

'Force' is the reaction force on the support: multiply by 4 to take the 2 symmetry planes into account.

LLD is equal to d1-d2,

where:

- d1 is the displacement in the $\vec{X}$ direction of the node located at coordinate ($x = 5$, $y = 20$, $z = 5$).
- d2 is the displacement in the $\vec{X}$ direction of the node located at coordinate ($x = -5$, $y = 0$, $z = 5$).
- CMOD is twice the displacement in the $\vec{Y}$ direction of the node located at coordinate ($x = -5$, $y = 0$, $z = 5$).

To evaluate the difference in loss of constraint between the two geometries $V(\sigma > \sigma_0)$ and σ_W should be reported. Note: the volume and Weibull stress for the entire specimen must be reported.

$V(\sigma > \sigma_0)$ is the total volume of material for which the maximal principal stress (σ) is larger than σ_0 where $\sigma_0 = 1.7 \, \sigma_{YS} = 703.8$ MPa and for which the plastic strain is larger than 0. Be careful that your FE model is only model ¼ of the total volume.

$$\sigma_W = \left(\int_{Vp} \sigma^m \frac{1}{V_0} dV \right)^{1/m} \tag{IC.3}$$

where σ is the maximal principal stress, $m = 6$, $V_0 = 1.25 \, 10^{-4}$ mm³ and Vp is the total volume for which the plastic strain is larger than 0. Be careful that your FE model is only model ¼ of the total volume. If Vpm is ¼ of the total volume of a precracked Charpy specimen for which the plastic strain is larger than 0, then:

$$\sigma_W = \left(4 \int_{Vpm} \sigma^m \frac{1}{V_0} dV \right)^{1/m} \tag{IC.4}$$

Any deviation from the recommendations in this guide should be reported, as well as the name and version of the finite element code used.

Shallow crack results

Displacement (mm)	Force (kN)	LLD (mm)	CMOD (mm)	$V(\sigma > \sigma_0)$ (mm³)	σ_W (MPa)
0	0	0	0	0	0
0.1					
0.2					
0.3					
0.4					
0.5					
0.6					
0.7					
0.8					
0.9					
1.0					
1.1					
1.2					

Deep crack results

Displacement (mm)	Force (kN)	LLD (mm)	CMOD (mm)	$V(\sigma > \sigma_0)$ (mm³)	σ_W (MPa)
0	0	0	0	0	0
0.05					
0.1					
0.15					
0.2					
0.25					
0.3					
0.35					
0.4					
0.45					
0.5					
0.55					
0.6					

IC.5. EXAMPLE OF INPUT FILE

ASCII input files with the information specified below can be obtained on request for the exercise. Each ASCII file contains a list of nodes and associated coordinate, a list of element and associated nodes. (Tabulations are used as separator.)

NODES

1   X_1 Y_1 Z_1
.
.
.
N X_N Y_N Z_N

ELEMENTS

1   N11 N21 N31 N41 N51 N61 N71 N81
.
.
.
E   N1E N2E N3E N4E N5E N6E N7E N8E

ID. TABULATED RESULTS FOR THE FINITE ELEMENT ROUND ROBIN PART 1

Laboratory 1: ABAQUS version 6.5-1

Force (kN)	LLD (mm)	CMOD (mm)
0	0	0
2.213932	0.05	0.0309392
4.07408	0.1	0.062641
5.0578	0.15	0.096275
5.6264	0.2	0.1307502
6.01588	0.25	0.1660936
6.30536	0.3	0.20232
6.532	0.35	0.239154
6.71744	0.4	0.276362
6.8746	0.45	0.313794
7.01156	0.5	0.351354

Laboratory 2: MSC-MARC

Force (kN)	LLD (mm)	CMOD (mm)
0	0	0
2.130806	0.05	0.0309627
4.2517464	0.1	0.06196678
5.290626	0.15	0.09581052
5.6654016	0.2	0.13019824
5.9754996	0.25	0.16505108
6.2085128	0.3	0.2008812
6.3661176	0.35	0.238475
6.5060932	0.4	0.2762372
6.6177972	0.45	0.3143944
6.7202828	0.5	0.3526048

Laboratory 3: ABAQUS 6.6

Force (kN)	LLD (mm)	CMOD (mm)
0	0	0
2.2156	0.05	0.03094
4.3117	0.1	0.06195
5.1809	0.15	0.09569
5.6004	0.2	0.12976
5.9203	0.25	0.1647
6.1682	0.3	0.20074
6.3544	0.35	0.23853
6.5063	0.4	0.27652
6.6291	0.45	0.31488
6.7333	0.5	0.35334

Laboratory 4: SYSTUS 2005

Force (kN)	LLD (mm)	CMOD (mm)
0	0	0
2.214	0.05	0.031
4.317	0.1	0.062
5.25	0.15	0.096
5.708	0.2	0.13
6.031	0.25	0.165
6.271	0.3	0.201
6.438	0.35	0.238
6.584	0.4	0.276
6.695	0.45	0.314
6.795	0.5	0.352

Laboratory 5: ANSYS version 9.0

Force (kN)	LLD (mm)	CMOD (mm)
0	0	0
2.3776	0.05	0.029556
4.6988	0.1	0.059166
5.4836	0.15	0.089646
6.0272	0.2	0.120342
6.4512	0.25	0.151894
6.7808	0.3	0.18441
6.9952	0.35	0.2183
7.1472	0.4	0.2525
7.2596	0.45	0.28678
7.338	0.5	0.32086

Laboratory 6.1: ABAQUS

Force (kN)	LLD (mm)	CMOD (mm)
0.000	0	0
2.227	0.05	0.031
4.407	0.1	0.072
5.158	0.15	0.106
5.608	0.2	0.141
5.917	0.25	0.177
6.145	0.3	0.213
6.321	0.35	0.25
6.472	0.4	0.288
6.592	0.45	0.325
6.668	0.5	0.352

Laboratory 6.2: ABAQUS

Force (kN)	LLD (mm)	CMOD (mm)
0.000	0	0
2.228	0.05	0.031
4.653	0.1	0.072
5.328	0.15	0.105
5.714	0.2	0.14
5.998	0.25	0.175
6.205	0.3	0.212
6.361	0.35	0.249
6.494	0.4	0.287
6.603	0.45	0.326
6.675	0.5	0.353

Laboratory 7.1: MSC-MARC 2005 r2

Force (kN)	LLD (mm)	CMOD (mm)
0	0	0
2.2157	0.05	0.030948
4.3193	0.1	0.061967
5.2744	0.15	0.095557
5.7581	0.2	0.12968
6.0972	0.25	0.16457
6.3536	0.3	0.20063
6.5539	0.35	0.23819
6.7119	0.4	0.27589
6.8487	0.45	0.31405
6.9707	0.5	0.35231

Laboratory 7.2: ABAQUS

Force (kN)	LLD (mm)	CMOD (mm)
0	0	0
2.2156	0.05	0.030936
4.318	0.1	0.061942
5.2544	0.15	0.09557
5.7112	0.2	0.12967
6.0388	0.25	0.16548
6.2772	0.3	0.2006
6.4456	0.35	0.238
6.5888	0.4	0.2758
6.7012	0.45	0.314
6.8028	0.5	0.3522

Laboratory 8: ABAQUS 6.3

Force (kN)	LLD (mm)	CMOD (mm)
0	0	0
2.216	0.05	0.0309366
4.316	0.1	0.061944
5.242	0.15	0.0955826
5.697	0.2	0.1296948
6.021	0.25	0.1646084
6.259	0.3	0.200576
6.426	0.35	0.238106
6.565	0.4	0.275878
6.672	0.45	0.314044
6.77	0.5	0.352274

Laboratory 9: ANSYS

Force (kN)	LLD (mm)	CMOD (mm)
0	0	0
2.38	0.05	0.0296
4.69	0.1	0.0592
5.47	0.15	0.0897
6.01	0.2	0.12
6.43	0.25	0.152
6.74	0.3	0.184
6.95	0.35	0.218
7.11	0.4	0.253
7.26	0.45	0.287
7.38	0.5	0.321

Laboratory 10: ABAQUS 6.3-1

Force (kN)	LLD (mm)	CMOD (mm)
0	0	0
2.205	0.05	0.031
4.303	0.1	0.062
5.238	0.15	0.096
5.692	0.2	0.13
6.018	0.25	0.165
6.257	0.3	0.2
6.424	0.35	0.238
6.567	0.4	0.276
6.681	0.45	0.314
6.782	0.5	0.352

IE. TABULATED RESULTS FOR THE FINITE ELEMENT ROUND ROBIN PART 2

Laboratory 1: ABAQUS version 6.7

Deep crack

Displ. (mm)	Force (kN)	LLD (mm)	CMOD (mm)	V(s>s0) (mm³)	sw (MPa)
0	0	0	0	0	0
0.05	1.6	0.045	0.027	0.3	3458
0.1	2.97	0.09	0.056	3.3	5182
0.15	3.79	0.135	0.086	9.2	6232
0.2	4.16	0.182	0.119	14.2	6782
0.25	4.37	0.23	0.152	17.8	7110
0.3	4.52	0.278	0.187	20.6	7353
0.35	4.64	0.327	0.221	22.6	7540
0.4	4.73	0.375	0.256	24.4	7692
0.45	4.82	0.423	0.291	26	7822
0.5	4.89	0.471	0.326	27.4	7931
0.55	4.95	0.52	0.361	28.8	8026
0.6	5.01	0.568	0.396	30.1	8109

Shallow crack

Displ. (mm)	Force (kN)	LLD (mm)	CMOD (mm)	V(s>s0) (mm³)	sw (MPa)
0	0	0	0	0	0
0.1	6.74	0.065	0.011	0.7	3907
0.2	10.58	0.126	0.028	5.5	5704
0.3	12	0.198	0.05	8.6	6375
0.4	12.73	0.274	0.074	12.3	6716
0.5	13.22	0.353	0.098	14.9	6954
0.6	13.59	0.433	0.124	17.8	7135
0.7	13.88	0.513	0.149	20.8	7281
0.8	14.13	0.594	0.175	22.7	7399
0.9	14.34	0.676	0.201	25.1	7502
1	14.52	0.757	0.228	27.3	7592
1.1	14.68	0.839	0.254	29.3	7672
1.2	14.82	0.921	0.28	31.7	7742

Laboratory 2: MSC-MARC

Deep crack

Displ. (mm)	Force (kN)	LLD (mm)	CMOD (mm)	V(s>s0) (mm³)	sw (MPa)
0	0	0	0	0	0
0.05	1.714	0.047	0.029	0.39	3782
0.1	3.262	0.095	0.058	3.97	5870
0.15	4.102	0.143	0.090	11.62	6665
0.2	4.343	0.193	0.125	15.85	6973
0.25	4.487	0.242	0.160	18.08	7167
0.3	4.621	0.291	0.195	20.18	7386
0.35	4.740	0.340	0.230	21.81	7584
0.4	4.842	0.390	0.265	23.76	7741
0.45	4.929	0.439	0.300	25.03	7849
0.5	5.004	0.488	0.335	26.44	7949
0.55	5.069	0.537	0.371	27.76	8037
0.6	5.127	0.586	0.406	28.90	8110

Shallow crack

Displ. (mm)	Force (kN)	LLD (mm)	CMOD (mm)	V(s>s0) (mm³)	sw (MPa)
0	0	0	0	0	0
0.1	7.856	0.075	0.012	1.13	4696
0.2	11.891	0.153	0.032	5.32	6305
0.3	12.458	0.239	0.059	7.35	6440
0.4	12.923	0.324	0.085	9.93	6777
0.5	13.340	0.408	0.111	12.80	7011
0.6	13.681	0.493	0.137	15.26	7195
0.7	13.958	0.577	0.163	18.25	7306
0.8	14.191	0.661	0.189	20.43	7368
0.9	14.391	0.745	0.215	24.04	7444
1	14.563	0.828	0.241	27.12	7516
1.1	14.712	0.912	0.267	29.91	7586
1.2	14.843	0.995	0.293	32.34	7656

Laboratory 3: ABAQUS 6.6

Deep crack

Displ. (mm)	Force (kN)	LLD (mm)	CMOD (mm)	V(s>s0) (mm³)	sw (MPa)
0	0	0	0	0	0
0.05	1.710	0.048	0.029	0.36	3476
0.1	3.120	0.095	0.059	3.70	5297
0.15	3.870	0.144	0.091	9.67	6227
0.2	4.170	0.193	0.125	13.70	6760
0.25	4.360	0.242	0.160	16.60	7109
0.3	4.500	0.291	0.195	19.00	7361
0.35	4.600	0.340	0.230	21.20	7553
0.4	4.690	0.389	0.265	22.60	7707
0.45	4.770	0.438	0.300	23.40	7834
0.5	4.830	0.487	0.336	24.60	7941
0.55	4.880	0.536	0.371	25.70	8033
0.6	4.930	0.585	0.407	26.70	8114

Shallow crack

Displ. (mm)	Force (kN)	LLD (mm)	CMOD (mm)	V(s>s0) (mm³)	sw (MPa)
0	0	0	0	0	0
0.1	7.540	0.073	0.013	0.97	4136
0.2	11.000	0.148	0.036	4.67	5467
0.3	12.000	0.229	0.061	7.67	6002
0.4	12.700	0.311	0.087	11.36	6324
0.5	13.100	0.394	0.114	16.07	6543
0.6	13.400	0.477	0.141	17.97	6701
0.7	13.600	0.560	0.168	20.98	6820
0.8	13.900	0.642	0.196	23.85	6913
0.9	14.000	0.725	0.224	25.74	6988
1	14.200	0.808	0.252	28.57	7051
1.1	14.300	0.891	0.280	30.52	7103
1.2	14.400	0.973	0.309	32.09	7147

Laboratory 4: SYSTUS 2006

Deep crack

Displ. (mm)	Force (kN)	LLD (mm)	CMOD (mm)	V(s>s0) (mm³)	sw (MPa)
0	0	0	0	0	0
0.05	1.719	0.047	0.029	0.44	3551
0.1	3.181	0.095	0.059	4.03	5352
0.15	3.999	0.143	0.091	10.75	6398
0.2	4.333	0.192	0.125	15.22	6888
0.25	4.531	0.241	0.159	18.50	7192
0.3	4.671	0.290	0.194	20.96	7416
0.35	4.780	0.340	0.230	23.06	7593
0.4	4.868	0.389	0.265	24.53	7736
0.45	4.942	0.438	0.300	25.96	7857
0.5	5.006	0.487	0.336	27.36	7961
0.55	5.061	0.535	0.371	28.16	8051
0.6	5.110	0.584	0.407	29.31	8130

Shallow crack

Displ. (mm)	Force (kN)	LLD (mm)	CMOD (mm)	V(s>s0) (mm³)	sw (MPa)
0	0	0	0	0	0
0.1	7.695	0.074	0.013	1.11	4222
0.2	11.404	0.150	0.035	4.56	5854
0.3	12.534	0.233	0.061	7.77	6402
0.4	13.135	0.318	0.087	10.94	6709
0.5	13.549	0.403	0.115	13.98	6923
0.6	13.864	0.488	0.142	17.13	7088
0.7	14.117	0.573	0.170	20.25	7222
0.8	14.326	0.658	0.197	23.08	7335
0.9	14.502	0.743	0.225	26.54	7434
1	14.653	0.827	0.253	31.64	7520
1.1	14.785	0.912	0.282	33.77	7599
1.2	14.900	0.996	0.310	35.67	7669

Laboratory 5: ANSYS version 9.0

Deep crack

Displ. (mm)	Force (kN)	LLD (mm)	CMOD (mm)	V(s>s0) (mm³)	sw (MPa)
0	0	0	0	0	0
0.05	1.833	0.049	0.030	0.54	3565
0.1	3.297	0.099	0.061	4.93	5351
0.15	4.085	0.148	0.094	11.91	6351
0.2	4.393	0.198	0.129	16.07	6808
0.25	4.578	0.247	0.164	19.10	7101
0.3	4.710	0.296	0.199	21.16	7315
0.35	4.814	0.346	0.235	23.16	7490
0.4	4.898	0.395	0.270	24.57	7630
0.45	4.968	0.444	0.306	26.20	7751
0.5	5.028	0.493	0.342	27.30	7852
0.55	5.079	0.542	0.377	28.31	7941
0.6	5.124	0.591	0.413	29.16	8020

Shallow crack

Displ. (mm)	Force (kN)	LLD (mm)	CMOD (mm)	V(s>s0) (mm³)	sw (MPa)
0	0	0	0	0	0
0.1	8.756	0.086	0.016	1.59	4072
0.2	11.962	0.171	0.042	5.41	5048
0.3	12.906	0.258	0.069	8.63	5464
0.4	13.426	0.346	0.097	11.84	5743
0.5	13.785	0.433	0.125	15.49	5970
0.6	14.058	0.520	0.153	18.43	6142
0.7	14.278	0.606	0.182	21.56	6290
0.8	14.461	0.692	0.210	24.39	6418
0.9	14.616	0.778	0.239	27.37	6534
1	14.749	0.864	0.268	30.22	6637
1.1	14.866	0.949	0.297	31.98	6718
1.2	14.969	1.034	0.326	34.75	6804

Laboratory 6: ABAQUS 6.6-1

Deep crack

Displ. (mm)	Force (kN)	LLD (mm)	CMOD (mm)	V(s>s0) (mm³)	sw (MPa)
0	0	0	0	0	0
0.05	1.730	0.048	0.029	0.44	3596
0.1	3.486	0.109	0.068	5.96	5748
0.15	4.126	0.158	0.101	12.86	6631
0.2	4.400	0.208	0.135	16.19	7017
0.25	4.574	0.257	0.170	19.27	7297
0.3	4.704	0.307	0.205	21.34	7512
0.35	4.808	0.357	0.240	23.40	7687
0.4	4.894	0.407	0.276	24.90	7832
0.45	4.968	0.457	0.311	26.10	7955
0.5	5.032	0.507	0.347	27.26	8063
0.55	5.090	0.558	0.382	28.35	8156
0.6	5.127	0.593	0.408	29.28	8218

Shallow crack

Displ. (mm)	Force (kN)	LLD (mm)	CMOD (mm)	V(s>s0) (mm³)	sw (MPa)
0	0	0	0	0	0
0.1	7.765	0.075	0.013	1.14	4265
0.2	11.888	0.176	0.043	5.62	6089
0.3	12.888	0.241	0.063	8.32	6458
0.4	13.363	0.307	0.084	11.06	6702
0.5	13.772	0.394	0.112	14.92	6938
0.6	14.094	0.481	0.140	18.55	7118
0.7	14.357	0.568	0.168	22.46	7262
0.8	14.582	0.656	0.197	25.98	7385
0.9	14.776	0.744	0.225	30.50	7490
1	14.943	0.832	0.254	33.42	7582
1.1	15.021	0.920	0.283	38.91	7664
1.2	15.183	1.023	0.317	44.27	7751

Laboratory 7: MSC-MARC 2005 r2

Deep crack

Displ. (mm)	Force (kN)	LLD (mm)	CMOD (mm)	V(s>s0) (mm³)	sw (MPa)
0	0	0	0	0	0
0.05	1.714	0.047	0.029	0.40	3809
0.1	3.274	0.095	0.058	4.16	5983
0.15	4.173	0.143	0.090	12.10	6862
0.2	4.490	0.192	0.124	17.29	7257
0.25	4.668	0.242	0.159	20.51	7511
0.3	4.817	0.291	0.194	22.61	7737
0.35	4.947	0.340	0.228	24.88	7941
0.4	5.056	0.389	0.264	26.89	8107
0.45	5.150	0.438	0.299	28.56	8240
0.5	5.232	0.487	0.334	30.41	8354
0.55	5.304	0.536	0.369	31.57	8454
0.6	5.368	0.585	0.405	32.89	8543

Shallow crack

Displ. (mm)	Force (kN)	LLD (mm)	CMOD (mm)	V(s>s0) (mm³)	sw (MPa)
0	0	0	0	0	0
0.1	7.779	0.075	0.013	1.19	4313
0.2	11.617	0.153	0.034	4.98	6002
0.3	12.836	0.237	0.059	8.81	6543
0.4	13.560	0.322	0.084	13.03	6886
0.5	14.080	0.407	0.110	17.55	7133
0.6	14.485	0.493	0.135	21.13	7324
0.7	14.817	0.578	0.161	26.70	7477
0.8	15.095	0.664	0.186	29.92	7609
0.9	15.299	0.749	0.212	34.28	7716
1	15.520	0.834	0.237	37.48	7812
1.1	15.708	0.919	0.262	39.95	7903
1.2	15.875	1.004	0.287	43.24	7986

Laboratory 8: ABAQUS 6.5

Deep crack

Displ. (mm)	Force (kN)	LLD (mm)	CMOD (mm)	V(s>s0) (mm³)	sw (MPa)
0	0	0	0	0	0
0.05	1.721	0.047	0.029	0.40	3535
0.1	3.183	0.095	0.059	3.95	5353
0.15	3.995	0.144	0.091	10.61	6406
0.2	4.326	0.193	0.125	14.98	6897
0.25	4.522	0.243	0.160	18.22	7211
0.3	4.664	0.293	0.195	20.61	7445
0.35	4.776	0.343	0.230	22.58	7633
0.4	4.868	0.393	0.266	24.36	7790
0.45	4.948	0.443	0.301	25.52	7923
0.5	5.018	0.493	0.337	26.57	8040
0.55	5.080	0.543	0.372	27.47	8143
0.6	5.136	0.593	0.408	28.91	8236

Shallow crack

Displ. (mm)	Force (kN)	LLD (mm)	CMOD (mm)	V(s>s0) (mm³)	sw (MPa)
0	0	0	0	0	0
0.1	7.727	0.074	0.013	1.10	4219
0.2	11.428	0.152	0.036	4.58	5851
0.3	12.571	0.236	0.062	7.80	6409
0.4	13.198	0.322	0.089	11.14	6727
0.5	13.643	0.409	0.116	14.58	6954
0.6	13.992	0.497	0.144	18.02	7132
0.7	14.260	0.584	0.172	21.31	7278
0.8	14.525	0.672	0.200	24.60	7403
0.9	14.739	0.761	0.229	27.60	7512
1	14.928	0.849	0.257	32.08	7611
1.1	15.098	0.938	0.285	35.62	7699
1.2	15.251	1.026	0.314	38.95	7780

114

Laboratory 9: ANSYS 8.1

Deep crack

Displ. (mm)	Force (kN)	LLD (mm)	CMOD (mm)	V(s>s0) (mm³)	sw (MPa)
0	0	0	0	0	0
0.05	1.727	0.047	0.029	0.43	3402
0.1	3.189	0.095	0.059	3.96	5261
0.15	4.004	0.144	0.091	10.75	6331
0.2	4.336	0.193	0.125	15.23	6824
0.25	4.529	0.242	0.160	18.45	7127
0.3	4.667	0.291	0.195	20.89	7350
0.35	4.774	0.340	0.230	22.90	7525
0.4	4.862	0.389	0.265	24.61	7667
0.45	4.935	0.438	0.300	25.83	7787
0.5	4.997	0.487	0.336	27.13	7889
0.55	5.052	0.536	0.371	28.12	7978
0.6	5.099	0.585	0.407	28.79	8057

Shallow crack

Displ. (mm)	Force (kN)	LLD (mm)	CMOD (mm)	V(s>s0) (mm³)	sw (MPa)
0	0	0	0	0	0
0.1	7.748	0.075	0.013	1.14	4148
0.2	11.429	0.152	0.035	4.69	5820
0.3	12.550	0.235	0.061	7.86	6361
0.4	13.145	0.320	0.088	10.99	6664
0.5	13.557	0.405	0.115	14.24	6876
0.6	13.870	0.490	0.142	17.22	7039
0.7	14.121	0.575	0.170	20.18	7171
0.8	14.327	0.661	0.198	23.09	7283
0.9	14.501	0.746	0.226	25.67	7381
1	14.651	0.831	0.254	29.09	7467
1.1	14.781	0.915	0.282	31.02	7545
1.2	14.894	1.000	0.311	33.37	7616

Laboratory 10: ABAQUS / Standard 6.6-2

Deep crack

Displ. (mm)	Force (kN)	LLD (mm)	CMOD (mm)	V(s>s0) (mm³)	sw (MPa)
0	0	0	0	0	0
0.05	1.730	0.047	0.029	0.44	3555
0.1	3.200	0.095	0.059	4.05	5360
0.15	4.030	0.144	0.091	10.86	6402
0.2	4.370	0.193	0.125	15.15	6873
0.25	4.570	0.242	0.160	18.36	7165
0.3	4.710	0.291	0.196	20.83	7380
0.35	4.810	0.340	0.231	22.53	7550
0.4	4.900	0.389	0.266	24.23	7689
0.45	4.970	0.438	0.302	25.70	7809
0.5	5.030	0.487	0.338	26.80	7911
0.55	5.090	0.536	0.373	27.89	8002
0.6	5.140	0.585	0.409	28.83	8082

Shallow crack

Displ. (mm)	Force (kN)	LLD (mm)	CMOD (mm)	V(s>s0) (mm³)	sw (MPa)
0	0	0	0	0	0
0.1	7.700	0.074	0.013	1.11	4226
0.2	11.410	0.151	0.035	4.59	5861
0.3	12.540	0.234	0.061	7.82	6410
0.4	13.140	0.318	0.087	10.99	6717
0.5	13.560	0.404	0.115	14.18	6932
0.6	13.870	0.489	0.142	17.25	7098
0.7	14.120	0.574	0.170	20.36	7234
0.8	14.330	0.659	0.197	23.11	7348
0.9	14.510	0.744	0.225	27.15	7448
1	14.660	0.829	0.253	31.91	7536
1.1	14.790	0.913	0.281	34.01	7615
1.2	14.900	0.998	0.310	35.93	7688

APPENDIX II
TOPIC AREA 2

IIA. MASTER CURVE DATASETS PROVIDED BY CRP-8 PARTICIPANTS FOR INVESTIGATING THE EFFECT OF LOADING RATE ON T_0

Tables IIA.1 and IIA.2 summarize the Master Curve T_0 results for the JRQ steel and other national steels.

TABLE IIA.1. MASTER CURVE DATASETS FOR JRQ STEEL

JRQ Block	Country code	W mm	B mm	B_N mm	Spec. type	Loading rate MPa√m/s	$T_0^{measured}$ °C	σ_{T0} K	$\sum n_i$
5JRQ12	BEL (SCK•CEN)	10	10	8	PCC	1.18E+00	-57.3	6.0	1.50
5JRQ12		10	10	8	PCC	3.67E+05	-14.7	6.8	1.07
5JRQ22	GER (FZD)	10	10	8	PCC	7.36E+05	-1.5	1.9	9.94
5JRQ33		10	10	8	PCC	1.20E+00	-59.0	5.2	1.60
5JRQ34		10	10	8	PCC	1.00E-01	-64.0	6.0	1.90
5JRQ34		10	10	8	PCC	7.00E-01	-59.0	5.4	1.40
5JRQ34		10	10	10	PCC	7.00E-01	-62.0	5.7	1.80
5JRQ34	RUS (RRC KI)	25	12.5	10	C(T)	4.00E-01	-61.0	5.4	1.80
5JRQ34		10	4	4	SE(B)	5.00E-01	-94.0	6.4	1.20
5JRQ34		10	4	3.2	SE(B)	5.00E-01	-75.0	6.6	1.14
5JRQ34		10	4	3.2	SE(B)	5.00E-01	-73.0	6.7	1.20
5JRQ53	CZR (NRI)	10	10	8	PCC	1.99E+00	-61.8	5.7	1.51
5JRQ53		10	10	10	PCC	5.91E+05	12.5	6.0	1.37
5JRQ45	USE (Westinghouse)	10	10	10	PCC	1.5E+02	-45.9	5.7	1.67
5JRQ45		10	10	10	PCC	1.4E+03	-40.0	5.9	1.43
6JRQ	JAP (JAEA)	10	10	8	PCC	2.00E+00	-75.8	N/A	N/A
6JRQ		10	10	8	PCC	7.27E+02	-43.1	N/A	N/A
6JRQ12	GER (FZD)	10	10	8	PCC	1.20E+00	-61.6	6.0	1.43
6JRQ12		10	10	8	PCC	1.20E+00	-55.9	6.3	1.19
6JRQ34		10	10	10	PCC	6.10E-01	-67.8	6.8	1.17
6JRQ34	ESP (CIEMAT)	10	10	10	PCC	1.00E+00	-53.5	4.1	3.21
6JRQ34		10	10	10	PCC	6.30E+00	-62.1	6.6	1.19
6JRQ34		10	10	10	PCC	6.30E+01	-54.2	7.1	1.00
6JRQ34		10	10	10	PCC	1.29E+03	-45.5	6.6	1.00
8JRQ33	KOR (KAERI)	10	10	10	PCC	1.00E+00	-57.3	N/A	1.20
8JRQ44		10	10	8	PCC	4.80E+05	12.8	N/A	1.20
8JRQ34		20	10	10	C(T)	5.30E-02	-57.4	5.0	2.17
8JRQ34		10	10	10	PCC	1.60E-01	-60.4	5.2	2.00
8JRQ52	MEX (ININ)	50.8	25.4	25.4	C(T)	9.41E-01	-45.5	5.2	1.86
8JRQ34		10	10	10	PCC	1.80E-01	-70.1	6.0	1.50
8JRQ34		10	10	10	PCC	2.70E+00	-51.7	5.2	1.86

TABLE IIA.1. MASTER CURVE DATASETS FOR JRQ STEEL (cont.)

JRQ Block	Country code	W mm	B mm	B_N mm	Spec. type	Loading rate MPa√m/s	$T_0^{measured}$ °C	σ_{T0} K	$\sum n_i$
8JRQ44	BEL (SCK•CEN)	10	10	8	PCC	7.16E+02	-48.0	5.4	1.71
8JRQ44		4	3	3	PCC	4.54E+03	-33.0	7.7	0.77
8JRQ44	GER (FZD)	10	10	8	PCC	1.00E+04	-19.3	5.7	1.43
8JRQ44		10	10	8	PCC	1.20E+00	-71.4	6.4	1.29
8JRQ44	JAP (CRIEPI)	10	10	8	PCC	4.10E+05	10.0	N/A	8.00
8JRQ44	RRE*	10	10	8	PCC	3.50E+05	-4.2	2.0	13.21

* RRE is the round robin exercise results

TABLE IIA.2. MASTER CURVE DATASETS FOR OTHER NATIONAL STEELS

Material ID	Code	Specimen type	W mm	B mm	B_N mm	Loading rate MPa√m/s	T_0 °C	σ_{T0} K	Σn_i
10 CrMo 9 10	GER (FZD)	PCC	10	10	8	1.20E+00	-111.4	5.7	1.29
10 CrMo 9 10	GER (FZD)	PCC	10	10	8	1.20E+00	-109.7	5.7	1.43
EUROFER97	BEL (SCK•CEN)	PCC	10	10	8	8.2E-01	-112.0	4.4	2.52
EUROFER97	BEL (SCK•CEN)	PCC	10	10	8	6.95E+02	-79.0	6.4	1.33
EUROFER97	BEL (SCK•CEN)	PCC	10	10	8	4.12E+05	-24.0	5.7	1.52
HX400	FIN (VTT)	PCC	10	10	8	1.00E-01	-27.0	N/A	N/A
HX400	FIN (VTT)	PCC	10	10	8	2.00E+00	-24.0	N/A	N/A
15X2MFA unirrad. (BM)	FIN (VTT)	PCC	10	10	8	1.00E+00	-133.0	6.0	1.50
15X2MFA irrad. (BM)	FIN (VTT)	PCC	10	10	8	1.00E+00	-102.0	6.3	1.40
15X2MFA unirrad. (BM)	FIN (VTT)	PCC	10	10	8	7.50E+05	-16.0	(5)	(>1)
15X2MFA irrad. (BM)	FIN (VTT)	PCC	10	10	8	7.50E+05	-1.0	(6)	(>1)
JSPS	JAP (JAEA)	PCC	10	10	8	9.00E-01	0.3	N/A	N/A
JSPS	JAP (JAEA)	PCC	10	10	8	1.07E+03	25.9	N/A	N/A
JSPS	BEL (SCK•CEN)	PCC	10	10	8	1.00E+00	-6.4	3.0	5.62
JSPS	BEL (SCK•CEN)	PCC	10	10	8	7.16E+02	14.0	5.9	1.45
JSPS	BEL (SCK•CEN)	PCC	10	10	8	4.83E+05	34.0	6.0	1.50
SFVQ1A (A508 Cl. 3)	JAP (CRIEPI)	C(T)	50.8	25.4	25.4	7.40E-03	-117.0	N/A	6.00
SFVQ1A (A508 Cl. 3)	JAP (CRIEPI)	C(T)	50.8	25.4	25.4	7.10E+00	-90.0	N/A	6.00
SFVQ1A (A508 Cl. 3)	JAP (CRIEPI)	C(T)	50.8	25.4	25.4	6.10E+01	-74.0	N/A	6.00
Steel A	JAP (JAEA)	PCVN	10	10	8	8.00E-01	-69.6	N/A	N/A
Steel A	JAP (JAEA)	PCVN	10	10	8	5.64E+01	-63.4	N/A	N/A
Steel A	JAP (JAEA)	PCVN	10	10	8	1.09E+03	-32.2	N/A	N/A
Steel A	JAP (JAEA)	PCVN	10	10	8	1.10E+03	-45.3	N/A	N/A
Steel L	JAP (JAEA)	PCVN	10	10	8	8.00E-01	-112.5	N/A	N/A
Steel L	JAP (JAEA)	PCVN	10	10	8	1.15E+03	-64.6	N/A	N/A
HSST-14	USA ORNL/USNA	C(T)	50.8	25.4	20.32	1.00E+00	-57.5	5.2	2.00
HSST-14	USA ORNL/USNA	C(T)	101.6	50.8		6.27E+03	-27.8	9.0	0.67
HSST-14	USA ORNL/USNA	C(T)	101.6	50.8		1.69E+05	-17.3	4.8	2.33

IIB. ASSESSMENT OF THE LOADING RATE IN A FRACTURE TOUGHNESS TEST

For fracture toughness tests in the ductile-to-brittle transition region, the current ASTM standard E1921-05 requires specimens to be loaded using a loading rate *dK/dt* between 0.1 and 2 MPa√m/s during the initial elastic portion. A table is also provided, which allows estimating the testing machine loading rate associated with this allowable range, both in terms of time to control load t_M or specimen load-line displacement rate $\dot{\Delta}_{LL}$. It has been proposed that the standard allow testing at higher loading rates, including precracked Charpy specimens tested with an instrumented pendulum machine (impact toughness tests). The revised version of ASTM E1921 would require test results (K_{Jc} or T_0) to be reported along with the relevant loading rate (*dK/dt*), and should therefore provide guidance on how to assess the value of *dK/dt* in a relatively simple, but reliable manner.

IIB.1. POSSIBLE OPTIONS FOR $\dot{K}$ EVALUATION IN A FRACTURE TOUGHNESS TEST

The loading rate is not constant during a fracture toughness test, particularly once plasticity is evident in the force/displacement record. However, for practical purposes it is necessary to specify a single value of *dK/dt* to be associated to the individual test result and reported with the measured data. This might also be prescribed in a future revision of ASTM E1921 or in the future ISO standard on impact toughness tests. In this paper, the following five options have been investigated.

(a) Average value of *dK/dt*, calculated using each individual force/time data point in a test up to cleavage or test termination. This option is the most time-consuming from a computational point of view. In practical terms, for the *N*-th data point $dK = K_N - K_{N-1}$ and $dt = t_N - t_{N-1}$.

(b) Ratio between stress intensity factor and corresponding time at cleavage or test termination (K_c/t_c). Since K_c is always calculated, the only additional parameter that needs to be evaluated is t_c.

(c) Estimation based on Table 3 of ASTM E1921-05 (reproduced below), which is intended to help the user choose the appropriate value of load-line displacement rate ($\dot{\Delta}_{LL}$) or t_M (time to control force P_M) corresponding to the required loading rate *dK/dt*. In the table, *a* is the crack size, *W* the specimen width, σ_Y the yield strength at the test temperature, $\dot{K}$ or $\dfrac{dK}{dt}$ the loading rate and *E* the Young's modulus.

SE(B) Specimen Rate Estimation			C(T) Specimen Rate Estimation		
a/W	$\dfrac{t_M \dot{K}}{\sigma_Y \sqrt{W}}$	$\dfrac{E\dot{\Delta}_{LL}}{\frac{dK}{dt}\sqrt{W}}$	a/W	$\dfrac{t_M \dot{K}}{\sigma_Y \sqrt{W}}$	$\dfrac{E\dot{\Delta}_{LL}}{\frac{dK}{dt}\sqrt{W}}$
0.45	0.346	5.064	0.45	0.412	3.475
0.50	0.333	5.263	0.50	0.386	3.829
0.55	0.318	5.522	0.55	0.361	4.212
0.60	0.302	5.851	0.60	0.336	4.635
0.65	0.283	6.267	0.65	0.312	5.118
0.70	0.263	6.798	0.70	0.287	5.696

By fitting the values in the third or sixth column as a function of a/W and solving the relationship for dK/dt, the loading rate can be easily calculated since all remaining variables (a, W, E and load-line displacement rate) are known.

(d) Ratio between stress intensity factor and corresponding time within the linear elastic region of the test record (K_{el}/t_{el}). This option requires only the determination of K_{el} and t_{el} at an arbitrarily chosen point along the linear elastic slope.

(e) Value of loading rate dK/dt at the instant preceding cleavage fracture (or test termination); i.e. if N corresponds to the instant of cleavage, the loading rate to be considered would be $(dK/dt)_{N-1} = (K_{N-1}-K_{N-2})/(t_{N-1}-t_{N-2})$.

IIB.2. INVESTIGATIONS PERFORMED

The study consisted in analysing data from 27 fracture toughness tests. More specifically, three steels with significantly different characteristics (all previously described) were chosen:

- EUROFER97;
- JRQ;
- JSPS.

Three displacement (loading) rate regimes were examined:

- quasi-static (machine crosshead displacement rate = 0.2 mm/min; sampling time = 1 s; digital precision A/D converter = 24 bit);
- intermediate/dynamic (displacement rate = 150 mm/min; sampling time = 0.2 ms; digital precision A/D converter = 24 bit);
- impact (tests performed on precracked Charpy specimens using an instrumented pendulum with impact velocities in the range 1.2–1.6 m/s; sampling time = 0.5 μs; digital precision A/D converter = 12 bit).

Tests were performed in accordance with ASTM E1921-05 (quasi-static and dynamic rates) and the ESIS TC5 Test Procedure (impact rates). Typical test records for the three loading rates are shown in Figure IIB.1 (JRQ steel in mid transition regime, K_{Jc} = 99 to 133 MPa√m).
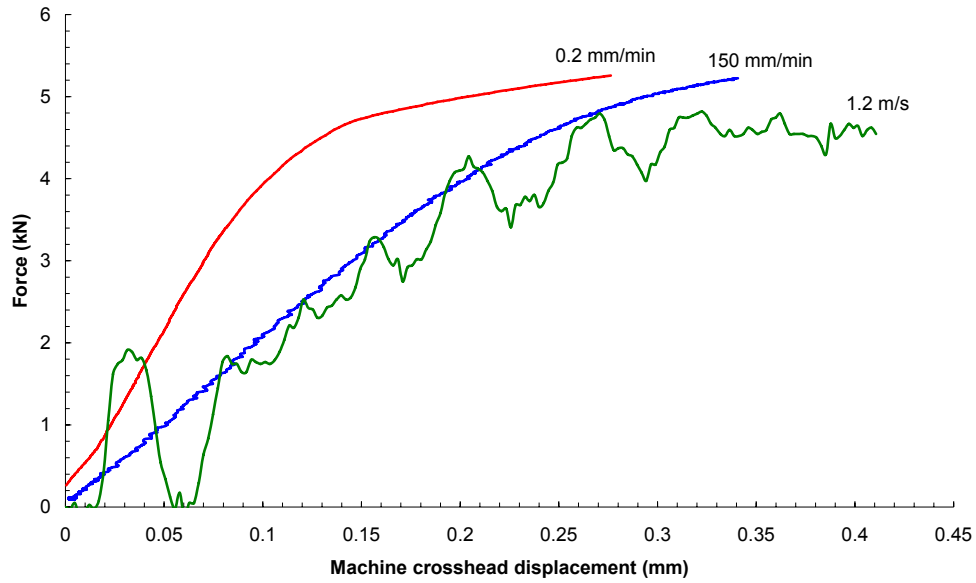
FIG. IIB.1. Typical test records for three different loading rates (JRQ steel).

Three different fracture toughness levels were considered (typical examples of test records are shown in Figure IIB.2 for the lowest loading rate, i.e. 0.2 mm/min):

- lower transition regime (K_{Jc} = 41–88 MPa√m);
- mid transition regime (K_{Jc} = 98–133 MPa√m);
- upper transition regime (K_{Jc} = 138–241 MPa√m).
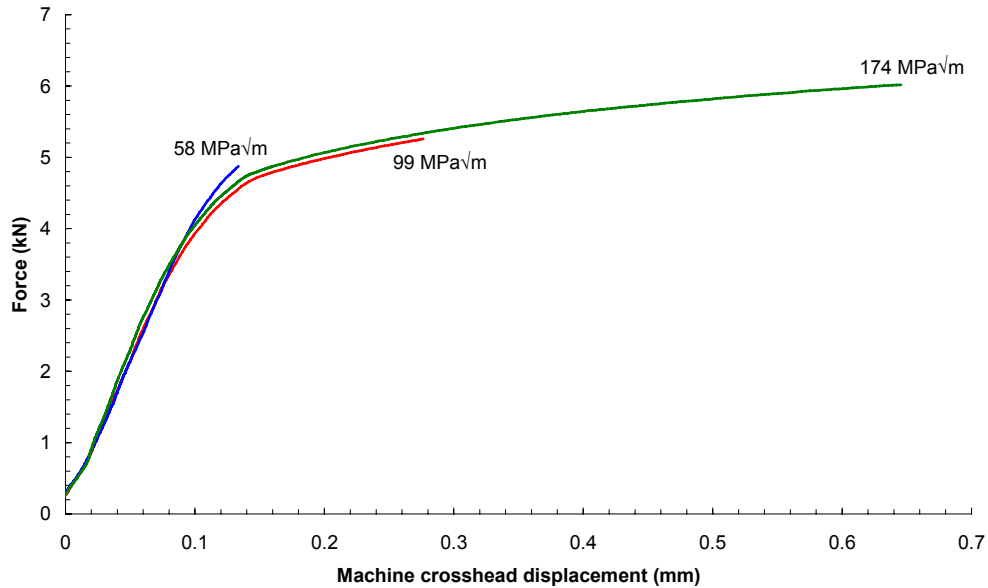
FIG. IIB.2. Typical test records for the three toughness levels (JRQ steel, 0.2 mm/min).

In order to illustrate four of the five investigated approaches, the force/time record for one of the tests (JRQ steel, 0.2 mm/min, K_{Jc} = 174 MPa√m) is shown in Figures IIB.3 and IIB.4 together with the evolution of the loading rate and the stress intensity factor, respectively. Options (a) and (e) are depicted in Figure IIB.3, while Figure IIB.4 illustrates options (b) and (d).
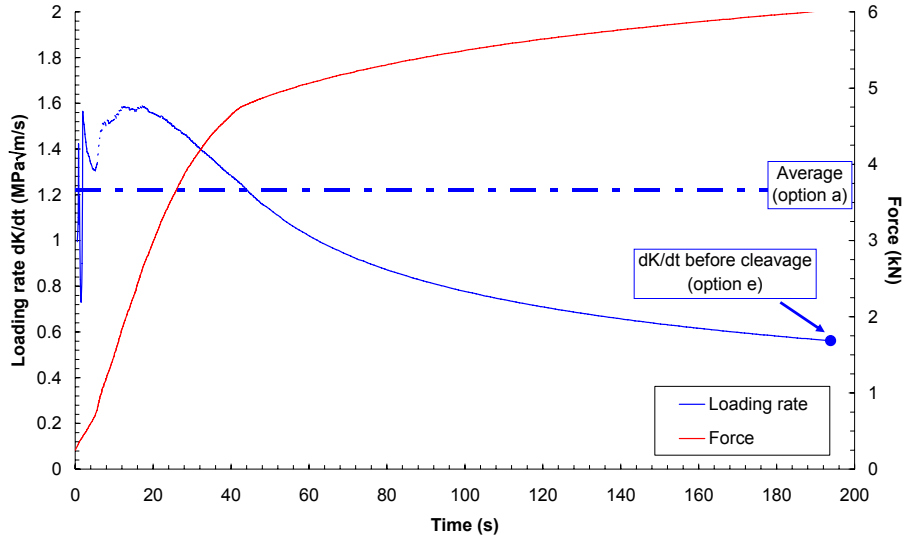
FIG. IIB.3. Loading rate and test record for a JRQ specimen tested at 0.2 mm/min. Options (a) and (e) are illustrated.
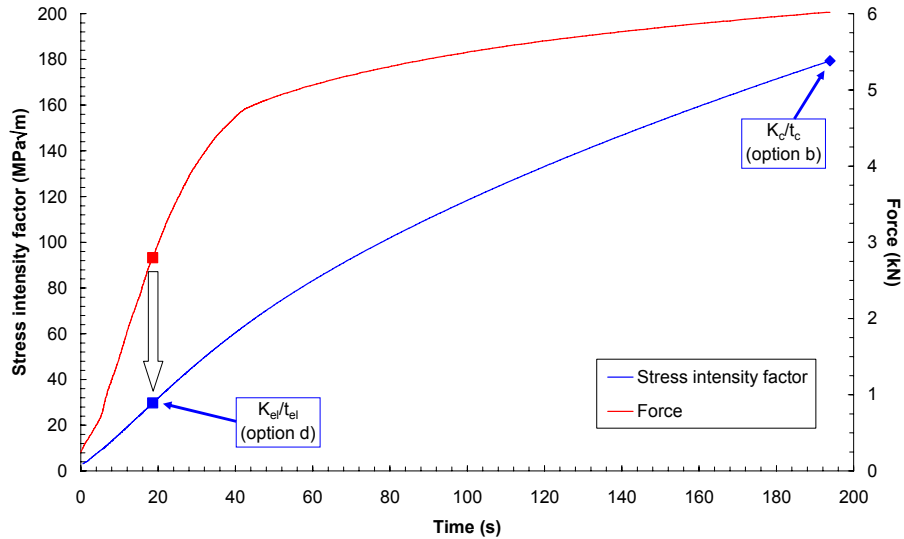
FIG. IIB.4. Stress intensity factor and test record for a JRQ specimen tested at 0.2 mm/min. Options (b) and (d) are illustrated.

As far as option (c) is concerned, the loading rate for a SE(B) specimen can be estimated from the left-hand side of Table 3 from ASTM E1921-05 using:

$$\frac{dK}{dt} = \frac{E \cdot \dot{\Delta}_{LL}}{Y \cdot \sqrt{W}} \tag{IIB.1}$$

where E is in MPa, $\dot{\Delta}_{LL}$ is in m/s, W is in m and Y is a function of a/W obtained by fitting a third-order polynomial curve through the values in the third column in the table and is given by:

$$Y\left(\frac{a}{W}\right) = 24.15 \cdot \left(\frac{a}{W}\right)^3 - 25.31 \cdot \left(\frac{a}{W}\right)^2 + 11.72 \cdot \left(\frac{a}{W}\right) + 2.272 \tag{IIB.2}$$

IIB.3. RESULT OBTAINED

The values of loading rate calculated using the five options previously listed for the 27 fracture toughness tests considered are presented in Table IIB.1.

As an example, results for tests conducted in the lower transition regime (K_{Jc} = 41 to 88 MPa√m) are illustrated in more detail using histograms in Figure IIB.5 (quasi-static loading rates), Figure IIB.6 (intermediate/dynamic) and Figure IIB.7 (impact).
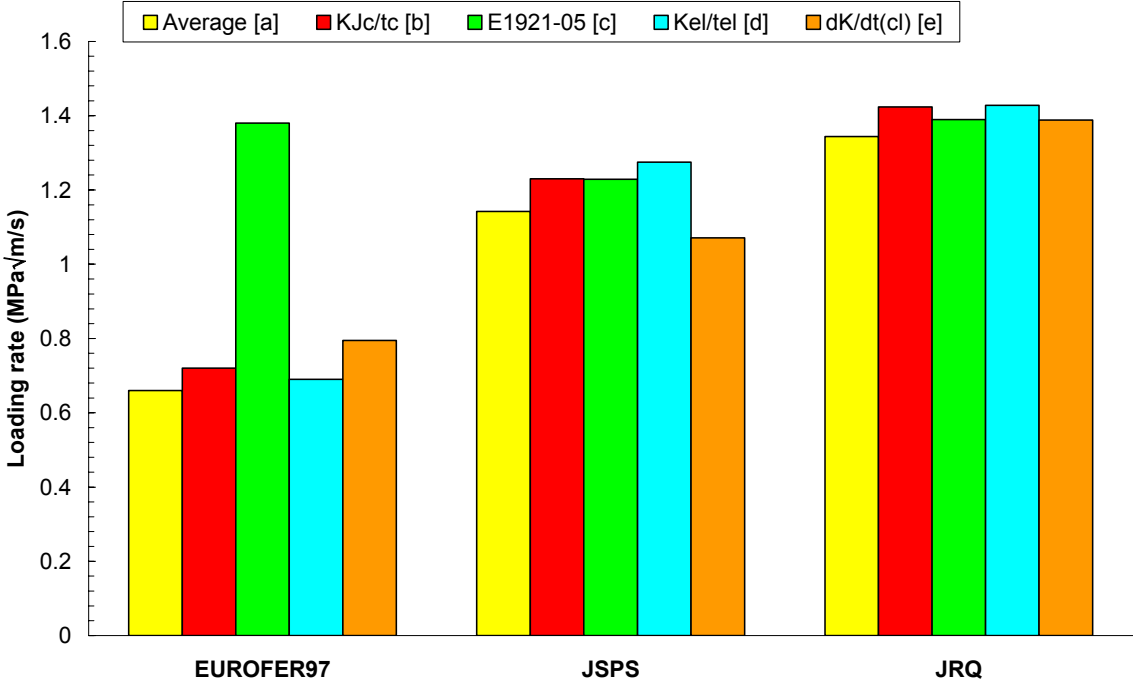
FIG. IIB.5. Comparison between different approaches for evaluating the loading rate under quasi-static conditions for tests conducted in the lower transition regime.

TABLE IIB.1. VALUES OF LOADING RATE CALCULATED USING THE 5 DIFFERENT OPTIONS

Material	Test speed	K_{Jc} (MPa√m)	Loading rate (MPa√m/s)				
			Average	K_{Jc}/t_c	E1921-05	K_{el}/t_{el}	dK/dt(cl)
EUROFER97	0.2 mm/min	47	**0.66**	0.72	1.38	0.69	0.79
		106	**0.72**	0.74	1.36	0.69	0.65
		184	**0.69**	0.69	1.33	0.67	0.41
JSPS		53	**1.14**	1.23	1.23	1.27	1.07
		102	**1.09**	1.07	1.26	1.47	0.71
		201	**0.80**	0.73	1.32	1.64	0.39
JRQ		58	**1.34**	1.42	1.39	1.43	1.39
		100	**1.36**	1.25	1.38	1.55	1.36
		174	**1.22**	0.93	1.38	1.60	0.56
EUROFER97	150 mm/min	54	**635**	654	974	634	1615
		99	**742**	752	972	638	1507
		192	**647**	654	985	694	426
JSPS		63	**751**	761	974	673	1728
		98	**760**	777	969	683	-83
		146	**587**	595	950	651	-16
JRQ		60	**674**	693	998	643	-181
		99	**753**	764	967	673	48
		155	**621**	630	932	708	834
EUROFER97	1.6 m/s	41	**8.31E+05**	8.40E+05	6.55E+05	8.42E+05	5.54E+05
		98	**6.78E+05**	6.04E+05	6.51E+05	6.47E+05	2.70E+05
		188	**6.25E+05**	5.04E+05	6.35E+05	6.43E+05	1.40E+05
JSPS	1.5 m/s	75	**6.40E+05**	6.47E+05	5.77E+05	6.38E+05	9.97E+05
		100	**5.53E+05**	5.56E+05	5.79E+05	6.18E+05	5.58E+05
		138	**4.80E+05**	4.82E+05	5.83E+05	6.54E+05	4.29E+05
JRQ	1.2 m/s	88	**3.90E+05**	3.88E+05	4.83E+05	3.86E+05	6.10E+05
		133	**3.85E+05**	3.85E+05	4.75E+05	4.38E+05	2.51E+04
		188	**2.90E+05**	2.90E+05	4.74E+05	4.30E+05	6.15E+04
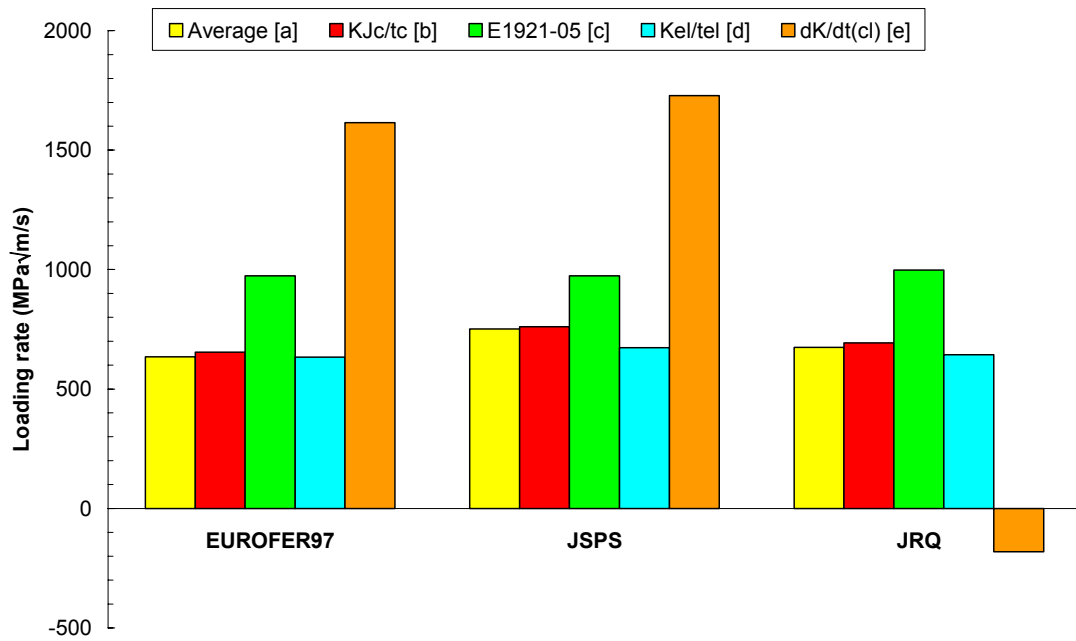
FIG. IIB.6. Comparison between different approaches for evaluating the loading rate under dynamic/intermediate conditions for tests conducted in the lower transition regime.
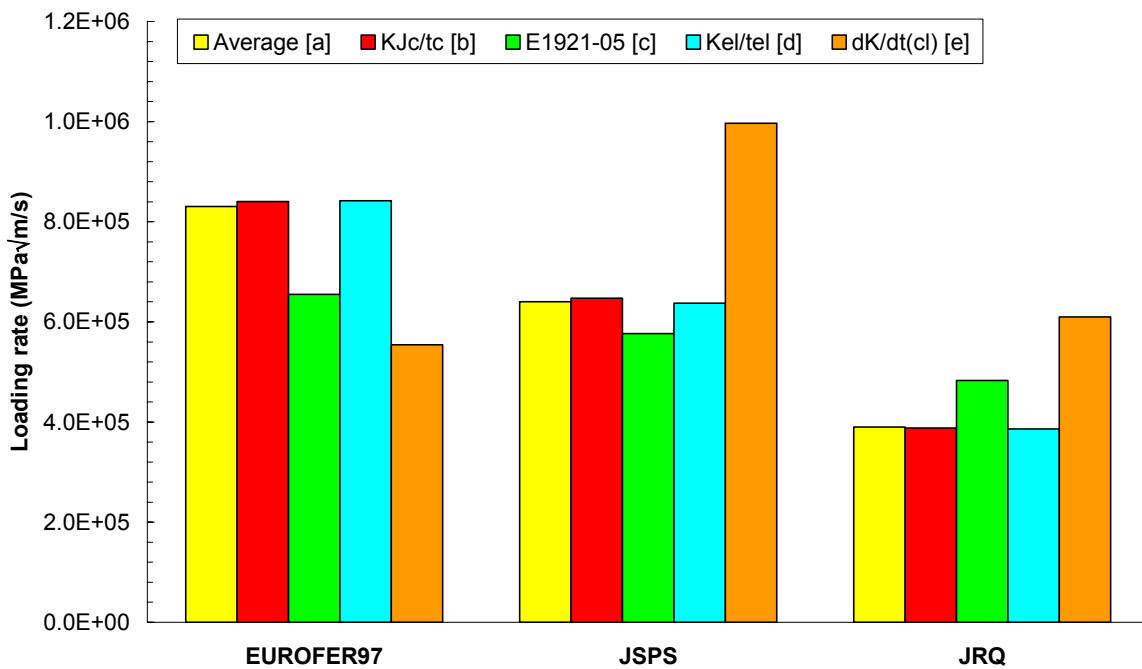
FIG. IIB.7. Comparison between different approaches for evaluating the loading rate under impact conditions for tests conducted in the lower transition regime.

IIB.4.DISCUSSION

It is clear, from the investigations performed but also from a merely intuitive standpoint, that loading rate changes continuously during a fracture toughness test and no unique value of *dK/dt* can be defined. However, the results obtained show that options (a) and (b) (and (d) as well, but only in the lower transition regime) provide substantially equivalent results and appear sufficiently representative of the effective loading rate for practical purposes.

In particular, K_c/t_c (option b) offers a straightforward and convenient way to estimate the overall loading rate in a fracture toughness test and, with respect to the average value of *dK/dt* (which can significantly vary during the test, see Figure IIB.8), it offers the advantage of being calculated in relation to the actual fracture event. Moreover, a similar approach is suggested by both ASTM E399-06 (Annex A10) and ASTM E1820-06 (Annex A13). However, one notable exception are tests where partial unloadings are performed in order to evaluate the current crack size; in this case, the time spent during the partial unloadings should be subtracted from the time to cleavage (t_c) used to calculate the loading rate. From a practical point of view, it might be advisable to use for such tests one of the other two approaches, i.e. average *dK/dt* (option a) or K_{el}/t_{el} (option d).

The two approaches which clearly emerge from our investigation as unsatisfactory and therefore should not be recommended are:

- the use of Table 3 from ASTM E1921-05 (option c), which often overestimates the average loading rate of the test;
- the value of *dK/dt* just before cleavage (option e), which can produce erratic or even negative results since the actual loading rate in some cases oscillates around its mean value, particularly for higher test velocities (an example in Figure IIB.8).
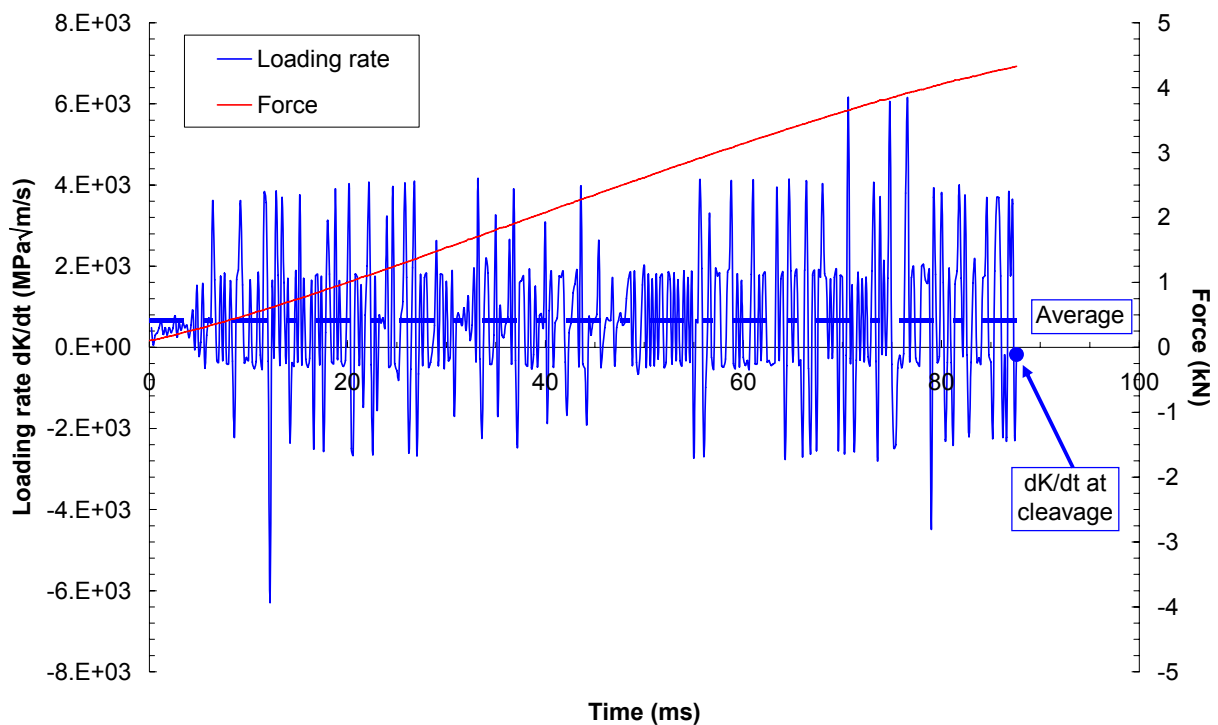
FIG. IIB.8. Loading rate and test record for a dynamic test (150 mm/min) on the JRQ steel.

IIB.5.CONCLUSIONS

Based on the investigations performed, the ratio between stress intensity factor and time at cleavage (or test termination), K_c/t_c, can be used to effectively estimate the average loading rate dK/dt in a fracture toughness tests, since:

- It is sufficiently close to the average loading rate of the test.
- It requires a minimum of additional computation (i.e. only the determination of the time at cleavage t_c).

However, in case partial unloadings are performed during the test (for instance during the linear elastic portion), K_c/t_c should not be used and other options (average dK/dt excluding the unloading periods or K_{el}/t_{el} evaluated before the first unloading) should be chosen.

The use of Table 3 from ASTM E1921-05 can grossly overestimate the average loading rate and is therefore not recommended. The reasons of this poor performance are not clear. Since the actual loading rate in a test tends to fluctuate around the average value, using dK/dt just before cleavage can lead to erratic results, including (albeit only in the case of dynamic tests) negative values which have no physical meaning. The results obtained do not appear to depend on material type or loading rate.

IIC. MASTER CURVE REFERENCE TEMPERATURES MEASURED AT QUASI-STATIC AND IMPACT LOADING RATES

IIC.1.REFERENCE TEMPERTURE DIFFERENCES BETWEEN QUASI-STATIC AND IMPACT LOADING RATES

SCK•CEN has collected reference temperature values obtained on unirradiated and irradiated RPV and ferritic/martensitic steels from tests conducted at quasi-static ($T_{0,\,qs}$) and impact ($T_{0,\,imp}$) loading rates using precracked Charpy specimens. For the two loading rate regimes, dK/dt corresponds to values of approximately 1 and 4×10^5 MPa√m/s, respectively.

The data presently included in the SCK•CEN database are shown in Table IIC.1. Differences between impact and quasi-static reference temperatures are plotted in Figures IIC.1 and IIC.2 as a function of $T_{0,\,qs}$ and $R_{y,\,T0sq}$ (yield strength measured at $T_{0,\,qs}$). The latter two parameters are both considered by the empirical model of Wallin for predicting the change of reference temperature due to an increase in loading rate.

Fair correlations are observed for the T_0 increase in Figures IIC.1 and IIC.2, with a significant amount of scatter, particularly for the relationship with $R_{y,\,T0sq}$. Reference temperature variations appear to decrease as $T_{0,\,qs}$ increases and $R_{y,\,T0sq}$ decreases.

IIC.2.YIELD STRENGTH TO BE USED AT LOADING RATES HIGHER THAN QUASI-STATIC

In the Master Curve analysis of fracture toughness data, the yield strength σ_{ys} is required for the calculation of the maximum K_{Jc} capacity of a specimen according to the expression:

$$K_{Jc(\text{limit})} = \sqrt{\frac{Eb_o\sigma_{ys}}{30\left(1-v^2\right)}} \tag{IIC.1}$$

where E is Young's modulus, b_o is the specimen uncracked ligament and ν is Poisson's ratio.

Ideally, σ_{ys} to be used in Equation IIC.1 should be measured at the same temperature and strain (loading) rate as the fracture toughness test. However, for tests conducted at loading rates higher than quasi-static (0.1–2 MPa√m/s), representative tensile data might not be available in practice.

TABLE IIC.1. RELATIONSHIP BETWEEN T_0 MEASURED UNDER QUASI-STATIC AND IMPACT LOADING RATES (SCK•CEN DATABASE)

Material	Condition	$T_{0, qs}$ (°C)	$R_{y, T0qs}$ (MPa)	$T_{0, imp}$ (°C)	ΔT_0 (°C)
73W	Baseline	-77	565	-29	48
	Irradiated	24	708	46	22
		39	642	78	39
18MND5	Baseline	-119	694	-71	48
	Irradiated	-85	744	-26	59
JSPS (A533B)	Baseline	-6	468	32	38
JRQ	Baseline	-70	539	-17	53
	Irradiated	15	586	58	43
A302B	Baseline	68	519	81	13
EUROFER97	Baseline	-115	717	-24	91
	Irradiated	-80	777	-13	67
F82H	Baseline	-118	731	-26	92
JRQ (CRP-4)	Baseline	-70	539	-3	67
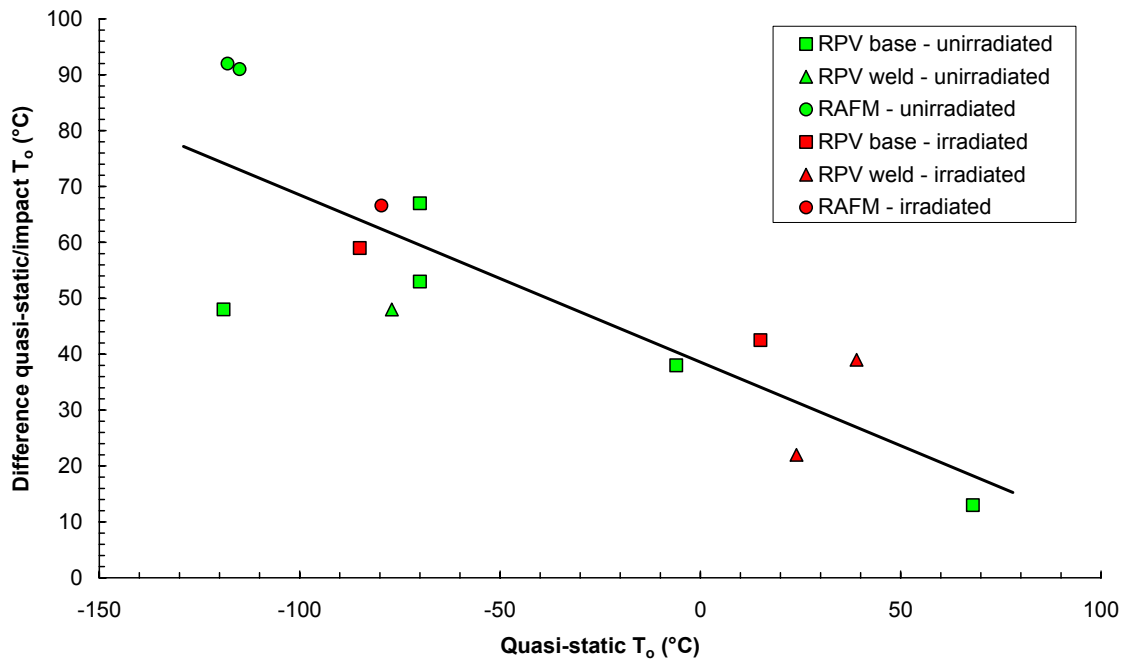
FIG. IIC.1. Influence of quasi-static reference temperature on the increase of T_0.
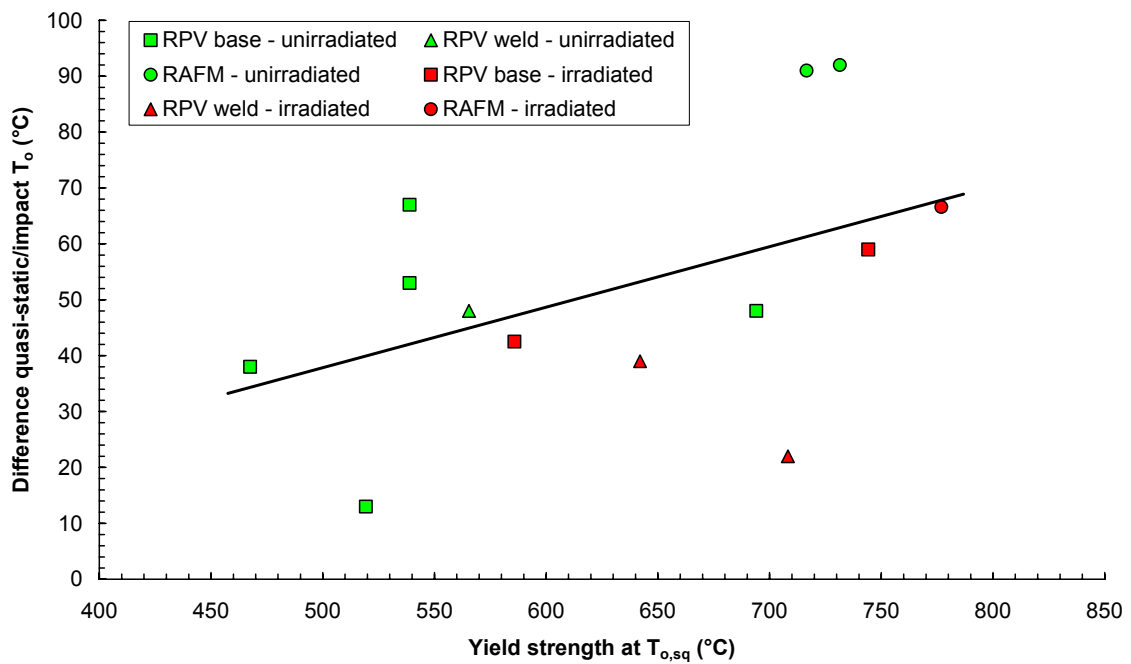
FIG. IIC.2. Influence of yield stress at quasi-static reference temperature on the increase of T_0.

In this case, the following options could be available:

- Using quasi-static tensile results, corresponding to strain rates in the order of 10^{-4} s^{-1}. Such values represent a conservative estimate of the yield strength measured at higher strain rates.

- Using dynamic tensile results, corresponding to strain rates in the order of 10 s⁻¹, which are considered to be representative of a Charpy impact test. If the fracture toughness test is not performed on a precracked Charpy specimen using an instrumented pendulum, dynamic values represent an unconservative estimate of the actual yield strength and could lead to the calculation of a non-conservative value of the reference temperature, due to a higher censoring limit.
- Using the Bennett-Sinclair parameter (BSP), which simultaneously accounts for temperature T and loading rate $\dot{\varepsilon}$ in a tensile test:

$$BSP = T \, \ln\left(\frac{A}{\dot{\varepsilon}}\right) \tag{IIC.2}$$

where A is a frequency factor whose value is around 10^{-8} s⁻¹. Yield strength values corresponding to different temperatures and strain rates can thus be represented on the same plot, as in the example provided in Figure IIC.3.
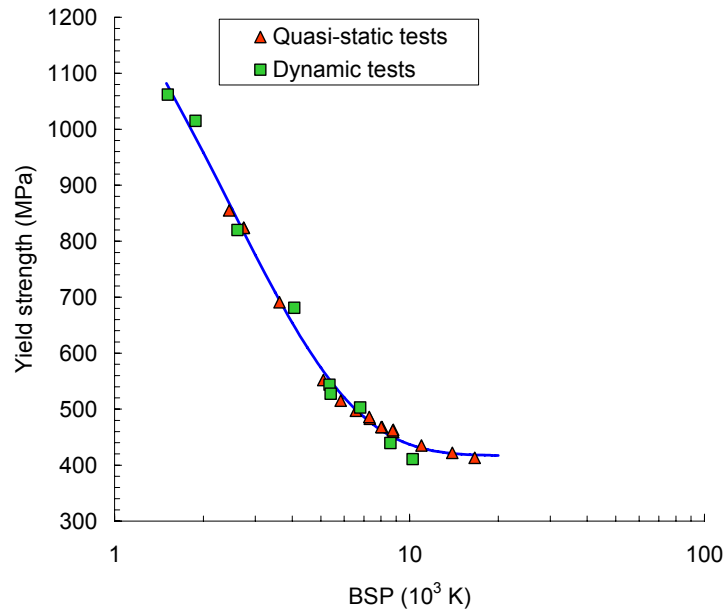
FIG. IIC.3. Example of BSP representation of tensile test results obtained at different temperatures and loading rates.

In the case of quasi-static tests, the loading rate for the fracture toughness test ($\dot{K} \sim 1$ MPa√m/s) corresponds to a tensile strain rate $\dot{\varepsilon} \sim 10^{-4}$ s⁻¹. For different loading rates, the following relationship holds:

$$\dot{\varepsilon}_{test} = \dot{K}_{test} \, \frac{\dot{\varepsilon}_{qs}}{\dot{K}_{qs}} \tag{IIC.3}$$

where $\dot{\varepsilon}_{qs}$ and $\dot{K}_{qs}$ are the above mentioned quasi-static values. Using the value of $\dot{\varepsilon}_{test}$ calculated from Equation IIC.3 into Equation IIC.2, the corresponding value of BSP_test can be determined for the test loading rate. The yield strength to be used for the Master Curve

analysis can therefore be estimated from a fitting curve like the one shown in Figure IIC.3 as the ordinate Y corresponding to the axis X = BSP$_{test}$.

The three options described above have been tested on three steels with different characteristics, namely EUROFER97 (9Cr ferritic/martensitic steel for fusion applications), JRQ and JSPS (Japanese A553B steel with low upper shelf toughness). Two loading rates have been investigated: 700 MPa√m/s (all steels) and 4500 MPa√m/s (only JRQ). The overall results are presented in Table IIC.2 and Figure IIC.4.

Differences in terms of T$_0$ for the investigated datasets are small and lower than 5°C in all cases. This can be also appreciated in Figure IIC.5, where T$_0$ values are plotted with their respective standard deviations.

TABLE IIC.2. MASTER CURVE REFERENCE TEMPERATURES AND MAXIMUM T$_0$ DIFFERENCES CALCULATED USING DIFFERENT VALUES OF YIELD STRENGTH

Material	Loading rate (MPa√m/s)	T$_0$ (°C)			Max Δ(°C)
		Quasi-static	Dynamic	Bennett-Sinclair	
EUROFER97	700 MPa√m/s	-75.0	-79.4	-79.0	4.4
JSPS		14.4	14.4	15.3	0.8
JRQ		-47.9	-48.5	-47.3	1.1
	4500 MPa√m/s	-35.3	-35.7	-33.5	2.2
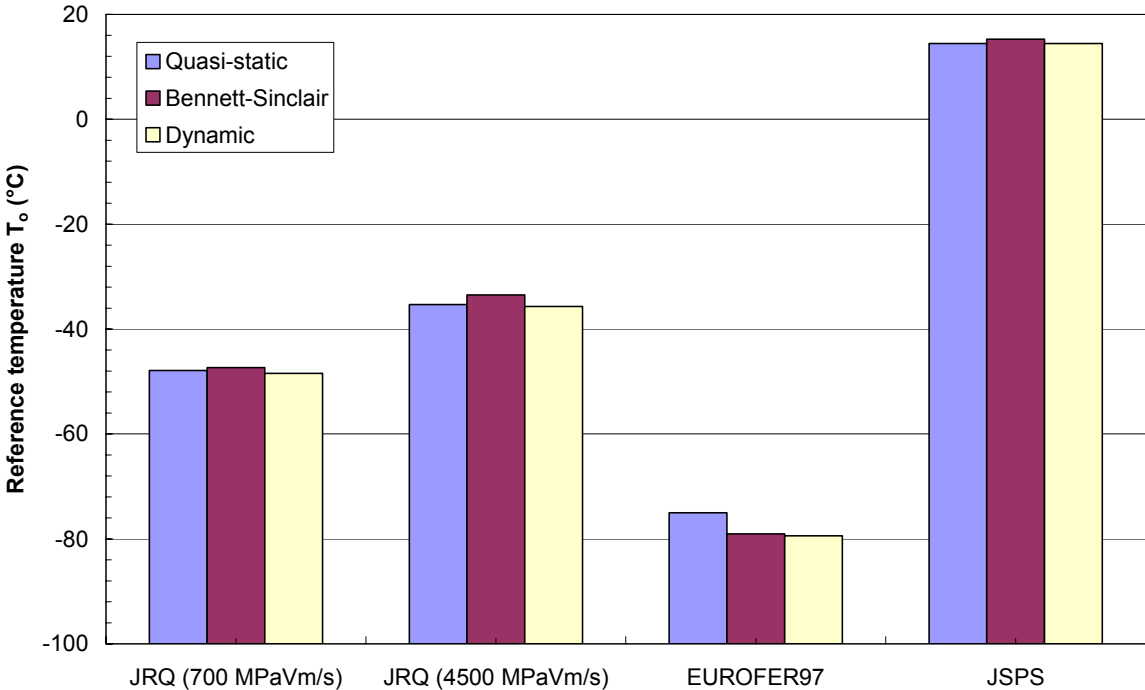
FIG. IIC.4. Master Curve reference temperatures calculated using different values of yield strength.
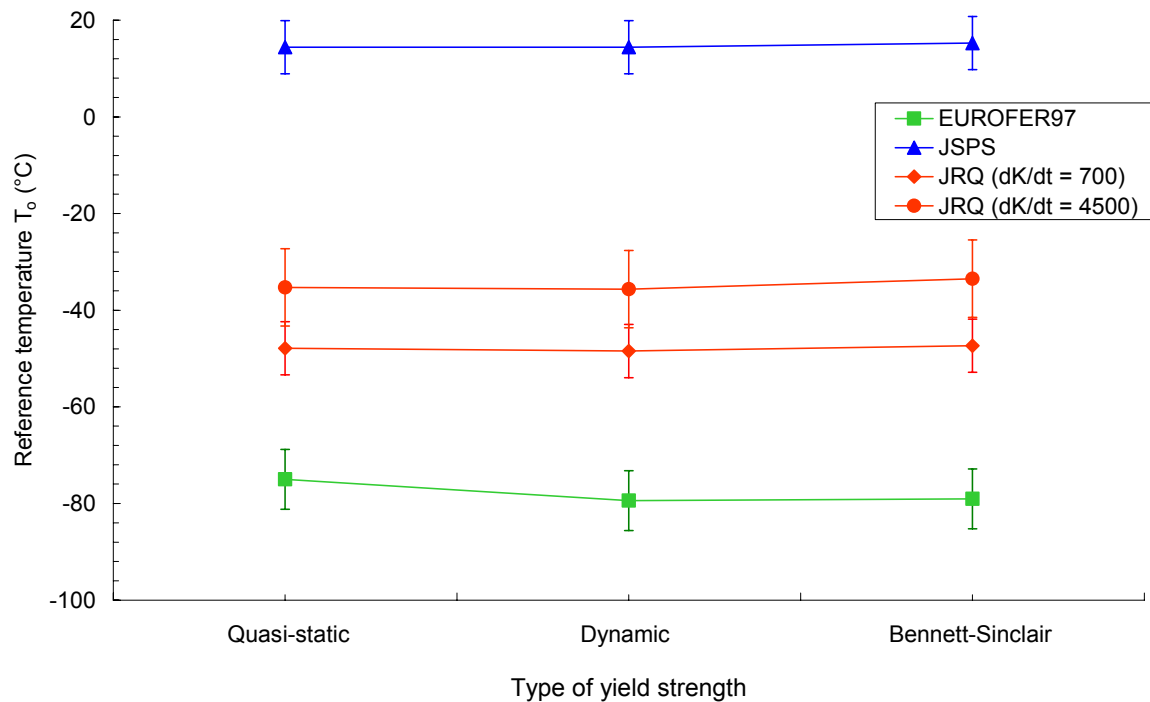
FIG. IIC.5. Master Curve reference temperatures calculated using different values of yield strength, with their corresponding standard deviations.

It is interesting to note that in three out of four cases the highest (most conservative) value of T_0 is obtained using the Bennett-Sinclair estimation, rather than the quasi-static value, as might somehow be expected. Conversely, the lowest (less conservative) values of T_0 correspond to the dynamic yield strength for three of the four datasets.

The following conclusions can be stated:

- The differences observed between the calculated values of T_0 are smaller than the uncertainties (standard deviations) of the individual reference temperatures. Therefore, a moderate effect of the yield strength choice can be expected, at least for datasets which do not contain a high number of censored data points.
- From a theoretical point of view, the Bennett-Sinclair approach appears more justified and should therefore be recommended.
- In the absence of relevant tensile test results, using the quasi-static yield strength is not necessarily the most conservative option.

IID. EFFECT OF LOADING PATTERN (MONOTONIC LOADING VS. PARTIAL UNLOADING)

ASTM E1921-05 allows loading test specimens both in the monotonous (M) and in the partial unloading (PU) mode. Partial unloading is recommended in case ductile crack extension needs to be measured.

This raises the question whether the applied loading mode influences the measured fracture toughness and consequently the reference temperature T_0.

PCC specimens of different JRQ blocks and of a German heat resistant steel plate 10 CrMo 9-10 were tested in the M and PU loading mode. Table IID.1 contains the values of T_0 evaluated by FZD and Figures IID.1 to IID.3 illustrate test results. Of the 24 monotonously loaded specimens of 5JRQ34, 12 were plane sided. The calculated T_0 for the 20% side grooved and plane sided specimens are -59°C and -62°C, respectively. Since both values are well within the respective standard deviations (Table IID.1), a common evaluation of both datasets was performed (T_0 = -60.5°C).

TABLE IID.1. REFERENCE TEMPERATURES CALCULATED FOR SPECIMENS TESTED IN THE MONOTONIC (M) AND PARTIAL UNLOADING (PU) MODE

Laboratory	Material	Loading mode	Σn_i	T_0 (°C)	σ (°C)
GER (FZD)	6JRQ12	PU	1.43	-61.6	6.0
	6JRQ12	M	1.19	-55.9	6.3
	10 CrMo 9-10	PU	1.29	-109.7	5.7
	10 CrMo 9-10	M	1.29	-111.4	5.7
RUS (RRC KI)	5JRQ33, 5JRQ34	PU	3.43	-61.6	3.9
	5JRQ34*	M	3.12	-60.5	4.0
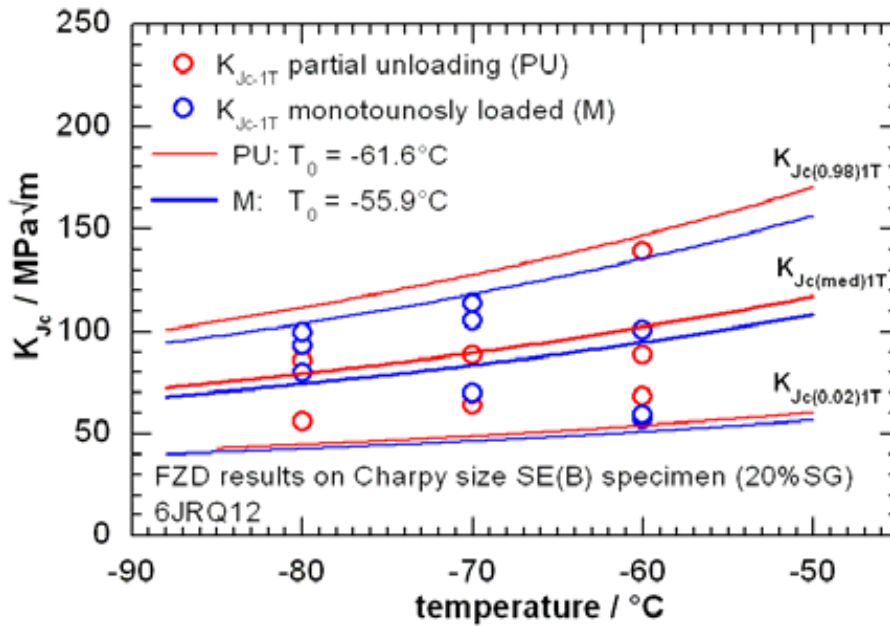
FIG. IID.1. Master Curve analysis of 6JRQ12 (loading rate UC and M: 1.2 MPa√m/s).
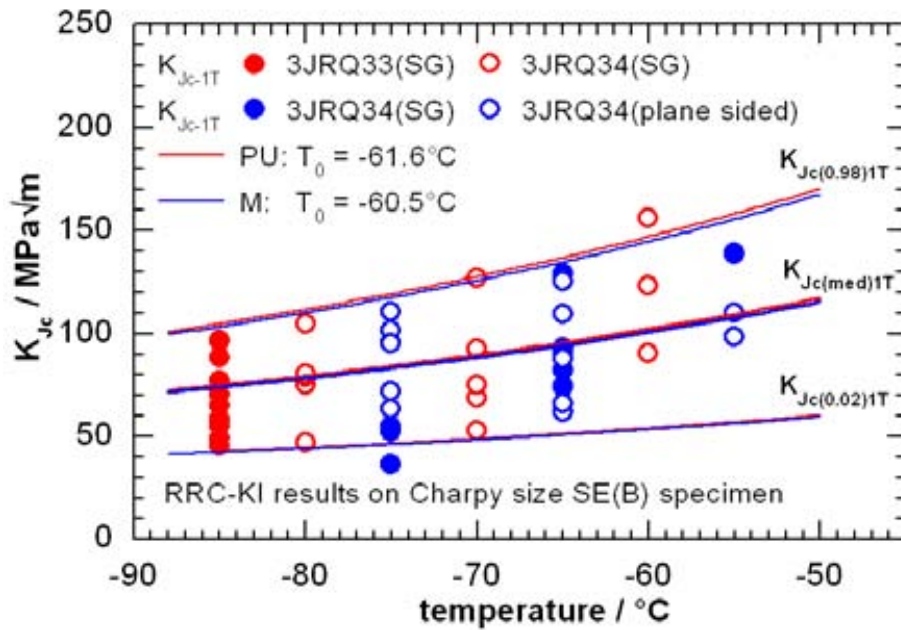
FIG. IID.2. Master Curve analysis of 5JRQ33 and 5JRQ34 datasets (loading rate UC: 0.1 MPa√m/s and 1.2 MPa√m/s, M: 0.7 MPa√m/s).
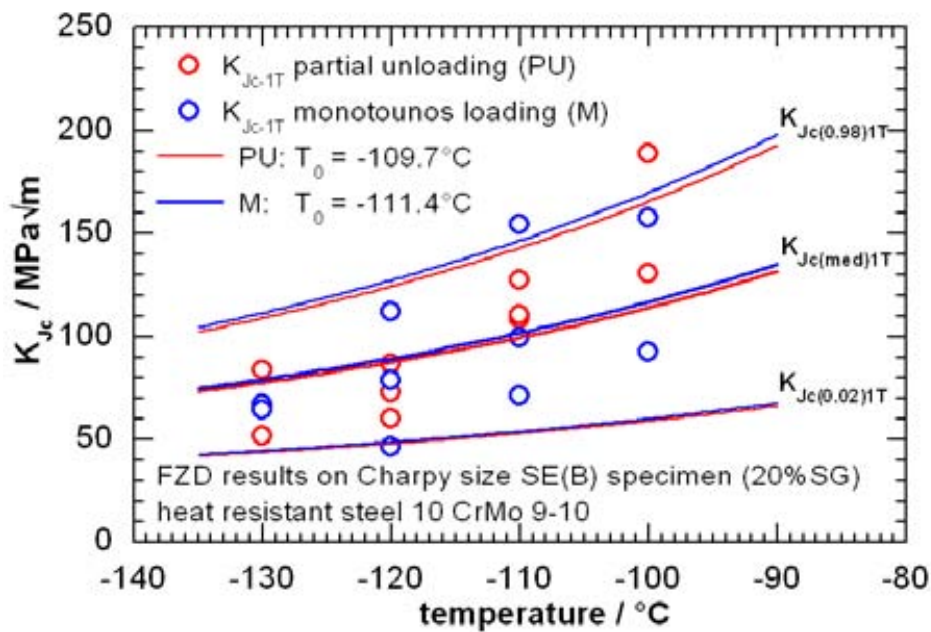
FIG. IID.3. Master Curve analysis of the German heat resistant steel 10 CrMo 9-10 (loading rate UC and M: 1.2 MPa√m/s).

The variation of the calculated T_0 values between the two loading modes is within the standard deviation for the investigated materials, therefore no influence of the loading mode on the Master Curve reference temperature can be detected.

IIE. ADDITIONAL ANALYSES OF THE ROUND ROBIN EXERCISE RESULTS

IIE.1. ASSESSMENT OF THE SUSPECT OUTLIER DATASET (LABORATORY 7)

A straightforward comparison of dial energy (KV) values reported by the participants, fitted by simple exponential curves, does not indicate any systematic difference among Laboratory 7 and the others (Figure IIE.1). This excludes that the outlier behaviour could be caused by material inhomogeneity or improper calibration of the pendulum machine.
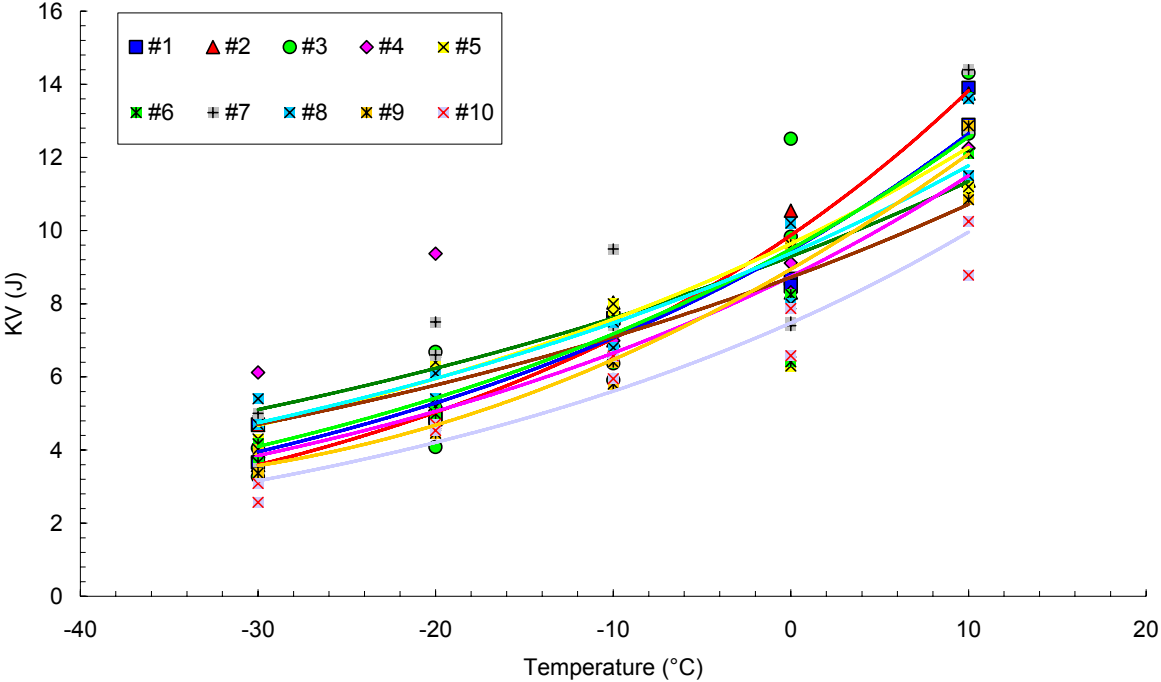
FIG. IIE.1. Dial energy (KV) values reported by round robin participants.

Since K_{Jc} values from impact toughness tests are calculated from time and force measurements and errors in time measurement can be excluded (no systematics can be observed in Figure IIE.2), the observed discrepancies can only derive from incorrect force measurements due to questionable calibration of the instrumented strikers. This appears to be confirmed by Figures IIE.3 to IIE.5, which compare test records at -30, -10 and 10°C for Laboratories 1 and 7 (with Laboratory 1 taken as an example of normal or non-outlier behaviour).
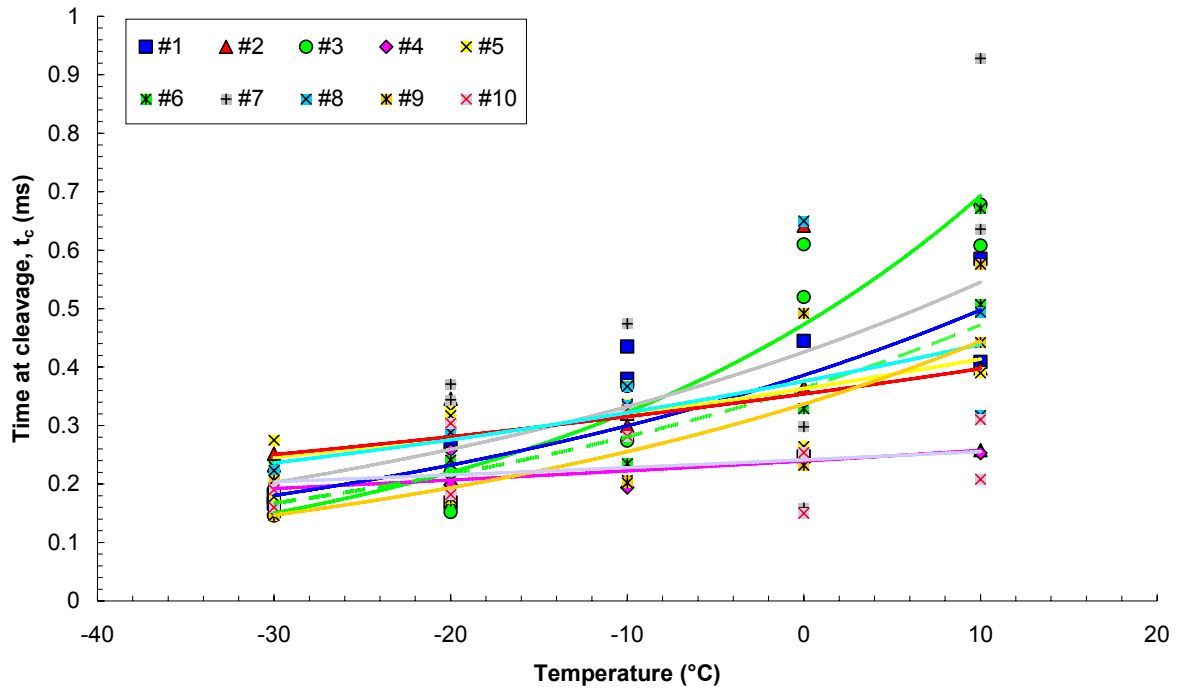
FIG. IIE.2. Values of time at cleavage fracture (t_c) reported by round robin participants.
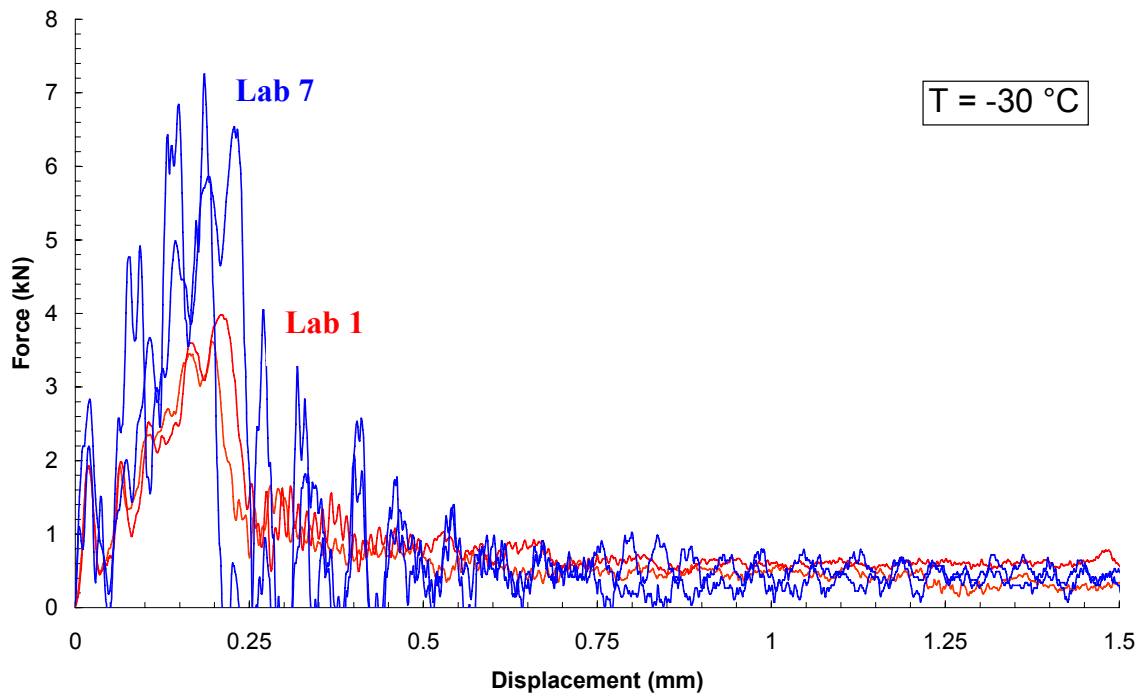
FIG. IIE.3. Test records supplied at -30°C by Laboratories 1 and 7 (two tests per laboratory).
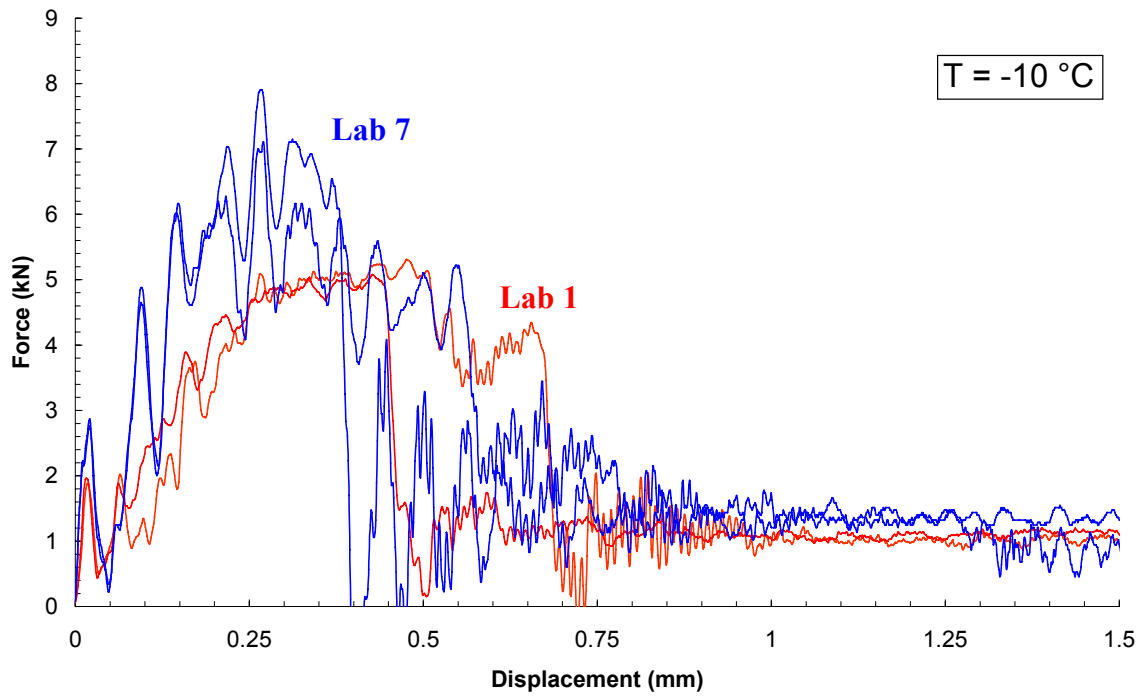
FIG. IIE.4. Test records supplied at -10°C by Laboratories 1 and 7 (two tests per laboratory).
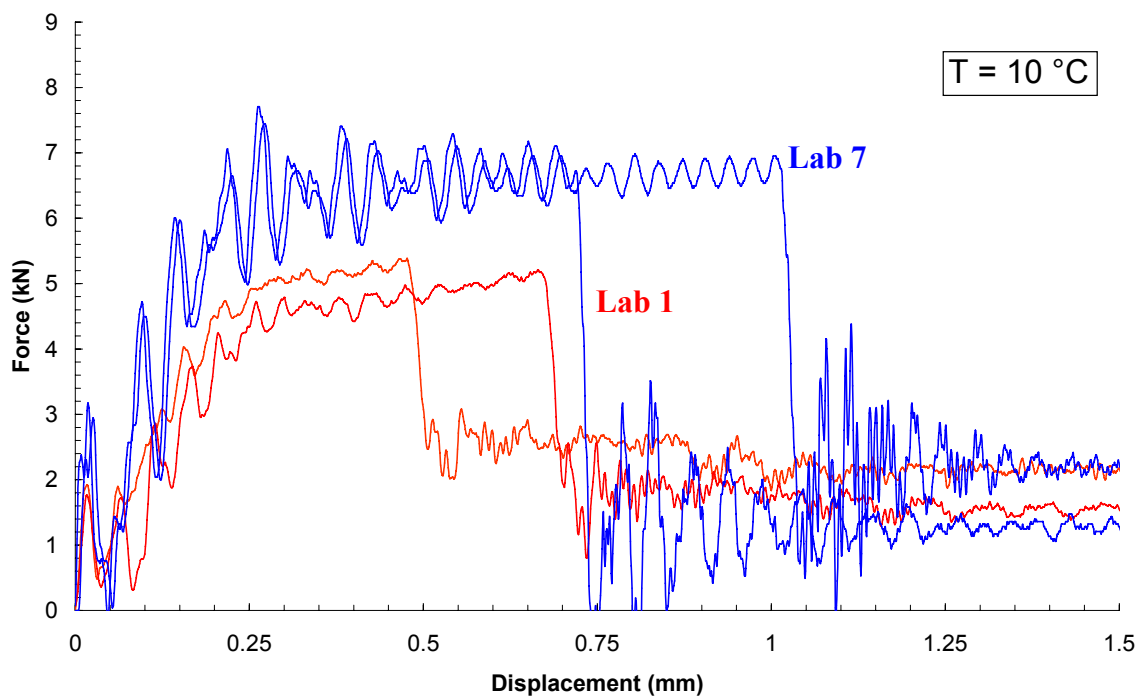
FIG. IIE.5. Test records supplied at 10°C by Laboratories 1 and 7 (two tests per laboratory).

Assuming that the striker calibration of Laboratory 1 is reliable, the figures clearly show that force values are too high for Laboratory 7.

Further evidence is offered by Figure IIE.6, which compares dynamic yield strength values reported by the participants.
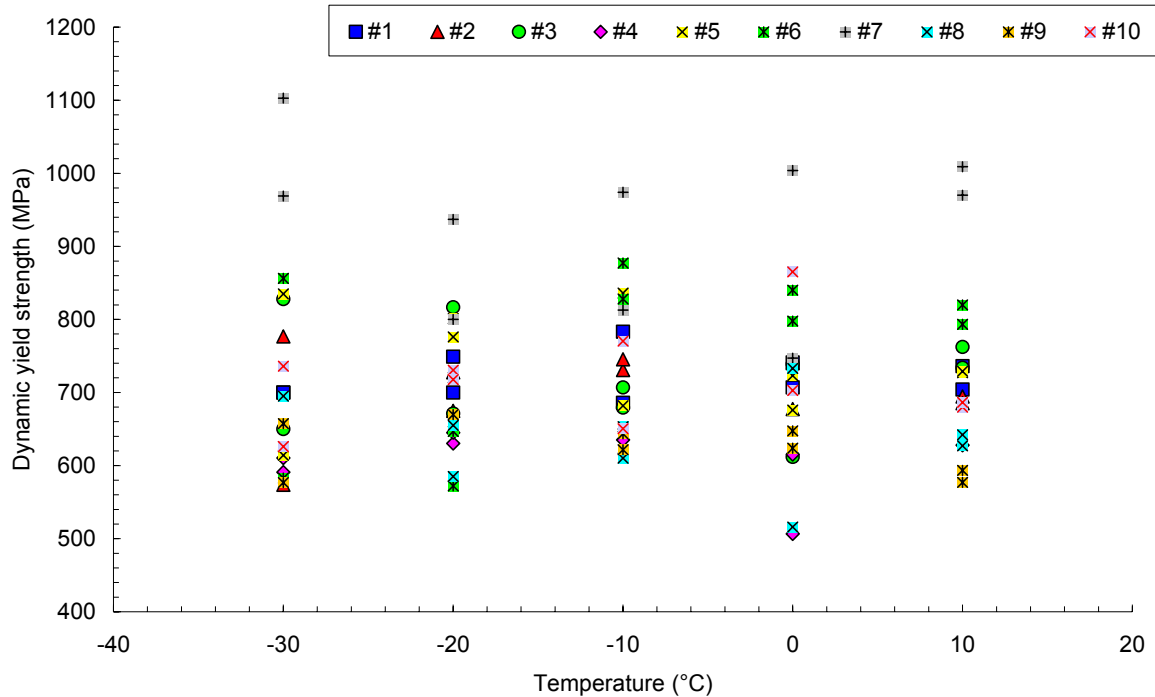
FIG. IIE.6. Dynamic yield strength values reported by participants.

An additional assessment of the suspected outlier dataset was performed using two recently published extensions of the Master Curve approach for the treatment of inhomogeneous datasets:

- Bi-Modal Master Curve (BMMC), developed for inhomogeneities governed by two separate populations;
- Multi-Modal Master Curve (MMMC), developed for the analysis of randomly inhomogeneous datasets consisting of multiple populations.

These approaches have been applied to selected individual datasets from the round robin exercise in order to confirm that the results provided by Laboratory 7 are not homogeneous with the remaining data and should therefore be excluded as outliers. The BMMC approach can also provide an estimation of the percentages corresponding to the two populations (A and B). The results are summarized in Table IIE.1 (note that for BMMC, non-homogeneity percentages for populations A and B are also indicated) and show that:

- Both BMMC and MMMC confirm that the results of Laboratory 7 do not belong to the overall population (represented in this case by Laboratory 1).
- Both approaches do not detect inhomogeneities between results from Laboratories 1, 2 and 5.
- Some indications of inhomogeneity is returned by BMMC for Laboratory 4, although MMMC is unable to detect random heterogeneity.

TABLE IIE.1. APPLICATION OF THE BI-MODAL AND MULTI-MODAL MASTER CURVE APPROACHES TO SELECTED DATASETS FROM THE ROUND ROBIN EXERCISE

Datasets analysed	Outcome BMMC	Outcome MMMC
#1 and #7	Not homogeneous (15/85)	Not homogeneous
#1 and #2	Homogeneous	Homogeneous
#1 and #5	Homogeneous	Homogeneous
#1 and #4	Not homogeneous (39/61)	Homogeneous

Following the investigations presented here, Laboratory 7 was requested to verify the force calibration of the instrumented strikers.

Additionally, an interlaboratory verification exercise was planned and conducted, consisting in each participant testing at room temperature two Charpy V-notched samples from the high energy (150 J) batch of certified reference specimens supplied by IRMM (Geel – Belgium).

IIE.2. REQUIREMENTS ON THE TIME TO FRACTURE/GENERAL YIELD

Impact toughness tests on precracked Charpy specimens are being standardized within both ASTM (American Society for Testing and Materials) and ISO (International Standards Organization). Both proposed procedures prescribe the following requirement on the time to fracture (t_f), if the test is to be analysed using a quasi-static approach (i.e. using forces and energies calculated from the test record):

$$t_f > 5\tau \qquad \text{(IIE.1)}$$

where τ is the period of oscillation of the force signal, which can be analytically evaluated as:

$$\tau = 3.36 \cdot \left(\frac{W}{S_0}\right) \cdot \sqrt{E' \cdot B_N \cdot C_S} \qquad \text{(IIE.2)}$$

with: W = specimen width, S_0 = speed of sound in steel, E' = plane strain Young's modulus, B_N = specimen net thickness and C_S = specimen compliance. The implication of Equation IIE.1 is that, provided fracture occurs after at least five oscillations, inertial effects are sufficiently dampened and a quasi-static loading condition has been reached in the specimen.

In the past, however, a less restrictive criterion had been proposed, i.e.:

$$t_f > 3\tau \qquad \text{(IIE.3)}$$

This requirement had been suggested and implemented in EPRI procedures in the late 1970s. Other model experiments have indicated that for PCC specimens (with a/W ~ 0.5) it may take more time (i.e. at least five oscillations) to come to an approximately quasi-static equilibrium of force, and the modified criterion (Equation IIE.1) was introduced in the experimental procedure issued by ESIS TC5, on which the current ASTM and ISO proposals are based. If the requirement on time to fracture is not fulfilled, the test has to be evaluated using fully dynamic measuring techniques which do not rely on forces measured by the instrumented striker.

Using W = 10 mm, S_0 = 5100 m/s, E' = 227472.5 MPa (E = 207000 MPa), B_N = 8 mm and C_S = 3.79 × 10^{-5} mm/N (calculated by FZD using FEM for a PCC specimen with a/W = 0.5), equation IIE.2 yields τ = 54.7 μs and the requirements (Equations IIE.1 and IIE.3) become $t_f > 274$ μs and $t_f > 164$ μs, respectively.

Times to fracture for the 98 impact toughness test results provided by RRE participants have been compared to the two requirements. It emerges that almost half of the tests performed fail to satisfy the more stringent requirement, i.e. for 48 out of 98 tests (49%), $t_f \leq 274$ μs; the temperature distribution of the rejected tests is: 19 at -30°C, 12 at -20°C, 4 at -10°C, 10 at 0°C and 3 at 10°C.

A much smaller portion (8 tests, or 8%) does not fulfil requirement of $t_f \leq 164$ μs; most tests (5) were performed at -30°C, 1 at -20°C and 2 at 0°C.

In order to investigate the effect of a possible t_f requirement on the RRE results, two approaches have been considered prior to performing an overall Master Curve analysis:

(a) simply removing the invalid tests, i.e. considering them as non-tests (such as specimens with invalid initial crack size in ASTM E1921);

(b) replacing the measured K_{Jc} with the values corresponding to t_f = 3τ (52.5 MPa√m) or 5τ (90 MPa√m), i.e. applying a sort of censoring procedure similar to that of ASTM E 1921, whereby if $K_{Jc} > K_{Jc(limit)}$, K_{Jc} is replaced by $K_{Jc(limit)}$ in the analysis.

The impact of the different requirements and approaches on the overall Master Curve analysis results is summarized in Table IIE.2. For comparison, results of the straightforward overall analysis are also included.

TABLE IIE.2. INFLUENCE OF TIME TO FRACTURE REQUIREMENTS ON THE OVERALL MASTER CURVE ANALYSIS

Requirement	Action	N	r	Σn_i	T_0 (°C)	σ_{T0} (°C)
None	None	98	85	13.21	-4.2	2.0
$t_f > 3\tau$	Remove data	90	77	12.02	-5.3	2.1
	Censor data	98	77[1]	12.02	-5.4	2.1
$t_f > 5\tau$	Remove data	50	37	6.14	-13.4	3.0
	Censor data	98	37	6.17	-17.8	3.0

Invalidating very short fracture times, i.e. very brittle tests, predictably tends to bias the reference temperature downwards (i.e. non conservatively). The bias is almost negligible (just above 1°C) in the case of the 'old' requirement, and removing or censoring does not make appreciable difference. However, if the more stringent requirement is enforced, the non-conservative shift of T_0 is more significant, particularly if the censoring approach is applied (shift of 13.6°C); if invalid data are removed, the resulting bias is less than 10°C (9.2°C). Therefore, based on the analysis of the RRE results, it appears more convenient to apply the less stringent requirement (Equation IIE.3), in order to avoid significant non-conservatism.

---

[1] Data with t_f < 3τ or 5τ are not included in the count of valid data, as in the case of data with $K_{Jc} > K_{Jc(limit)}$.

IIE.3. ADDITIONAL ANALYSES OF THE ILC RESULTS

A statistical analysis was conducted on the original ILC data in accordance with ASTM E691-05, in order to determine their repeatability and reproducibility. According to the standard, the repeatability concerns the variability between independent test results obtained within a single laboratory; the within-laboratory consistency statistics k, is calculated as:

$$k = \frac{s}{s_r} \tag{IIE.4}$$

where s is the standard deviation for one laboratory and s_r is the repeatability standard deviation of the material, given by:

$$s_r = \sqrt{\frac{\sum_1^p s^2}{p}} \tag{IIE.5}$$

Figure IIE.7 shows the values of within-laboratory statistic k for F_{gy} and F_m calculated from the original ILC results; the critical value of k is indicated at the 0.5% significance level, which depends on the number of laboratories and the number of tests per laboratory (in this case, $k_{crit} = 2.41$).
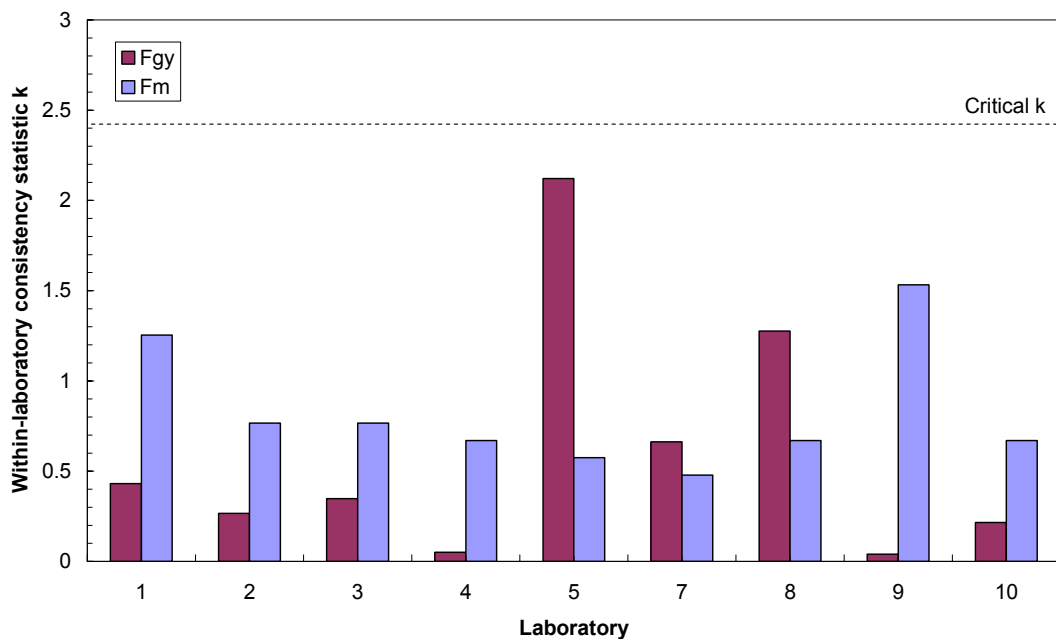
FIG. IIE.7. Within-laboratory consistency statistic k for the original ILC data.

On the other hand, reproducibility deals with the variability between single test results obtained in different laboratories. The between-laboratory consistency statistic h is calculated as:

$$h = \frac{d}{s_{\overline{X}}}$$

(IIE.6)

where d is the deviation of the laboratory average from the average of the laboratory averages and $s_{\overline{X}}$ is the standard deviation of the laboratory averages. The values of h calculated for each laboratory from the original results are shown in Figure IIE.8, together with the critical values of h at the 0.5% significance level, which only depend on the number of laboratories (in this case, $h_{crit} = \pm 2.23$).
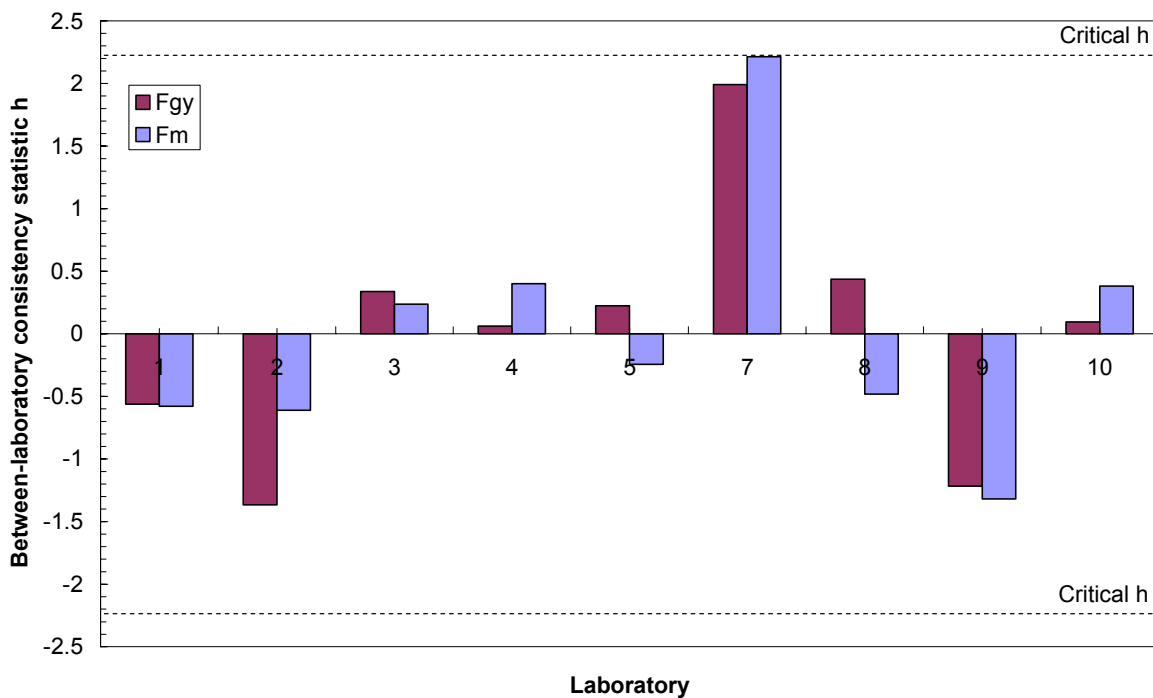
FIG. IIE.8. Between-laboratory consistency statistic h for the original ILC data.

From Figures IIE.9 and IIE.10, we remark that no laboratory exceeds the critical k value for F_{gy}, or F_m, while Laboratory 7 is quite close to the upper h limit for F_{gy} and extremely close for F_m, thus confirming the anomaly recorded in the analyses of the RRE results. This circumstance is confirmed by Figure IIE.11, where instrumented curves are compared between Laboratories 2, 5 and 7.

The effect of the dynamic correction on the within-laboratory and between-laboratory consistency statistics can be appreciated in Figures IIE.9 (k) and IIE.10 (h).

We observe that the within-laboratory consistency (Figure IIE.9) remains quite acceptable, whereas the between-laboratory consistency (Figure IIE.10) is somewhat improved, particularly in the case of Laboratory 7.
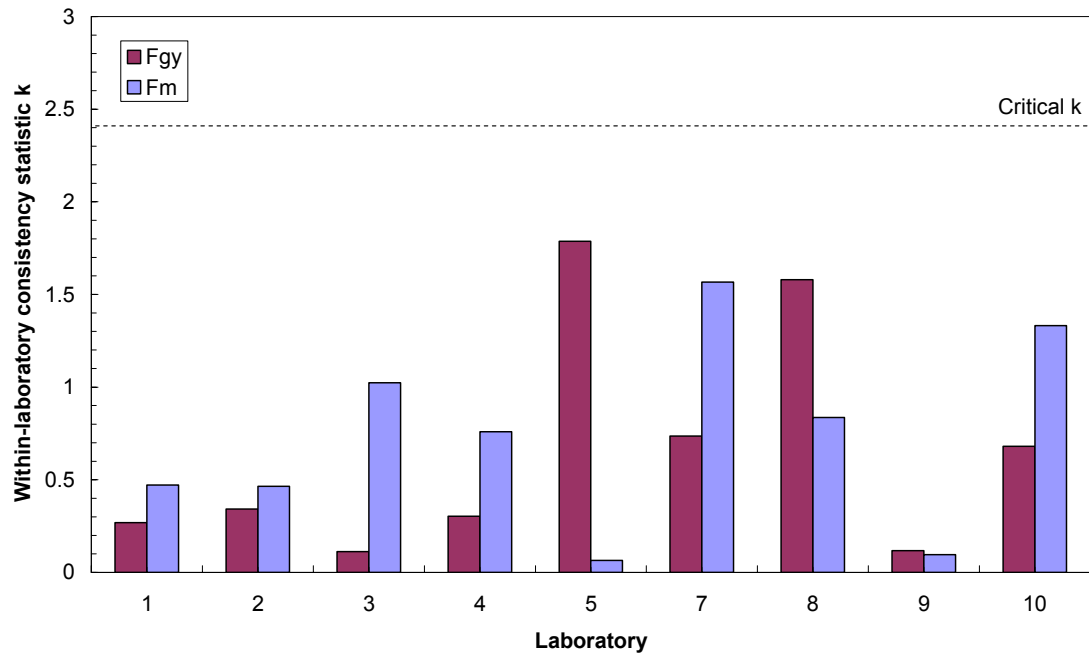
FIG. IIE.9. Within-laboratory consistency statistic after dynamic force correction.
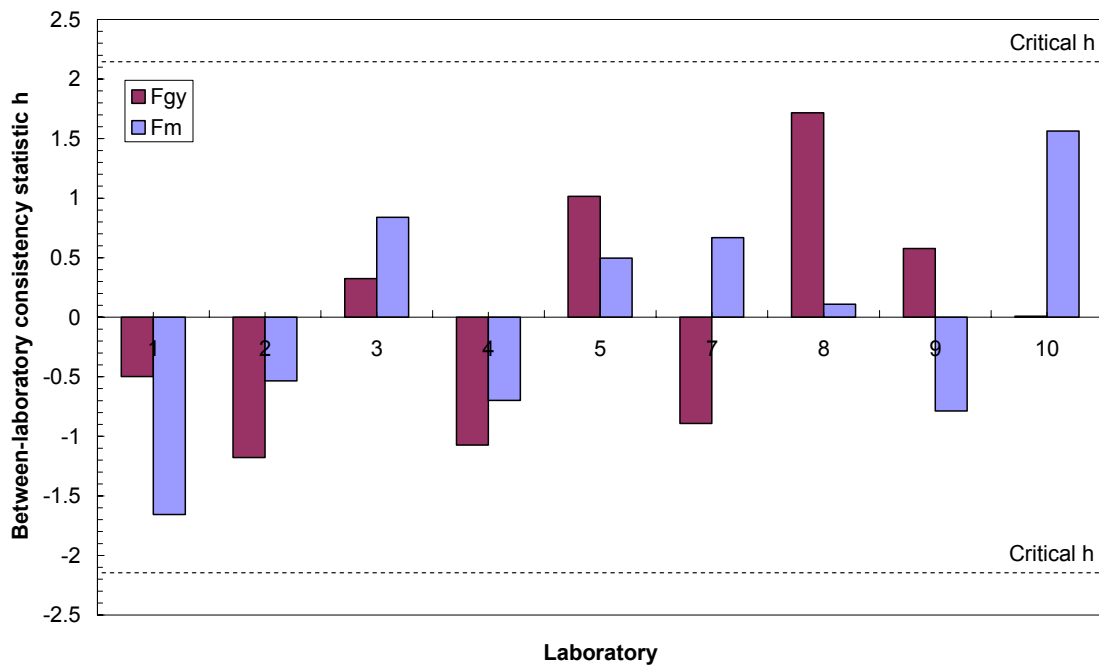
FIG. IIE.10. Between-laboratory consistency statistic after dynamic force correction.
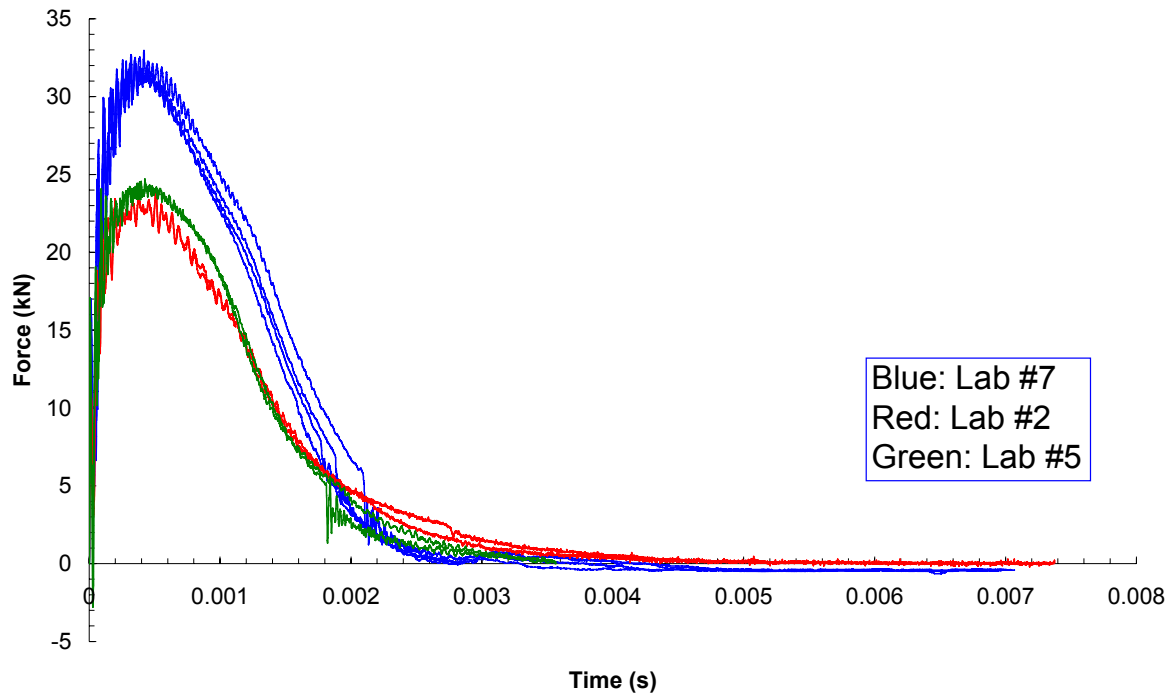
FIG. IIE.11. Instrumented curves for ILC tests performed by Laboratories 2, 5 and 7.

IIE.4. INFLUENCE OF STRIKER RADIUS

A possible influence of the instrumented striker radius (2 mm vs. 8 mm) was also investigated, although only one third of the ILC participants (Laboratories 3, 8 and 10) used an 8 mm striker. Figure IIE.12 shows no significant effect of striker radius for the original results.
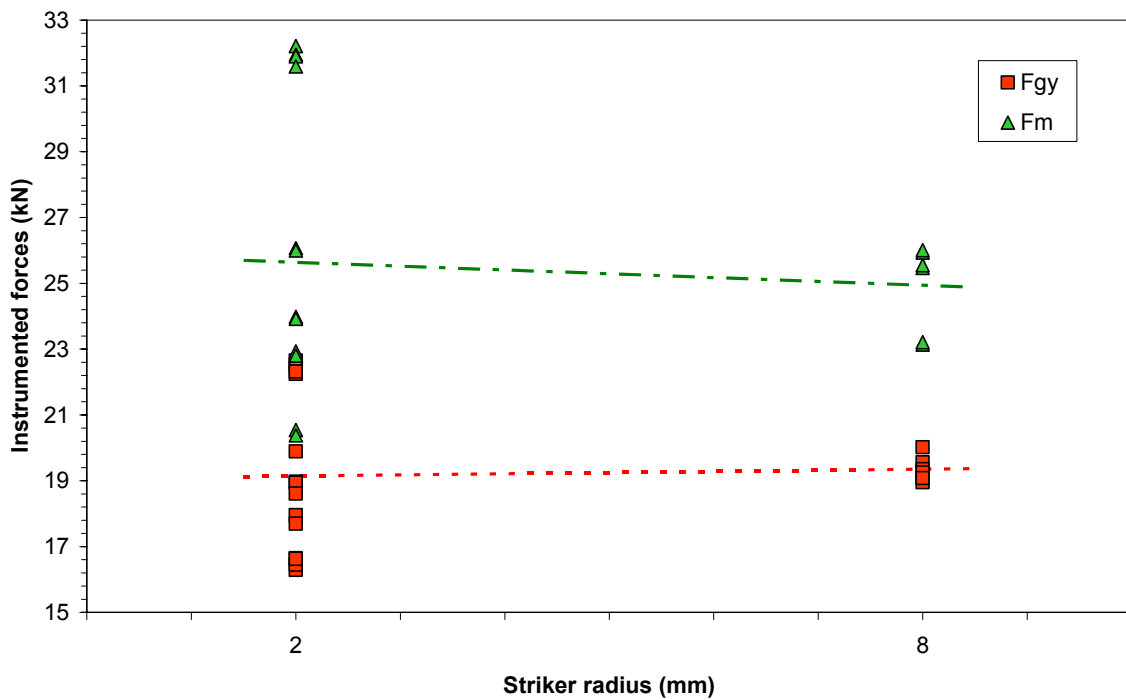
FIG. IIE.12. Effect of striker radius on the original ILC results.

A slight influence of striker radius is now visible on the corrected force values (Figure IIE.13 – forces increasing with striker radius), which would anyhow need confirmation by a larger number of tests conducted using an 8 mm striker.
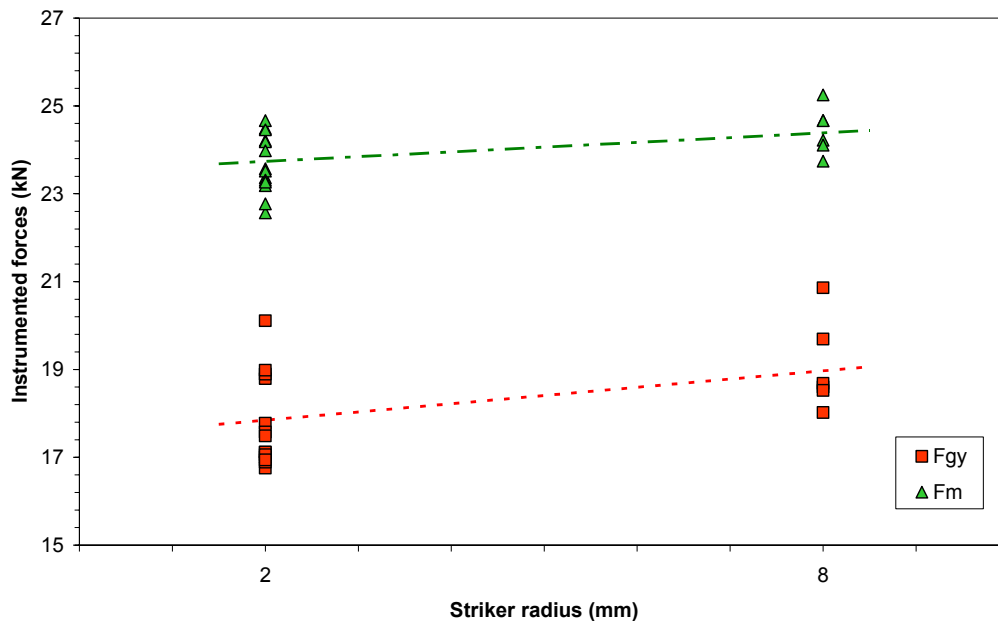
FIG. IIE.13. Effect of striker radius on the dynamically corrected ILC results.

IIF. CORRELATIONS

IIF.1. RELATIONSHIP BETWEEN CRACK ARREST FORCES FROM INSTRUMENTED CHARPY TESTS AND NDT FROM PELLINI TESTS

Licensing rules related to safety against brittle fracture of nuclear reactor pressure vessels (RPV) are based on the nil ductility transition temperature (NDT), which is measured by drop-weight (Pellini) tests in accordance with ASTM E208. The reference temperature RT_{NDT}, which is used for indexing both the initiation (K_{Ic}) and arrest (K_{Ia}) fracture toughness curves of the vessel, is obtained by combining Pellini and Charpy test information for the unirradiated condition, while the increase ΔRT_{NDT} caused by irradiation is assumed to be equal to the shift of the Charpy energy curve at the 41 J (30 ft-lb) level.

The use of crack arrest forces F_a from instrumented Charpy tests to correlate NDT was first proposed by GKSS; more recently, Wallin, Iskander and Fabry have used Charpy F_a forces to describe the crack arrest behaviour of RPV steels.

A. Fabry proposed a 'crack arrest master curve' formulation for the temperature dependence of arrest forces, based on the following equation:

$$F_a(T) = 3 \cdot \exp(\lambda T - NDT) \tag{IIF.1}$$

where $\lambda = 0.020$ for $T < NDT$ and $\lambda = 0.026$ for $T > NDT$ and the nil ductility temperature NDT corresponds to a median crack arrest force indexing level of 3 kN. This indexing level provides an accuracy of ±15°C in NDT determination at the 95% confidence level, based on the investigation of 26 RPV steels (Figure IIF.1). Other force values have been proposed for

the determination of NDT, such as 4 kN in and 2.45 kN in, leading to accuracies of ±10°C and ±11°C respectively but based on a more limited database (7 and 8 materials).

The excellent correlation between NDT values measured from Pellini drop-weight tests and median 3 kN crack arrest force temperature from Charpy tests is shown in Figure IIF.2, which is based on data given in Table IIF.1.

As part of the Fabry's work , it was also shown that the temperature T_A at which the median arrest fracture toughness K_{Ia} is equal to 100 MPa√m (arrest reference temperature) corresponds to a Charpy arrest force indexing level of 5.05 kN (Figure IIF.3); it was also demonstrated that:

$$T_A = NDT + 20°C \qquad\qquad (IIF.2)$$

with an uncertainty of ±12°C at the 95% confidence level (2σ). This compares favourably with results from Wallin who proposed:

$$T_{Fa4} = T_A - 10°C \qquad\qquad (IIF.3)$$

(2σ = ±27 °C) where T_{Fa4} is the temperature at which the median crack arrest force is 4 kN. Based on Equation IIF.3, this transforms in:

$$T_A = NDT + 21°C \qquad\qquad (IIF.4)$$

which is very similar to equation IIF.2.
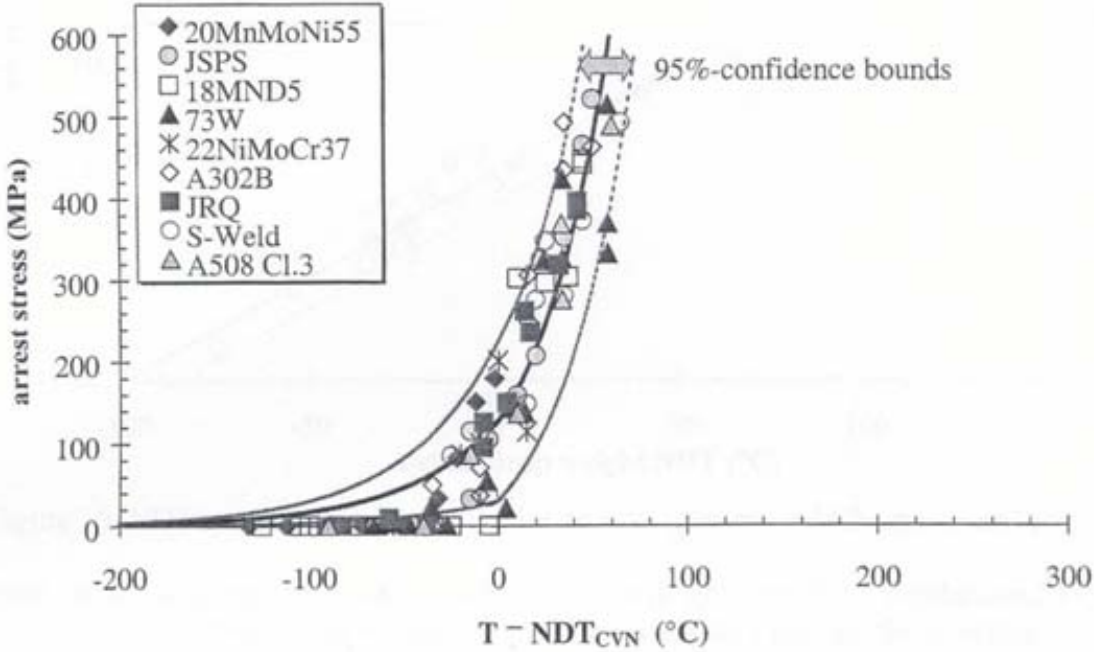
FIG. IIF.1. Master Curve regression of arrest stress values from instrumented Charpy tests.
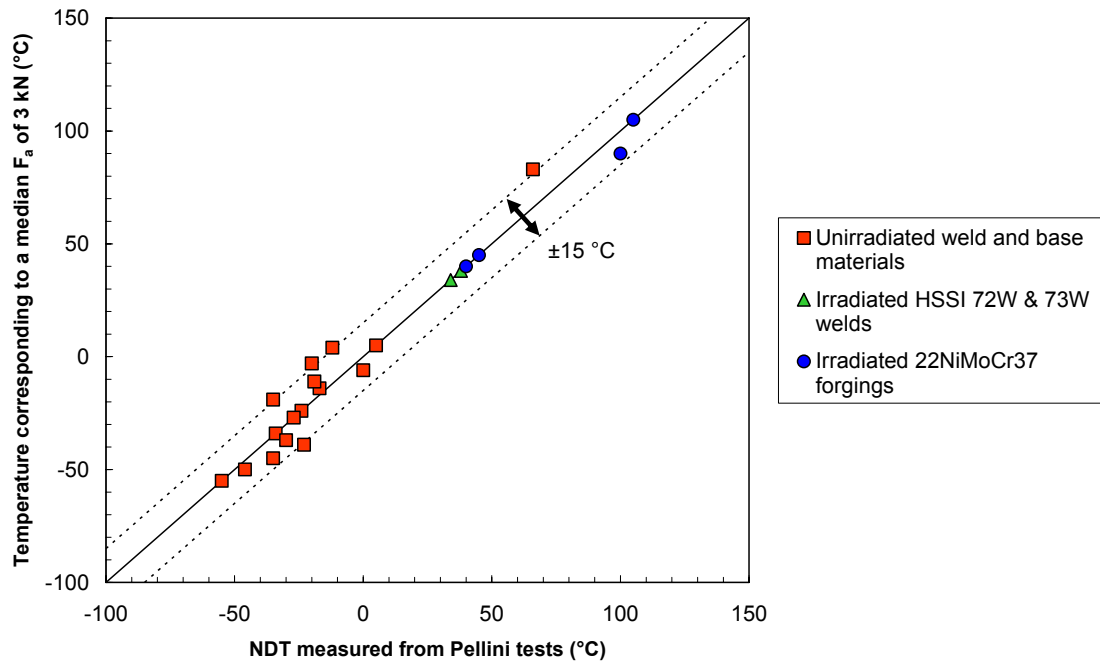
FIG. IIF.2. Correlation between NDT and temperature corresponding to a Charpy median crack arrest force of 3 kN .

TABLE IIF.1. DATA USED FOR FIGURE IIF.2

Steel	Condition	NDT Pellini (°C)	3 kN median F_a (°C)
A302B	Unirradiated	-17	-14
HSST-02		-19	-11
HSST-03		-12	4
KS-01 22NiMoCr37		5	5
KS-02 22NiMoCr37		0	-6
A508 Cl.2 (PTSE-1)		66	83
Belgian surv. forging 1		-24	-24
Belgian surv. forging 2		-35	-19
22NiMoCr37 surv. forging		-20	-3
HSSI 72W		-27	-27
HSSI 73W		-34	-34
Linde-80 weld		-23	-39
Quad Cities-2 surv. weld		-46	-50
Belgian surv. weld		-30	-37
22NiMoCr37 surv. weld		-35	-45
Midland vessel weld		-55	-55
KS-01 (2E19 n/cm²)	Irradiated	45	45
KS-01 (7E19 n/cm²)		100	90
KS-02 (2E19 n/cm²)		40	40
KS-02 (8E19 n/cm²)		105	105
HSSI 72W (1.5-2E19 n/cm²)		34	34
HSSI 73W (1.5-2E19 n/cm²)		38	38
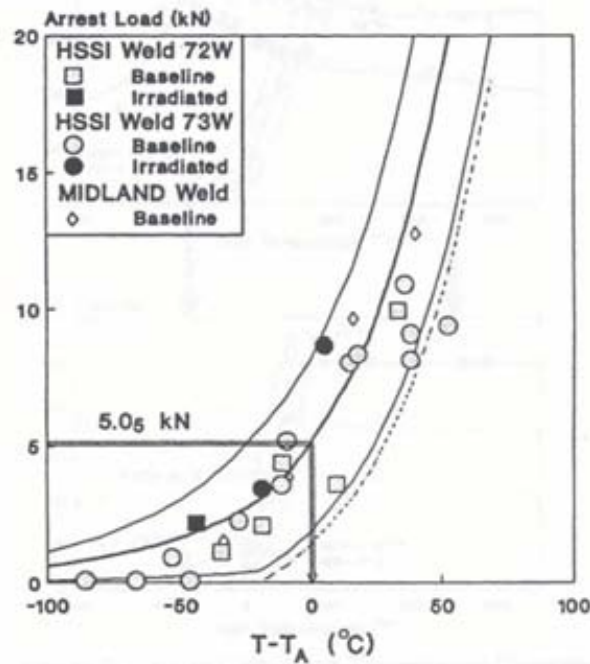
FIG. IIF.3. Measuring crack arrest toughness from instrumented Charpy tests.

IIF.2. CORRELATION BETWEEN T_0 AND T_{41J}

Using data included in the databases of FZD and SCK•CEN, empirical correlations have been established between measured values of T_{41J} (from Charpy tests) and T_0 (from fracture toughness tests analysed using the Master Curve approach), considering both base and weld materials, in the unirradiated and irradiated conditions. The relationship obtained considering only base materials, imposing unity for the slope of the linear fit, is:

$$T_0 = T_{41J} - 56°C \tag{IIF.5}$$

with a standard deviation of 30°C (Figure IIF.4).

If weld metal data are included, the experimental scatter is significantly increased and the correlation becomes:

$$T_0 = T_{41J} - 53°C \tag{IIF.6}$$

with an almost identical intercept but a markedly higher standard deviation of 50°C (Figure IIF.5).

Both relationships are considerably different from the one proposed by Sokolov and Nanstad and presently included in ASTM E1921-05 (§8.4, Test Temperature Selection):

$$T_0 = T_{41J} - 24°C \tag{IIF.7}$$
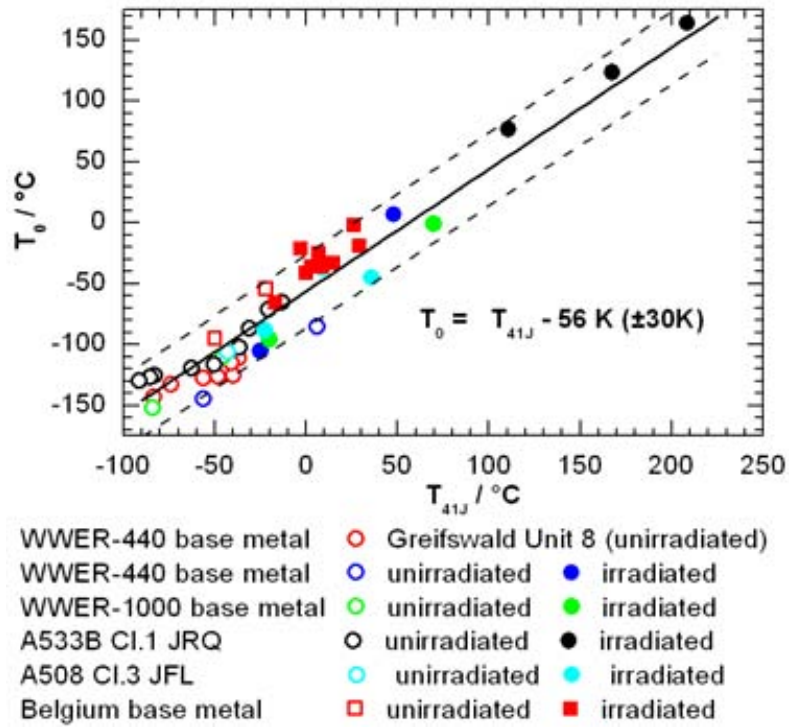
FIG. IIF.4. Relationship between T_0 and T_{41J} for base materials.
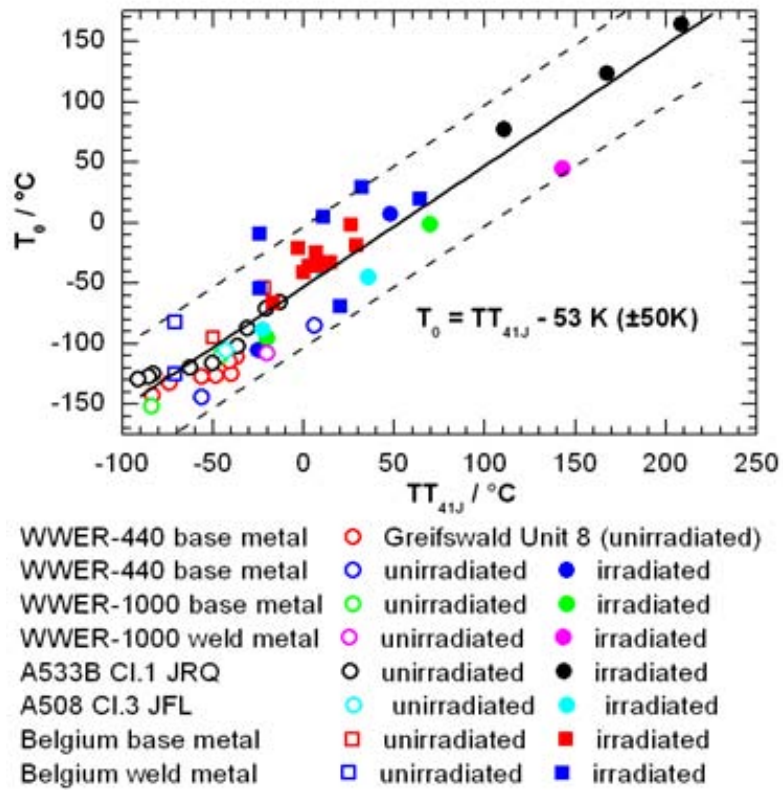
FIG. IIF.5. Relationship between T_0 and T41J for base and weld materials.

IIIA. MATERIALS EVALUATED FOR TOPIC AREA 3

The materials reviewed in Topic area 3 are shown in Table IIIA.1. The materials consisted of mostly different reactor pressure vessel (RPV) base and weld metals from various surveillance and test programmes.

TABLE IIIA.1. SUMMARY OF MATERIAL DATA PROVIDED FOR TOPIC AREA 3

Material [1]	Fluence (E >1 MeV)	T_o (^{o}C)	Condition [2]	Remarks
VVER 440 BM & WM	$<1.1 \times 10^{21}$ n/cm^2 (E>0.5 MeV)	+15…+240	I	
IAEA RRE WM		+42…+60	I	
Material A			R	
NiCrMo WM	2.2×10^{19} n/cm^2		I	40-50 mm WOL specimen
JFL, JRQ	20×10^{19} n/cm^2		I	
VVER 440 BM			I	IGF ≈ 20%
JFL		-45…-37		
JRQ		+124 and +164	I	
VVER 440 Weld 502		+30…+84	I	
VVER 1000		+31	I	High Ni cont.
JRQ		+62	I	
A533B-1 (mod.)		-6 +6 (SINTAP)	A+I	0.057% P content
1.	1.9×10^{19} n/cm^2	+117 (SINTAP)	A+I	Tests at 90°C
2.	5.3×10^{19} n/cm^2	+218 (SINTAP)	A+I	Tests at 200°C
Mod. 9Cr-1Mo-V		-68		Ferritic-martens. steel
JRQ			A	Incl. IGF (program on going)
16MND5 (A508Cl.3)		$\Delta T_0 \approx 90^o$C	A	
HSSI WM 72W, 73W			R, I	
KS-01 WM		ΔT_0=160°C	R, I	
Midland WM	3.4×10^{19} n/cm^2		R, I	
EUROFER 97 F82H, T91, HT9	High fluence		I	Ferritic-martens. steels
Western steels Linde 80 WM			R & I	
VVER 440 WM			R, I, IA etc.	
22NiMoCr37 (Mat. A)	3.1×10^{19} n/cm^2	+69 (irradiated)	R, I	
PTSE-1 (15X2MFA)		+80…+163	A	Diff. size specimens, various depth
VVER 440 WM	$\approx 10^{21}$ n/cm^2 (E>0.5 MeV)	+228	I	Reconstituted specimens

[1] BM: base metal, WM: weld metal
[2] R: reference, I: irradiated, A: annealed

IIIB. EFFECT OF DUCTILE TEARING

The ductile tearing often preceding brittle fracture in the upper transition region tends to decrease the measured fracture toughness by increasing the volume ahead of the crack tip where cleavage fracture may potentially initiate. This means growing probability for cleavage fracture initiation with the amount of ductile crack growth. The model has been applied, together with the standard MC approach, on thermally embrittled and irradiated RPV steels which showed abnormal transition curve shape.

The possibility of ductile tearing increases when approaching the upper transition region. As a consequence of ductile tearing the probability of cleavage fracture initiation is increasing with the growing volume of the process zone as the crack advances. Besides affecting this statistical sampling volume of potential cleavage initiators, ductile tearing also tends to change the crack tip stress distribution. In both cases, the effect is dependent on the amount of ductile crack growth. A simplified expression for the fracture probability (P_f) at stress intensity (K_I), considering a small amount of ductile tearing ($\Delta a \leq 1$ mm), is given as follows:

$$P_f = 1 - \exp - \left[\frac{B}{B_0} \left(\frac{K_I - K_{min}}{K_0 - K_{min}} \right)^4 \cdot \left(1 + \frac{2\Omega^2 \cdot \Delta a}{K_I^2 \cdot (2m+1)} \right) \right] \tag{IIIB.1}$$

where m and Ω are material dependent constants, B is specimen thickness, B_0 and K_0 are scale factors and $K_{min} = 20$ MPa√m. The Equation IIIB.1 can thus be used to correct the fracture probability to correspond to the increased sampling volume ahead of the crack tip due to ductile tearing.

In Figure IIIB.1, the ductile tearing correction (Equation IIIB.1) has been used to calculate the toughness of a thermally aged pressure vessel steel (PTSE-1) which has T_0 as high as +163°C. The analysis shows that the correction moves the upper transition region to the right, but has negligible effect on the value of T_0 and on the behaviour near the lower shelf. In this case, however, the total deviation of the high temperature values from the prediction cannot be explained by ductile crack growth alone.
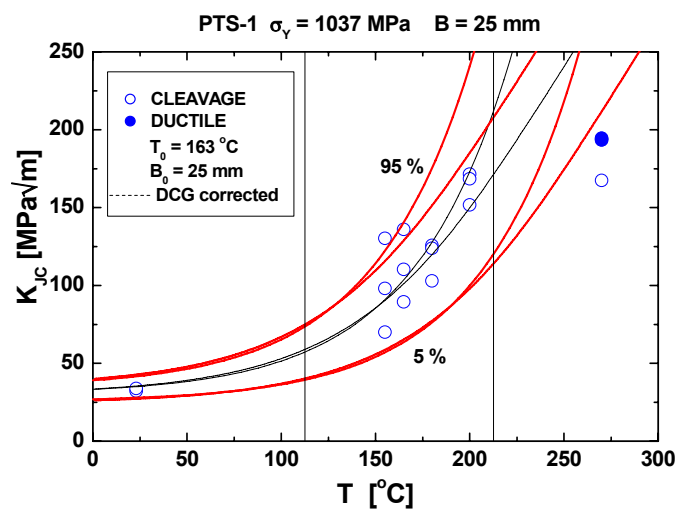
FIG. IIIB.1. Effect of ductile tearing on the Master Curve prediction of a thermally aged pressure vessel steel (PTSE-1).

The effect of ductile tearing on the measured J-integral is generally considered in test standards which limit the amount of ductile crack growth (to avoid an excessive plastic part of J), and procedures exist to correct the effect of small crack growth. In general, the consideration of ductile tearing is more relevant with high strength steels which also typically have a low strain hardening exponent. The proposed ductile tearing model is applicable to estimate the statistical effect of small ductile crack growth on the cleavage fracture probability in comparison to the normal MC prediction and to the measured fracture toughness.

As ductile tearing preceding cleavage initiation tends to increase the probability of cleavage initiation and thus decrease the fracture toughness, loss of constraint on the contrary tends to increase the fracture toughness. This effect is shown in Figure IIIB.2 describing the evaluation made for low and very low toughness structural steels (LT and VLT) by SCK•CEN.
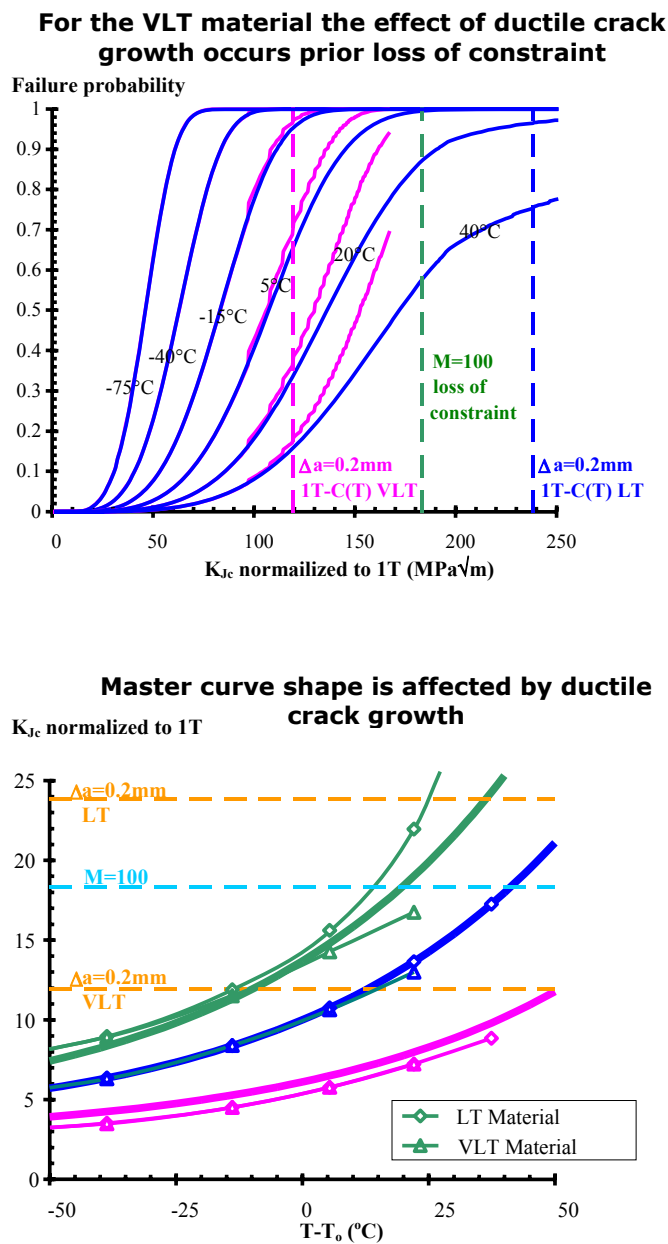
FIG. IIIB.2. Fracture toughness analysis for two structural steels (LT and VLT) showing the effect of ductile crack growth and loss of constraint at high K_{Jc} (analyses by SCK•CEN).

IIIC. THE UPPER SHELF CORRELATION

IIIC.1. DEVELOPMENT OF A MODEL DESCRIBING UPPER SHELF TOUGHNESS

This model described the temperature dependence of the upper shelf toughness derived based on the thermal term of the Zerilli-Armstrong (ZA) equation describing the dependence of the yield strength of ferritic steels on temperature. The basis for using the thermal portion of the ZA equation as the functional form for the upper shelf toughness temperature-dependence was the fact that both yield behaviour and ductile initiation fracture toughness behaviour are controlled by the ability of a material to move dislocations through the matrix. Zerilli and Armstrong demonstrated that this temperature dependence was the same for all materials of a given lattice structure implying that all ferritic steels would exhibit the same temperature dependence of yield behaviour. Therefore, it was deemed appropriate to use the same form of the thermal term in the ZA yield equation to describe the temperature dependence of the upper shelf initiation toughness for all ferritic steels.

The criteria for fracture on the upper shelf should not change the functional form of the temperature dependence of ductile initiation toughness, but only magnify or reduce the temperature dependence described by the flow equation. To empirically evaluate this idea, the ZA dislocation-based flow model for BCC materials was re-arranged to isolate the thermal terms, as follows (stress and temperature are expressed in MPa and °C, respectively):

$$\sigma_f = \left\langle \Delta\sigma'_G + C_4\varepsilon^n + k/\sqrt{d} \right\rangle + \left\{ C_1 \cdot \exp\left[-C_2(T+273.15) + C_3(T+273.15)\cdot \ln(\dot{\varepsilon}) \right] \right\} \qquad \text{(IIIC.1)}$$

Here, the first term, i.e. $\langle \ldots \rangle$, is the athermal part of the flow stress, which depends on the effects of prior hardening ($\Delta\sigma'_G$), strain hardening under load ($C_4\varepsilon^n$), and grain size ($k/\sqrt{d}$). Conversely, the second term, i.e. $\{\ldots\}$, is the part of the flow stress that depends on temperature and strain rate. To isolate the thermal term the value of the flow stress at a fixed temperature, T_{ref}, was subtracted from Equation IIIC.1. Based on Equation IIIC.1, the flow strength at T_{ref} can be expressed as follows:

$$\sigma_{f(ref)} = \left\langle \Delta\sigma'_G + C_4\varepsilon^n + k/\sqrt{d} \right\rangle + \left\{ C_1 \cdot \exp\left[-C_2\left(T_{ref}+273.15\right) + C_3\left(T_{ref}+273.15\right)\cdot \ln(\dot{\varepsilon}) \right] \right\} \text{(IIIC.2)}$$

Subtracting Equation IIIC.2 from Equation IIIC.1 produces:

$$\Delta\sigma_f \equiv \sigma_f - \sigma_{f(ref)} = \left\{ C_1 \cdot \exp\left[-C_2(T+273.15) + C_3(T+273.15)\cdot \ln(\dot{\varepsilon}) \right] \right\} - \sigma_{T=Tref}^{thermal} \qquad \text{(IIIC.3)}$$

Where:

$$\sigma_{T=Tref}^{thermal} = \left\{ C_1 \cdot \exp\left[-C_2\left(T_{ref}+273.15\right) + C_3\left(T_{ref}+273.15\right)\cdot \ln(\dot{\varepsilon}) \right] \right\}$$

In Equation IIIC.3, $\Delta\sigma_f$ represents the difference between the flow strength at any given temperature and the flow strength at the reference temperature T_{ref}. For ARMCO Iron, ZA give the following coefficients for the temperature / strain rate terms: C_1 = 1033 MPa, C_2 = 0.00698/K, C_3 = 0.000415/K. The physical expectation, which is borne out by other data presented by ZA, is that these coefficients are the same for all ferritic steels.

The temperature dependence expressed by Equation IIIC.3 was compared with the temperature dependence exhibited by a large collection of J_{Ic} data from ferritic steels and normalized by the J_{Ic} at 288°C to determine whether Equation IIIC.3 adequately describes the

temperature dependence on upper shelf toughness. This database contains 91 datasets that collectively have a total of 809 measured J_{Ic} values. The database includes nuclear pressure vessel steels, ship steels, and mild steels; materials that exhibit a wide range of upper shelf impact toughness values (from ≈50 to 300 J upper shelf energy) as measured by the Charpy V-notch specimen. Comparison of this J_{Ic} data to Equation IIIC.3 confirmed the postulate that the temperature dependence of J_{Ic} is indeed similar to that of the ZA flow model, and revealed that the following model (see FIG. IIIC.1) with a value of $\alpha = 1.75$ mm provides a good representation of the temperature dependence for the overwhelming majority of the 91 datasets considered:

$$\Delta J_{Ic} \equiv J_{Ic}(T) - J_{Ic(Tref)} = \alpha\left\{ C_1 \cdot \exp\left[- C_2(T + 273.15) + C_3(T + 273.15) \cdot \ln(\dot{\varepsilon})\right] - \sigma_{T=Tref}^{thermal} \right\} \quad \text{(IIIC.4)}$$

The empirically derived coefficient α has units of mm to convert from the stress units, MPa, inside the {...} to J units, kJ/m^2, on the left hand side of Equation IIIC.4.
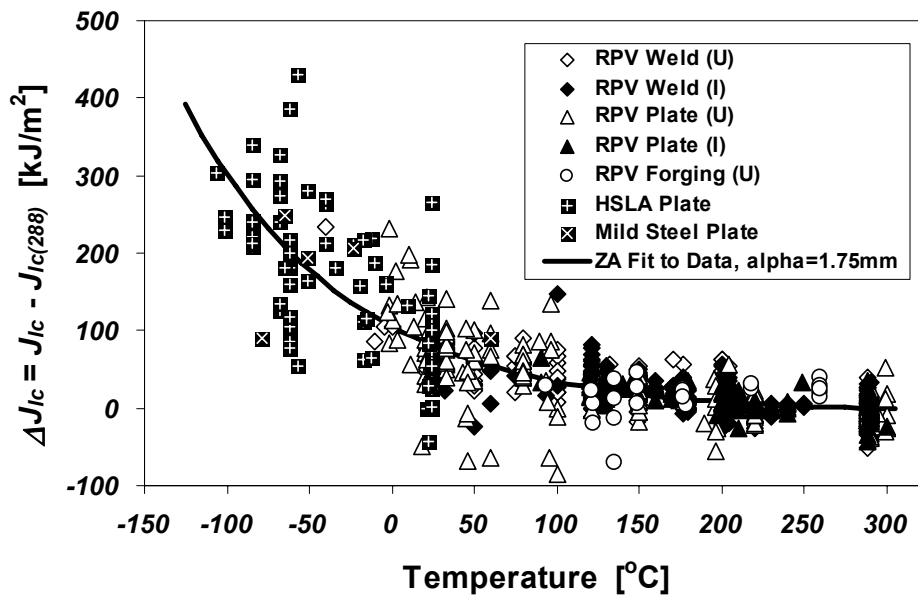
FIG. IIIC.1. Model of J_{Ic} temperature dependence.

A model for the variability of J_{Ic} at any fixed temperature was also determined from the empirical database. The following model shows that the variability in J_{Ic} depends only on temperature, increasing as temperature decreases.

$$\sigma_{\Delta J_{Ic}} = 51.2 \cdot e^{-0.0056T} \quad \{\sigma_{\Delta Jlc} \text{ in kJ/m}^2, \text{ temperature in } °C\} \quad \text{(IIIC.5)}$$

Further work, using a large dataset (50 specimens tested at 7 different temperatures) from the Euro forging, suggested that the variability in J_{Ic} may depend not only on the temperature, but also on the absolute magnitude of J_{Ic}. This premise was further studied using the 91 datasets from the original analysis to develop an upper shelf model. Results suggest the following relationship between the standard deviation of J_{Ic}, the test temperature, and the absolute magnitude of J_{Ic} on the upper shelf:

$$\sigma_{\Delta J_{Ic}} = A \cdot e^{\left(B \cdot \hat{T}\right)} \tag{IIIC.6}$$

where:

$$\hat{T} = T - 288°C$$
$$A = 9.03 \cdot e^{(1.12 \cdot P)}$$
$$B = MIN\{0, 0.0009 - 0.0045 \cdot P\}$$
$$P = MIN\{1, MAX[0, MIN(P_1, P_2)]\}$$
$$P_1 = \frac{J_{Ic(288)}}{120} - 0.46$$
$$P_2 = \frac{J_{Ic(288)}}{800} + 0.51$$

Equation IIIC.6 is shown with actual datasets in Figure IIIC.2, demonstrating the variation in scatter in J_{Ic} with absolute value of J_{Ic}.

IIIC.2. DEVELOPMENT OF A RELATIONSHIP BETWEEN THE UPPER SHELF MODEL AND THE TRANSITION TOUGHNESS MODEL FOR FRACTURE TOUGHNESS

Combining Equation IIIC.1 with Wallin's Master Curve for fracture mode transition permits identification of a temperature above which upper shelf behaviour occurs, thereby signalling the upper limit of cleavage fracture behaviour and the onset of upper shelf, where ductile fracture processes manifest. Fitting a master curve through K_{Jc} data and fitting Equation IIIC.4 through J_{Ic} data defines the temperature at which the Wallin Master Curve and the upper shelf Master Curve intersect, which we label T_{US}. T_{US} is defined for a particular dataset as the temperature at the intersection of the Wallin Master Curve:

$$K_{Jc} = 30 + 70 \cdot \exp\left(0.019\left(T - T_o\right)\right) \tag{IIIC.7}$$

and the upper shelf Master Curve proposed in Equation IIIC.4. The intersection point is defined when both curves are expressed in J-units, so Equation IIIC.6 becomes:

$$J_c = \frac{\{30 + 70 \cdot \exp\left(0.019\left(T - T_o\right)\right)\}^2\left(1 - \upsilon^2\right)}{E} \tag{IIIC.8}$$

where $E = \{207200 - 57.1 \cdot T\}^{13}$, T is in °C, E is in MPa, and $\nu = 0.3$.
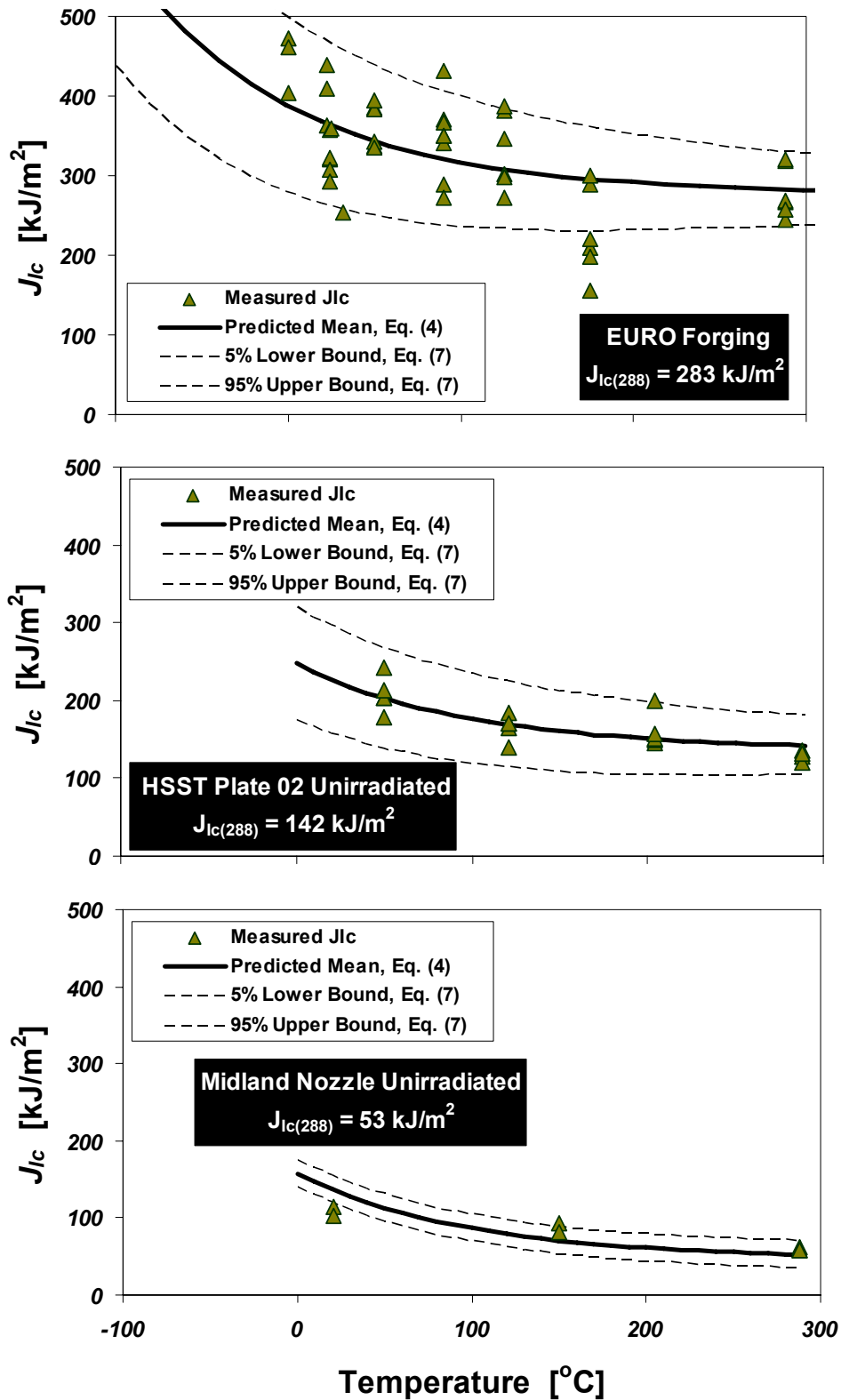
FIG. IIIC.2. Comparison of the revised J_{Ic} model, Equations IIIC.4 and IIIC.6, with J_{Ic} data from steels having three different upper shelf toughness ($J_{Ic(288)}$) values.

Plotting the intersection of the mean transition and upper shelf master curves (see Figure IIIC.3), defined as T_{US}, versus T_0 for a series of datasets contained within the EPRI database shows a clear trend between these two values that is shown in Figure IIIC.4. The

data in Figure IIIC.4 includes both irradiated and unirradiated nuclear RPV steels (including different product forms and the so-called low upper shelf welds) as well as the higher-strength copper precipitation hardened steels ASTM A710 and HSLA-100 used by the US Navy in surface ship fabrication. These data exhibit an extremely consistent trend over T_0 values spanning nearly 350°C. Fitting a linear relationship to all 54 (T_0, T_{US}) pairs produces the following relationship, as shown in Figure IIIC.4:

$$T_{US} = 50.1 + 0.794 T_o \quad \text{(temperature in °C)} \tag{IIIC.9}$$

The linear correlation coefficient and the standard deviation of the fit represented by Equation IIIC.9 are $R^2 = 0.985$ and $\sigma = 8.2$°C. The consistency of this relationship across such a broad range of materials suggests that Equation IIIC.9 can be used to define an upper limit of applicability for the ASTM E1921 transition toughness Master Curve that is more physically motivated than the current $T_0 + 50$°C limit as shown in Figure IIIC.5.
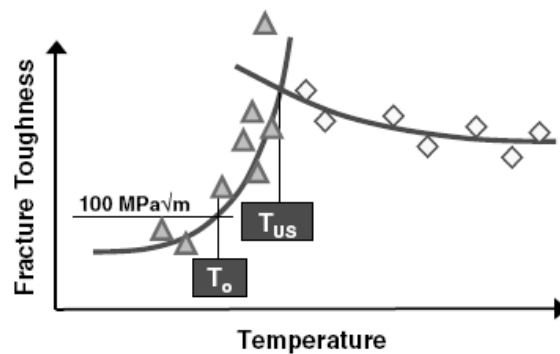
FIG. IIIC.3. Schematic illustrating the relationship between the transition and upper shelf toughness, and defining the value T_{US} as the intersection of the Master Curve and the upper shelf temperature curve.
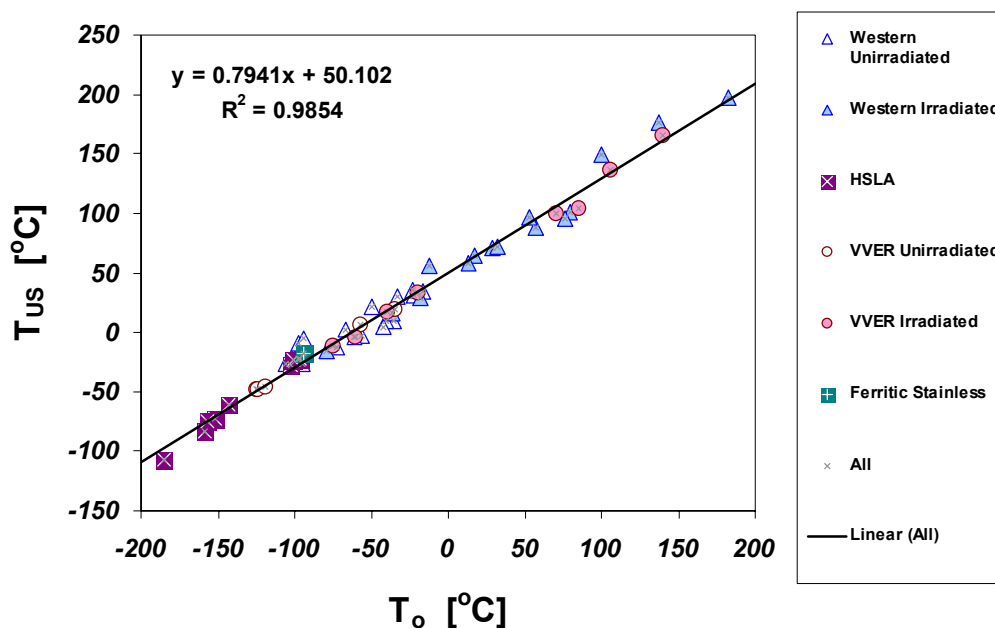
FIG. IIIC.4. Relationship between T_{US} and T_0.
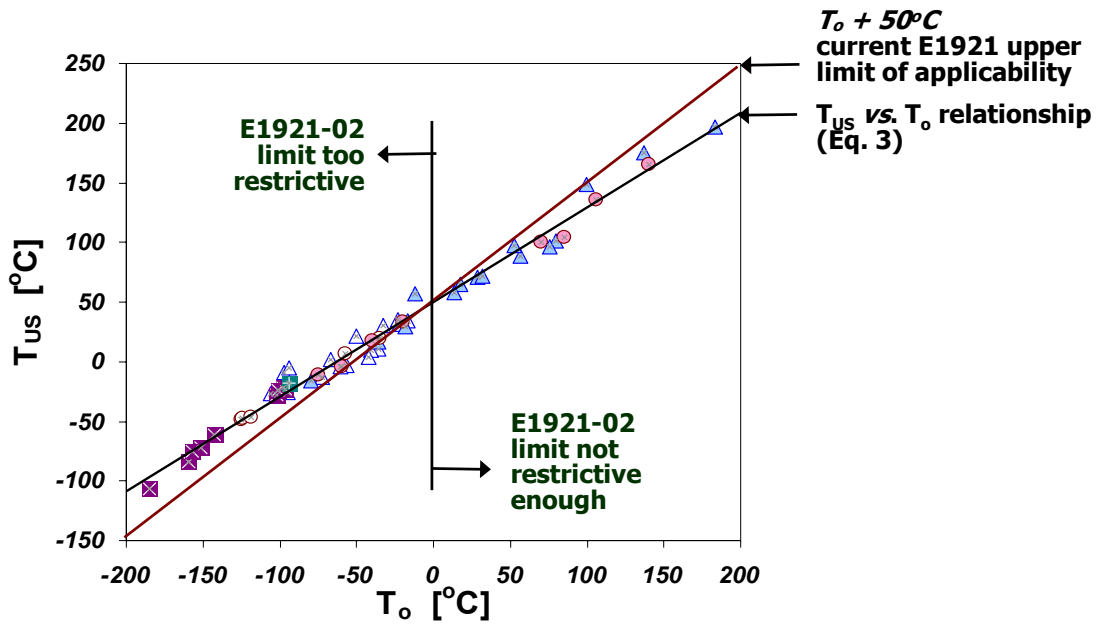
FIG. IIIC.5. The data of Figure 3 overlaid with the ASTM E1921-02 limits on (transition) Master Curve applicability.

IIID. COMPARISON OF MASTER CURVE VS. UNIFIED CURVE

To compare the Master Curve (MC) and Unified Curve predictions, three datasets, i.e. the irradiated welds 72W and 73W tested by ORNL and a special heat KS22, were analysed with both methods. In case of welds 72W and 73W, the maximum likelihood fitted temperature dependence followed closely the MC prediction and moderately also the Unified Curve prediction (Figure IIID.1).

| (a) | (b) |
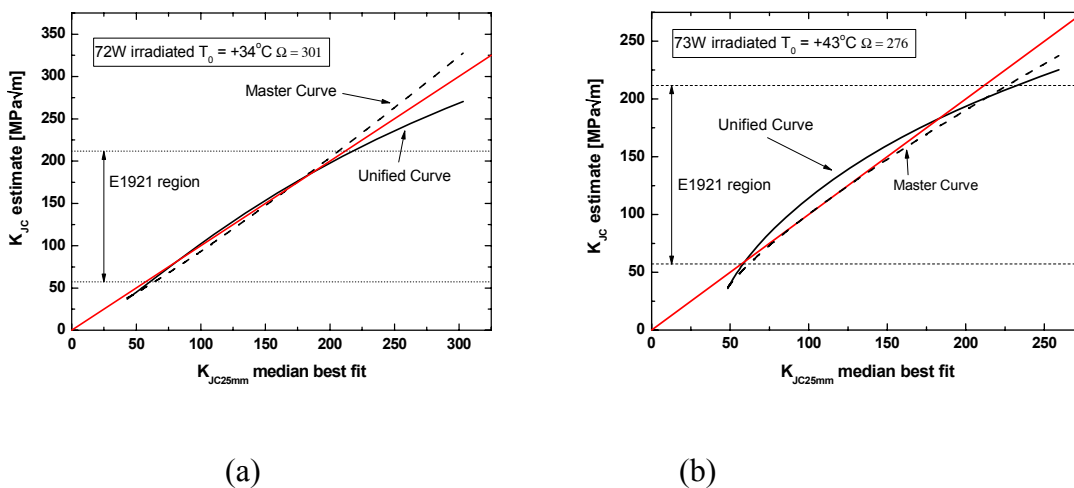
FIG. IIID.1. Comparison of Master Curve and Unified Curve predictions on (a) irradiated 72W weld and (b) 73W weld.

The KS22 data analysed both by the standard Master Curve and the Unified Curve gave a totally different result than the previous ones (Figure IIID.2). The standard Master Curve form seemed to be too steep for this material. At least partly this behaviour may be explained by the large proportion of ductile tearing. The Unified Curve, however, provides a strongly over-conservative prediction of the materials temperature dependence and does not predict the actual cleavage fracture values occurring above 200 MPa√m.

The performed study suggests that the Unified Curve tends to over-predict the shape change due to irradiation. Also, it is noted that the upper limit prediction included in the Unified Curve model for cleavage fracture has not been verified.

As for the temperature dependence the KS22 data evidently represents an extreme case which cannot be analysed satisfactorily with the standard MC procedure, but not fully either with the UC procedure. In this case, assuming that the data reflects the true temperature dependence, the shape adjusted MC estimation is suggested to provide the most realistic description of the fracture toughness behaviour outside the standard ±50°C validity window.
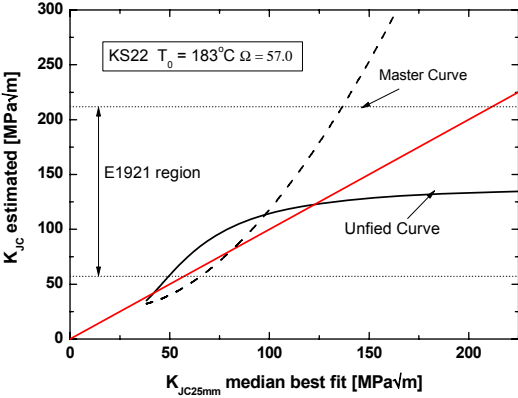
FIG. IIID.2. Comparison of Unified Curve and Master Curve predictions
on special heat KS22.

In the UC procedure the parameter Ω describes the degree of embrittlement of the material. As the degree of embrittlement increases, the parameter Ω decreases. The decreasing Ω thus means also a gradually decreasing slope of the transition curve. This effect is clarified in Figure IIID.3, which compares the UC predictions of K_{Jc} vs. T with the values of Ω ranging from 50 to 5000 MPa√m and the corresponding MC prediction. The difference between the MC and the UC estimates is clear when Ω is less than about 500 MPa√m, but negligible when Ω is between 1000–5000 MPa√m (Figure IIID.3).

160
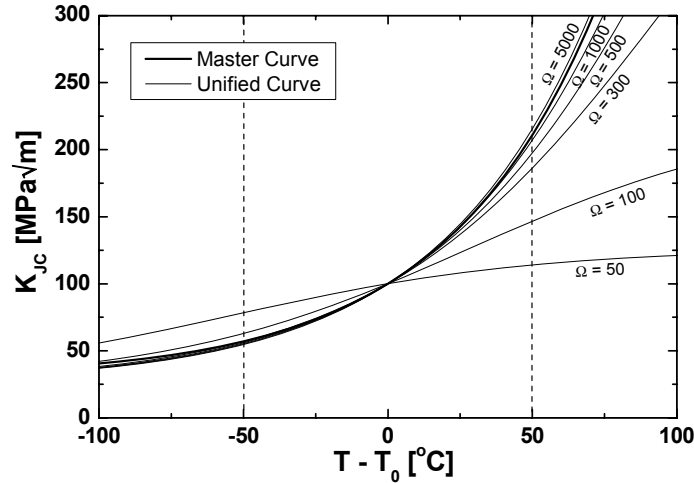
FIG. IIID.3. Comparison of fracture toughness temperature dependence according to the MC and the UC with different values of parameter Ω.

IIIE. CLEAVAGE FRACTURE MODEL DEVELOPMENT

The fracture model used in the Master Curve approach was recently calibrated to provide more accurate predictions of fracture toughness using the new microstructural and mechanical property information. Utilising the new understanding of cleavage initiation mechanisms and materials fracture behaviour, a new version of the original cleavage fracture model was developed by simulating the fracture behaviour of a 0.5-TCT specimen and by applying the recent experimental results on cleavage fracture initiation and microstructures. The new model is still based on the assumption of cleavage initiation to be controlled by carbides, but now the model includes also the effect of matrix strain on the carbide stress. The model is capable of quantitatively predicting correctly (comparable to the Master Curve) the statistical size effect on fracture toughness as well as the respective shape of the ductile-to-brittle transition region fracture toughness decrease.

Besides the specimen thickness dependency, the commonly observed trends for the volumetric dependency of fracture toughness and the lower shelf assumption, the above results confirm the temperature dependency and the Master Curve shape assumption. The evaluation was made for the 0.5-T specimen geometry by carrying out analyses over the temperature range of the Eurocurve dataset. In Figure IIIE.1, the simulated K_{Jc} vs. T curves are given together with the experimental Material A data using the number of particles in a volume element (N_v) as the scale parameter and by varying the constant term of the particle surface energy (γ_p^α).
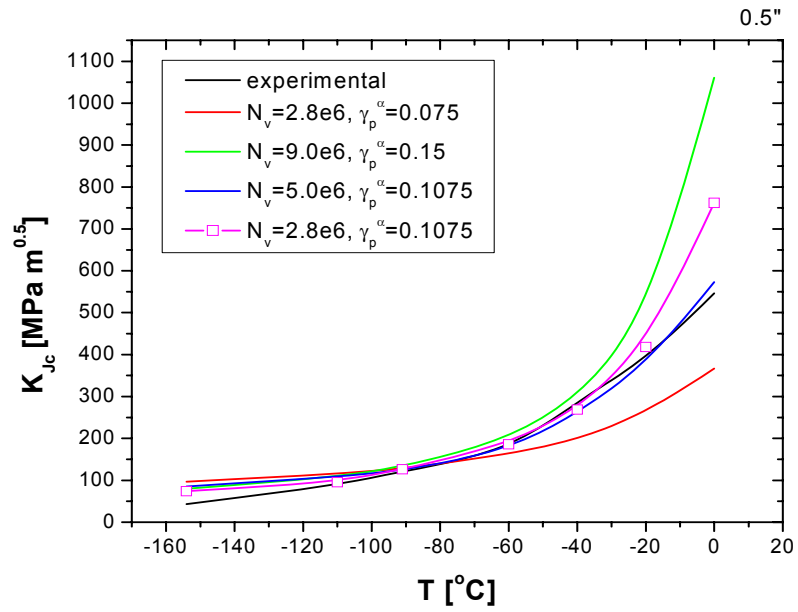
FIG. IIIE.1. Comparison of fracture toughness Master Curve (curve experimental) estimated for the Euro Reference Material A and various WST model predictions made with the new model version.

ABBREVIATIONS

AEKI	Atomic Energy Research Institute
ASME	American Society of Mechanical Engineers
ASTM	American Society for Testing and Materials
BM	Base metal
BMMC	Bi-Modal Master Curve
BSP	Bennett-Sinclair parameter
CFR	Code of Federal Regulations
CIEMAT	Centro de Investigaciones Energéticas, Medioambientales y Tecnológicas, Spain
CMOD	Crack mouth opening displacement
CPU	Central processing unit
CRIEPI	Central Research Institute of Electric Power Industry
CRP	Coordinated Research Programme
CT / C(T)	Compact tension specimen
CTOD	Crack tip opening displacement
CVN	Charpy V-notch
DOF	Degree of freedom
EFPY	Effective full power years
EN	European norm
EOL	End of life
EPFM	Elastic-plastic fracture mechanics
ESIS	European Structure Integrity Society
F_{gy}	Force at general yield
F_m	Maximum force
FZD	Forschungszentrum Dresden, Germany
FZR	Forschungszentrum Karlsruhe, Germany
GBF	Intergranular fracture
HAZ	Heat affected zone
HSST	Heavy section steel technology
IGF	Intergranular fracture
ILC	Interlaboratory comparison
ININ	Instituto Nacional de Investigaciones Nucleares, Mexico
IRMM	Institute for Reference Materials and Measurements, Geel, Belgium
JAEA	Japan Atomic Energy Agency

JEAC/JEA	Japanese Electric Association
J-R	J-integral-resistance
JRC	Joint Research Centre
JRQ	Japan Reference Quality
JSPS	Japanese steel with low upper shelf toughness
KAERI	Korea Atomic Energy Research Institute
KCV	Impact strength (measured value in CVN impact test)
K_I	Stress intensity factor
$K_{IC;}K_{JC}$	Fracture toughness
KTA	Nuclear Technical Commission
KV	Absorbed energy
LEFM	Linear elastic fracture mechanics
LLD	Load line displacement
LWR	Light water reactor
MC	Master Curve
MMMC	Multi-Modal Master Curve
NDT	Nil-ductility temperature
NPP	Nuclear power plant
NRC	Nuclear Regulatory Commission
NRI	Nuclear Research Institute Řež, Czech Republic
ORNL	Oak Ridge National Laboratories
PCC	Precracked Charpy
PCCv	Precracked Charpy V-notch specimen
PCVN	Precracked Charpy V-notch specimen
P-T	Pressure-temperature
PTS	Pressurized thermal shock
PWR	Pressurized water reactor
R_m	Ultimate tensile strength
$R_{p0.2}$	Yield strength
RPV	Reactor pressure vessel
RRC-KI	Russian Research Centre – Kurchatov Institute
RRE	Round robin exercise
RT_{NDT}	Reference temperature
SCK•CEN	Dosimetry Measurement Laboratory, Mol, Belgium

| SEB | / | Single edge bend specimen |
| SE(B) | | |

SSC	Structures, systems and components
T_{irr}	Irradiation temperature
T_k	Ductile-brittle transition temperature; critical temperature of brittleness
T_{k0}	Initial ductile-brittle transition temperature
TT	Transition temperature
T_{US}	Upper shelf temperature
UC	Unified Curve
USE	Upper shelf energy
VTT	Valmistustekniikka Turvallisuustekniikka (Technical research center in Finland)
WWER	Water-water energy reactor
W/B	Width to thickness ratio
WM	Weld metal
WST	Weibull statistical model
W_t	Integrated absorbed energy

CONTRIBUTORS TO DRAFTING AND REVIEW

Blasset, S.	AREVA NP GmbH, Germany
Brumovský, M.	Nuclear Research Institute Řež plc, Czech Republic
Falcník, M.	Nuclear Research Institute Řež plc, Czech Republic
Gillemot, F.	Atomic Energy Research Institute Budapest, Hungary
Horvath, M.	Atomic Energy Research Institute Budapest, Hungary
Kang, K.S.	International Atomic Energy Agency
Korshunov, M.	Russian Research Centre Kurchatov Institute, Russian Federation
Kupca, L.	International Atomic Energy Agency
Kytka, M.	Nuclear Research Institute Řež plc, Czech Republic
Lapeña, J.	CIEMAT, Spain
Lee, B.S.	Korea Atomic Energy Research Institute, Republic of Korea
Lucon, E.	Belgium Nuclear Research Centre, Belgium
Minnebo, P.	Institute for Energy EC-Joint Research Centre, Netherlands
Miura, N.	Central Research Institute of Electric Power Industry, Japan
Nanstad, R.K.	Oak Ridge National Laboratory, USA
Onizawa, K.	Japan Nuclear Safety Research Center, Japan
Perosanz, F.	CIEMAT, Spain
Planman, T.	Technical Research Centre of Finland, Finland
Rosinski, S.T.	Electric Power Research Institute, USA
Scibetta, M.	Belgium Nuclear Research Centre, Belgium
Server, W.L.	ATI Consulting, USA
Spanner, J.	Electric Power Research Institute, USA
Viehrig, H.W.	Forschungszentrum Rossendorf e.V., Germany

Research coordination meetings
Budapest, Hungary: 11–13 May 2005
Dresden, Germany: 6–10 November 2006
Vienna, Austria: 7–9 April 2008

Consultant meetings
Vienna, Austria: 20–22 October 2004
Budapest, Hungary: 16–17 May 2005
Dresden, Germany: 9–10 November 2006
Vienna, Austria: 10–11 April 2008

IAEA

International Atomic Energy Agency

Where to order IAEA publications

In the following countries IAEA publications may be purchased from the sources listed below, or from major local booksellers. Payment may be made in local currency or with UNESCO coupons.

Australia
DA Information Services, 648 Whitehorse Road, Mitcham Victoria 3132
Telephone: +61 3 9210 7777 • Fax: +61 3 9210 7788
Email: service@dadirect.com.au • Web site: http://www.dadirect.com.au

Belgium
Jean de Lannoy, avenue du Roi 202, B-1190 Brussels
Telephone: +32 2 538 43 08 • Fax: +32 2 538 08 41
Email: jean.de.lannoy@infoboard.be • Web site: http://www.jean-de-lannoy.be

Canada
Bernan Associates, 4611-F Assembly Drive, Lanham, MD 20706-4391, USA
Telephone: 1-800-865-3457 • Fax: 1-800-865-3450
Email: order@bernan.com • Web site: http://www.bernan.com

Renouf Publishing Company Ltd., 1-5369 Canotek Rd., Ottawa, Ontario, K1J 9J3
Telephone: +613 745 2665 • Fax: +613 745 7660
Email: order.dept@renoufbooks.com • Web site: http://www.renoufbooks.com

China
IAEA Publications in Chinese: China Nuclear Energy Industry Corporation, Translation Section, P.O. Box 2103, Beijing

Czech Republic
Suweco CZ, S.R.O. Klecakova 347, 180 21 Praha 9
Telephone: +420 26603 5364 • Fax: +420 28482 1646
Email: nakup@suweco.cz • Web site: http://www.suweco.cz

Finland
Akateeminen Kirjakauppa, PL 128 (Keskuskatu 1), FIN-00101 Helsinki
Telephone: +358 9 121 41 • Fax: +358 9 121 4450
Email: akatilaus@akateeminen.com • Web site: http://www.akateeminen.com

France
Form-Edit, 5, rue Janssen, P.O. Box 25, F-75921 Paris Cedex 19
Telephone: +33 1 42 01 49 49 • Fax: +33 1 42 01 90 90 • Email: formedit@formedit.fr

Lavoisier SAS, 14 rue de Provigny, 94236 Cachan Cedex
Telephone: + 33 1 47 40 67 00 • Fax +33 1 47 40 67 02
Email: livres@lavoisier.fr • Web site: http://www.lavoisier.fr

Germany
UNO-Verlag, Vertriebs- und Verlags GmbH, August-Bebel-Allee 6, D-53175 Bonn
Telephone: +49 02 28 949 02-0 • Fax: +49 02 28 949 02-22
Email: info@uno-verlag.de • Web site: http://www.uno-verlag.de

Hungary
Librotrade Ltd., Book Import, P.O. Box 126, H-1656 Budapest
Telephone: +36 1 257 7777 • Fax: +36 1 257 7472 • Email: books@librotrade.hu

India
Allied Publishers Group, 1st Floor, Dubash House, 15, J. N. Heredia Marg, Ballard Estate, Mumbai 400 001,
Telephone: +91 22 22617926/27 • Fax: +91 22 22617928
Email: alliedpl@vsnl.com • Web site: http://www.alliedpublishers.com

Bookwell, 24/4800, Ansari Road, Darya Ganj, New Delhi 110002
Telephone: +91 11 23268786, +91 11 23257264 • Fax: +91 11 23281315
Email: bookwell@vsnl.net • Web site: http://www.bookwellindia.com

Italy
Libreria Scientifica Dott. Lucio di Biasio "AEIOU", Via Coronelli 6, I-20146 Milan
Telephone: +39 02 48 95 45 52 or 48 95 45 62 • Fax: +39 02 48 95 45 48

Japan
Maruzen Company, Ltd., 13-6 Nihonbashi, 3 chome, Chuo-ku, Tokyo 103-0027
Telephone: +81 3 3275 8582 • Fax: +81 3 3275 9072
Email: journal@maruzen.co.jp • Web site: http://www.maruzen.co.jp

Korea, Republic of
KINS Inc., Information Business Dept. Samho Bldg. 2nd Floor, 275-1 Yang Jae-dong SeoCho-G, Seoul 137-130
Telephone: +02 589 1740 • Fax: +02 589 1746
Email: sj8142@kins.co.kr • Web site: http://www.kins.co.kr

Netherlands
Martinus Nijhoff International, Koraalrood 50, P.O. Box 1853, 2700 CZ Zoetermeer
Telephone: +31 793 684 400 • Fax: +31 793 615 698 • Email: info@nijhoff.nl • Web site: http://www.nijhoff.nl

Swets and Zeitlinger b.v., P.O. Box 830, 2160 SZ Lisse
Telephone: +31 252 435 111 • Fax: +31 252 415 888 • Email: infoho@swets.nl • Web site: http://www.swets.nl

New Zealand
DA Information Services, 648 Whitehorse Road, MITCHAM 3132, Australia
Telephone: +61 3 9210 7777 • Fax: +61 3 9210 7788
Email: service@dadirect.com.au • Web site: http://www.dadirect.com.au

Slovenia
Cankarjeva Zalozba d.d., Kopitarjeva 2, SI-1512 Ljubljana
Telephone: +386 1 432 31 44 • Fax: +386 1 230 14 35
Email: import.books@cankarjeva-z.si • Web site: http://www.cankarjeva-z.si/uvoz

Spain
Díaz de Santos, S.A., c/ Juan Bravo, 3A, E-28006 Madrid
Telephone: +34 91 781 94 80 • Fax: +34 91 575 55 63 • Email: compras@diazdesantos.es
carmela@diazdesantos.es • barcelona@diazdesantos.es • julio@diazdesantos.es
Web site: http://www.diazdesantos.es

United Kingdom
The Stationery Office Ltd, International Sales Agency, PO Box 29, Norwich, NR3 1 GN
Telephone (orders): +44 870 600 5552 • (enquiries): +44 207 873 8372 • Fax: +44 207 873 8203
Email (orders): book.orders@tso.co.uk • (enquiries): book.enquiries@tso.co.uk • Web site: http://www.tso.co.uk

On-line orders:
DELTA Int. Book Wholesalers Ltd., 39 Alexandra Road, Addlestone, Surrey, KT15 2PQ
Email: info@profbooks.com • Web site: http://www.profbooks.com

Books on the Environment:
Earthprint Ltd., P.O. Box 119, Stevenage SG1 4TP
Telephone: +44 1438748111 • Fax: +44 1438748844
Email: orders@earthprint.com • Web site: http://www.earthprint.com

United Nations (UN)
Dept. I004, Room DC2-0853, First Avenue at 46th Street, New York, N.Y. 10017, USA
Telephone: +800 253-9646 or +212 963-8302 • Fax: +212 963-3489
Email: publications@un.org • Web site: http://www.un.org

United States of America
Bernan Associates, 4611-F Assembly Drive, Lanham, MD 20706-4391
Telephone: 1-800-865-3457 • Fax: 1-800-865-3450
Email: order@bernan.com • Web site: http://www.bernan.com

Renouf Publishing Company Ltd., 812 Proctor Ave., Ogdensburg, NY, 13669
Telephone: +888 551 7470 (toll-free) • Fax: +888 568 8546 (toll-free)
Email: order.dept@renoufbooks.com • Web site: http://www.renoufbooks.com

Orders and requests for information may also be addressed directly to:

Sales and Promotion Unit, International Atomic Energy Agency
Vienna International Centre, PO Box 100, 1400 Vienna, Austria
Telephone: +43 1 2600 22529 (or 22530) • Fax: +43 1 2600 29302
Email: sales.publications@iaea.org • Web site: http://www.iaea.org/books